HIGH RESOLUTION SEQUENCE STRATIGRAPHIC ARCHITECTURE OF A MID-CONTINENT MISSISSIPPIAN OUTCROP IN SOUTHWEST MISSOURI

By

MIRANDA CHILDRESS

Bachelor of Science in Geology

Oklahoma State University

Stillwater, OK

2012

Submitted to the Faculty of the
Graduate College of the
Oklahoma State University
in partial fulfillment of
the requirements for
the Degree of
MASTER OF SCIENCE
May, 2015

HIGH RESOLUTION SEQUENCE STRATIGRAPHIC

ARCHITECTURE OF A MID-CONTINENT MISSISSIPPIAN

OUTCROP IN SOUTHWEST MISSOURI

Thesis Approved:

Dr. G. Michael Grammer

Thesis Adviser

Dr. Jim Puckette

Dr. Jay Gregg

Name: MIRANDA CHILDRESS

Date of Degree: MAY, 2015

Title of Study: HIGH RESOLUTION SEQUENCE STRATIGRAPHIC ARCHITECTURE OF A MID-CONTINENT MISSISSIPPIAN OUTCROP IN SOUTHWEST MISSOURI

Major Field: GEOLOGY

Abstract: The Mid-Continent Mississippian Limestone represents a geologically complex system containing different depositional environments and dynamic diagenetic and tectonic histories. This thick (up to 500 ft) carbonate unit was deposited in an east-west oriented belt with a northern and southern boundary within 5°-30° of the paleo-equator. Its subsurface equivalent is an unconventional oil and gas play in Oklahoma and Kansas with well-exposed outcrops in Missouri and Arkansas. The Mississippian-age strata in this area has been interpreted by some to be deposited in a shelf margin environment based on over-simplified paleo-depositional maps. In this study, detailed outcrop analysis has revealed the depositional environment is more consistent with a distally steepened ramp and that complex and dynamic facies mosaics exist across the distally steepened ramp due to lateral migration of facies, complicating the lithology-based nomenclature used throughout the Mid-Continent.

Understanding how primary depositional facies fit into a sequence stratigraphic framework will increase predictability of reservoir facies. The high resolution sequence stratigraphic architecture study at the Jane outcrop provides a basin specific analog for identification of reservoir facies in the subsurface. This study includes analyses of facies vertically and horizontally to identify geometries and vertical stacking patterns on the third-, fourth-, and fifth-order scales. Using an integrated sequence stratigraphic approach combining Gigapan imaging, thin section analysis, scanning electron microscopy, and spectral gamma ray logs identified a repeated shallowing-upward succession of facies ranging from bryozoan-crinoidal wackestones to bryozoan crinoidal grainstones, likely at the 4th order scale.

Integrating this sequence stratigraphic approach with an understanding of the probable complexity of facies mosaics from modern analogs has led to a modified time-series of paleo-depositional maps that better illustrate the complex facies mosaics associated with Milankovitch-scale sea level change. The high resolution sequence stratigraphic architecture developed at the Jane outcrop provides a datum for a more accurate interpretation of how Mississippian lithofacies fit into the sequence stratigraphic framework. A high resolution sequence stratigraphic architecture study that incorporates primary facies, depositional environments, and gamma ray response within a larger scale 2-D geometry for an outcrop can be used as a basin specific analog to identify reservoir facies in the subsurface.

TABLE OF CONTENTS

I. INTRODUCTION 1
Mississippian Play History 1
Problems 3
Questions and Hypotheses 7
Objectives 10
Geologic Setting 11
Depositional Environment 11
Sea Level and Cycle Hierarchy 14
Paleotemperature 19
Regional Stratigraphy 20
Bachelor Formation 21
Compton Formation 21
Northview Formation 23
Pierson Formation 24
Sequence Stratigraphy 25
Reservoir-Scale Modeling 28
Vertical/Lateral Significance 28

II. HIGH RESOLUTION SEQUENCE STRATIGRAPHIC ARCHITECTURE OF A MID-CONTINENT MISSISSIPPIAN-AGE OUTCROP IN SOUTHWEST MISSOURI 30

Introduction 30
Geologic Setting 33
Sea Level 33
Outcrop Stratigraphy 34
Methods 39
Gigapan EPIC Pro 40
High Resolution Vertical Sections 40
Thin Section Petrography 43
Scanning Electron Microscopy 43
Spectral Gamma Ray 44
Results 45
Facies Descriptions 45
Depositional Model 51

Chapter Page

Outcrop Sequence Stratigraphy 53
Idealized Facies Succession 60
High Resolution Vertical Sections 60
Spectral Gamma Ray 74

Discussion 78
Section/Cycle Thickness 78
Application to Reservoir 79

III. OUTRUNNER BLOCKS 81

Introduction 81
Previous Studies 82
Questions and Hypothesis 85
Geologic Setting 86
Outcrop Observations 87
Outrunner Blocks and Debris Flow 97
Methods 91
Gigapan Imaging 91
Thin Section Analysis 92
Literature Comparison 92
Results 92
Evidence for Outrunner Blocks 92
Thin Section Analysis 98
Formation and Flow Mechanism 103
Triggering Mechanism 106
Outrunner Block Example 110
Finneidfjord Slide 110
Depositional Model 112
Sequence Stratigraphy 114

IV. SUMMARY AND CONCLUSIONS 116

Anomalous Stratigraphy 117
Sequence Stratigraphy 118
Alternative Explanations 119
Time Slice Models 123

Conceptual Model 132
Conclusions 133

REFERENCES 136

APPENDICES 146

Appendix A (thin section photomicrographs) 146
Appendix B (SEM images) 240
Appendix C (outcrop field photographs) 246

LIST OF TABLES

1. Cycle Hierarchy 15

2. Thin Section Image Labels..... 44

3. Block Terminology and Structural Attributes 84

4. Block Dimensions 91

LIST OF FIGURES

Figure Page

1. Mississippian Sequence Stratigraphy 3
2. Mississippian Play Map 6
3. Paleo-Depositional Map 9
4. Blakey Map 13
5. Global Sea Level and Onlap Curves for the Carboniferous 18
6. Milankovitch Orbital Patterns 19
7. Milankovitch-Band Frequency Patterns 20
8. Greenhouse and Icehouse Conditions throughout Geologic Time 22
9. Systems Tract Deposition relative to Eustasy vs. Time 27
10. Study Area Location Maps 32
11. Partial Gigapan Photograph of the study area 36
12. Outcrop photograph of the Northview Formation 37
13. Tidal Flat Evidence within the Northview Formation 38
14. Complete Gigapan Photograph and Bedding Geometry of Jane Outcrop 42
15. Thin Section Photomicrographs of the Depositional Facies 47
16. SEM Images of Each Primary Depositional Facies 50
17. Pore Size Classification 51

Figure Page

18. Distally Steepened Ramp Depositional Model 53

19. Biostratigraphic Range Chart 56

20. Jane Outcrop Conodont Zonation 57

21. Eustatic Sea Level Curve Illustrating 3rd Order Sequences 58

22. Third Order Sequences Overlain on Jane Outcrop 59

23. Idealized Facies Succession 61

24. Vertical Section 1 63

25. Vertical Section 2 64

26. Vertical Section 2-3c 65

27. Vertical Section 3 66

28. Compton Formation Field Photograph with Sequences at VS 2 67

29. Compton Formation Field Photograph with Sequences at VS 2-3c 68

30. Northview Formation Field Photograph with Sequences at VS 2 69

31. Pierson Formation Field Photograph with Sequences at VS3 70

32. Sequence Stratigraphy of Jane Outcrop Based on 3rd Order Sequences and 4th Order High Frequency Sequences 71

33. Sequence Stratigraphic Architecture 73

34. Spectral Gamma Ray Results 77

35. Outrunner Blocks and Debris Flow within the Compton Formation 88

36. Debris Flow Sample 89

37. Density Flow Types 90

38. Geopetal Structures 95

39. Northview Compactional Draping 96

40. Intraformational Truncation Features 97

41. JC1 Thin Section Photomicrographs 99

42. Block 2 Thin Section Photomicrographs 99

43. Block 3 Thin Section Photomicrographs 100

44. Block 4 Thin Section Photomicrographs 100

45. Block 5 Thin Section Photomicrographs 101

46. Block 6 Thin Section Photomicrographs 101

47. Debris Flow Thin Section Photomicrographs 102

48. Outrunner Block Formation and Flow Diagram 104

49. Glide Track within the Compton Formation 105

50. Mechanisms for Block Initiation 108

51. Finneidfjord Slide Morphology 111

52. Block Deposition on a Distally Steepened Ramp 113

53. Anomalous Stratigraphy throughout the Mid-Continent 121

54. Cross-Sectional Distally Steepened Ramp Models 123

55. Time Slice: Bachelor Deposition 124

56. Time Slice: Compton Deposition 125

57. Time Slice: Block Deposition 126

58. Time Slice: Northview Deposition 127

59. Time Slice: Anomalous Northview Deposition 128

60. Time Slice: Pierson Deposition (TST)..... 129

61. Time Slice: Pierson Deposition (HST) 130

62. Shifting Facies Conceptual Model..... 132

.

CHAPTER I

INTRODUCTION

Mississippian Play History

The Mississippian play in the Mid-Continent, often referred to as the "Mississippian Lime" play, is one of many unconventional resource plays that yields prolific hydrocarbons by horizontal drilling and multistage hydraulic fracturing techniques. Unconventional resource plays are typified by large volumes of hydrocarbons that are difficult to develop (Seale and Snyder, 2011). They commonly require stimulation and exhibit limited flow capacity. Due to limited drainage areas, horizontal drilling is often the method used to access the recoverable reserves (Roundtree et al., 2010; Cox et al., 2008). In general, horizontal drilling enhances reservoir contact and well productivity. The large contact area provided by the horizontal well enhances well injectivity for enhanced oil recovery in the Mississippian. Because of the complex heterogeneities within Mississippian carbonates of the Mid-Continent, horizontal drilling helps to intersect multiple pay zones within the targeted units (Joshi, 1991). Technological advancement in horizontal drilling and multi-stage fracturing has allowed access to previously uneconomic reserves within the "Mississippian Lime" play (Seale and Snyder, 2011).

Reservoir equivalent facies to subsurface production in Kansas and Oklahoma are exposed in outcrop in the tri-state region of Oklahoma, Arkansas, and Missouri. In outcrop, these units are Kinderhookian and Osagean in age (Figure 1) and consist of the Reeds Spring Limestone, Pineville tripolite facies, and Mississippian “chat”. “Chat” serves as an informal name for diagenetically-altered cherty limestone (Elebiju et al., 2011; Rogers, 2001). The primary Mississippian oil and gas reservoirs targeted today can be seen in Figure 2. Complex interactions of diagenesis, structure, deposition, and sea level change have created heterogeneities that complicate every formation within the Mississippian (Elebiju et al., 2011).

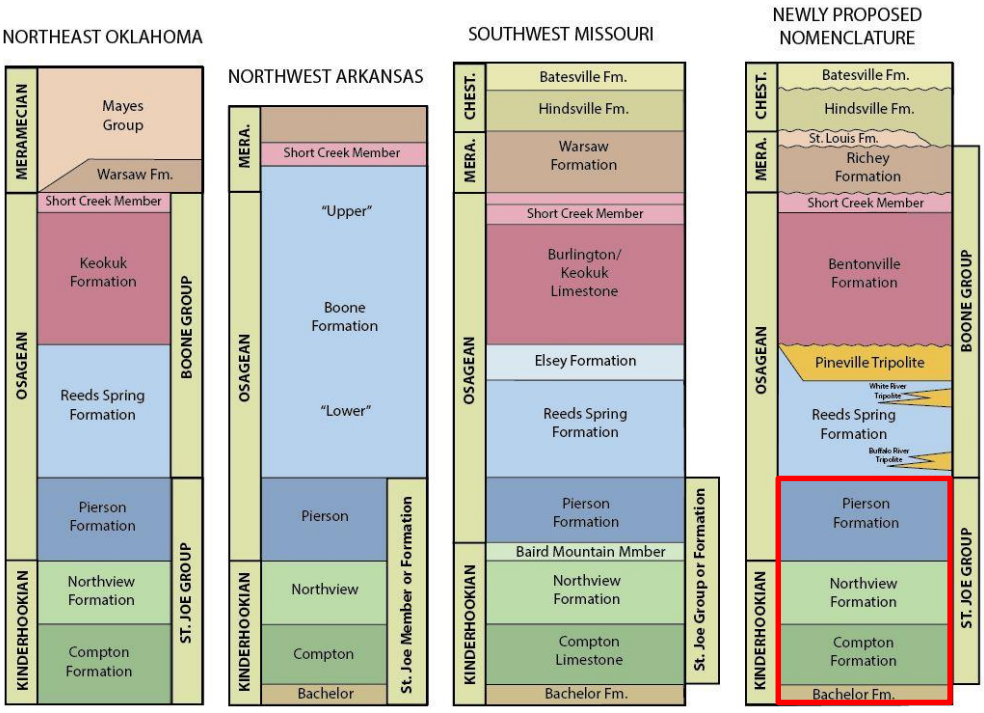

Figure 1: Stratigraphic nomenclature of the entire Mississippian period for northeast Oklahoma, northwest Arkansas, and southwest Missouri. Multiple names for each formation exist within each state, complicating outcrop and subsurface investigations. A new standardized stratigraphic nomenclature was proposed for the formations present in the tri-state area (right column). On this column, the formations investigated in this study are outlined in red and include the Bachelor, Compton, Northview, and Pierson Formations, which were deposited from the Kinderhookian to Early Osagean stages. Note Meramecian and Chesterian stages are abbreviated (i.e. Mera. and Chest.) (Modified from Mazzullo et al., 2013).

Problems

The Mississippian-age rock units throughout the Mid-Continent of the United States represent a geologically complex system of facies. The emphasis of work on the Mississippian covered in this study is in the tri-state region and includes the states of Oklahoma, Missouri, and Arkansas. The Mississippian rocks in this study are

associated with outcrop exposures containing Kinderhookian and Osagean strata equivalent to subsurface reservoir facies distributed throughout Kansas and Oklahoma (Figure 1; Figure 2). From an application standpoint, the key problem with this unconventional "Mississippian Lime" resource play is the significant heterogeneity in facies and reservoir quality, which results in compartmentalized reservoir systems. Complex and dynamic shifts in facies exist across the study area due to lateral migration of facies and facies belts, complicating the lithology-based nomenclature used throughout the Mid-Continent. These complex and dynamic shifts in facies are not well-represented by the current paleo-depositional model applied to the Mississippian carbonates in the Mid-Continent region. Figure 3 represents the current generalized paleo-depositional map with a very simplified facies distribution. From modern analogs of carbonate systems as well as examples of Mississippian carbonate strata in other parts of the world, facies mosaics are expected to be much more complex than represented by this map (Westphal et al., 2004; Sonnenfeld, 1996; Read, 1995; Elrick and Read, 1991; Mitchum and Van Wagoner, 1991). An additional problem is that this model is both "static" and "normalized" as it attempts to represent facies distribution for the entire Lower to Middle Mississippian. The simplification of this model has led to the industry-wide application of lithostratigraphic nomenclature to Mississippian-age formations without any consideration of the chronostratigraphy of the system. This nomenclature leads to the incorrect use of formation names across the Mid-Continent based purely on the lithologic character of the rock, and does not

integrate the complex facies mosaics associated with changes in sea level that are ubiquitous in carbonate systems.

Based on simplification of the paleo-depositional model in Figure 3, the Mississippian-age strata in the tri-state region has been interpreted to have been deposited in a shelf margin environment (Figure 3; Gutschick and Sandberg, 1983; Lane and De Keyser, 1980). Detailed outcrop analysis in this study has revealed a depositional environment more consistent with a distally-steepened ramp interpretation, a model that better illustrates the complexities in facies shifts associated with relative changes in sea level. Anomalous features associated with this distally steepened ramp model have been referred to as *in situ* bioherms or "mud mounds" and also as "slump blocks" (Morris and Mazzullo, 2013; Unrast, 2012; Evans et al., 2011). Determining whether these features are truly *in situ* or have been transported will assist in constructing an accurate sequence stratigraphic framework for this outcrop study.

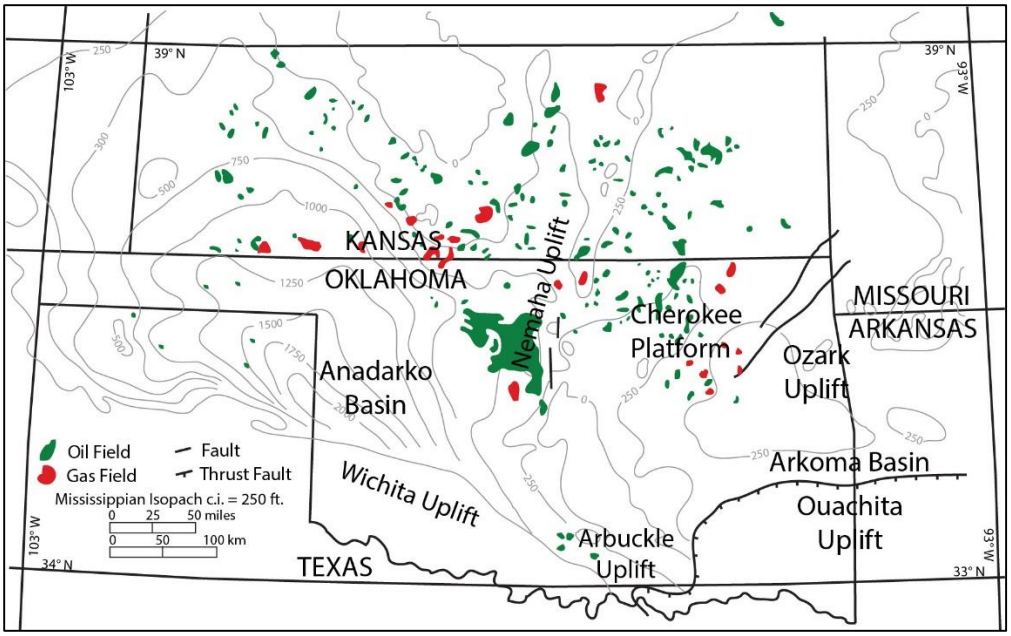

Figure 2: Mississippian play map showing the distribution of oil (green) and gas (red) fields throughout Oklahoma and Kansas. Thickness of the Mississippian section is represented by the gray contours. Note the contour interval is 250ft (76.2 m) (Modified from Harris, 1987).

In addition to the overly simplified paleo-depositional model, limitations exist in defining the temporal extent of sequences within the Mid-Continent formations of the Mississippian. Haq and Schutter (2008) have identified global sea level changes on the order of one to six million years throughout the Lower and Middle Mississippian. This span of sea level fluctuations relates to deposition of sequences tens to hundreds of meters thick and can generally be constrained by biostratigraphy (Read, 1995). In the Mississippian, distinctive conodont types are used to consistently recognize biostratigraphical correlations and help to confirm sea level fluctuation curves with a resolution of 1-3 million years (Boardman, 2013; Boardman, D.R. and Nestell, M.K., 1992). Although this provides a time constraint on sequences that are ten to hundreds of meters thick, it does not constrain thinner

(meters to tens of meters thick) higher frequency events which may occur on the order of 20,000-400,000 years (i.e. Milankovitch scale) that are superimposed on the one to three million year sequences (Read, 1995). These higher frequency events are significant as they control facies stacking patterns, the lateral distribution of facies, and ultimately the potential reservoir distribution throughout the system (Grammer et al., 1996).

In determining vertical stacking patterns within potential reservoir units, potential problems may occur when distinguishing vertical facies successions. Autocyclic and allocyclic processes could factor into depositional processes, potentially producing and/or modifying meter-scale cycles (Rankey, 2002; Wilkinson and Drummond, 1993). Relative changes in sea level can occur, leading to slight reorganizations in the depositional system that are not representative of laterally adjacent environments and facies, such as local changes in subsidence and sedimentation rates (Rankey, 2002). Understanding the distribution and migration of depositional facies within the system can help identify true high frequency sequences and cycles (Rankey, 2002; Drummond and Wilkinson, 1993). Analysis of the Mid-Continent Mississippian sequence stratigraphy at a high resolution scale will allow for more accurate characterization of the complex and dynamic reservoirs and facies mosaics distributed throughout the Mid-Continent region.

Questions and Hypotheses

Fundamental questions that stem from these problems that are addressed in this study are as follows:

1. Do high frequency sequences and cycles (probable 4th and 5th order, with a duration of tens to hundreds of thousands of years) exist in the Mississippian of the Midcontinent?
2. What is the vertical and lateral variability of these facies and how do they fit into the sequence stratigraphic framework?
3. Can a regional model be developed to capture the dynamic nature of the system?
4. Are the “mud mounds” in the Compton Formation truly *in situ* bioherms, or are they mobilized blocks?

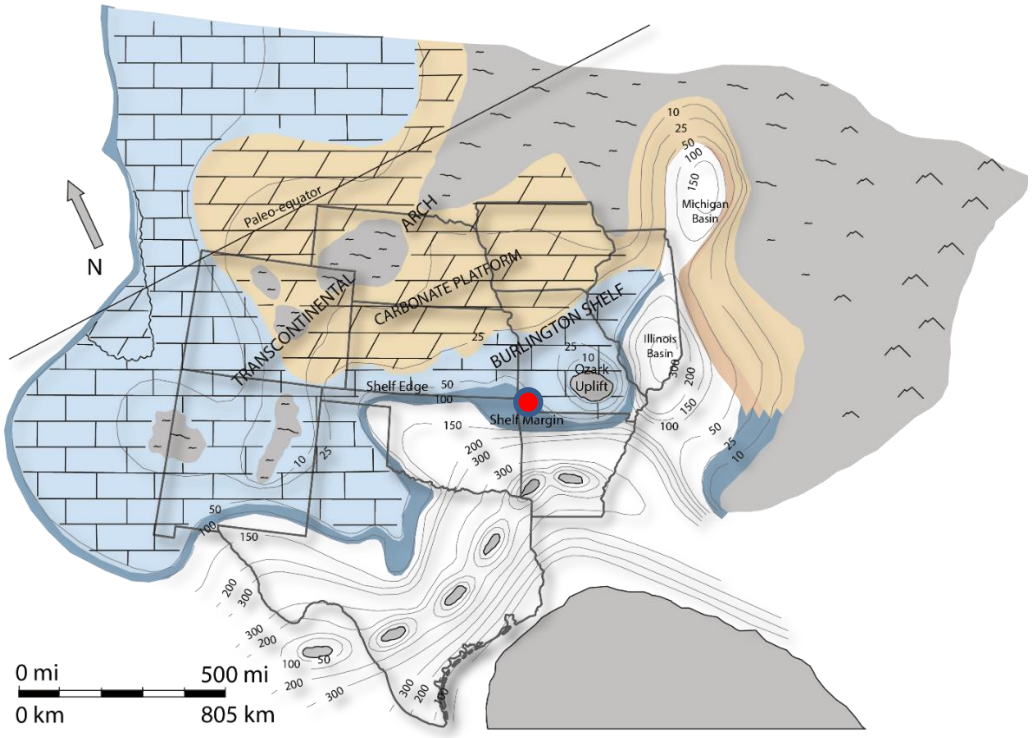

Figure 3: Generalized paleo-depositional model of the Mid-Continent region of the U.S., showing distribution of the Burlington Shelf and the Transcontinental Arch during the Mississippian. The shelf margin, originally named by Lane and De Keyser (1980), marks the region where the Mississippian carbonates being examined in this study were deposited. The red dot is the location of the study area, west of the Ozark Uplift and North of the Ouachita Uplift in water depths of 50 – 100m (164ft – 328ft). Paleo-bathymetric contours are in meters and show a significant difference between the eastern and southern edges of the shelf margin. The shelf margin grades into the Illinois Basin within 15 – 20 miles as water depth increases from 50 – 100m (164ft – 328ft). The southern margin of the shelf deepens from 50m –100m (164ft – 328ft) over a distance of 150 miles (Modified from Gutschick and Sandberg, 1983).

Multiple hypotheses were created to help answer the above questions. The first hypothesis is that the evaluation of the stratigraphy from a high frequency sequence and/or high frequency cycle framework (4th and 5th order) will complement the current biostratigraphic data (3rd order). An additional hypothesis is the identification of facies types and vertical stacking patterns at the higher frequency scale will define the controls and distribution of reservoir heterogeneity observed within the units of the Jane outcrop. Lastly, through integration of the sequence stratigraphic framework and an understanding of the probable complexity of facies mosaics from modern analogs, a modified time-series of paleo-depositional maps should be able to be created that better illustrate the complex facies mosaics associated with Milankovitch-scale (4th and 5th order) sea level change.

Objectives

In order to accurately build the high resolution sequence stratigraphic architecture for the Mississippian-age formations, it is necessary to identify the fundamental objectives of this study. The primary objective was to identify common rock facies and vertical stacking patterns of those facies through outcrop samples and thin section analysis. The second objective was to identify the sequence stratigraphic architecture formed by probable high frequency relative sea level changes. This was completed through identifying vertical stacking patterns of facies and evidence of flooding and/or subaerial exposure. The third objective was to refine the sequence stratigraphic framework defined by biostratigraphy. Through each of these objectives,

an enhanced understanding of the facies heterogeneity resulting from higher frequency sea level changes should increase the predictability of potential reservoir units in the subsurface and allow for a more accurate interpretation of how Mississippian lithofacies fit into the sequence stratigraphic framework.

Geologic Setting

Depositional Environment – Although not well defined, deposition of Mississippian-aged carbonates in the Mid-Continent has been generally interpreted as occurring in a shallow, tropical sea on the southern margin of a broad and shallow carbonate platform known as the Burlington Shelf (Figure 3; Gutschick and Sandberg, 1983). The paleogeographic map by Blakey (2013) shows the study area during the Mississippian and suggests deposition in the study area occurred at 10-15 degrees south latitude (Figure 4). The area of southwestern Missouri is interpreted as the shelf margin, which is also present in north-central Arkansas and continues west into the area of the Tri-State Mining District where it is present in the south-central Kansas subsurface (Lane and De Keyser, 1980). The Burlington Shelf extends from central Illinois to southwestern Kansas and parallels the eastern margin of the Transcontinental Arch, a subaerial physiographic element (Figure 3; Lane and De Keyser, 1980). The southern margin of North America served as the boundary between a transequatorial seaway connecting the Iapetus and Panthalassic seas. Laurasia and Gondwana converged, closing off the transequatorial seaway in the Late Carboniferous. This formed a series of borderland basins filled with siliciclastic sediments overlain by Permian carbonates and evaporites

at the southern margin of North America (Noble, 1993). Landward from these borderlands in the Early and Middle Osagean, the Burlington Shelf formed in the platform region of North America and was bordered on the south by a shelf margin where Mississippian carbonates were deposited (Figure 3; Lane, 1978).

Mississippian-age rocks in the Mid-Continent of the United States consist of various lithologies ranging from green, calcareous shales to crinoidal-bryozoan packstones and grainstones, which reflect the transgressive and regressive sequences that occurred throughout this time (Lisle, 1983). Inner shelf, main shelf, and shelf margin are the three carbonate depofacies of the Burlington Shelf as defined by Lane and De Keyser (1980). The inner shelf facies flanks the Transcontinental Arch, the main shelf facies is just seaward of the inner shelf facies, and the shelf margin facies follows the seaward edge of the main shelf. The inner shelf facies consists of crinoidal-bryozoan, grain-supported rocks that have been partially to completely dolomitized. The main shelf facies is the most aerially extensive of the depofacies and consists of thicker grain-supported rocks that have not been dolomitized. The shelf margin facies consists of red and green, mud-supported argillaceous limestone overlain by cherty lime mudstone and/or wackestone (Figure 3; Lane and De Keyser, 1980).

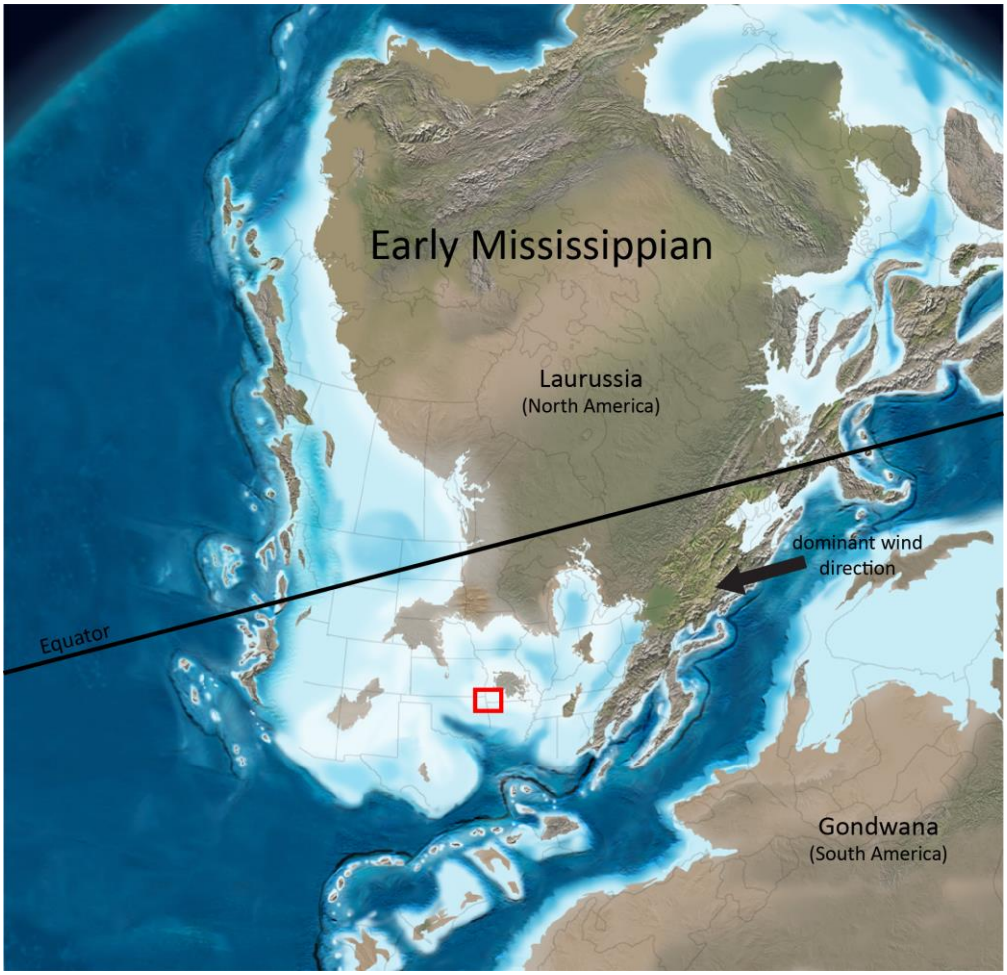

Figure 4: Paleogeography of the study area during the Mississippian. The study area is outlined in red and located 10-15° south latitude, in shallow tropical seas. (Modified from Blakey, 2013).

The current interpretation for deposition of Mississippian strata of the Mid-Continent is in a foreland ramp setting as part of a system of shallow-water carbonate facies bordered by deep-water deposits to the south and west. These facies are said to be deposited during tectonic events that overprinted the lithostratigraphy, biostratigraphy, and sequence stratigraphic framework of the Mississippian-age strata (Mazzullo et al., 2011). Boardman (2013) describes the geometry of Osagean strata as

diachronous prograding carbonate wedges, determined by application of a new conodont zonation. Progradation of these wedges eventually led to a homoclinal to distally steepened ramp depositional setting for Mississippian-age strata (Wilhite et al., 2011). Despite the new distally-steepened ramp interpretation, terminology associated with shelf margin settings is still presently being used, complicating the lithology-based nomenclature used throughout the Mid-Continent.

Sea Level and Cycle Hierarchy – The two factors responsible for global sea level change with time are changes in ocean basin volume from heat flow through mid-ocean ridges and variations in global ice volume. The combination of these two mechanisms creates a hierarchy of sea level fluctuations referred to as sequences and cycles (Table 1). Each sea level sequence or cycle is distinguished by characteristics including duration, magnitude, and processes responsible for sea level change (Read, 1995). First order sequences are 200-300 million years in length and are associated with opening and closing of ocean basins and tectonic plate movement (Read, 1995). Second order sequences range from 10-50 million years in length and are controlled by tectonics, changes in ocean basin volume, and variations in global ice volume (Read, 1995). Third order sequences are superimposed on second order sequences, which range in duration from 1 to 10 million years (Read, 1995). It should be noted that there is no accepted mechanism or periodicity for 3rd order sequences, but most researchers believe the sequences are generally less than 3 million years in duration and are caused by tectonics and ocean floor spreading (Haq and Schutter, 2008; Plint et al., 1992) or waxing and waning of continental ice sheets (Read, 1995). Haq and Schutter recognize 21

transgressive-regressive cycles on the order of 1-6 million years (possibly 3rd order) throughout the Mississippian that can be correlated world-wide (Figure 5).

Cycle Hierarchy				
Tectono-Eustatic Cycle Order	**Sequence Stratigraphic Unit**	**Duration (n = my)**	**Relative Sea Level Amplitude (m)**	**Relative Sea Level Rise/Fall Rate (cm/1000 yrs)**
First	Supersequence	> 100		< 1
Second	Supersequence	10 – 100	50 – 100	1 – 3
Third	Depositional Sequence, Composite Sequence	1 – 10	50 – 100	1 – 10
Fourth	High-Frequency Sequence, Parasequence, and Cycle Set	0.1 – 0.4	1 – 150	40 – 500
Fifth	Parasequence, High-Frequency Cycle	0.02 – 0.04	1 – 150	60 – 700

Table 1: Cycle hierarchy chart showing the difference between first through fifth order sea level sequences and cycles. The 3rd order depositional sequences are known to exist within Mississippian-age carbonate rocks throughout the Mid-Continent and can be tied to conodont biostratigraphy. The 4th order high frequency sequences and 5th order high frequency cycles range in duration from 20,000 to 400,000 years and have not yet been tied to Mississippian-age carbonate rocks of the Mid-Continent (Re-drafted from Kerans and Tinker, 1997)

Superimposed on 3rd order sequences are 4th order high frequency sequences (HFS) and 5th order high frequency cycles (HFC), which are most likely forced by Milankovitch-band glacio-eustacy (Kerans and Tinker, 1997; Read, 1995). Milankovitch

cycles, which are a function of orbital variations of the Earth, are responsible for climate change, which in turn causes eustatic sea level change (Read, 1995). The three Milankovitch-band frequencies are eccentricity, obliquity, and precession, and can be seen in Figure 6 and Figure 7 (Read, 1995). Eccentricity, the change in shape of the earth's orbit, occurs on a 4^{th} order scale every 100,000 years and 400,000 years. Obliquity, the tilt of the earth's axis, occurs on a 5^{th} order scale every 40,000 years. Precession, the wobble of the axis of the earth, occurs on a 5^{th} order scale every 20,000 years (Kerans and Tinker, 1997; Read, 1995).

Sea level fluctuations are related primarily to the volume of continental ice present during a given sequence or cycle, which is correlative to the change in greenhouse and icehouse conditions through geologic time (Read, 1995). High frequency sequences and cycles (4^{th} and 5^{th} order) directly relate to the icehouse/greenhouse cycles of the Phanerozoic, which determine differences in lithofacies continuity, preservation of depositional topography, and formation of diagenetically enhanced porosity (Kerans and Tinker, 1997). During global greenhouse conditions, Milankovitch sea level fluctuations were small (likely less than 10m) and dominated by precession cycles (Read, 1995; Read and Horbury, 1993). In contrast, during global icehouse conditions Milankovitch sea level fluctuations were generally large (up to 100m or more) and dominated by eccentricity cycles (Read, 1995; Read and Horbury, 1993).

Overall, the Mississippian was a period of global regression and occurs between Devonian submergence and Carboniferous emergence (Buggisch et al., 2008; Ettensohn, 1993). During the mid-Visean (late Osage/Meramecian) sea level began to significantly decline relative to the sea level during the Tournaisian (Kinderhookian and early Osagean), reaching a low in the late Mississippian/Serpukovian (Chesterian) (Figure 5; Haq and Schutter, 2008). This represents a transitional period from greenhouse conditions present during the Devonian to icehouse conditions present during the Pennsylvanian and Permian (Figure 8). Obliquity cycles are likely more important during these transitional periods (Read, 1995).

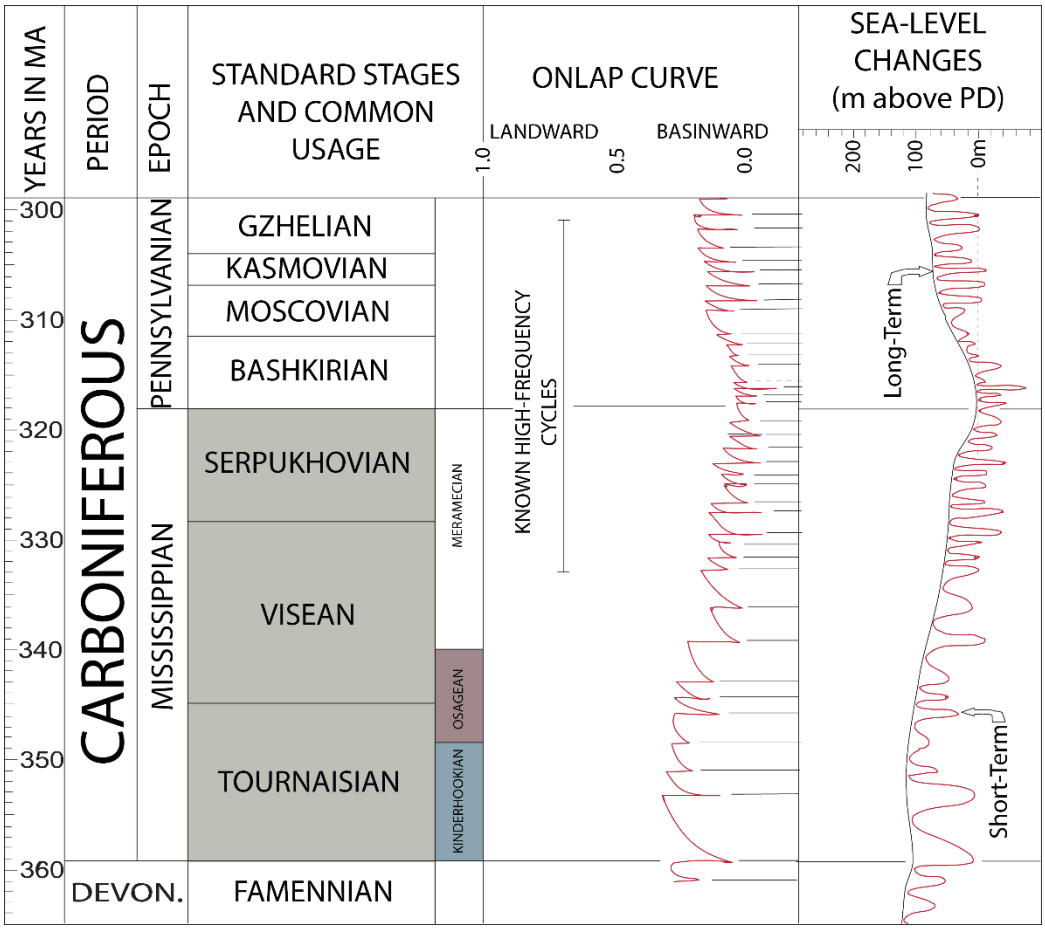

Figure 5: Global sea level fluctuations throughout the Carboniferous Period. Stages of the Mississippian are highlighted in gray. Kinderhookian and Osagean strata correspond to the Tournaisian through Middle Visean Stages over approximately 20 MY. Haq and Schutter (2008) use "known high-frequency cycles" to identify 3rd order sequences. Up to eight 3rd order sequences spanning 1-6 million years have been globally identified throughout the Kinderhookian and Osagean. 4th order high frequency sequences and 5th order high frequency cycles have been interpreted by several workers (Westphal et al., 2004; Elrick and Read, 1991), but are not identified in this figure (Modified from Haq and Schutter, 2008).

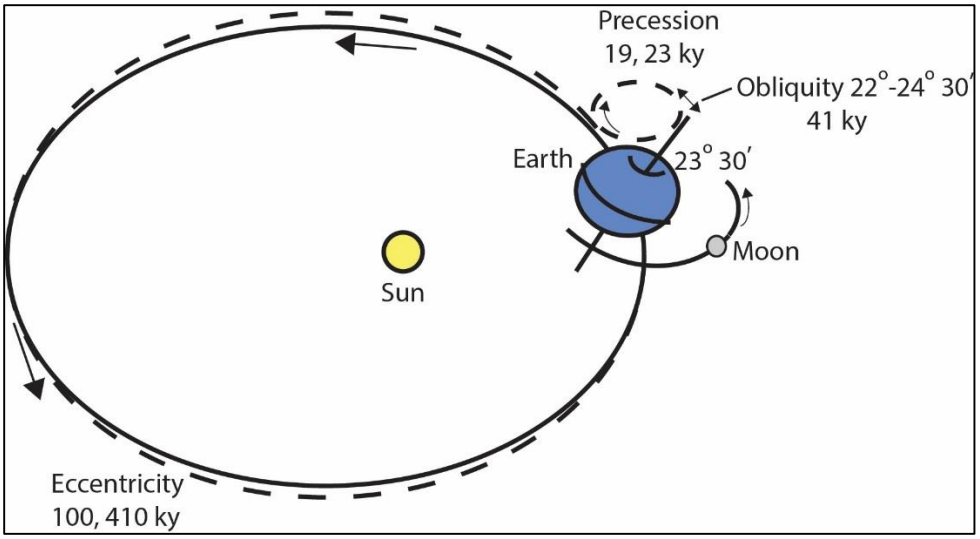

Figure 6: Relationship between Milankovitch orbital patterns of eccentricity, obliquity (tilt), and precession (modified from Read, 1995). Eccentricity, the change in shape of the earth's orbit, occurs approximately every 100,000 years and 400,000 years. Obliquity, the tilt of the earth's axis, occurs approximately every 40,000 years. Precession, the wobble of the axis of the earth, occurs approximately every 20,000 years (Re-drafted from Kerans and Tinker 1997).

Paleotemperature – Buggisch et al. (2008) reconstructed the history of average sea surface temperature during the Mississippian using oxygen isotope ratios measured on conodont apatite. In the early Tournaisian, low latitude sea surface temperatures averaged around 25 to 30˚C. Sea surface temperature dropped to 17˚C towards the end of the Tournaisian, which Buggisch suggests may be due to waxing of ice sheets and climatic cooling (Figure 7). Tournaisian-aged, meter-scale, upward-shallowing cycles in Montana and Wyoming were interpreted by Elrick and Read (1991) as an initial effect of the Carboniferous glaciation.

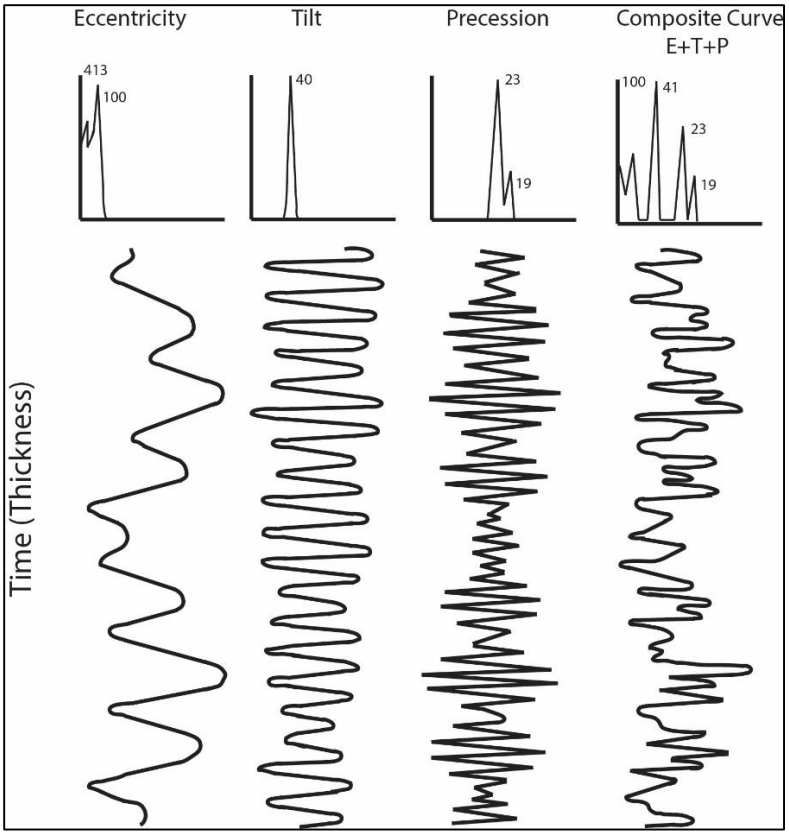

Figure 7: Milankovitch-band frequencies responsible for sea-level fluctuations and sequences. The composite curve shows the relationship of the combined frequencies, which reinforce and interfere with each other (Modified from Read, 1995).

Regional Stratigraphy

Mississippian lithostratigraphic nomenclature throughout the Mid-Continent varies by state, leading to uncertainty in recognizing the formation being studied. The most sought-after potential reservoir facies of the Mississippian were deposited during Kinderhookian and Osagean times (Mazzullo et al., 2013; Mazzullo, 2011). The Kinderhook interval is comprised of the Bachelor, Compton, and Northview Formations. The Osage, from base to top, consists of the Pierson, Reeds Spring, Pineville Tripolite, and Bentonville Formations, as well as the Short Creek Member above the Bentonville

Formation (Figure 1; Mazzullo et al., 2013). The Bachelor, Compton, Northview, and Pierson Formations represent the Lower and Middle Mississippian and are the primary focus for this study.

Bachelor Formation – The Bachelor Formation is the lowermost unit of the Mississippian, which uncomformably overlies the Devonian Woodford (Chattanooga) Shale. The general lithology consists of quartzarenite sandstones and green calcareous shale (Friesenhahn, 2012; Kreman, 2011). Thickness of the Bachelor varies little throughout southwestern Missouri, reaching a maximum thickness of approximately 3.9 feet (1.2 meters) with an average thickness of 1 foot (0.3 meters) (Manger and Shanks, 1976; Mehl, 1961).

Compton Formation – The Compton Formation is Kinderhookian in age and overlies the Bachelor Formation in the lower Mississippian. Lithologically, the Compton is comprised of light gray crinoidal-bryozoan packstones and grainstones (Kreman, 2011; Manger and Shanks, 1976). The average thickness ranges from 5 to 15 feet (1.5-4.6 meters), but can reach up to 30 feet (9 meters) in some regions (Thompson and Fellows, 1970). Near Jane, Missouri, the thickness of the Compton increases from south to north (Wilhite et al., 2011). According to the interpretation of Lane (1978), deposition of the Compton occurred in a shelf margin environment.

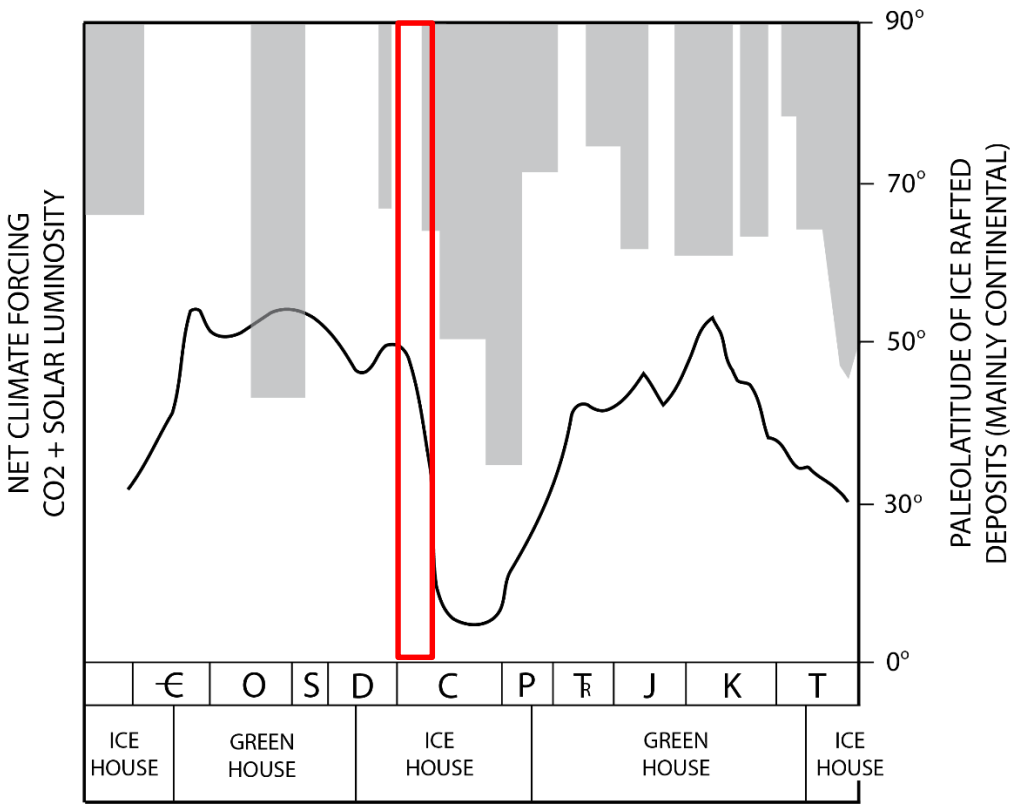

Figure 8: Icehouse and greenhouse conditions throughout geologic time. The Lower and Middle Mississippian is outlined in red. It can be seen from climate change by variation in CO^2 and solar intensity (solid line) in combination with marine ice-rafted deposits (gray) that Lower to Middle Mississippian deposition occurred during a transition from greenhouse conditions (Devonian) to icehouse conditions (Pennsylvanian and Permian) (Modified from Read, 1995).

Over forty “mounds” have been identified within the Compton interval in a belt trending east-west through southwestern Missouri (Manger and Thompson, 1982). Manger and Thompson (1982) describe the mounds as a core of homogeneous carbonate mudstone that developed during a regression in the later stages of Lower Mississippian deposition. Evans et al. (2011) refers to the mounds as “slump blocks” which can be found in isolated locations along Highway 71 in Missouri and Arkansas and interprets them as evidence for somewhat deeper-water deposition during the

Kinderhookian. Stratigraphic evidence for the slump blocks include debris flow breccias at the base, no flank beds within the Compton Formation, and a homogenous structureless lime mudstone fabric (Evans et al., 2011). Mazzullo (2011) interprets these carbonate mounds as displaced bioherms. This interpretation is not universally accepted and olistoliths may be another explanation. An Olistolith is defined in the McGraw-Hill Science & Technology Dictionary as "an exotic block or other rock mass that has been transported by submarine gravity sliding or slumping and is included in the binder of an olistostrome. Tennyson et al. (2008) suggest an explanation of soft-sediment deformation caused by intense shaking of slightly dipping sediments during an earthquake. This interpretation applies specifically to the Bella Vista fault in northwestern Arkansas, which underlies a valley. In this interpretation, faulting occurred at least as early as the Kinderhookian, as indicated by the olistoliths. Transportation of the sediments contributing to the olistolith was facilitated by the Northview Formation, which served as a surface of sliding because its dip is about 3˚ towards the fault.

Northview Formation – The Northview Formation is the top unit of the Kinderhookian stage. It conformably overlies the Compton Limestone and is unconformably overlain by the Pierson Limestone. The Northview unit occurs throughout southwestern Missouri, northwestern Arkansas, and northeastern Oklahoma (Shoeia, 2012). Huffman (1960) describes the lithology as olive green, calcareous shale or marlstone with an average thickness of 2 to 5 feet (0.6-1.5 meters), although it may reach over 80 feet (24m) in places. This thick section was deposited in an east-west trending trough near the middle of the Burlington Shelf (Wilhite et al.,

2011; Lane, 1978). The amount of shale within the formation increases northward, while the formation becomes more calcareous to the south (Shoeia, 2012). The Northview, along with the Bachelor, Compton, and Pierson, thins to the south (Wilhite et al., 2011).

The Northview Formation has been previously referred to as the "Northview Shale," and interpreted as a deeper water facies due to contradicting lithologic correlations and lack of evidence to support a definite age assignment (McDuffie, 1964). A more recent interpretation refers to the Northview as a conformable highstand wedge deposited between the Compton and Pierson Formations (Shoeia, 2012). Based on personal observations made in the field at the Jane outcrop, the Northview is 2 to 5 feet (0.6-1.5 meters) thick and contains flaser bedding, lenticular bedding, multiple subaerial exposure surfaces, and bi-directional ripples. The lithologies throughout the Northview include skeletal wackestones, packstones, and grainstones separated by two thin, discontinuous shale-like beds. Each of these outcrop observations has led to the current interpretation that the Northview Formation was deposited in a tidal flat environment.

Pierson Formation – The Pierson Formation occurs at the base of the Osagean, and unconformably overlies the Kinderhookian-aged Northview Formation. It is unconformably overlain by the Reeds Spring Limestone and has been described as a fine-grained, buff, gritty limestone (Shoeia, 2012; Heinzelmann, 1964,). The Compton and Pierson Formations are often noted to be lithologically similar and differentiated primarily through the identification of the over- and underlying strata, particularly through the identification of the intervening Northview Formation (Manger and Shanks,

1976). Regionally, the Pierson can be found in southwestern Missouri, northeastern Oklahoma, and northwestern Arkansas (Wilhite et al., 2011).

The Pierson consists of grainstones and packstones, suggestive of a relatively high energy depositional environment. Average thickness of the Pierson is 4 to 18 feet (1.2-5.5 meters) (Kreman, 2011; Wilhite et al., 2011). Huffman (1960) describes the lithology as a gray, thick-bedded, finely crystalline limestone. A glauconite zone exists at the base of the Pierson Limestone and serves as a marker bed for the base of the Osage (Krueger, 1965; Heinzelmann, 1964). The glauconite occurs as small, dark green, rounded nodules in a dark calcareous shale or argillaceous limestone (Krueger, 1965). A brown-weathering dolomite has been found within the lower portion of the Pierson in west-central Missouri. Fossils are preserved within cherty layers and include internal and external molds and silicified corals. Brachiopods and corals are the most common skeletal component within this unit (Spreng, 1952).

Sequence Stratigraphy

Sequence stratigraphy is a stratigraphic method that packages sedimentary sections deposited during the same rise and fall in sea level (Kerans and Tinker, 1997). Much of the nomenclature used for Mississippian-age formations of the Mid-Continent is based on lithostratigraphy, a classification scheme based solely on rock characteristics such as allochem types, fabric, and sedimentary structures. This can lead to the incorrect use of formation names across the Mid-Continent and incorrect correlations between formations that are assumed to be vertically and laterally continuous. The use

of sequence stratigraphy increases the predictability of heterogeneous units with the use of a suite of systems tracts and lithofacies tracts tied to a sinusoidal curve (Figure 9; Tinker and Kerans, 1997). Using this method in conjunction with subsurface cores and wireline logs is often referred to as high resolution sequence stratigraphy and is used to define reservoir-scale sequence descriptions associated with 4^{th} order high frequency sequences and 5^{th} order high frequency cycles (Tinker and Kerans, 1997).

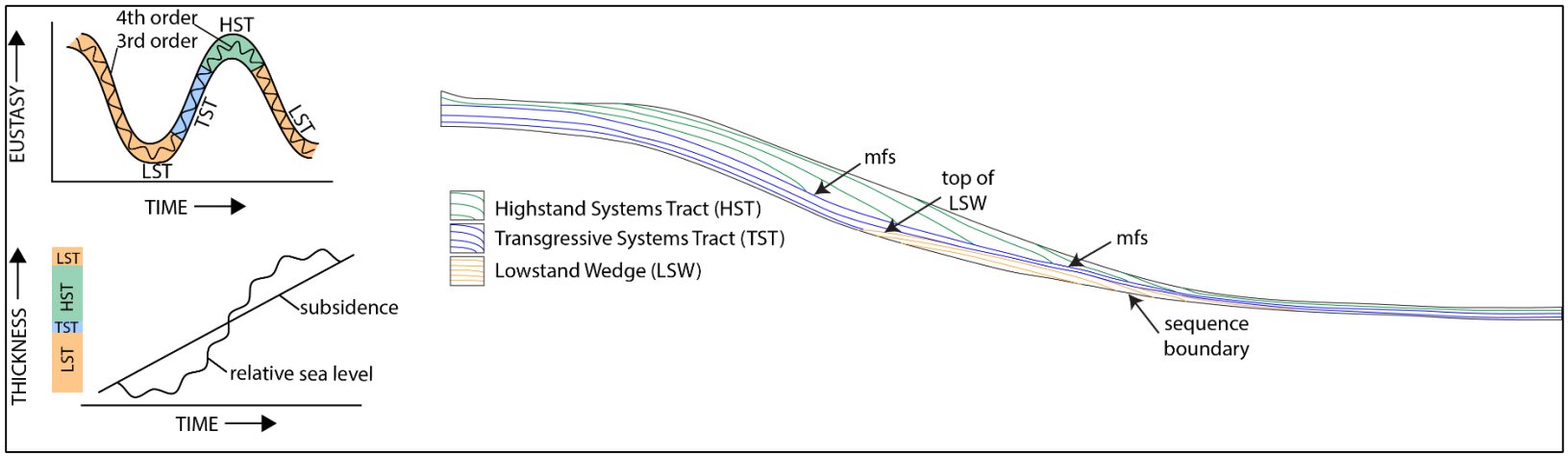

Figure 9: The above diagram shows variations in sea level through time in relation to 3rd and 4th order depositional sequences. The two graphs at the left show eustasy versus time and thickness versus time. The right side of the figure shows each systems tract, which demonstrates deposition of the lowstand wedge (LSW), transgressive systems tract (TST), and highstand systems tract (HST). The LST (orange) is deposited when the subsidence rate is higher than sea level. As sea level starts to rise above the subsidence rate, transgression begins and the transgressive systems tract (blue) is deposited. The maximum flooding surface (mfs) separates the underlying TST from the overlying highstand systems tract (HST). The HST (green) is deposited when sea level is greater than the rate of subsidence, just before sea level falls again (Grafe and Wiedmann, 1998; Kerans and Tinker, 1997).

Reservoir-Scale Modeling – The use of high resolution sequence stratigraphy in understanding the Middle and Upper Mississippian-age strata of the Mid-Continent has only recently been utilized (Le Blanc, 2014; Price, 2014). In order to link high resolution sequence stratigraphy to reservoir-scale modeling, it is necessary to identify the nature of genetically-related stratigraphic units, facies distribution within the genetic units, and facies partitioning with regard to position within the vertical stacking pattern of genetic units and lower frequency cycles (Eberli and Grammer, 2004).

Layer models for reservoir description, volumetric calculations, and fluid flow modeling are all products of recognizing and describing the interval of interest at a high-frequency cycle scale. Through this process, scale-sensitive depositional models can be developed for use in forward modeling of reservoir strata (Kerans, 1995). To successfully complete the process of describing and modeling carbonate reservoirs at the high-frequency scale, identification of sedimentary facies and the interpretation of depositional environments must be completed. Once an interpretation has been made, a distinction is likely to be seen between genetic units and their vertical stacking patterns. These stacking patterns must be interpreted to determine facies partitioning in landward and seaward stepping units. Lateral continuity can then be predicted by comparing sedimentology in different units (Eberli and Grammer, 2004).

Vertical/Lateral Significance – Determining vertical and lateral trends in facies is crucial to understanding lateral variability within cycles, the lateral extent of reservoir units and seals, and the direction of migration for potential reservoir facies. Facies

partitioning is used to better understand major changes in accommodation in a vertical section and to evaluate lateral facies shifts. This concept helps to distinguish between the different facies successions that will develop during transgressive and regressive phases (Eberli and Grammer, 2004). Variations in water depth through time are shown by the vertical succession of depositional environments, which is a measure of the change in accommodation. Lateral facies distribution within a genetic unit is a result of a combination of relative sea level change, the carbonate factory, the redistribution of sediment, and the existence or creation of topography. Variations in the vertical and lateral filling of changing accommodation space are responsible for lateral facies variations (Lerat et al., 2000). Accommodation space is produced by tectonic subsidence and sea level rise. The rate at which this space is produced, along with sediment supply, determines the stratigraphic architecture (Eberli and Grammer, 2004).

CHAPTER II

HIGH RESOLUTION SEQUENCE STRATIGRAPHIC ARCHITECTURE OF A MID-CONTINENT MISSISSIPPIAN OUTCROP IN SOUTHWEST MISSOURI

Introduction

Significant heterogeneities in facies and reservoir quality exist in the Mid-Continent formations of the Mississippian, resulting in compartmentalized reservoir systems. Complex interactions of diagenesis, structure, deposition, and sea level change have created heterogeneities that complicate each formation within the Mississippian (Elebiju et al., 2011). In turn, sections of the "Mississippian Limestone" play can be considered unconventional as they commonly require stimulation and exhibit limited flow capacity (Seale and Snyder, 2011; Roundtree et al., 2010; Cox et al., 2008).

The primary focus of this study is to examine the vertical and lateral facies variability within Lower and Middle Mississippian strata to understand the hierarchy of cyclicity within the sequence stratigraphic architecture. Conodont biostratigraphy has constrained 3rd order sequences throughout the Mid-Continent, but only recently has work focused on high frequency cyclicity within Mississippian strata in the region (Le Blanc, 2014; Price, 2014).

This study utilizes an outcrop exposure of the Bachelor, Compton, Northview, and Pierson Formations exposed along Highway 71, near Jane, Missouri (Figure 10). At the study location, the primary depositional facies are vertically repetitive throughout each formation and form a shallowing-upward idealized facies succession. The idealized facies succession was used to construct high resolution vertical sections to delineate high frequency sequence and cycle boundaries. Each vertical section was laterally linked across the outcrop to build the sequence stratigraphic architecture, reflecting the distribution of vertical and lateral heterogeneity that is often controlled by high frequency cyclicity (Grammer et al., 1996). The resulting high resolution sequence stratigraphic architecture can be utilized as a predictive tool to model potential reservoir units when coupled with subsurface data as it provides a basin-specific analog for identification of reservoir facies in the subsurface.

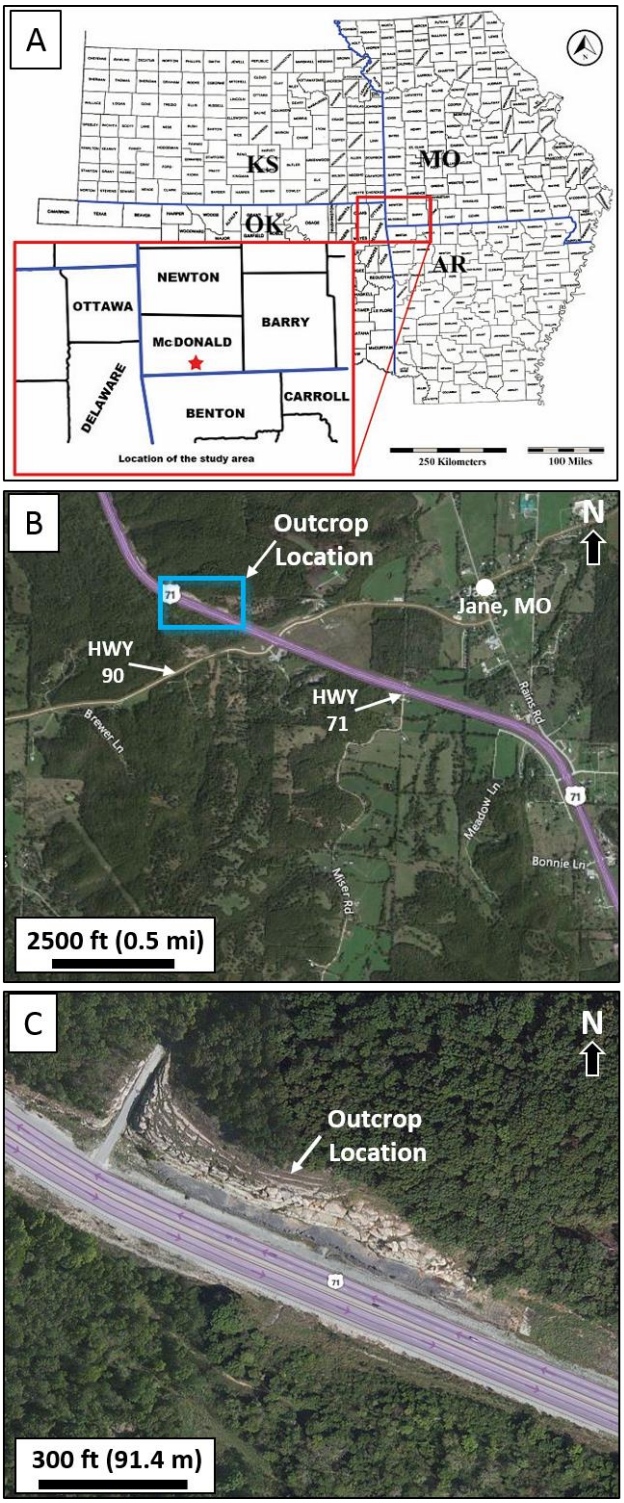

Figure 10: (A) Location of the outcrop study area is in McDonald County, MO. (B) Google Earth image of the outcrop location along Highway 71. (C) Close up view of outcrop exposure along Hwy 71. The outcrop is oriented parallel to the NW-SE regional Mississippian strike direction (Google Earth, 2014; After Shoeia, 2012).

Geologic Setting – Although not well defined, deposition of Mississippian-aged carbonates in the Mid-Continent has been generally interpreted as occurring in a shallow, tropical sea on the southern margin of a broad shallow carbonate platform known as the Burlington Shelf (Gutschick and Sandberg, 1983). The Burlington Shelf formed in the platform region of North America and was bordered on the south by a shelf margin where Mississippian carbonates were deposited (Lane, 1978). One of the current interpretations for deposition of Mississippian strata of the Mid-Continent is in a foreland ramp setting as part of a system of shallow-water carbonate facies bordered by deep-water deposits to the south and west. Progradation of diachronous carbonate wedges eventually led to a homoclinal to distally steepened ramp depositional setting for Mississippian-age strata in the Mid-Continent (Boardman, 2013; Wilhite et al., 2011). Despite the relatively new interpretation for deposition on a distally-steepened ramp, terminology associated with shelf margin settings is still being used, complicating the lithology-based nomenclature used throughout the Mid-Continent.

Sea Level – The Mississippian-age strata at the Jane outcrop were deposited during a transitional period from greenhouse conditions present during the Devonian to icehouse conditions present during the Pennsylvanian and Permian (Haq and Schutter, 2008; Read, 1995). During global greenhouse conditions, Milankovitch sea level fluctuations were small (likely less than 10m) and dominated by precessional cycles (Read, 1995; Read and Horbury, 1993). In contrast, during global icehouse conditions Milankovitch sea level fluctuations were generally large (up to 100m or more) and dominated by eccentricity cycles (Read, 1995; Read and Horbury, 1993). As the strata

investigated in this study was deposited during a transitional greenhouse/icehouse period, sea level fluctuations would likely have been on the order of 20-70 m (Read, 1995). In a distally steepened ramp depositional setting, sea level fluctuations at this scale can significantly influence shifts in facies belts.

Outcrop Stratigraphy – The Kinderhookian and Osagean strata examined in this study include the Bachelor, Compton, Northview, and Pierson Formations. Each of these formations lie above the Woodford (Chattanooga) shale (Figure 11). The Bachelor Formation is the lowermost formation of the Mississippian Epoch in this region, lying just above the Devonian Woodford (Chattanooga) Shale, above the unconformity that exists between the Devonian and Kinderhookian strata. From outcrop observation and thin section analysis, the general lithology of the Bachelor Formation at the Jane outcrop is a gray to green calcareous shale, reaching a thickness of no more than a few inches at the study area. Due to the thin nature and shaly lithology, the Bachelor is often absent between the Woodford and Compton Formations at the Jane outcrop.

The Compton Formation is Kinderhookian in age and overlies the Bachelor Formation in the Lower Mississippian. Lithologically, the Compton consists of light gray crinoidal-bryozoan wackestones, packstones, and grainstones. The average thickness of the Compton at the Jane outcrop ranges from 10 to 12 ft (3.0-3.7 m), increasing slightly from south to north. Figure 11 shows the Compton Formation, which contains an anomalous feature that has been outlined. Identifying terms for this feature have ranged from “Waulsortian-type mound” to “displaced bioherm” to “slump block”

(Morris and Mazzullo, 2013; Unrast, 2012; Evans et al, 2011). A detailed description of this feature and implications associated with it are discussed in Chapter III.

The Northview Formation is the top-most formation of the Kinderhookian. It conformably overlies the Compton Formation and is unconformably overlain by the Pierson Formation. At the Jane Outcrop, the Northview is 2 to 5 ft (0.6-1.5 m) thick and contains flaser bedding, lenticular bedding, clay drapes, bi-directional ripples, and multiple subaerial exposure surfaces (Figure 12; Figure 13). There are also two separate beds of dark gray shale and light brown to gray silty to shaly sediment. A very thinly bedded tan mud-lean packstone to grainstone exists at the top of the shallowing-upward succession. These observations were made during the field work conducted as a part of this study and indicate the Northview Formation was deposited in a tidal flat depositional environment. This differs significantly from the Compton and Pierson Formations, as the Northview Formation consists of the most regressive facies.

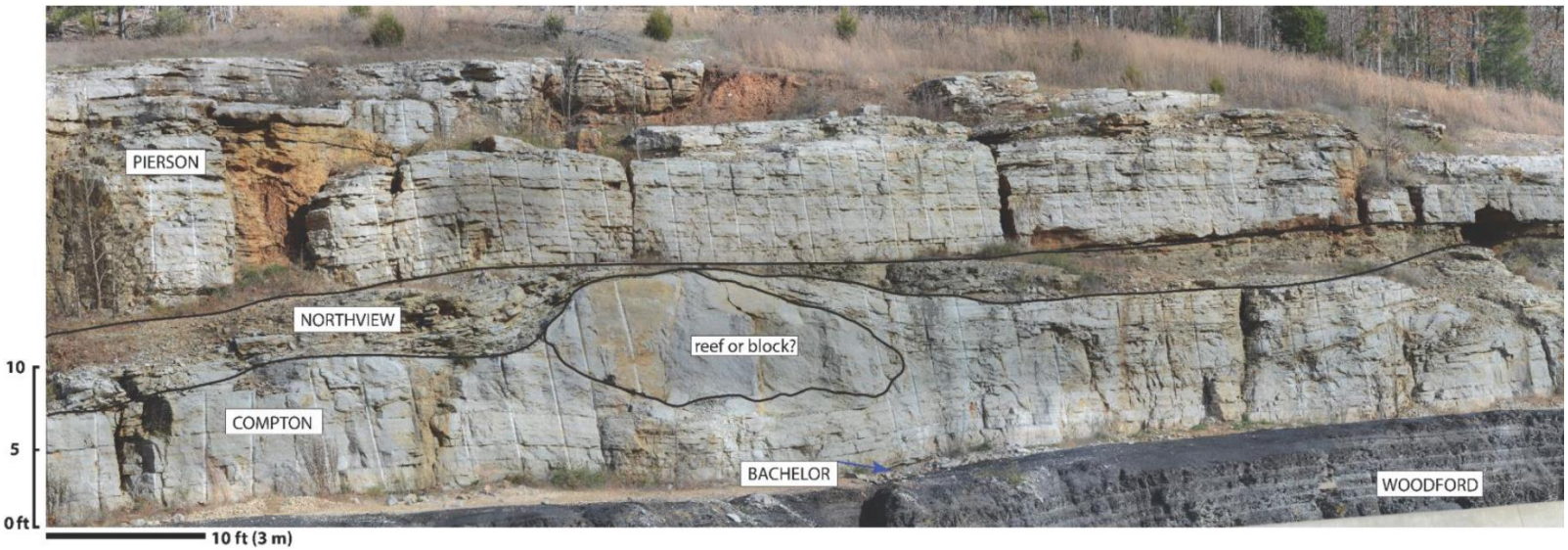

Figure 11: Partial Gigapan photograph of the study area illustrating the Kinderhookian and Osagean strata exposed at the Jane outcrop location, which was deposited above the Woodford (Chattanooga) Shale. The formations examined in this study include, from base to top, the Bachelor, Compton, Northview, and Pierson Formations. The Bachelor Formation consists of a gray to green calcareous shale of only 1-3 inches in thickness. The Compton Formation is 10-12 ft (3.0-3.6 m) thick and primarily consists of light gray crinoidal-bryozoan wackestones and packstones. Within the Compton Formation, a “bioherm” or “block” is outlined. The Northview Formation is 2-5 ft (0.6-1.5 m) thick and consists of crinoidal wackestones, packstones, and grainstones. The Pierson Formation is 15-18 ft (4.5-5.4 m) thick and primarily consists of skeletal mud-lean packstones and grainstones.

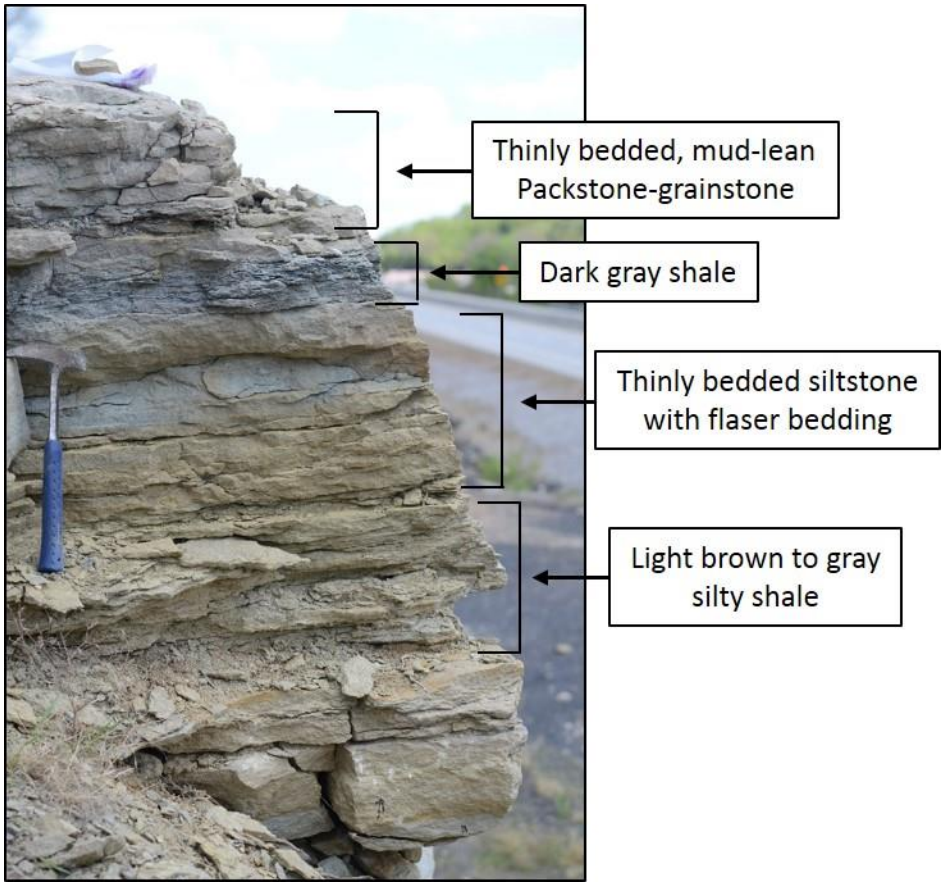

Figure 12: Photograph of the Northview Formation at the Jane outcrop, above the Compton Formation and below the Pierson Formation. The view of the photograph is facing southeast. The depositional environment of the Northview is interpreted as a tidal flat (see text for discussion). This section is 3.5 ft thick (1.06 m) and includes, from base to top, light brown to gray silty shale, thinly bedded siltstone with lenticular bedding, dark gray shale, and a thinly bedded mud-lean packstone to grainstone. See rock hammer for scale.

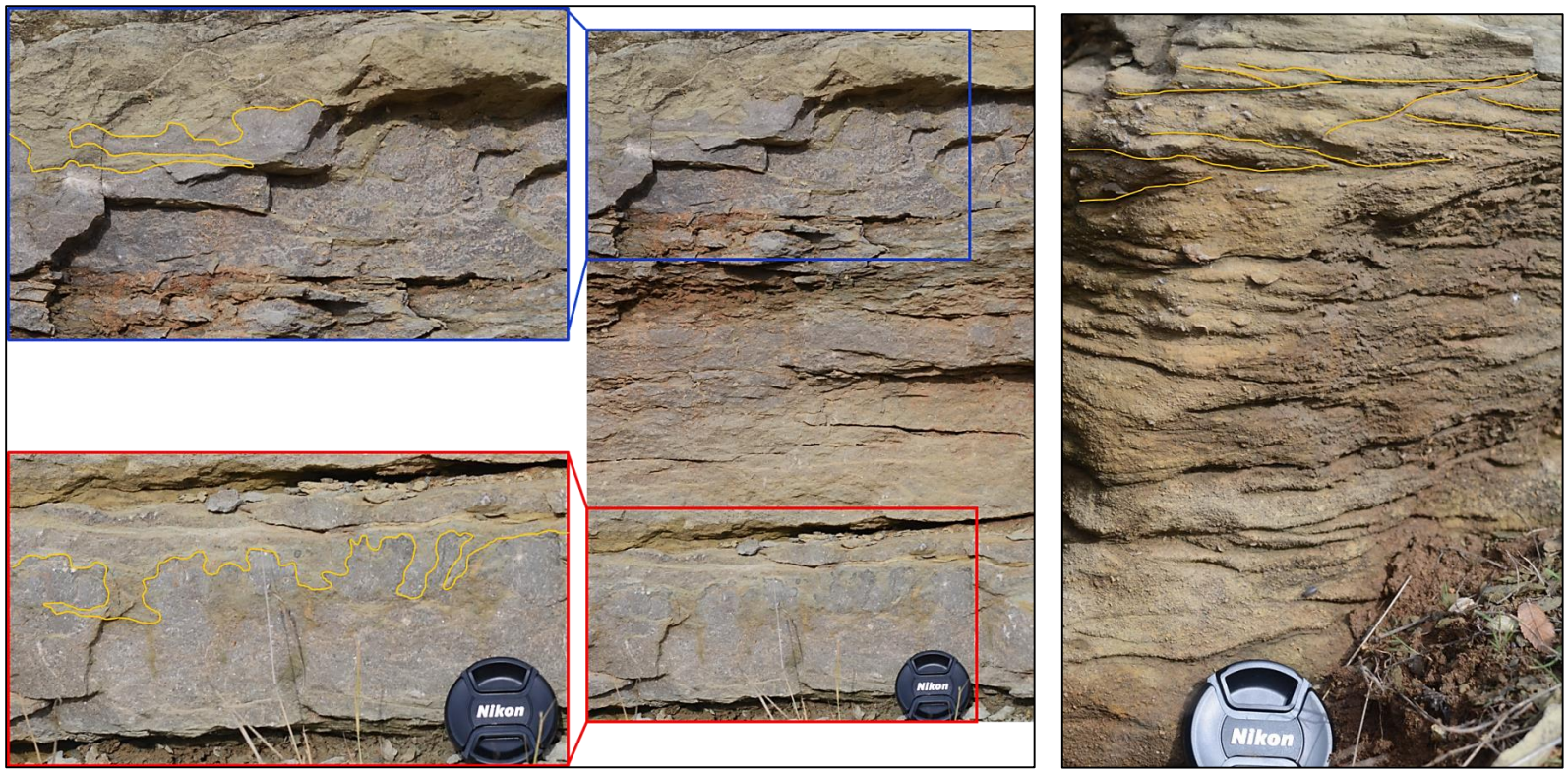

Figure 13: Field outcrop photographs of the subaerial exposure surfaces (left) and bi-directional ripples (right) found within the Northview Formation at the Jane Outcrop. Multiple exposure crusts can be traced laterally for 10 ft (3 m) along the surface. At the right, some of the ripples at the top of the photograph have been highlighted to show their bi-directional trend within the Northview section. Note the lens cap (~7 cm diameter) for scale.

The Pierson Formation is the basal formation of the Osage and unconformably overlies the Northview Formation. The Pierson is lithologically similar to the Compton Formation, differing in an increased number of grainstone facies and separated from the Compton by the Northview Formation. At the Jane outcrop, the Pierson ranges in total thickness from 15 to 18 ft (4.5 – 5.5 m) between two ledges. The dominating primary facies types are mud-lean crinoidal-bryozoan packstones to crinoidal grainstones. Other skeletal grain types include brachiopods and ostracods, all indicative of a normal marine environment.

Methods

The primary focus of this study was to identify high frequency sequences and cycles within the Kinderhookian and Osagean strata of the Mississippian in the Mid-Continent through identification of vertical stacking patterns of facies, subaerial exposure surfaces, and evidence of flooding surfaces. Through identification of a hierarchy of cyclicity, the resulting sequence stratigraphic architecture reveals lateral variability within cycles, the lateral extent of reservoir units and seals, and the direction of migration for potential reservoir facies (Eberli and Grammer, 2004). This study utilized the biostratigraphic framework provided by Shoeia (2012), who used conodonts for biostratigraphic analysis to constrain 3rd order relative sequences. The sequence stratigraphic framework defined by biostratigraphy was then refined to delineate 4th order high frequency sequences and 5th order high frequency cycles.

Gigapan EPIC Pro: Gigapan EPIC Pro hardware and software was used to generate a high resolution photograph of the outcrop, which, when coupled with detailed facies analysis, allows for determination of 2-D facies geometry and continuity. The Gigapan system allowed for over 800 individual high magnification photographs of the outcrop to be stitched together to produce a very high-resolution, seamless photograph of the entire outcrop where individual beds and sedimentary structures are visible down to the centimeter scale (Figure 14A). Once the high resolution image was stitched together, individual beds within each formation were traced in Adobe Illustrator to show bedding geometry and continuity, an important component in understanding the depositional environment and sequence stratigraphic framework (Figure 14B).

High Resolution Vertical Sections – In order to define the controls and distribution of heterogeneity observed within the units of the Jane outcrop, vertical sections were measured and sampled to identify facies types and vertical stacking patterns. Analysis of facies vertically and horizontally was conducted to identify depositional environments, geometry of depositional environments, and to understand the vertical facies stacking patterns within the sequence stratigraphic framework. Sample locations were selected based on changes in bedding thickness, fabric, and composition (Figure 14A). This sampling strategy was utilized to help interpret the controls and distribution of heterogeneity within the formations at the Jane outcrop.

The location of Vertical Section 1 was already established by Shoeia (2012) for his study on conodont biostratigraphy. Boardman (2013) defined the conodont zonation from Shoeia's (2012) high resolution sampling, thereby establishing the sequence stratigraphic framework for 3rd order sequences at the Jane outcrop. Samples from Shoeia's (2012) study were used in addition to the newly sampled Vertical Section 2 and 3 of this study. The location of Vertical Section 1 is at the northwestern-most end of the outcrop. Vertical Section 2 is located at the southeastern-most end of the outcrop. The third and final vertical section, Vertical Section 3, is in the middle of the outcrop between Vertical Section 1 and Vertical Section 2. Each of the vertical sections and sampling locations can be seen overlain on the Gigapan photograph of the outcrop in Figure 14A.

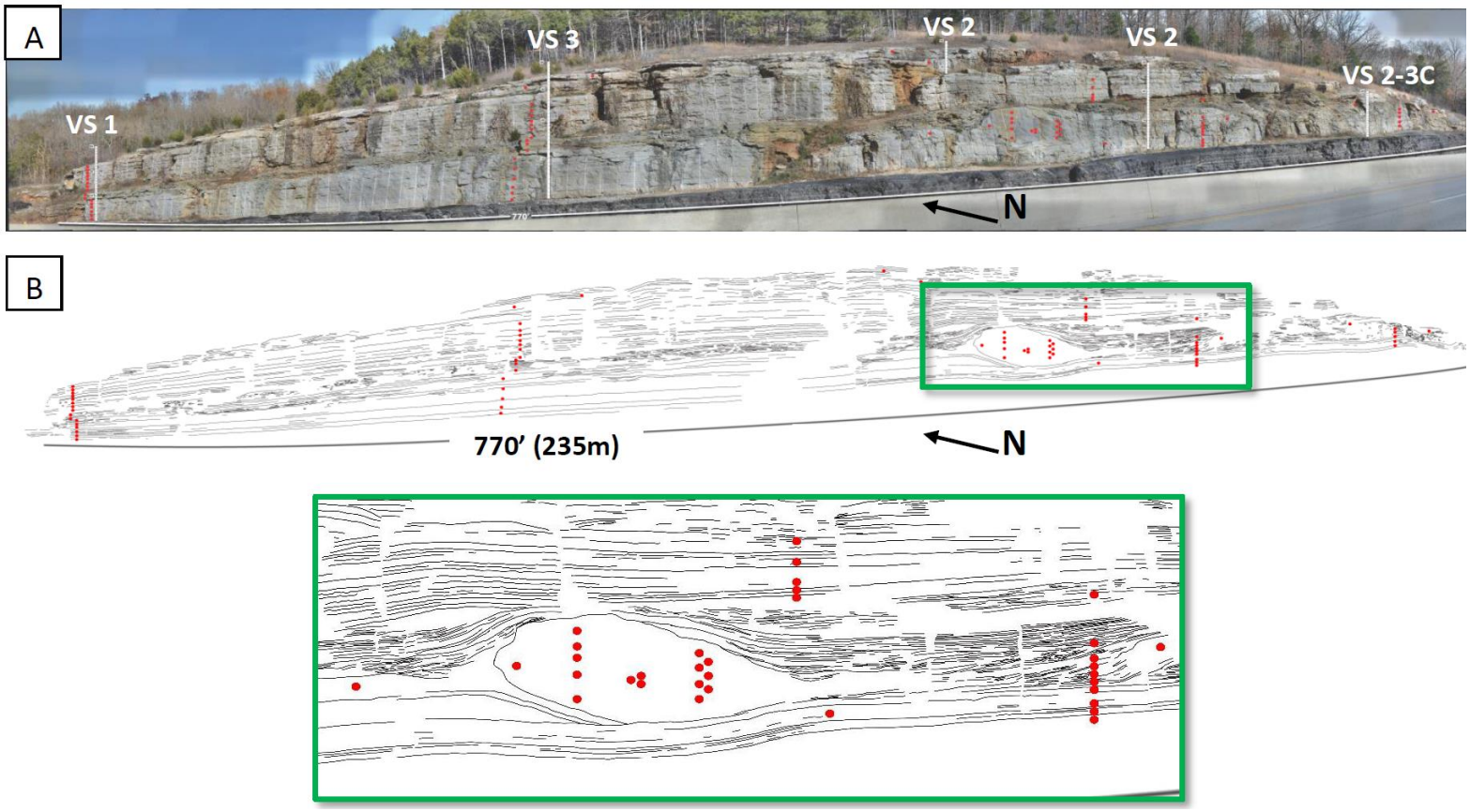

Figure 14: **A.** Gigapan photograph of entire Jane outcrop, showing the locations of Vertical Section 1 (VS 1), Vertical Section 2 (VS 2), a sub-section of Vertical Section 2 (Vertical Section 2-3C), and Vertical Section 3 (VS 3). Sample locations are marked with red dots. **B.** A line interpretation of bed architecture of the entire outcrop. Beds were traced using the high resolution Gigapan image in A. Bed tracing revealed lateral continuity and geometry of each bed, an important step in understanding the depositional environment and building the sequence stratigraphic framework. **C.** Magnified view of bed interpretation. Note the length of the entire outcrop is 770 ft (235 m) along strike (NW-SE).

Thin Section Petrography: Thin section petrography was conducted to determine vertical stacking packages within the sequence stratigraphic framework through identification of primary depositional facies types. Examination of 86 thin sections, sampled at specific intervals of the outcrop based on changes in texture, composition, and bed geometry, was completed to identify the details of the primary depositional facies. Thin sections were made from samples taken from the sampling locations across the outcrop, near Vertical Section 1, 2, and 3, seen in Figure 14. Thin sections used in this study were standard size (27 mm by 46 mm or 1 in by 1.8 cm) and vacuum-impregnated with blue epoxy to highlight presence of porosity. Classifications from Dunham (1962) and Choquette and Pray (1970) were used to define textural analysis, classification, and pore types seen throughout each thin section photomicrograph. A reference for thin section labels can be seen in Table 2.

Scanning Electron Microscopy: Scanning electron microscopy (SEM) can be used as a tool for understanding microstructural and physical properties such as texture, composition, and pore networks (Camp, 2013). This is an invaluable tool due to the micro- to nano-scale pore architecture present within the unconventional sections of Mississippian-aged rocks throughout the Mid-Continent. Four samples were hand-polished then argon ion-milled for ten hours each to obtain a polished surface to eliminate surface topography and shadowing effects, allowing a clear view of nano-pores within the rock. After coating each sample with gold palladium, SEM images were taken at different magnifications to illustrate the pore networks present in each facies type.

Thin Section Image Labels					
Feature Key				Porosity Key	
BR	brachiopod	MW	mud wisp	FR	fracture
BY	bryozoan	MC	mud clasts	IP	interparticle
C	coral	O	ostracod	IX	intercrystalline
CC	calcite cement	OIL	oil/dead oil	MO	moldic
CR	crinoid	PH	phosphate	VU	vug
D	dolomite	PY	pyrite	WP	intraparticle
FR	fracture	Q	quartz	WX	intracrystalline
GST	gastropod	S	stylolite		
L	lamination	SP	spicule		
M	mud/mudstone	T	trilobite		

Table 2: Thin section image labels. Porosity types are based on the classification by Choquette and Pray (1970).

Spectral Gamma Ray: An Exploranium GR-320 envi-SPEC scintillometer was used to measure spectral gamma ray response for each of the three vertical sections of the outcrop to help constrain high frequency sequence and cycle boundaries within the Mississippian-age strata at the Jane outcrop. Variations in the intensity of gamma ray response can distinguish the depositional facies defined in outcrop and thin section, as well as the hierarchy of shoaling-upward packages that range from a few meters thick to tens of meters thick. Unlike standard gamma ray measurements, spectral gamma ray differentiates between each source of emission, individually (K-40, Th, and U). Low Th and K usually indicate a pure carbonate, as the ions of each are insoluble (Glover, 2012). Organisms concentrate and store U very well, so U can be used as a proxy for organic material. Highly oxidized uranium ions are insoluble, while non-oxidized uranium ions

are more soluble and often present in carbonates (Glover, 2012). Readings were collected at six inch intervals at each vertical section location across the outcrop. Using the collected field data in conjunction with spectral gamma ray can help to constrain the high frequency sequence boundaries within these Mississippian-age strata. The gamma ray response associated with each of the vertical sections was used to help delineate the sequence stratigraphic framework.

It should be noted that gamma ray readings may be affected by post-depositional processes that can produce inaccurate results representative of conditions present during carbonate deposition. Some of these processes include pressure dissolution, formation of stylolites, and karstic weathering which concentrate insoluble minerals along seams in the rock. This would generate results showing high uranium content, which is not an accurate reflection of conditions present during carbonate deposition (Glover, 2012; Doveton, 1994).

Results

Facies Descriptions – Four primary depositional facies types were identified from the analysis of outcrop and thin sections. Classifications from Dunham (1962) and Choquette and Pray (1970) were used to define texture, classification, and pore types seen throughout each thin section photomicrograph. Use of the Dunham classification aids in the interpretation of the depositional environment due to the emphasis on textural distinction between mud-dominated versus grain-dominated lithofacies and a distinction between pore types. Four primary lithofacies, Facies 1 through Facies 4, were

defined based on specific attributes, which include sedimentary structures, texture and fabric, composition, size and geometry of grains, bedding geometry, and stratigraphic stacking patterns (Figure 15).

Facies 1 can be described as a crinoidal-bryozoan wackestone that is very fine to coarse grained (62.5µ - 500µ), and poorly sorted. Types of bryozoans include encrusting and fenestrate. Brachiopods are also locally present. Localized dolomite rhombs and blocky calcite cement is observed throughout the thin section. Facies 1 in Figure 15 was sampled from the Compton Formation at Vertical Section 3, a few inches above the top of the Bachelor Formation. Facies 1 is the most distal facies, as it contains 30% skeletal grains, 65% micrite matrix, and 5% blocky calcite cement (visual estimation).

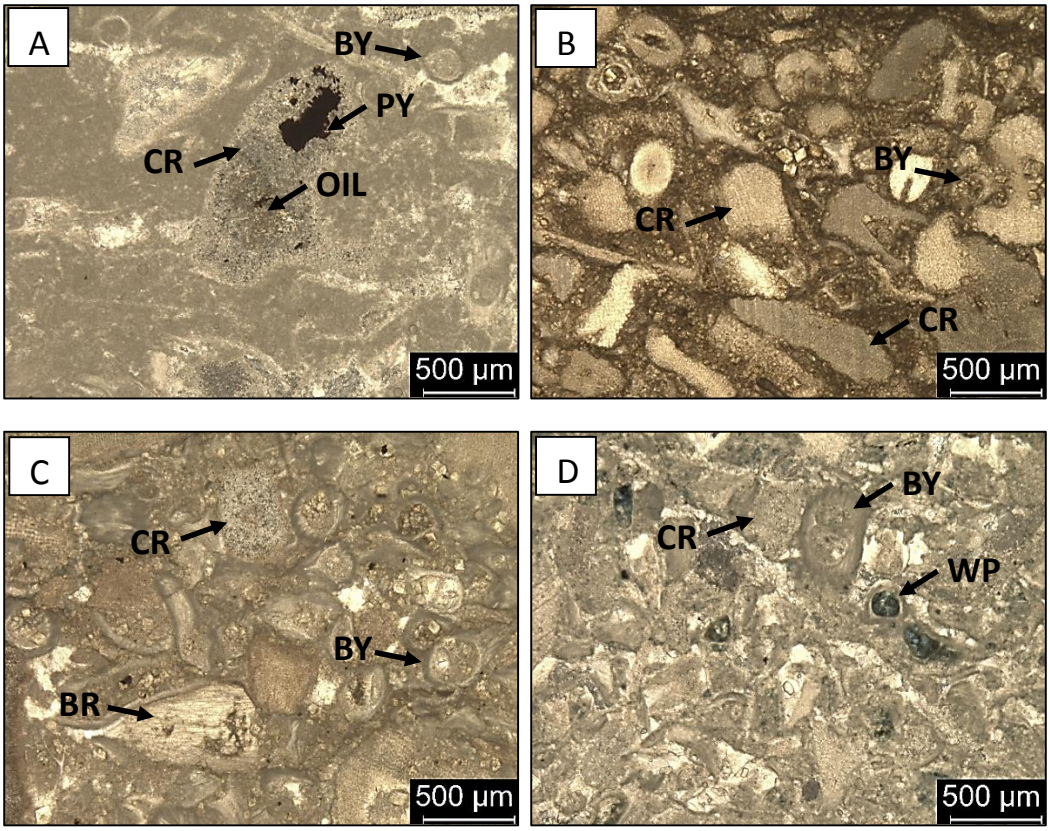

Figure 15: Thin section photomicrographs of the primary depositional facies types defined within the Mississippian-age strata at the Jane outcrop. Classifications from Dunham (1962) and Choquette and Pray (1970) were used to define texture, classification, and pore types seen throughout each thin section photomicrograph. Each thin section is shown in CPL. **A.** Facies 1, crinoidal-bryozoan wackestone, very fine to coarse grained (62.5µ - 2mm), poorly sorted. **B.** Facies 2, crinoidal wackestone to packstone, medium to coarse grained (250µ – 500µ), poorly-moderately sorted. **C.** Facies 3, crinoidal-bryozoan mud-lean packstone to grainstone, fine to very coarse grained (125µ - 2mm), moderately to poorly sorted. **D.** Facies 4, skeletal grainstone, very fine to medium grained (62.5µ - 500µ), moderately to well sorted. The skeletal types in each facies are representative of a normal marine depositional environment. Each of these facies types occur throughout all Kinderhookian and Osagean strata exposed at the Jane outcrop. This repetitive stacking pattern consists of a shallowing-upward sequence from a more distal facies (Facies 1) to a shallower, more proximal facies (Facies 4).

Facies 2 in Figure 15 is described as a crinoidal wackestone-packstone that is medium to coarse grained (250µ – 500µ), poorly to moderately sorted, and includes wispy stylolites (low amplitude (< 1mm) stylolites that are often lined with clay) (Alsharhan and Sadd, 2000). Facies 2 contains 50% skeletal grains, 45% micrite mud, and 5% dolomite rhombs (visual estimation).

Facies 3 is a crinoidal-bryozoan mud-lean packstone to grainstone. This facies is fine to very coarse grained (125µ - 2mm), moderately to poorly sorted, and contains very thin, clay-lined wispy stylolites and localized blocky calcite cement. Grain types include crinoids (250µ – 2mm), bryozoans (125µ – 500µ), and brachiopods (250µ – 400µ). Facies 3 contains 60% skeletal grains, 38% micrite matrix, and 2% blocky calcite cement and localized dolomite rhombs (visual estimation).

Facies 4 is a skeletal grainstone that is very fine to medium grained (62.5µ - 500µ) and moderately to well sorted. Primary grains include fenestrate bryozoans (125µ - 500µ) and crinoids (250µ - 500µ). This facies contains 85% skeletal grains, 5% micrite matrix, and 10% blocky calcite cement, pyrite, dead oil, and porosity (visual estimation). Facies 4 is the highest energy facies, as it contains no detectable mud, and is interpreted as the shallowest facies. Each of the primary depositional facies contain normal marine skeletal grains and are vertically repetitive throughout all Kinderhookian and Osagean formations exposed at the Jane outcrop. This repetitive stacking pattern consists of a shallowing-upward sequence from a more distal facies (Facies 1) to the shallowest facies likely deposited in a more proximal position (Facies 4).

Thin section analysis has revealed the pore types in these rocks consist of fracture, vuggy, interparticle, and intraparticle pores. Nano- to micropores below the resolution of thin section petrography were characterized through scanning electron microscopy (Figure 16). The pore classification scheme used in this study was proposed by Loucks et al. (2012) shown in Figure 17. Based on a combination of thin sectional analysis and SEM, Facies 3 contains the highest amount of porosity relative to the other facies. Facies 3 is dominated by vuggy and Intraparticle porosity. Pore sizes in Facies 3 fall into the nano- to micropore class, while pore throats fall into the nanopore class as defined by Loucks et al. (2012). The vugs in each facies are typically filled with a combination of calcite crystals, pyrite, and clay.

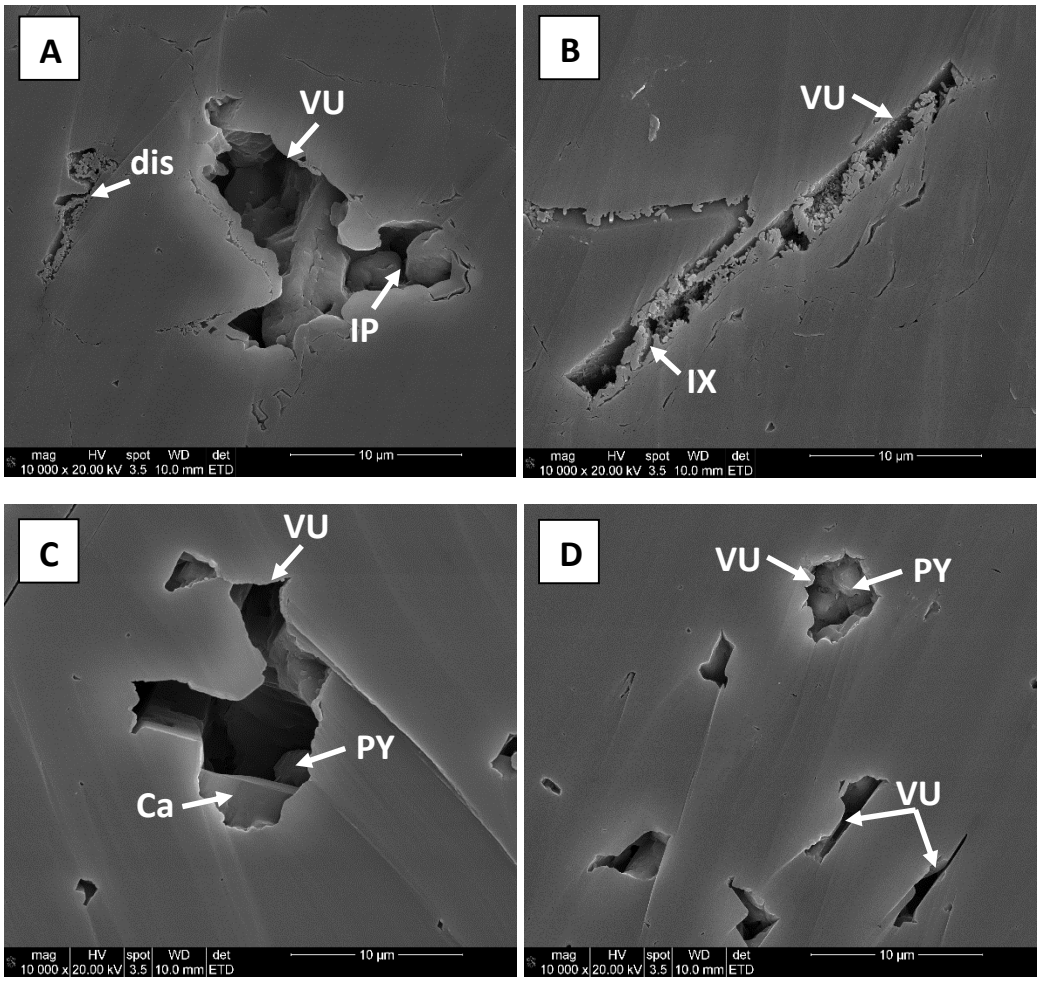

Figure 16: SEM photographs of each facies type at a magnification of 10,000. **A.** Facies 1, vug (VU) containing interparticle porosity (IP). The curved features surrounding the main vug may be dissolution-related features (dis). Pores and pore throats fall into the micro- to nanopore classes. **B.** Facies 2 demonstrates a rectangular-shaped pore along a cleavage plane. Interparticle porosity (IP) occurs within the vugs. Pores fall into the micro- to nanopore classes, while pore throats are primarily in the nanopore class. **C.** Facies 3 is dominated by vuggy and Intraparticle porosity. Pore-filling pyrite (PY) and calcite crystals (Ca) can be seen lining the walls within the vugs. There are significantly more pores present within Facies 3 relative to Facies 1, 2, and 4. Pore size falls into the micropore class. Facies 3 contains the largest pore throats, which fall into the nano- and micropore classes. **D.** Facies 4 contains vuggy and interparticle porosity. The largest vug has been partially filled by clay and pyrite. Pores fall into the micro- to nanopore classes, while pore throats are primarily in the nanopore class. See Appendix B for additional SEM photographs at higher magnifications.

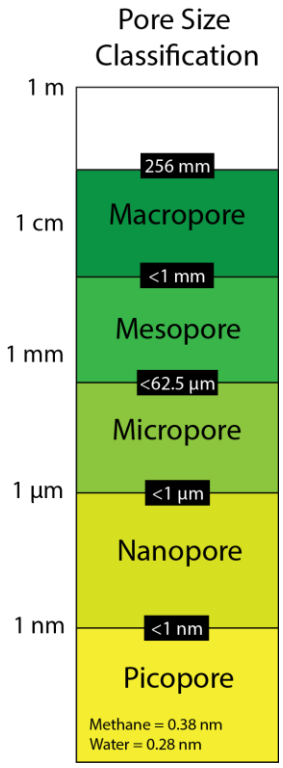

Figure 17: Classification used to define pore sizes seen in SEM photos in this study, originally after Loucks et al. (2012) and redrafted by Vanden Berg and Grammer (2014).

Depositional Model – Depositional models assist in understanding sediment deposition, geometries, and facies stacking patterns of the area under study. After the area under study has been fit into a depositional model, it can then be linked to outcrop and modern analogs. This assists in the demonstration of subsurface reservoir distribution, with only some constraints caused by exposure (Grammer et al., 2004). The best fit for a depositional model is a distally steepened ramp, as each of the facies defined in this study are similar to facies deposited in other distally steepened ramp settings (Grafe and Wiedmann, 1998; Kerans et al., 1994; Handford and Loucks, 1993; Handford, 1986). Dominating facies types at the Jane outcrop range from crinoidal-

bryozoan wackestones to crinoidal-bryozoan mud-lean packstones with an average ratio of 65% skeletal grains to 35% micrite mud. These mud-supported facies types fall between the boundaries of fair weather wave base and storm wave base in a distally steepened ramp setting. This succession of lower-energy facies suggests deposition more distal and further from the shelf margin region originally defined by Gutschick and Sandberg (1983) and Lane and De Keyser (1980). Significant complexity and heterogeneity of facies distribution exists within the Mississippian-age distally steepened ramp setting. Figure 18 is a schematic diagram illustrating deposition along a distally steepened ramp, between fair weather wave base and storm wave base. Deposition of the Jane outcrop facies would have likely occurred within the red outline of Figure 18, which includes the tidal flat environment of the Northview Formation and the “blocks” seen within the Compton Formation.

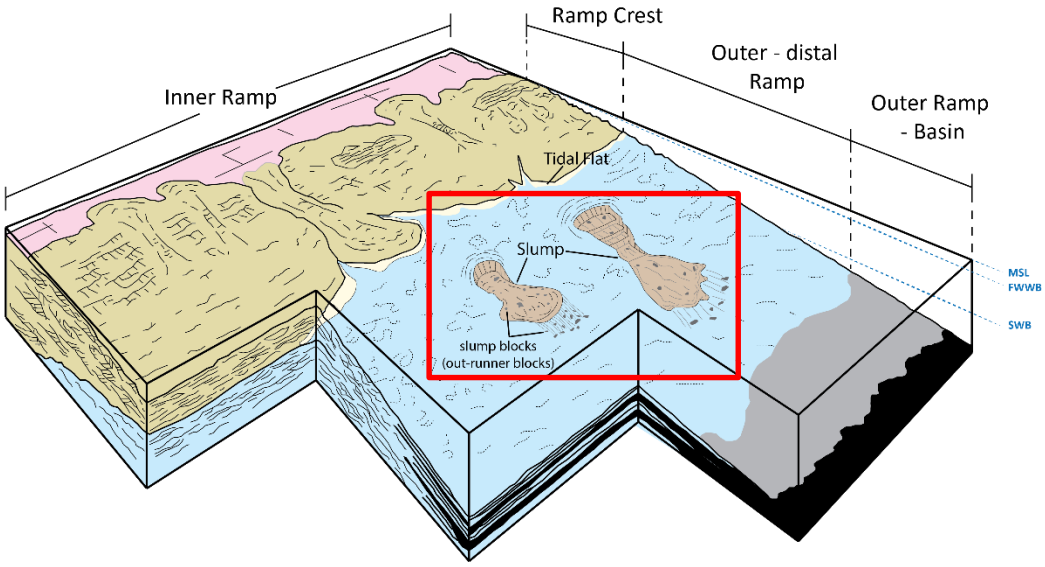

Figure 18: Schematic diagram illustrating distribution of depositional environments at the Jane outcrop on a distally steepened ramp between fair weather wave base and storm wave base. Deposition of the primary facies defined at the Jane outcrop would have likely taken place within the red outlined region, which includes the tidal flat environment of the Northview Formation and anomalous features (blocks or bioherms?) similarly seen within the Compton Formation (Modified from Handford, 1986).

Outcrop Sequence Stratigraphy – Boardman (2013) developed a new range chart for the biostratigraphically most significant taxa of the Mississippian-aged strata throughout the Mid-Continent (Figure 19). The overlapping conodont ranges were charted against the biostratigraphic zones, each representing a period of 1-2 million years throughout the Kinderhookian and Osagean. Boardman (2013) also defined the conodont biostratigraphy at the Jane outcrop, which may be linked to 3rd order depositional sequences as conodont biostratigraphy has a resolution of 1 to 3 million years and occur in overlapping zonations at this location (Figure 20). These 3rd order

sequences establish a base for defining a hierarchy of sequences and cycles within the sequence stratigraphic architecture at the Jane outcrop.

Boardman's (2013) newly defined conodont zonations do not definitively correlate to the eustatic sea level changes throughout the Kinderhookian and Osagean (Figure 21). The eustatic sea level curve shows three 3rd order sequences in the Kinderhookian and two 3rd order sequences in the Early Osagean. Based on conodont biostratigraphy at the Jane outcrop, there is only one 3rd order sequence in the Kinderhookian-age formations and one 3rd order sequence in the Osagean-age formations. The discrepancy between the biostratigraphic zones and 3rd order sequences in the Kinderhookian strata at the Jane outcrop could be related to a sequence lost in deposition of the blocks and breccia beds throughout the Compton Formation and/or erosion at the top of the Northview Formation. The discrepancy between the biostratigraphic zones and 3rd order sequences in the Osagean strata at the Jane outcrop could be related to a combination of the incomplete Osagean section and erosion at the top of the Pierson Formation. An integration of stacking patterns and the well-defined exposure surface at the top of the Northview Formation has allowed identification of two 3rd order sequences present within the exposed strata at the Jane outcrop (Figure 22).

In carbonates, due to the differences between facies and water depth, transgressive and regressive phases of a cycle can be graphically displayed on a stratigraphic column using a combination of red and blue triangles. The blue triangle

represents the transgressive phase of the cycle, while the red triangle represents the regressive phase of the cycle. At the outcrop, the transgressive leg of the first 3rd order sequence is represented by the Bachelor and Compton Formations, which contain a higher number of Facies 1 and 2. The regressive leg is represented by the Northview Formation, which is interpreted to be deposited in a tidal flat depositional environment. The second 3rd order sequence is represented by the Pierson Formation, deposited during a highstand systems tract after a flooding event. Evidence for the flooding event is not present at the outcrop, but is inferred due to the exposure surface at the top of the Northview Formation. During the highstand, the Pierson Formation aggraded to base level and prograded seaward (Figure 22).

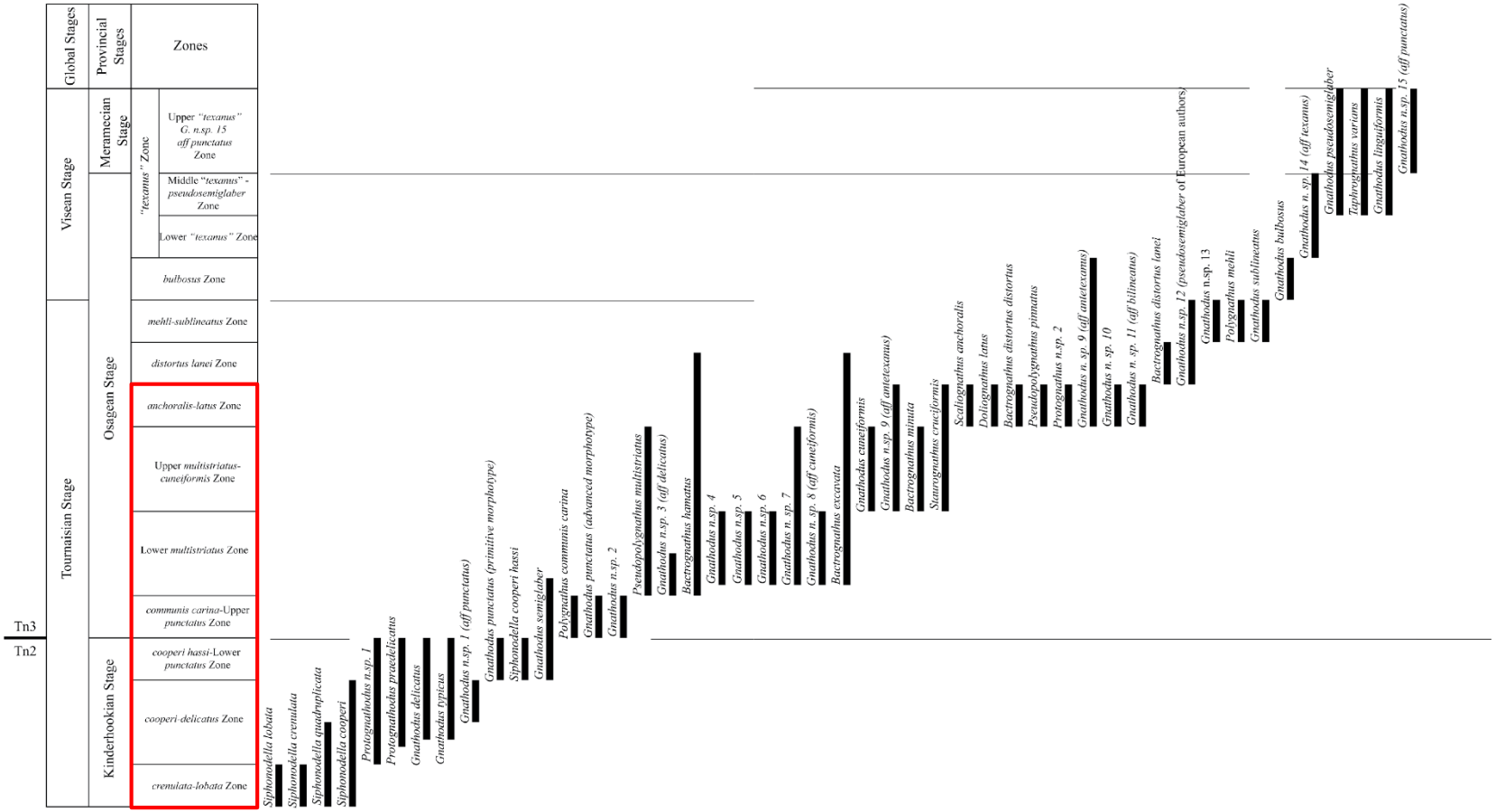

Figure 19: New range chart for the biostratigraphically most significant taxa of Boardman's (2013) study. The conodont ranges are charted against the biostratigraphic zones and chronostratigraphic designations on the left side of the figure. This figure illustrates the overlap of each conodont range throughout the Kinderhookian and Osagean. Each biostratigraphic zone within the Kinderhookian and Osagean represents 1-2 million years of time. The formations at the Jane outcrop contain each zone through the *anchoralis-latus* Zone (red box) (After Boardman, 2013).

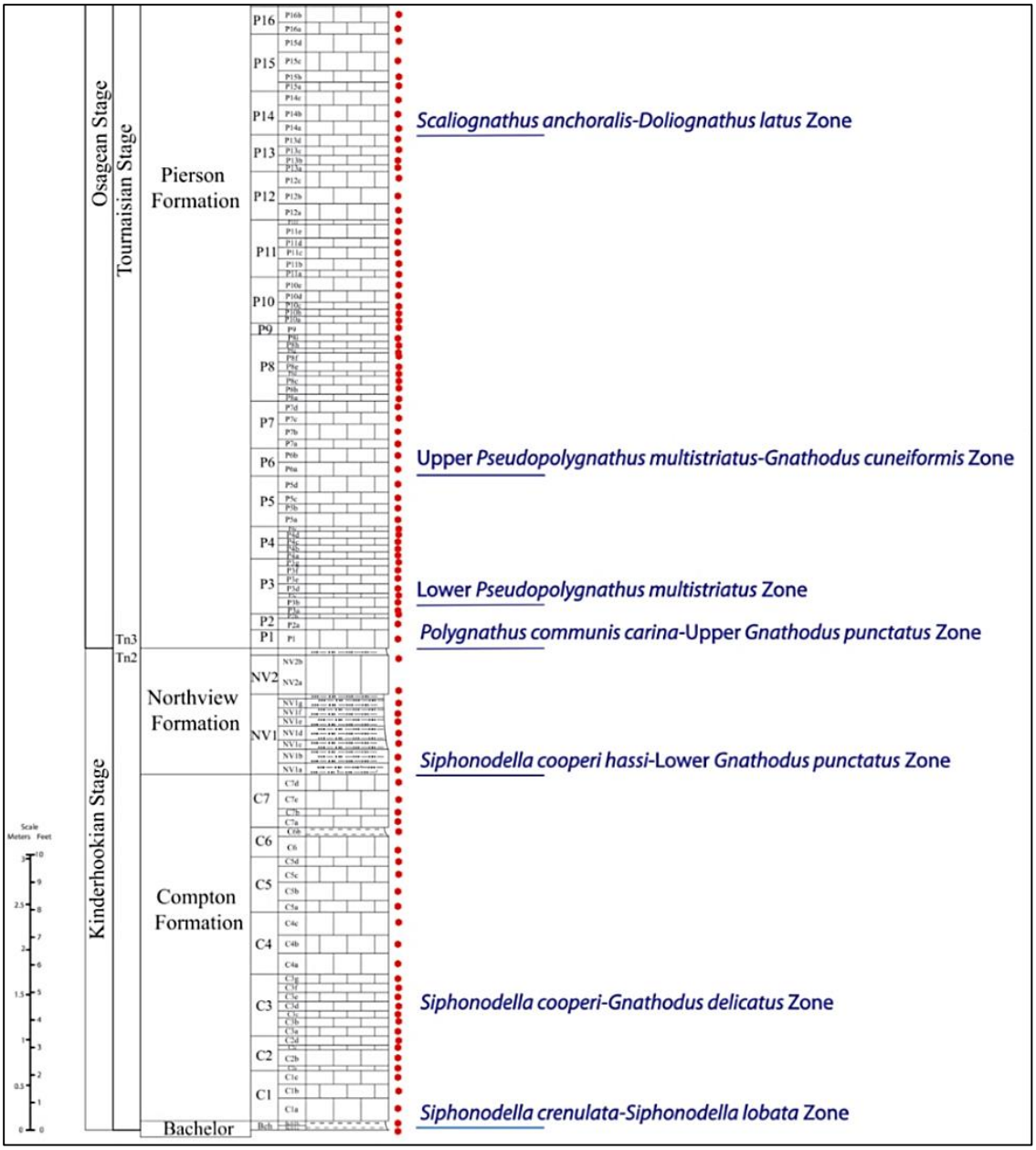

Figure 20: Updated conodont zonation for the Middle Tournaisian-Lower Visean (middle Kinderhookian-basal Meramecian) strata of the Jane outcrop. This type of conodont biostratigraphy may be tied to 3rd order sequences known within the Mississippian. The established biostratigraphic framework provides a base for determining a hierarchy of sequences and cycles within the stratigraphic framework of the Jane outcrop. Sampling intervals of Boardman (2013) are shown by small red dots. The stratigraphic position of the appearance of each zone is indicated by a thin blue line with the Biozone name in blue. Each biozone overlaps and represents 1 to 3 million years, indicating two 3rd order sequences exist within the Bachelor, Compton, Northview, and Pierson Formations (After Boardman, 2013).

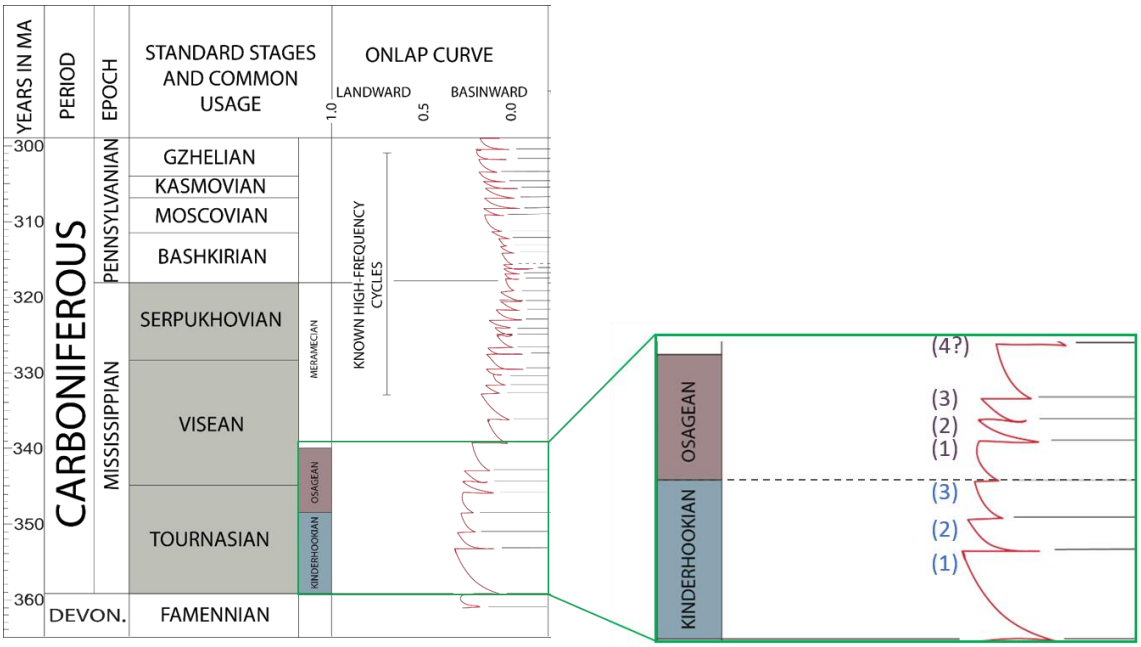

Figure 21: Haq and Schutter (2008) eustatic sea level curve illustrating three 3rd order sequences throughout the Kinderhookian and two 3rd order sequences throughout the Early Osagean. There is no clear correlation between the number of 3rd order sequences defined by eustatic sea level and the number of 3rd order sequences defined by the conodont biostratigraphy defined by Boardman (2013) in Figure 19 (Modified from Haq and Schutter, 2008).

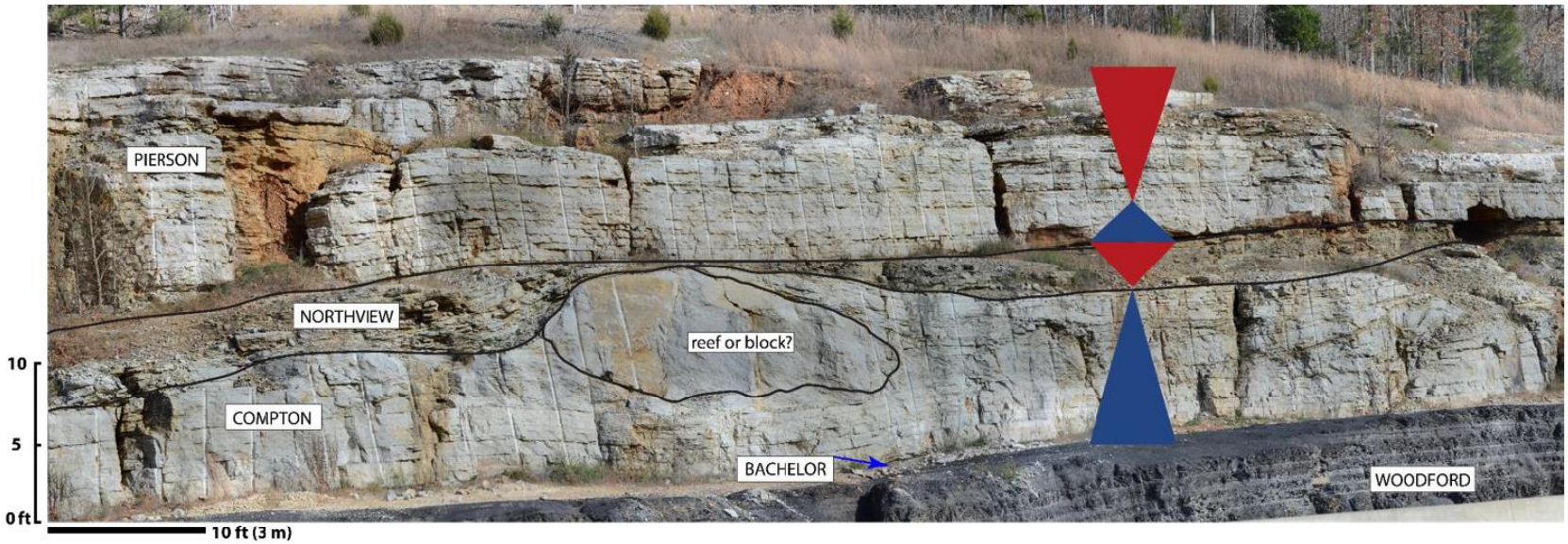

Figure 22: Partial Gigapan photograph of the Jane outcrop including 3rd order sequences constrained by biostratigraphy (Boardman, 2013; Shoeia, 2012). Overall, there are two 3rd order sequences represented at the Jane outcrop. The transgressive leg of the first 3rd order sequence is represented by the Bachelor and Compton Formations. The regressive leg is represented by the Northview Formation, which is interpreted as a tidal flat depositional environment. The second 3rd order sequence is represented by the Pierson Formation, deposited during a highstand systems tract after a flooding event. Evidence for the flooding event is not present at the outcrop, but is inferred due to the exposure surface at the top of the Northview Formation. During the highstand, the Pierson Formation aggraded to base level and prograded seaward.

Idealized Facies Succession –Since the four primary depositional facies are repetitive throughout each formation, an idealized facies succession was recognized within the biostratigraphically and eustatically constrained 3rd order sequences. Each facies, displayed in an asymmetrical, shallowing-upward sequence, is shown in Figure 23 and represents the facies deposited during one rise and fall in sea level. The idealized facies succession begins with deposition of Facies 1 (bryozoan-crinoidal wackestone) at the base of the cycle. This is the facies containing the highest mud content and represents the transgressive portion of the succession. The succession is dominated by the regressive portion of the sequence, which starts with deposition of Facies 2 (crinoidal wackestone-packstone), followed by Facies 3 (crinoidal mud-lean packstone-grainstone) and Facies 4 (crinoidal grainstone facies). Within the Northview Formation at Vertical Section 2, Facies 3 and 4 contain bi-directional ripples and subaerial exposure surfaces supporting the interpretation that the Northview Formation was deposited in a tidal flat environment. The repetitive packages range in thickness from 3 – 10 ft (1 – 3 m). This repetition illustrates the same system was migrating laterally during specific times of deposition for the Bachelor, Compton, Northview, and Pierson Formations. This succession, and associated facies partitioning, allows for recognition of a hierarchy of sequences and cycles, which can increase the predictability of facies distribution related to the reservoir architecture in the subsurface (Eberli and Grammer, 2004).

High Resolution Vertical Sections – Since 3rd order sequences have been previously constrained by a combination of biostratigraphy and eustatic sea level (Boardman, 2013; Shoeia, 2012; Haq and Schutter, 2008), the focus of this study has

been to delineate the higher frequency sequences and cycles within the system. As evidenced from the repetitive nature of each facies within the idealized facies succession, a hierarchy of sequences and cycles exists within the sequence stratigraphic architecture. In this study, the higher frequency events superimposed on the biostratigraphically and eustatically constrained 3rd order sequences will be referred to as 4th order high frequency sequences and 5th order high frequency cycles, unrelated to time. It is not possible to constrain the time element well enough to determine an average cycle duration, but evaluation of a general cycle hierarchy is useful for determining stratigraphic ordering (Kerans and Tinker, 1997).

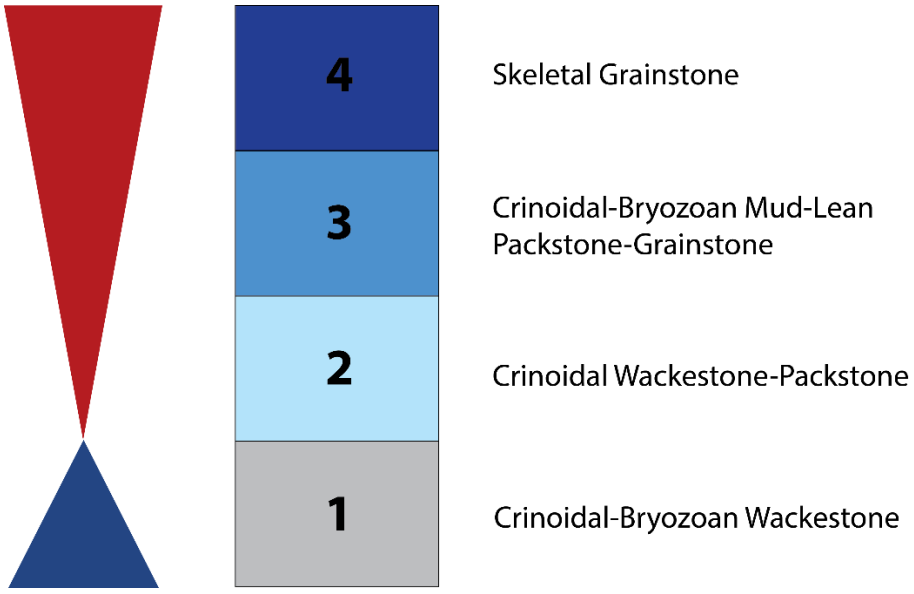

Figure 23: Idealized facies succession showing primary depositional facies deposited during one rise and fall in sea level. The blue triangle represents the transgressive phase of the cycle and the red triangle represents the regressive phase of the cycle. The cycle shallows upward and is vertically repetitive across the outcrop throughout Vertical Section 1, 2, and 3. Within the Northview Formation at Vertical Section 2, Facies 3 and Facies 4 contain bi-directional ripples and subaerial exposure surfaces supporting the interpretation that the Northview represents deposition in a tidal flat environment.

The high resolution vertical sections of this study are shown in figures 24 – 27. Each vertical section displays the bedding geometry, sample locations, 3rd order sequences, 4th order high frequency sequences (HFS), 5th order high frequency cycles (HFC), depth, and lithology. Figures 28 – 31 are field photographs that show individual 4th order high frequency sequences and 5th order high frequency cycles overlain on the outcrop. These outcrop photographs show how the sequence boundaries were picked based on the occurrence of vertical stacking patterns, flooding surfaces, and subaerial exposure surfaces. Together, each of these vertical sections were laterally correlated across the outcrop to show the hierarchy of high frequency sequences and cycles present at the Jane outcrop. Figure 32 shows the high resolution sequence stratigraphy of 3rd order sequences and 4th order high frequency sequences laterally linked across the outcrop. This breakdown of the sequence stratigraphic hierarchy shows increased vertical and lateral variability in each of the Mississippian-age formations across the Jane outcrop.

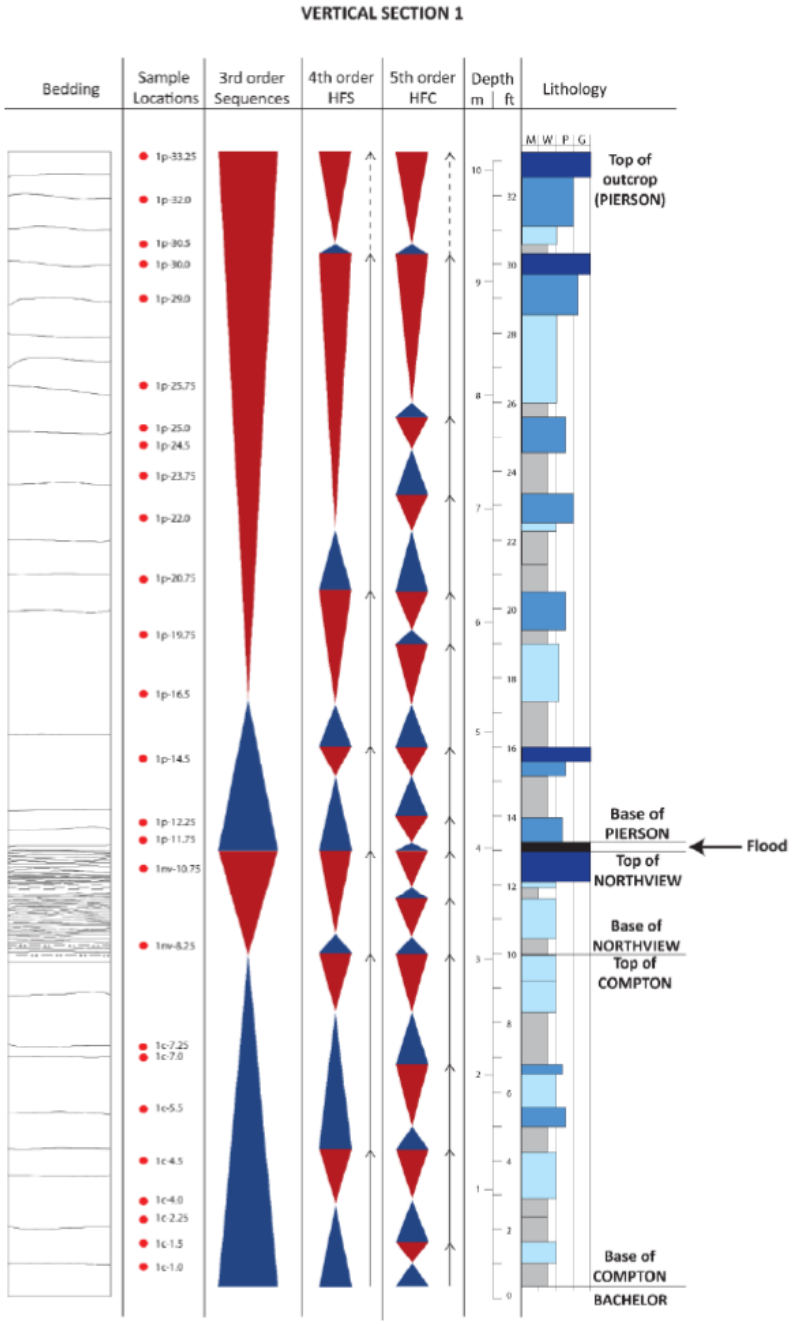

Figure 24: Vertical Section 1, located at the northwestern-most end of the outcrop (Figure 16A). Columns from left to right include bedding geometries traced from the Gigapan photograph, sample locations, 3rd order sequences, 4th order high frequency sequences (HFS), 5th order high frequency cycles (HFC), vertical depth, and lithology based on Dunham's (1962) classification. A series of shallowing-upward sequences can be seen in each of the formations. The general pattern of the idealized facies succession in Figure 23 repeats itself vertically. Each of the sequence and cycle boundaries were picked based on the vertical stacking patterns, flooding surfaces, and exposure surfaces present at the outcrop.

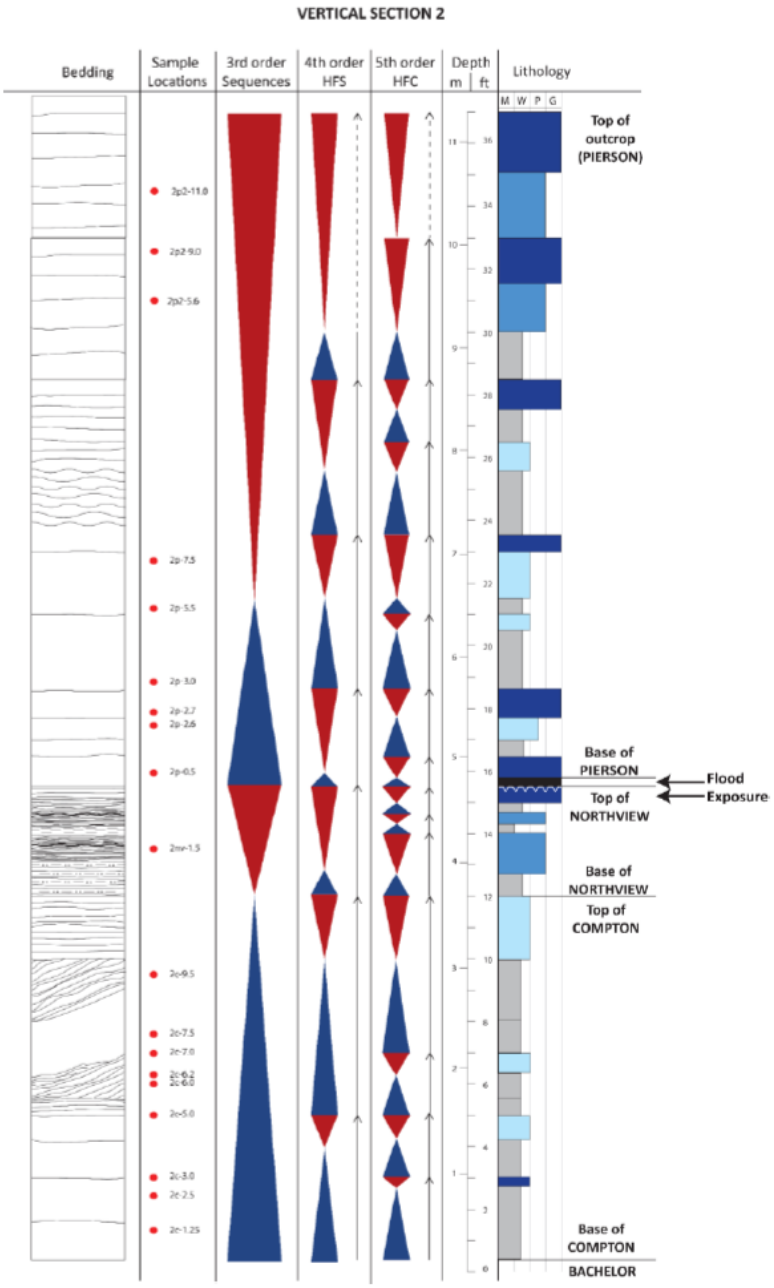

Figure 25: Vertical Section 2, located at the southeastern-most end of the outcrop (Figure 16A). Columns from left to right include bedding geometries traced from the Gigapan photograph, sample locations, 3rd order sequences, 4th order high frequency sequences (HFS), 5th order high frequency cycles (HFC), vertical depth, and lithology based on Dunham's (1962) classification. A series of shallowing-upward sequences can be seen in each of the formations. The general pattern of the idealized facies succession in Figure 23 repeats itself vertically. Each of the sequence and cycle boundaries were picked based on the vertical stacking patterns, flooding surfaces, and exposure surfaces present at the outcrop.

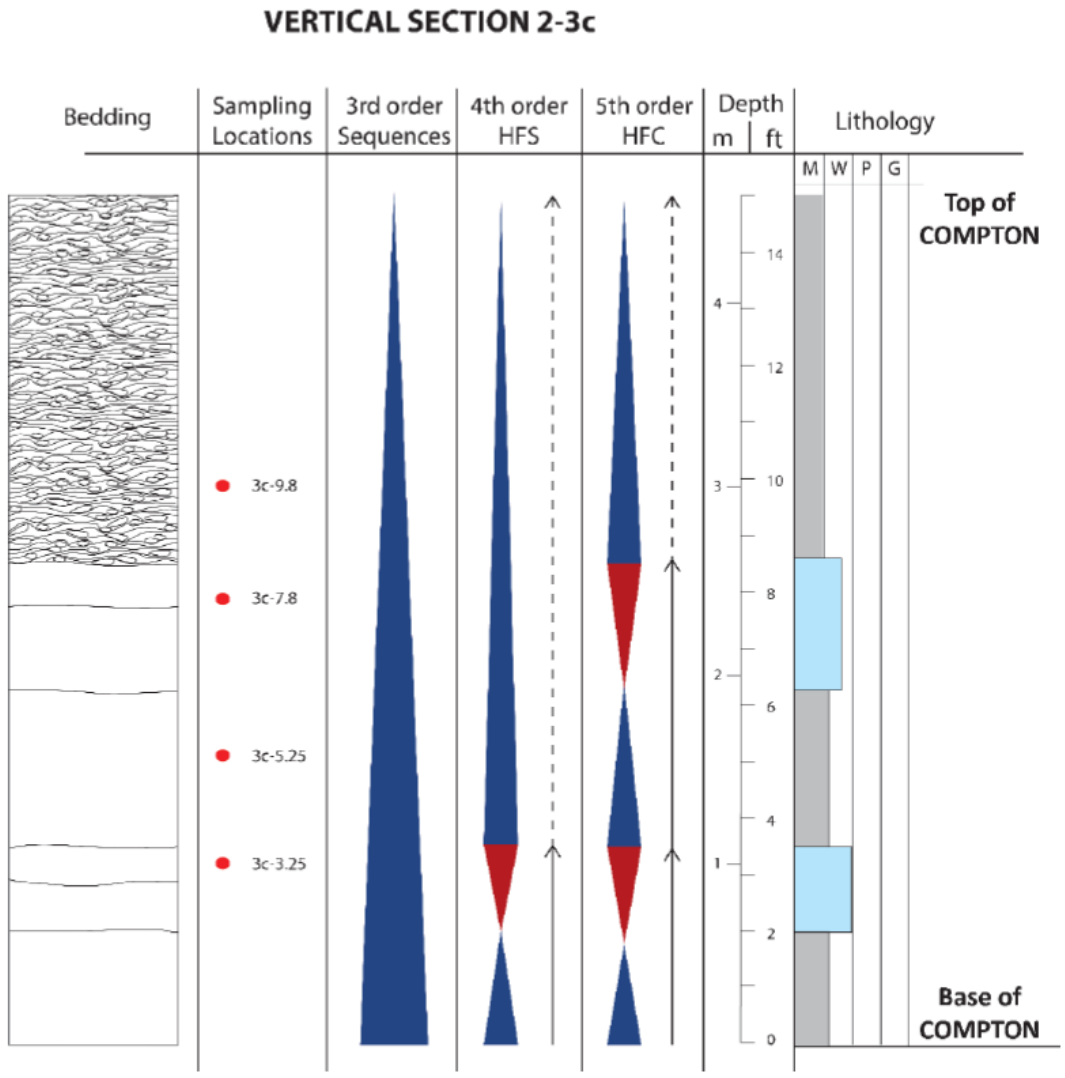

Figure 26: Vertical Section 2-3c, located at the southeastern-most end of the outcrop (Figure 16A). Columns from left to right include bedding geometries traced from the Gigapan photograph, sample locations, 3rd order sequences, 4th order high frequency sequences (HFS), 5th order high frequency sequences (HFC), vertical depth, and lithology based on Dunham's (1962) classification. The general facies stacking pattern seen in this vertical section is not complete due to erosion of the top of the Compton and the overlying Northview and Pierson Formations. Each of the sequence and cycle boundaries were picked based on the vertical stacking patterns, flooding surfaces, and exposure surfaces present at the outcrop. The upper portion of the bedding geometry column is related to the mud-dominated facies associated with the "block" features within the Compton Formation.

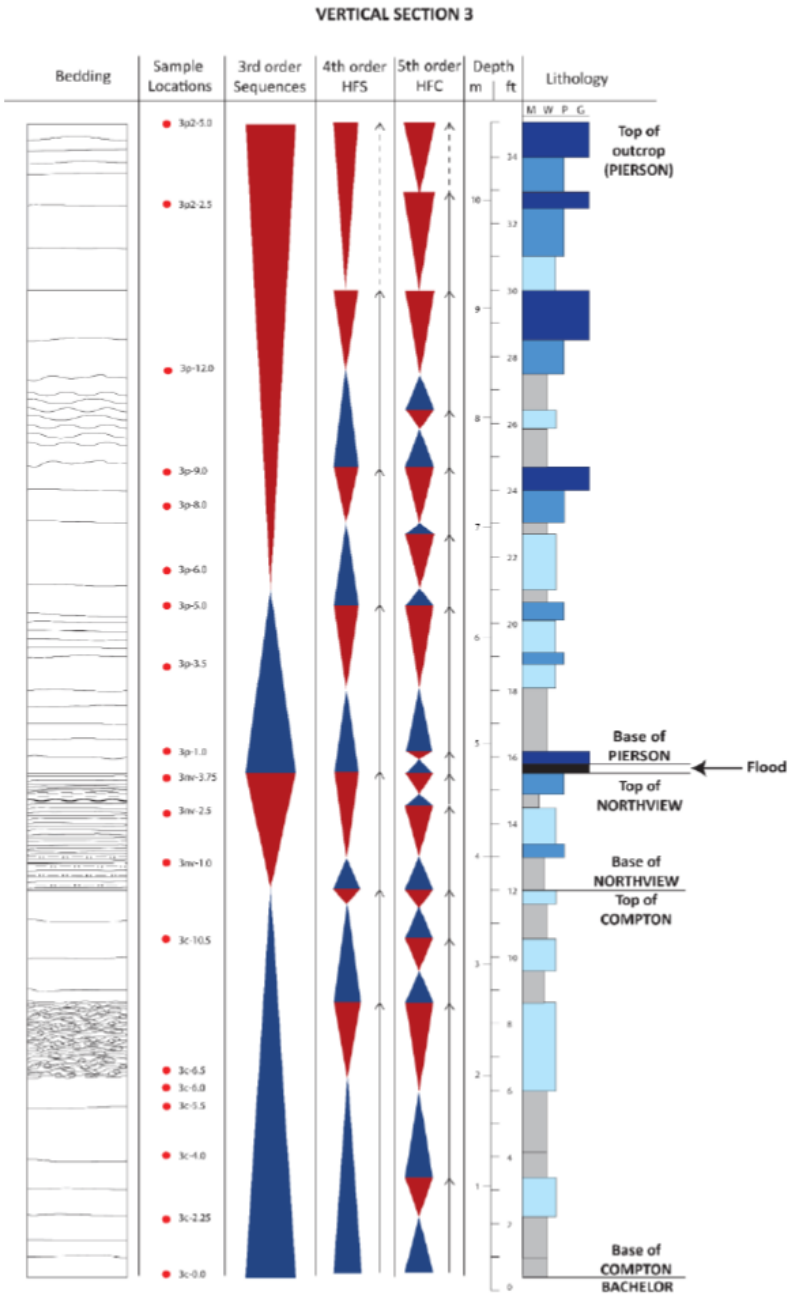

Figure 27: Vertical Section 3, located in the middle of the outcrop, between Vertical Section 1 and 2. (Figure 16A). Columns from left to right include bedding geometries traced from the Gigapan phtograph, sample locations, 4th order high frequency sequences (HFS), 5th order high frequency cycles (HFC), vertical depth, and lithology based on Dunham's (1962) classification. A series of shallowing-upward sequences can be seen in each of the formations. The general pattern of the idealized facies succession in Figure 23 repeats itself vertically. Each of the sequence and cycle boundaries were picked based on the vertical stacking patterns, flooding surfaces, and exposure surfaces present at the outcrop.

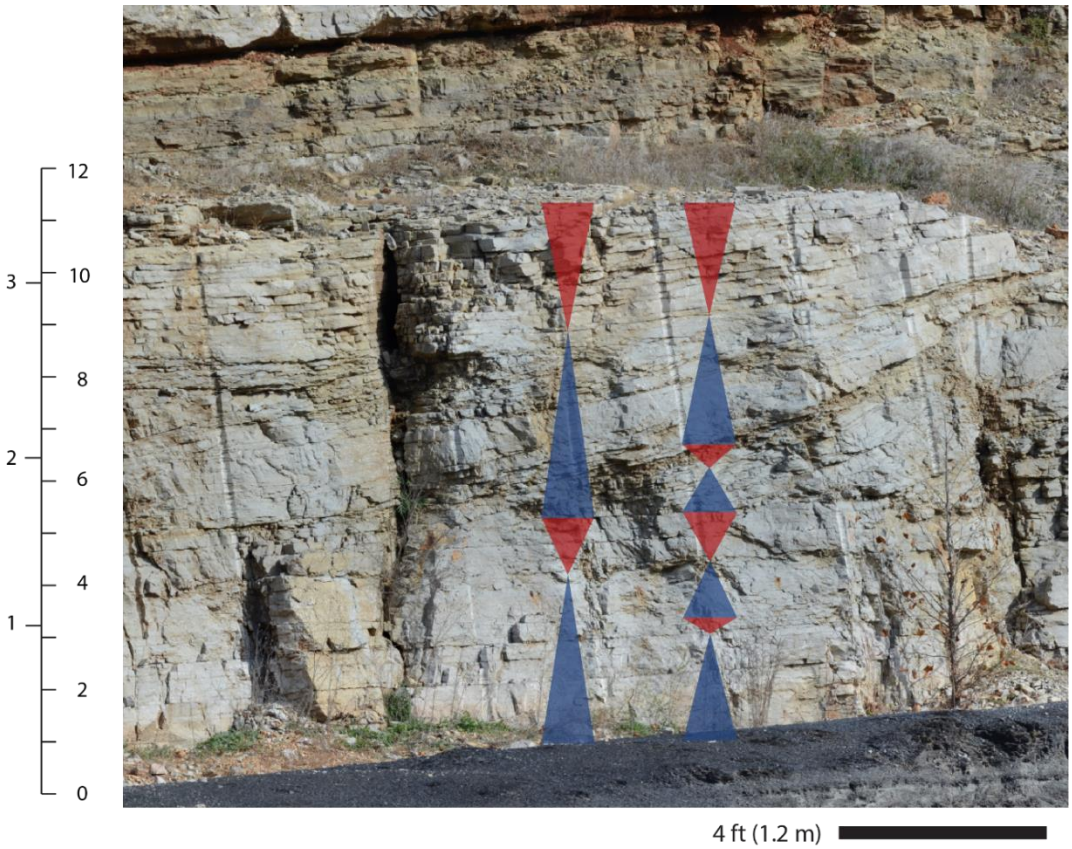

Figure 28: Field photograph of 4th order high frequency sequences (left) and 5th order high frequency cycles (right) overlain on the Compton Formation at Vertical Section 2. Each of the sequence and cycle boundaries were picked based on vertical stacking patterns, flooding surfaces, and exposure surfaces present at the outcrop. Four probable 5th order high frequency cycles can be seen within two probable 4th order high frequency sequences. In this figure, 5th order high frequency cycle boundaries are related to the debris beds, as high frequency sea level changes likely contributed to block movement.

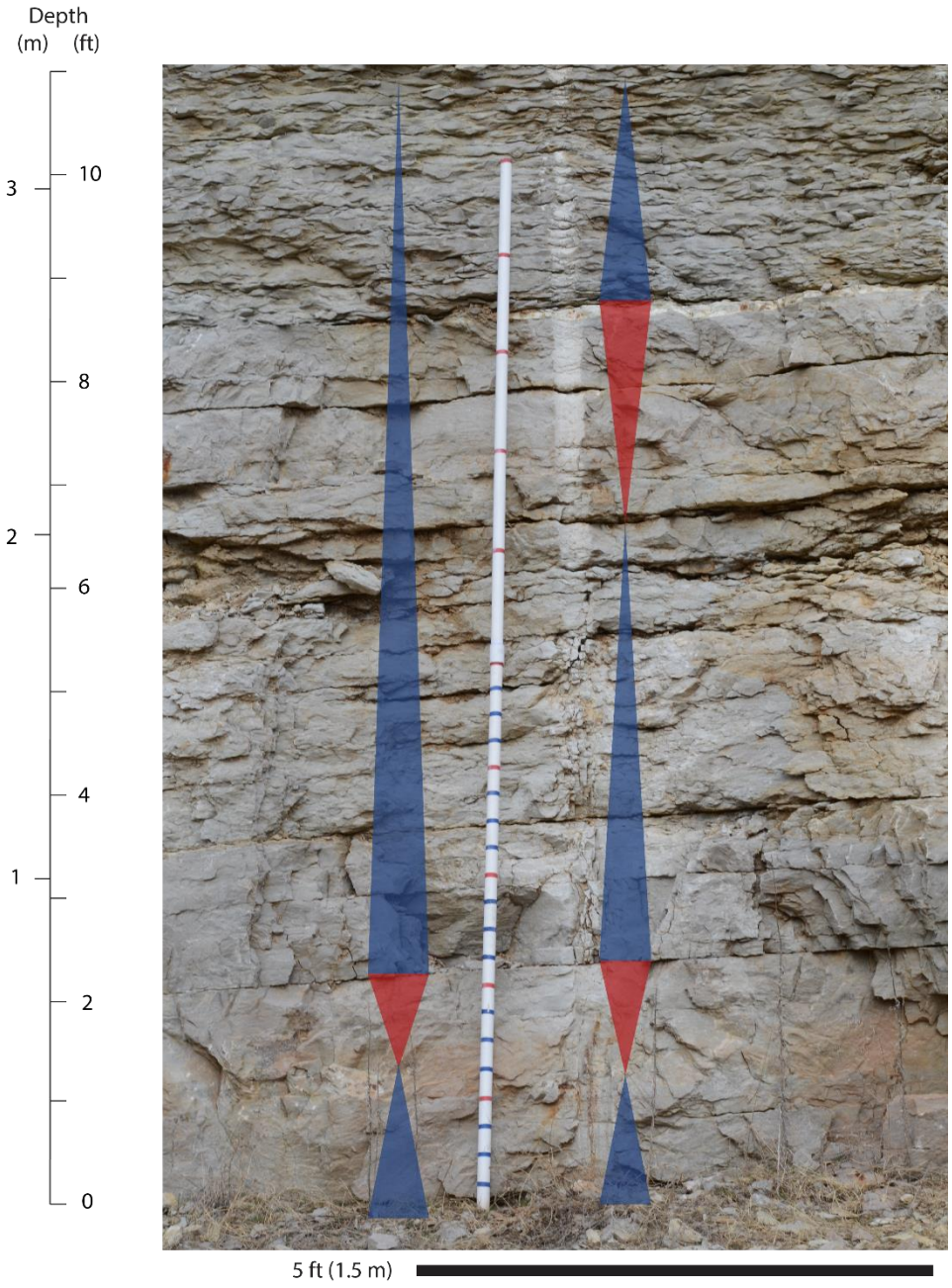

Figure 29: Field photograph of 4th order high frequency sequences (left) and 5th order high frequency cycles (right) overlain on the Compton Formation at Vertical Section 2-3c. Each of the sequence and cycle boundaries were picked based on vertical stacking patterns, flooding surfaces, and exposure surfaces present at the outcrop. Three probable 5th order high frequency cycles can be seen within two probable 4th order high frequency sequences. The change in facies types seen at 8.5 ft (2.6 m) is related to the "block" features associated with the Compton Formation.

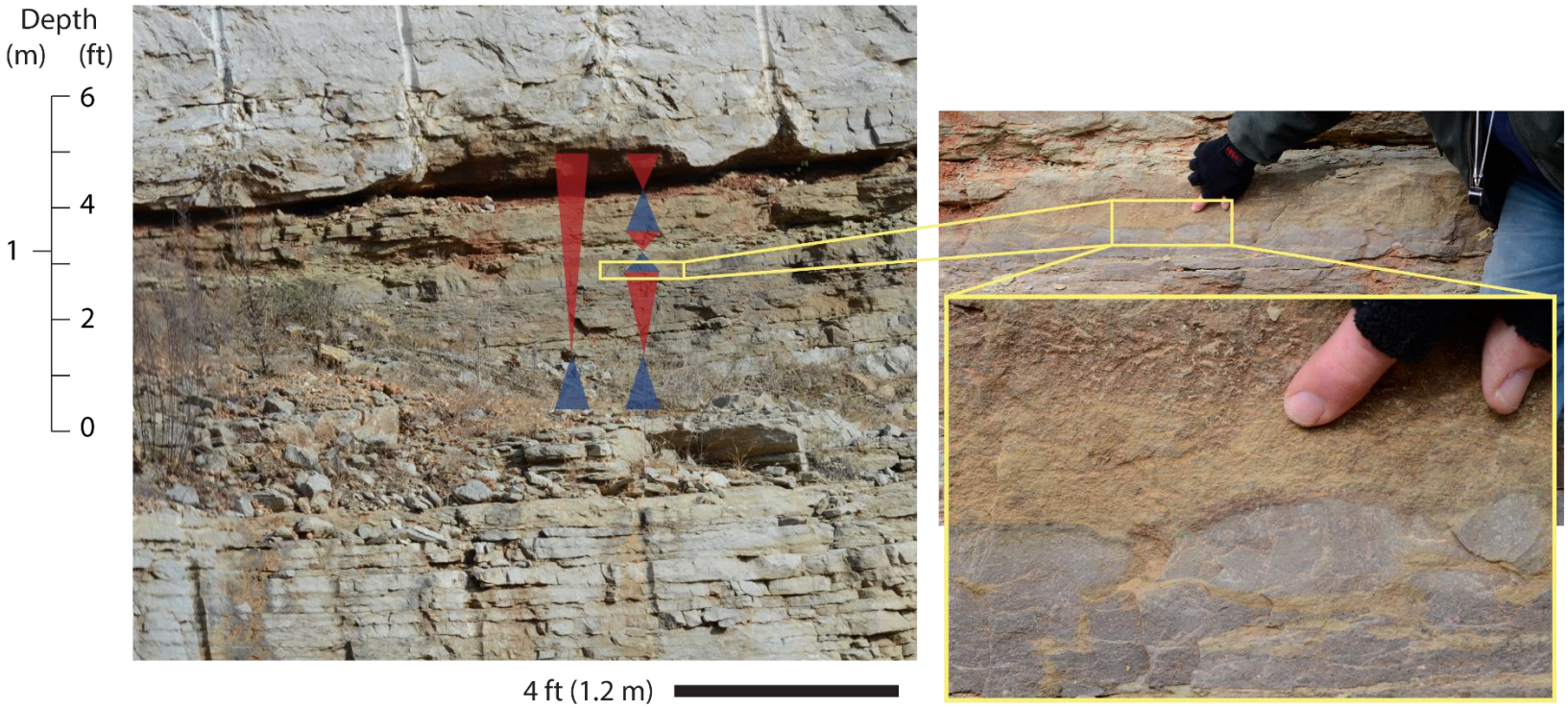

Figure 30: Field photograph of 4th order high frequency sequences (left) and 5th order high frequency cycles (right) overlain on the Northview Formation at Vertical Section 2. Each of the sequence and cycle boundaries were picked based on vertical stacking patterns, flooding surfaces, and exposure surfaces present at the outcrop. Three probable 5th order high frequency cycles can be seen within one probable 4th order high frequency sequences. The magnified photo on the right shows a subaerial exposure surface and microkarst, evidence for a sequence boundary formed when relative sea level was low and sediments of the Northview Formation were exposed.

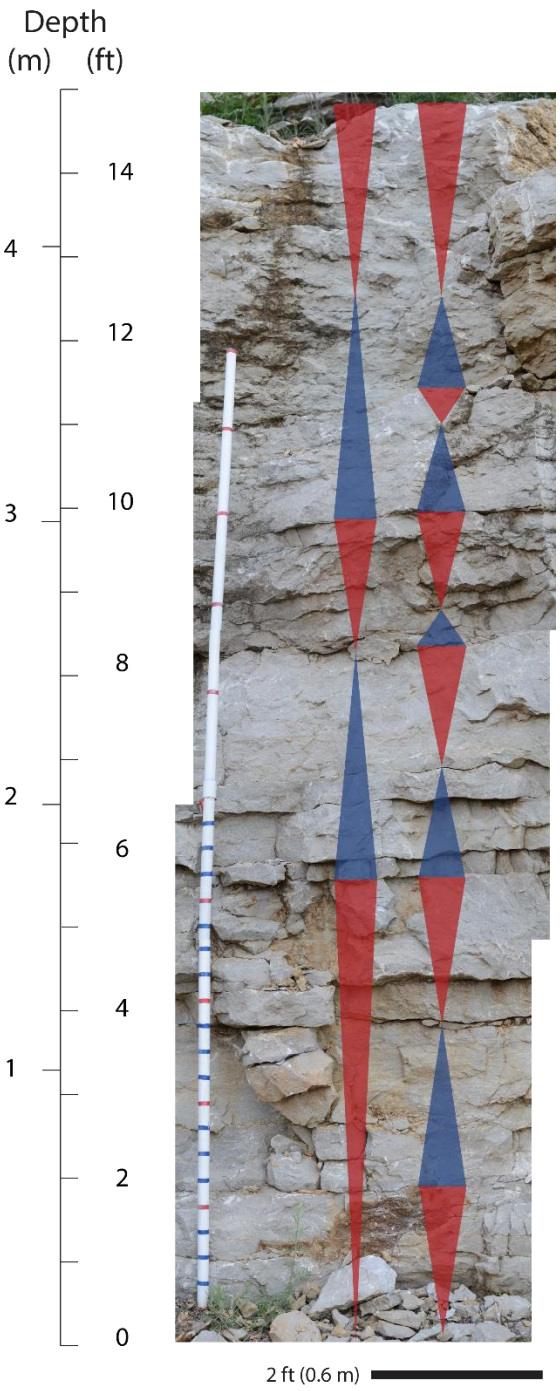

Figure 31: Field photograph of 4th order high frequency sequences (left) and 5th order high frequency cycles (right) overlain on the first ledge of the Pierson Formation at Vertical Section 3. Each of the sequence and cycle boundaries were picked based on vertical stacking patterns, flooding surfaces, and exposure surfaces present at the outcrop. Six probable 5th order high frequency cycles can be seen within three probable 4th order high frequency sequences.

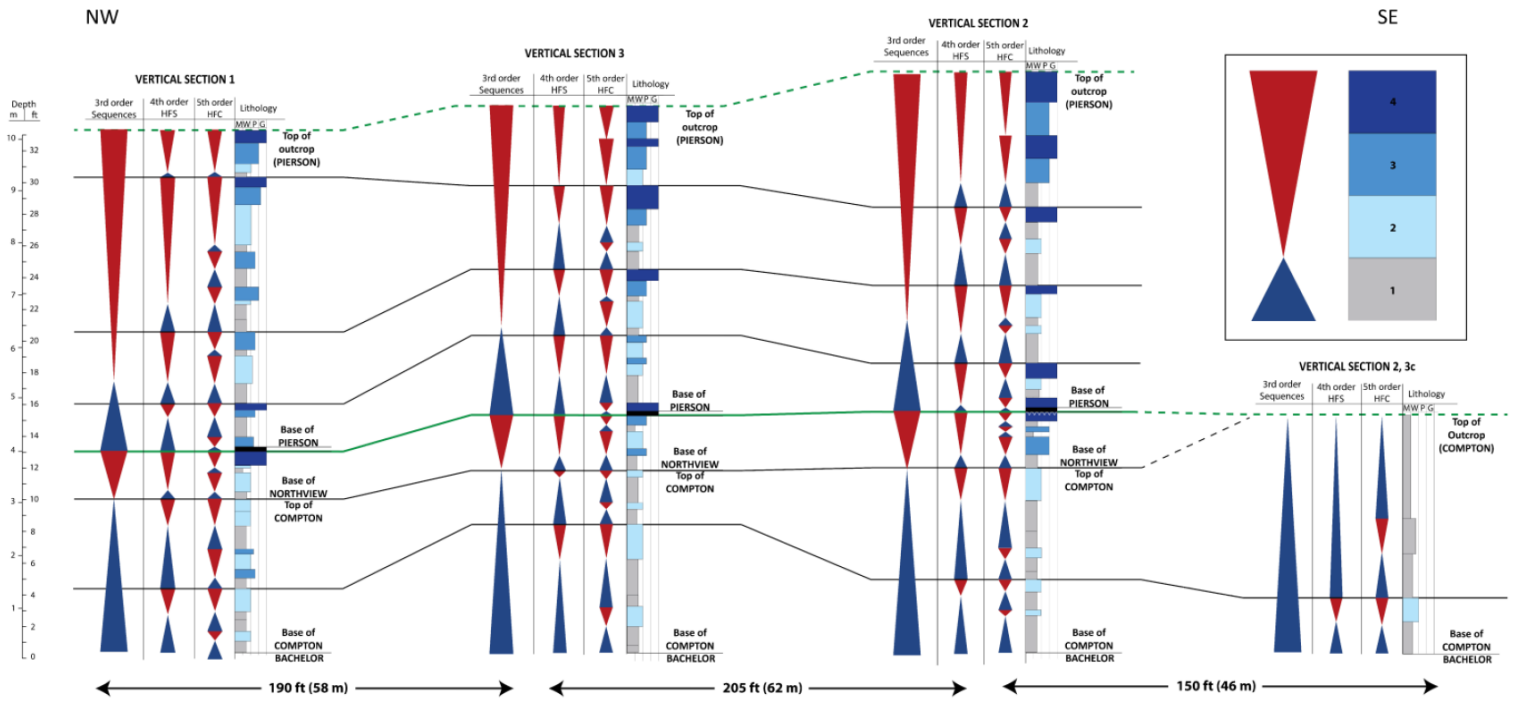

Figure 32: High resolution sequence stratigraphy of the Jane outcrop based on 3rd order sequences and 4th order high frequency sequences. Each of the vertical sections were laterally linked across the outcrop and contain the same colors for facies designation as the idealized facies succession in Figure 23 and in the upper right-hand corner. Sequence and cycle boundaries were picked based on a combination of vertical stacking patterns, flooding surfaces, and subaerial exposure surfaces. The two 3rd order sequences are correlated across the length of the outcrop as green lines. Superimposed on the 3rd order sequences are the probable 4th order high frequency sequences correlated across the length of the outcrop as black lines. As indicated by the stacking patterns and subaerial exposure surfaces seen at Vertical Section 2, a flooding event occurred after deposition of the Northview Formation and before deposition of the Pierson Formation. This figure demonstrates the stratigraphic hierarchy that is discernible at the Jane outcrop.

Using the correlated 4th order high frequency sequences from Figure 32, boundaries for 5th order high frequency cycles were picked using a combination of vertical stacking patterns, flooding surfaces, and subaerial exposure surfaces. Difficulty in choosing boundaries for 5th order high frequency cycles exists as the stratigraphic architecture can change systematically in conjunction with varying accommodation conditions (Tinker and Kerans, 1997). Using the established 4th order high frequency sequences in conjunction with thin section analysis and bedding geometry helped determine boundaries chosen for 5th order high frequency cycles in this study. Through identifying the 5th order high frequency cycles that are superimposed on the 4th order high frequency sequences, the sequence stratigraphic architecture was built by incorporating continuity of facies laterally across the length of the outcrop (Figure 33). This was a vital step in building the high resolution sequence stratigraphic architecture of the Jane outcrop because higher frequency sea level fluctuation is often responsible for controlling vertical and lateral reservoir heterogeneity within a formation, as shown in many carbonate reservoirs (Grammer et al., 1996). Figure 33 also shows the distribution of Facies 3, likely the best reservoir facies based on porosity observed in thin section analysis and SEM. This facies is most prevalent in the Northview and Pierson Formations and occurs towards the top of each shallowing-upward facies succession.

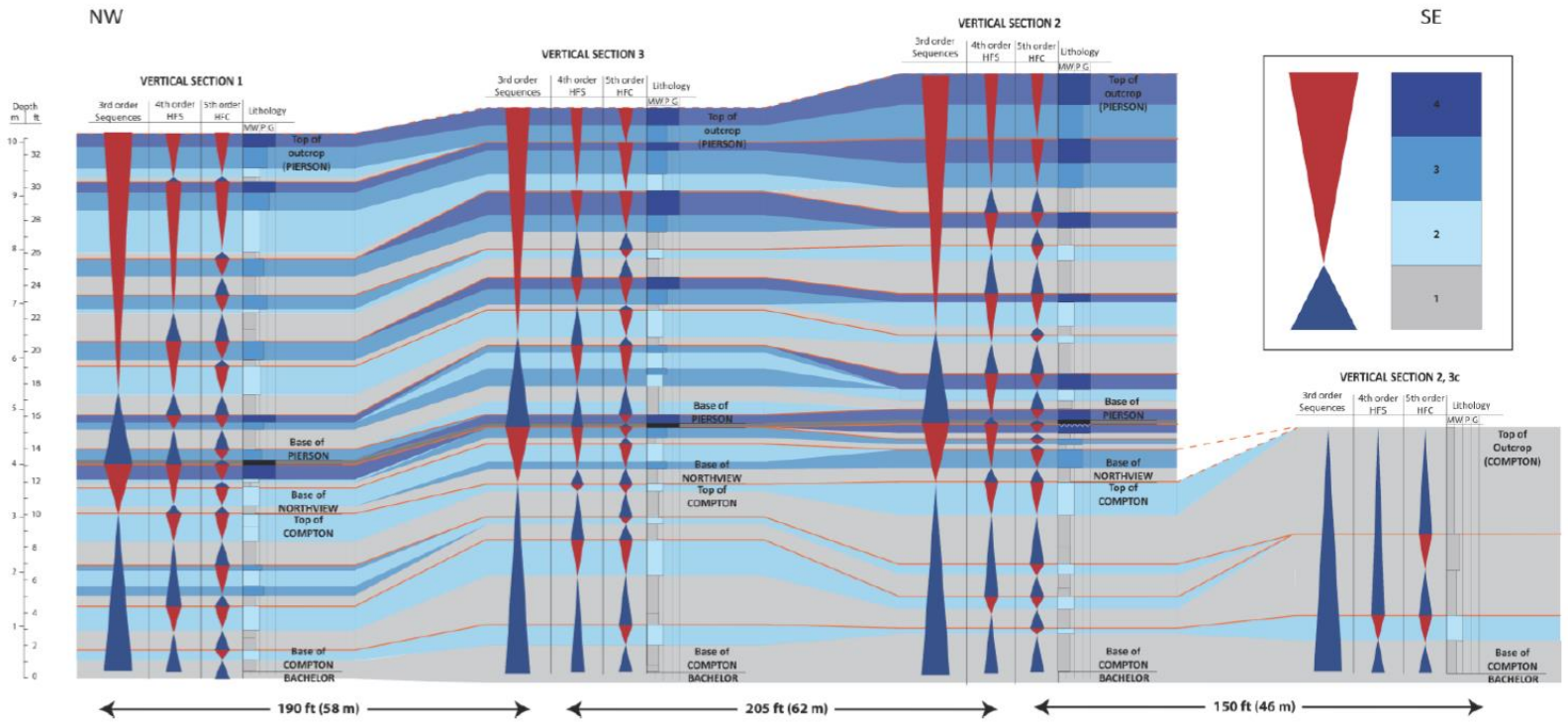

Figure 33: Sequence stratigraphic architecture of the Jane outcrop defined by 5th order high frequency cycles. Each lithology is represented by the same colors seen on the idealized facies succession in the upper right corner. The Compton Formation is dominated by wackestones and packstones, which transitions into packstones and grainstones in the Pierson Formation. From a reservoir perspective, Facies 3 (mud-lean packstone to grainstone) would likely be the best reservoir flow unit based on porosity seen in thin section and SEM. This facies is most prevalent in the Northview and Pierson Formations and occurs towards the top of each shallowing-upward facies succession.

Spectral Gamma-Ray – Gamma-ray signatures of the Mississippian-age strata at the Jane outcrop can be seen in Figure 34. Overall, the spectral gamma-ray measurements are relatively low in potassium, thorium, and uranium throughout each vertical section, with the exception of the Northview Formation. The Northview displays the most significant trend throughout each of the vertical sections, containing the highest gamma-ray signal (40 – 100 API units) relative to the Compton and Pierson Formations. This agrees with the interpretation that the Northview was deposited in a tidal flat environment, as the low uranium content reflects an oxidizing environment that likely produced the subaerial exposure surfaces seen within the Northview Formation at Vertical Section 2 (Doveton, 1994). The highest gamma-ray signal in all three vertical sections corresponds to the mud-lean packstone facies present at the turnaround point of the first 4^{th} order HFS and 5^{th} order HFC within the Northview Formation (Figure 34).

Within the Compton and Pierson Formations, it is difficult to link the gamma-ray signal to 4^{th} order high frequency sequence boundaries and associated facies. Overall, the spectral gamma-ray readings for the Pierson formation range from 0 to 20 total API units, reflecting low amounts of K, Th, and U, indicating clean carbonate deposition of the mud-lean packstones and grainstones that dominate the formation. The Compton Formation averages between 30 and 50 total API units, which may be due an increased number of stylolites throughout the formation as stylolites have potential to locally concentrate U, clays, and organic matter (Glover, 2012). An additional possibility for the higher gamma-ray signal throughout the Compton Formation could be an increase in

the number of mud-dominated facies relative to the Pierson Formation, which is dominated by mud-lean packstones and grainstones (Doveton, 1994).

Additionally, spectral gamma-ray response allowed for determination of the thorium (Th) to uranium (U) ratio at all three vertical sections, which is linked to the depositional environment. When the ratio is less than two (uranium-rich), the depositional environment is commonly marine. This is due to uranium mobilization under reducing conditions. If this ratio is greater than seven (uranium-poor), uranium mobilization through weathering and/or leaching likely occurred, which is an indication of a terrestrial depositional environment (Doveton, 1994). Additionally, potassium (K) and thorium (Th) are directly related to siliciclastic content, while Uranium is uncorrelated to potassium and thorium and determined by diagenetic processes involving changes in oxidation state. As a product of these correlations, K-Th-dominated gamma-ray peaks likely indicate major marine transgressions, whereas U-dominated gamma-ray peaks reflect minor transgressions (Ehrenberg and Svana, 2001; Doveton, 1994).

From the base to top of each vertical section, the total gamma-ray signal decreases as there is an increase in Th at the top of the outcrop. Th/U ratio spikes occur throughout each of the vertical sections, but not consistently along the same stratigraphic interval or facies. In Vertical Section 2, there are two Th/U ratio spikes within the Northview Formation that likely reflect the two subaerial exposure surfaces found at the outcrop. Subaerial exposure occurs under oxidizing conditions, which are

linked to high amounts of K and Th, and low amounts of U (Glover, 2012). This is the only Th/U ratio that can be correlated to a stratigraphic surface.

The logs shown in Figure 34 are not very effective in clearly defining high frequency cyclicity (4^{th} and 5^{th} order) that could aid in the interpretation of the sequence stratigraphic framework of the Jane outcrop. No certain facies directly correlates to a specific gamma-ray signature, with the exception of the skeletal mud-lean packstone facies in the Northview Formation. These results demonstrate the importance of using the rock data collected at the outcrop in addition to electric logs to accurately characterize and predict potential reservoir units within the sequence stratigraphic framework.

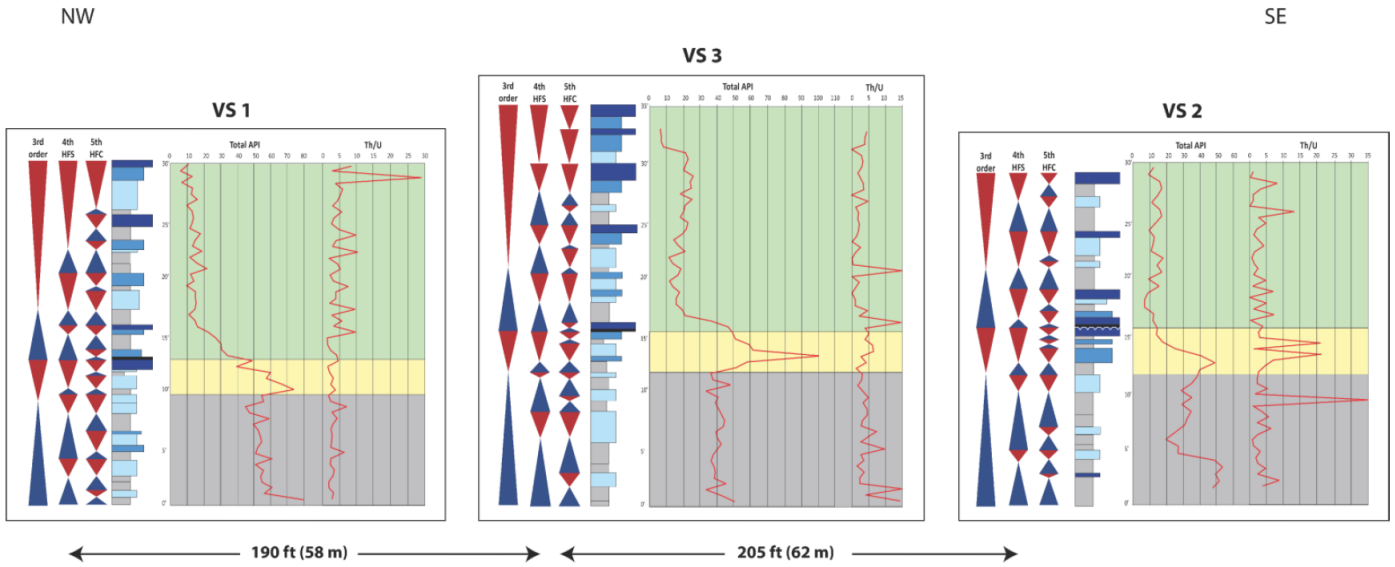

Figure 34: Gamma-ray signatures of the Compton (gray), Northview (yellow), and Pierson (green) Formations at the Jane outcrop. From left to right each vertical section displays, 3rd order sequences, 4th order high frequency sequences (HFS), 5th order high frequency cycles (HFC), gamma-ray signature (total API units), and the Th/U ratio. The Northview (yellow) displays the most significant trend throughout each of the vertical sections, containing the highest total gamma-ray (ranging from 40 – 100 API units) relative to the other formations. This signal helps define the 3rd order fall in sea level that occurred during deposition of the Northview Formation. The spectral gamma-ray readings for the Pierson formation range from 0 to 20 total API units, reflecting low amounts of K, Th, and U, indicating clean carbonate deposition of the mud-lean packstones and grainstones. The Compton Formation averages between 30 and 50 total API units, which may be due an increased amount of stylolites found throughout the formation. In Vertical Section 2, there are two Th/U ratio spikes within the Northview Formation that likely reflect the two subaerial exposure surfaces found at the outcrop at this location. Subaerial exposure occurs under oxidizing conditions, which are linked to high amounts of K and Th, and low amounts of U (Glover, 2012). This is the only Th/U pattern that can be correlated to a stratigraphic surface. Correlation between higher frequency cyclicity (4th and 5th order) and the gamma-ray signatures is poor and ineffective in aiding interpretation of the sequence stratigraphic framework of the Jane outcrop.

Discussion

Section/Cycle Thickness – Overall, 3rd order sequences established by conodont biostratigraphy have provided the framework for determining boundaries for the hierarchy of cyclicity seen within the Kinderhookian and Osagean formations at the Jane outcrop (Boardman, 2013; Shoeia, 2012). The first 3rd order sequence includes the Bachelor, Compton, and Northview Formations, spanning a total thickness of 12-15 ft (3.7-4.6 m). The Pierson Formation represents the second 3rd order sequence and is 15-18 ft (4.6-5.5m) thick. Multiple 4th order high frequency sequences are superimposed on the 3rd order sequences and have thicknesses ranging from 3-10 ft (0.9-3 m) across the outcrop. Furthermore, 5th order high frequency cycles are superimposed on 4th order high frequency sequences and range from 1 to 4 ft (0.3-1.2 m) thick.

Determining thicknesses of individual high frequency sequences and cycles confirmed the hierarchy of cyclicity that exists within the Mississippian-age formations of the Jane outcrop as shown in this study. Recognizing and describing intervals at this high frequency scale enables the use of models for reservoir description, volumetric calculations, and fluid flow modeling that includes critical heterogeneities within the system (Kerans, 1995). This high resolution analysis also helps to develop depositional models for use in forward modeling of reservoir strata (Kerans, 1995). Determining high frequency sequences and cycles is critical for reservoir framework construction, as the individual cycles demonstrated above are too thin to be mapped based solely on log response (Kerans and Tinker, 1997).

The facies architecture in Figure 33 demonstrates that facies in each high frequency sequence can vary laterally on outcrop scale. These lateral facies and subtle thickness variations are directly related to the stacking of the genetic units in the third order sequences that have been constrained by biostratigraphy and eustatic sea level (Boardman, 2013; Haq and Schutter, 2008; Westphal et al., 2004). The facies architecture readily displays the repetitive vertical stacking pattern of the idealized facies succession and shows a general facies change from wackestone- to packstone-dominated to mud-lean packstone- and grainstone-dominated in the upper portion of the outcrop. The sequences that characterize the lower portion of the outcrop (Bachelor and Compton Formations) are much thicker (4-8 ft; 1.2-2.4 m) than the sequences in the upper portion of the outcrop (Northview and Pierson Formations, which are 1.5 ft (0.5 m) in average thickness. This may imply the lower portion of the outcrop was deposited during a period of more accommodation during the flooding phase of the first 3rd order sequence than was available during deposition of the Northview and Pierson Formations (Kerans and Tinker, 1997).

Application to Reservoir

Although significant heterogeneities in facies and reservoir quality exist within the Mississippian-age formations throughout the Mid-Continent, high resolution sequence stratigraphy can be utilized as a predictive tool to delineate the vertical and lateral heterogeneities and compartmentalization within the system, as demonstrated in this study. These higher frequency events are extremely significant as they control

facies stacking patterns, lateral distribution of facies, and potential reservoir distribution throughout the system (Grammer et al., 1996). Determining vertical and lateral trends in facies is crucial to understanding lateral variability within cycles, the lateral extent of reservoir units and seals, and the direction of migration for potential reservoir facies (Eberli and Grammer, 2004).

This high resolution sequence stratigraphic architecture study reveals the locations of vertical and lateral continuity of the reservoir facies (Facies 3) in the outcrop, which can increase the predictability of equivalent reservoir units in the subsurface (Eberli and Grammer, 2004). Facies 3 is most prevalent in the Northview and Pierson Formations of the Jane outcrop and tends to be discontinuous throughout the Northview Formation. Facies 3 (bryozoan-crinoidal mud-lean packstone) contains similar characteristics to the reservoir facies in Le Blanc's (2014) study of subsurface Mississippian-age strata in Oklahoma and may be a common reservoir quality facies throughout the Mid-Continent region. This study shows the impact of identifying a hierarchy of cyclicity to delineate heterogeneities and compartmentalization within the reservoir architecture of the system.

CHAPTER III

OUTRUNNER BLOCKS

Abstract: The Mid-Continent Mississippian Limestone represents a geologically complex system containing different depositional environments as well as dynamic diagenetic and tectonic histories. This unit was deposited in an east-west oriented belt 10-15°S of the paleo-equator. In southwestern Missouri, Kinderhookian and Osagean strata exposed at the Jane outcrop includes the Bachelor, Compton, Northview, and Pierson Formations. This study specifically focuses on the Kinderhookian Compton Formation, as it contains multiple anomalous features, commonly referred to as "displaced bioherm," "Waulsortian-type *in situ* mound," "slump block," and "olistolith." The use of these different classification schemes and terminology leads to significant confusion and potential errors in interpretation of the depositional system.

The current high resolution sequence stratigraphic study has interpreted that deposition of the Kinderhookian and Osagean strata exposed at the Jane outcrop occurred on a distally steepened ramp based on evidence from thin section analysis, sedimentary structures seen at the outcrop, and lateral continuity and geometry of bedding. The dominating facies types present throughout the outcrop range from wackestones to mud-lean packstones, indicating deposition in a distal, lower energy environment. Common features often associated with distally steepened ramps are mass transport deposits, including slumps and debris flows. The anomalous features deposited within the Compton Formation are interpreted as "outrunner blocks" in this study, as they have been deposited within a debris flow bed observed at the outcrop. Debris flows are often produced from a slump as broken clasts supported by a mud matrix. Often associated with the slump rotation and debris flow are outrunner blocks, defined as nearly intact pieces of debris that detach from a slowing-down slide and flow ahead of the front. Development of the blocks is due to hydroplaning, acceleration, and final detachment of the head of submarine landslides and debris flows (Tripsanas et al., 2008; Ilstad et al., 2004). Gigapan imagery has revealed multiple lines of outcrop evidence to support movement of the outrunner blocks. This study examines the outrunner blocks at the Jane outcrop in detail to understand mass transport failure in a distally steepened ramp setting. Integrating mass transport movement with the distally steepened ramp depositional model can assist in clarifying the high resolution sequence stratigraphic architecture within the Compton Formation at the Jane outcrop.

Introduction

The Compton Formation at the Jane outcrop contains anomalous features that have been the subject of various studies, all of which differ in terms and depositional environment interpretations. The use of these different classification schemes and terminology leads to significant confusion and potential errors in interpretation of the depositional system. The features found within the Compton Formation have been previously termed "displaced bioherm" (Morris and Mazzullo, 2013; Mazzullo, 2011), "Waulsortian-type *in situ* mound" (Unrast, 2012), "slump block" (Evans et al., 2011), "olistolith" (Tennyson et al., 2008), and "mound" (Manger and Thompson, 1982). The focus of this chapter is to examine these anomalous features in close detail to correctly identify their composition, if they have moved, how they were developed, and document how these features fit into the high resolution sequence stratigraphic framework of the Jane outcrop.

The interpretation from this study favors the term "outrunner blocks" because the features are set within a debris flow, which is a type of mass transport deposit composed of clasts supported by a mud matrix (Table 3; Asmus and Grammer, 2013). Mass-transport refers to gravity-driven downslope movement of "en masse" sediment particles where the main sediment transport mechanism is non-fluid turbulence. Final emplacement or accumulation of sediment resulting from those processes are termed mass-transport deposits (MTDs) (Asmus and Grammer, 2013). Attributes used to distinguish between different MTD deposits include flow type, flow behavior, flow

cohesion, flow character, dominant sediment support mechanism, sediment concentration (volume percent of solid grains), and architectural elements (Cook and Mullins, 1983; Lowe, 1979; 1982; Mulder and Alexander, 2001). Table 3 summarizes the terminology and the architectural attributes commonly used for MTDs (Asmus and Grammer, 2013).

Previous studies – Many previous studies have observed the blocks found within the Compton Formation at the Jane outcrop and named them based upon general observations. These blocks have been the subject of much debate in recent publications (Morris and Mazzullo, 2013; Unrast, 2012). Morris and Mazzullo (2013) use the term "reefs," and define them as "limestone lithosomes of convex-up lensoid geometery with presumed relief above the sea floor during deposition whose allochemical composition is dominated by what are regarded as impoverished Mississippian reef building biota" (Morris and Mazzullo, 2013). They then fit the "reef" into their regional tectonic model of forebulge and backbulge basins that resulted from convergence and compression caused by the Laurussian-Gondwanan continental suture zone (Morris and Mazzullo, 2013; Wilhite et al., 2011). In this case, the term "reef" may be more consistent with the term "bioherm," defined by Wilson (1950) as consisting of any dome-like, mound-like or other mass, built exclusively or mainly by organisms such as corals, stromatoporoids, algae, brachiopods, Mollusca, crinoids, etc. and enclosed in normal rock of different lithologic character.

Flow Type		Flow Behavior	Flow Cohesion	Flow Character	Dominant Sediment Support Mechanism	Sediment Concentration (volume % of solid grains)	Architectural Elements
Source: Lowe (1982)	Source: Mulder and Alexander (2001)	Source: Lowe (1979, 1982); Mulder and Alexander (2001)	Source: Lowe (1979, 1982); Mulder and Alexander (2001)	Source: Lowe (1979, 1982); Mulder and Alexander (2001)	Source: Lowe (1979, 1982); Mulder and Alexander (2001)	Source: Mulder and Alexander (2001)	Source: Cook and Mullins (1983); Lowe (1979, 1982); Mulder and Alexander (2001)
Turbidity Current	Low-Density Turbidity Current	Fluid	Non-cohesive	Turbulent	Fluidal Turbulence	0–10%	Variable bed thicknesses (millimeters-to-meters); basal scour marks; dewatering structures occuring at the base or top of individual depositional packages; partial-to-complete Bouma sequences; long travel distances (100s of kilometers); and cyclical stratigraphic occurence (i.e., cyclical stacking of in dividual depositional packages).
Fluidized Flow	High-Density Turbidity Current	Fluid	Non-cohesive	Turbulent	Escaping Pore Fluids (completely support solid grains)	10–40%	Dewatering structures occuring at the base or top of individual depositional packages; collapse structures; slight-to-moderate grading; and basal load structures. Liquified flows exhibit greater runout distances compared to fluidized flows due to increased sediment concentrations of fine sand sized grains within the flow body.
Liquified Flow	Concentrated Density Flow	Fluid/Plastic	Non-cohesive	Turbulent/ Laminar	Escaping Pore Fluids (partially support solid grains)/Dispersive Pressure (grain-to-grain collision)/ Bouyancy	10–40%	
Grain Flow	Hyperconcentrated Density Flow	Plastic	Non-cohesive	Laminar	Dispersive Pressure (grain-to-grain collision)/Bouyancy	25–90%	Massive bedding; sharp upper and lower bedding contacts; basal erosional features; local inverse grading; and sediment concentrations dominated by gravel-, sand-, and silt-sized grains.
Debris Flow		Plastic	Cohesive	Laminar	Matrix Strength/ Bouyancy/Pore Pressure	30–90%	Massive bedding; clasts may exhibit random and chaotic fabrics with variations in size, roundness, and composition; clasts and matrix may contain shoal-water and basin fauna; internal deformational shearing; local inverse grading; and clast protrusion into underlying and/or overlying strata.
Slide	Slump (rotational)	Elastic/Plastic	na	na	na	na	Spoon-shaped external geometry; minimal internal deformation of bedding along central axis of flow body; significant internal deformation of bedding along basal surface and exterior margins of flow body; microfolding and microfaulting are common.
	Glide (translational)	Elastic/Plastic	na	na	na	na	Continuous bedding; planar basal surfaces; minimal internal deformation; local faulting (strike-slip and listric) and folding may occur along the base and margins of the flow body

Table 3: Terminology and structural attributes associated with turbidites and MTDs. This table highlights specific characteristics of the debris flow and slump, the flow types associated with mass transport in this study (Modified from Asmus and Grammer, 2013).

Unrast (2012) focused on Waulsortian and Waulsortian-type mounds of the Mississippian at multiple outcrop locations throughout the Mid-Continent and compared them to Waulsortian mounds found in Ireland. Unrast (2012) recognized two "mounds" at the Jane outcrop, classified them as "Waulsortian-type," and interpreted them as being *in situ*. Evidence used by Unrast (2012) to support the term "Waulsortian-type" included examples of various geopetal structures documented to be at the same angle.

Questions and Hypothesis – Fundamental questions addressed in this study that arise from previous studies are as follows:

1. Are the anomalous features in the Compton Formation at the Jane outcrop truly "*in situ* bioherms", or are they "outrunner blocks"?
2. What outcrop evidence supports the term "outrunner block" for the anomalous features associated with the Compton Formation at the Jane outcrop?
3. How many outrunner blocks were deposited within the Compton Formation at the Jane outcrop, and what is the composition of each?
4. How do the outrunner blocks effect the sequence stratigraphic architecture within the Jane outcrop?

The primary data set created to help answer these questions was detailed outcrop analysis using the integration of Gigapan imagery, thin section analysis, bedding

geometries, and the incorporation of a depositional model to explain movement and composition of each block within the Compton Formation. Once this information was identified, the blocks were integrated into the established high frequency sequence stratigraphic architecture of the Jane outcrop.

Geologic Setting – Deposition of Mid-Continent Mississippian carbonates occurred at 10-15 degrees south latitude in a foreland ramp setting as part of a system of shallow water facies bordered by deep water deposits to the south and west (Mazzullo et al., 2013). Conodont biostratigraphy by Boardman (2013) on Lower to Middle Mississippian strata in this region revealed a geometry consisting of diachronous prograding carbonate wedges. Progradation of these wedges eventually led to a homoclinal to distally steepened ramp depositional setting for Mississippian-age strata (Wilhite et al., 2011).

The study area is located in southwestern Missouri, near Jane, Missouri, where Kinderhookian and Osagean strata are exposed. This location is approximately 100 miles west of the Ozark Uplift and 150 miles north of the Arkoma Basin. The formations exposed at the Jane outcrop, from base to top, include the Bachelor, Compton, Northview, and Pierson Formations. This chapter focuses specifically on the Compton Formation, which is generally described as a light gray crinoidal-bryozoan wackestone to packstone unit (Kreman, 2011; Manger and Shanks, 1976). Near Jane, Missouri, the thickness of the Compton increases from south to north and has an average thickness of 10-12 ft (3.0-3.7 m) (Wilhite et al., 2011).

Outcrop Observations

Outrunner Blocks and Debris Flow – The Gigapan photograph in Figure 35 highlights multiple outrunner blocks shaded in gray, each of which is set within a debris flow shaded in orange. Figure 36 shows the characteristics of the debris flow more closely. Tripsanas et al. (2008) defines a debris flow as a plastic, poorly sorted flow in which clasts 'float' in a fine-grained matrix with finite shear strength. This sample shows subrounded clasts ranging in grain size from very coarse sand to very coarse pebbles (2mm – 2.5 in) supported by a mud matrix, confirming it is a debris flow. Figure 37 helps to clarify differences between the dynamics of a debris flow relative to other types of subaqueous sedimentary density flows. There are a total of six blocks set within the outlined debris flow in Figure 35 and the size of each can be compared in Table 4.

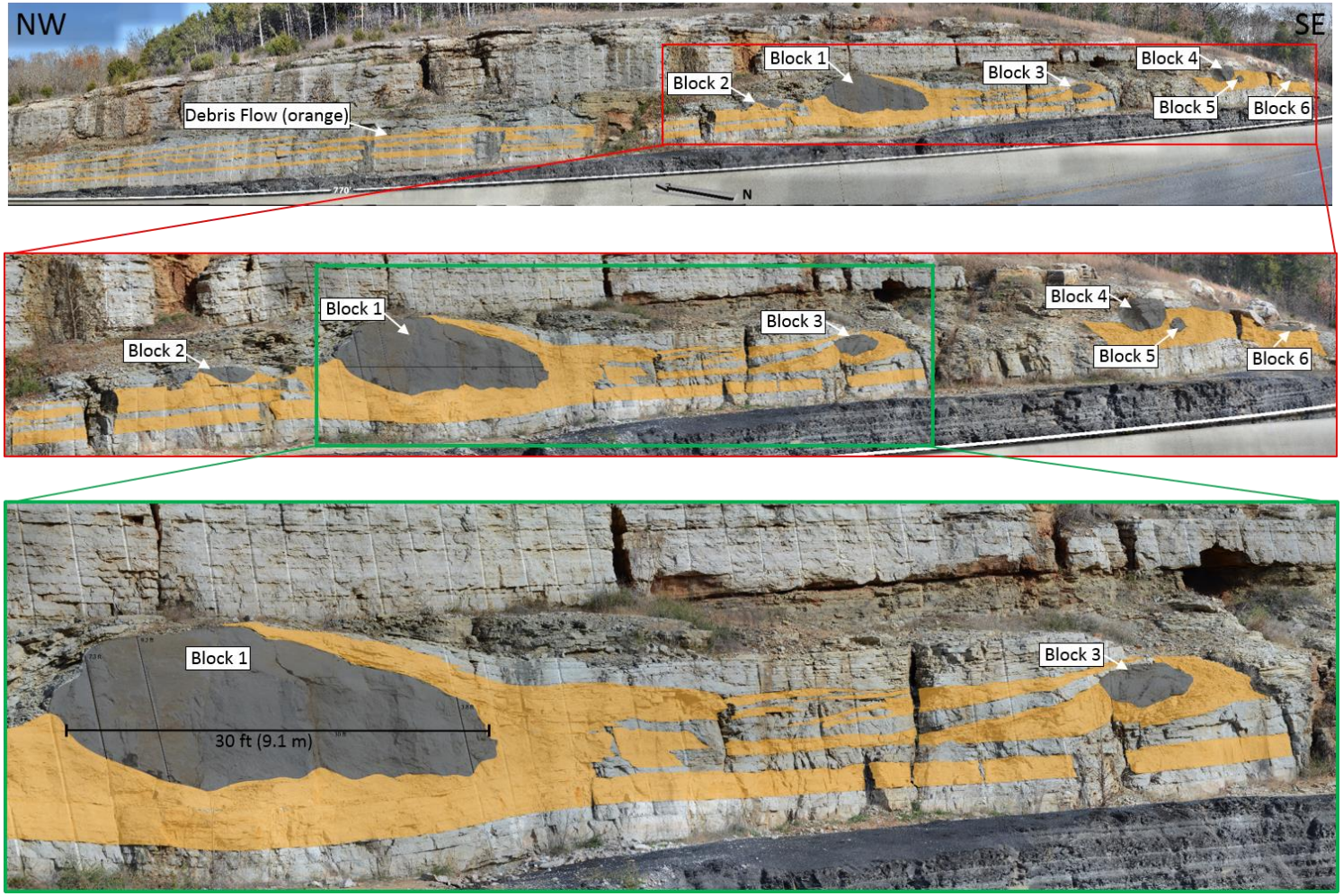

Figure 35: Gigapan photographs showing the debris flow bed highlighted in orange. Each outrunner block is shaded in gray. Block 1 is the primary outrunner block and largest in size with dimensions of 9.2 ft (2.8 m) high and 30.0 ft (10.2 m) wide. The debris flow bed occurs throughout the entire outcrop and thins out to the northwest.

Figure 36: Sample of the debris flow bed within the Compton Formation. Mud clasts ranging in grain size from very coarse sand to very coarse pebbles (2 mm – 2.5 in) are set within a crinoidal-bryozoan micrite matrix very similar to the composition of the Compton Formation. Note the scale is in centimeters and the up direction is to the left.

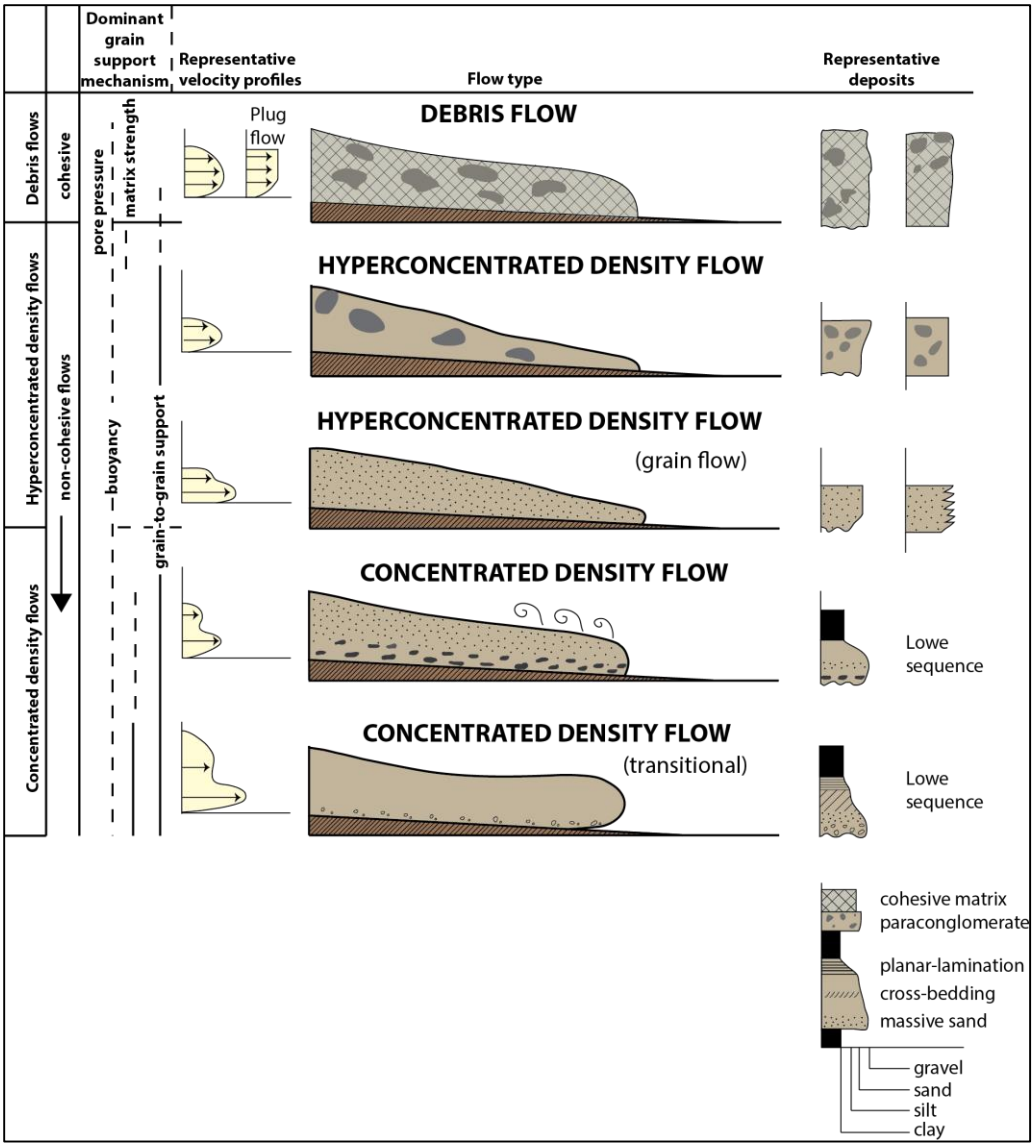

Figure 37: Schematic definition diagram for subaqueous sedimentary density flows, indicating dominant grain-support mechanisms, idealized velocity profiles, idealized flow shape, and schematic sedimentary logs. Two types of hyperconcentrated density flows are presented to represent end-members depending on load characteristics. Two types of concentrated density flows are presented to represent the large range of sediment concentrations in this category and the associated variation in sediment types. Diagrammatic velocity profiles for positions within each flow (near the flow front) are presented to show inferred variation between flow types. Two velocity profiles are presented for debris flows to illustrate the difference between plug and non-plug flow conditions. This diagram helps to clarify differences between the dynamics of a debris flow relative to other types of subaqueous sedimentary density flows (Modified from Mulder and Alexander, 2001).

Block #	Width	Height
Block 1	30 ft (10.2 m)	9.2 ft (2.8 m)
Block 2	6.5 ft (2.0 m)	2.1 ft (0.6 m)
Block 3	5.4 ft (1.6 m)	2.5 ft (0.8 m)
Block 4	7.2 ft (2.2 m)	3.5 ft (1.1 m)
Block 5	2.1 ft (0.6 m)	1.8 ft (0.5 m)
Block 6	3.1 ft (0.9 m)	0.7 ft (0.2 m)

Table 4: Width and height dimensions for the six blocks within the Compton Formation at the Jane outcrop for comparison.

Methods

Gigapan Imaging – Gigapan EPIC Pro hardware and software was used in this study to allow over 800 individual photographs of the outcrop to be stitched together to produce a very high-resolution, seamless photograph of the entire outcrop where individual beds and sedimentary structures are visible down to the centimeter scale (Figure 35). Once the high resolution image was stitched together, individual blocks and beds were traced for lateral continuity and geometry, an important step in distinguishing each block from the surrounding bedding. This also highlighted multiple lines of evidence supporting block movement.

Thin Section Analysis – Each outrunner block at the Jane outcrop was sampled in this study for thin section analysis to aid in determining its composition. The debris flow was also sampled at multiple locations to investigate its composition relative to the composition of the blocks. Fifteen thin section photomicrographs from the six outrunner blocks and four thin section photomicrographs from the debris flow were examined and classified based on Dunham (1962) and Choquette and Pray (1970) classification schemes. Thin sections used in this study were standard size (27 mm by 46 mm or 1 in by 1.8 in) and vacuum impregnated with blue epoxy to illustrate presence of porosity. The abbreviations used to label skeletal grains is shown in Table 2 of Chapter II.

Literature Comparison – Once the characteristics of the outrunner blocks were constrained, comparisons were made to similar features described in the published literature. This enabled identification of mechanisms of block movement and block development, which was then tied to the depositional model for the region. Integration of the characteristics of outrunner blocks and the distally steepened ramp depositional model allowed for further development of the high resolution sequence stratigraphic architecture of the system.

Results

Evidence for Block Movement – In addition to the debris flow outlined in Figure 35, multiple lines of evidence to support movement of the blocks can be seen at the Jane outcrop using the Gigapan hardware and software. Evidence for block movement includes geopetal structures, inclined Northview beds, and truncated Compton beds.

Geopetal fabrics can serve as guides to the normal or inverted position of strata within complex stratigraphic settings (Honjo et al., 1965). These features are partial sedimentary infillings of rock cavities that may form during times of minimal sedimentation and/or rapid burial (Wieczorek, 1979). Multiple geopetal structures in the form of partially infilled brachiopods were found at angles ranging from 15 – 45 degrees on the exposed surface of Block 1, indicating the feature is a block that underwent multiple phases of movement and/or rotation (Figure 38).

Additional evidence for movement is in the overlying, dipping beds of the Northview Formation. The angle of this bedding suggests compression of the Northview strata after it was deposited on top of Block 1 (Figure 39). This is also evidence that the Blocks were originally sourced from within the Compton Formation at a location further up-dip, before deposition of the Northview Formation. The Northview Formation represents a tidal flat environment based on sedimentary structures observed at the outcrop, including bi-directional ripples and multiple subaerial exposure surfaces. Once relative sea level fell during deposition of the Northview Formation, cementation of exposed strata would have likely prevented any potential break-up of sediment (Shinn, 1983).

Additional evidence for movement of the blocks can be found within the bedding between Block 1 and Block 3. Movement of each block likely occurred during different times, as evidenced by the parallel bedding between the debris flow and the blocks. If one event stemmed the movement of every block in the Compton Formation

simultaneously, the debris flow bed surrounding the blocks would be a continuous, homogeneous deposit with no intervening parallel bedding. As Figure 35 shows, the debris flow bed (orange) is heterogeneous and intermixed with flat-lying, horizontal bedding in between the blocks. This is evidence that at least two of the five blocks moved at different times, complicating the bedding geometry within the Compton Formation. In the same area between Block 1 and Block 3, intraformational truncation surfaces occur throughout the bedding (Figure 40). These were likely produced as blocks moved along truncation surfaces. Similar truncation surfaces have been observed within a base-of-slope carbonate apron (western Newfoundland) and are interpreted to represent deposition on an unstable sloping surface (Coniglio, 1985).

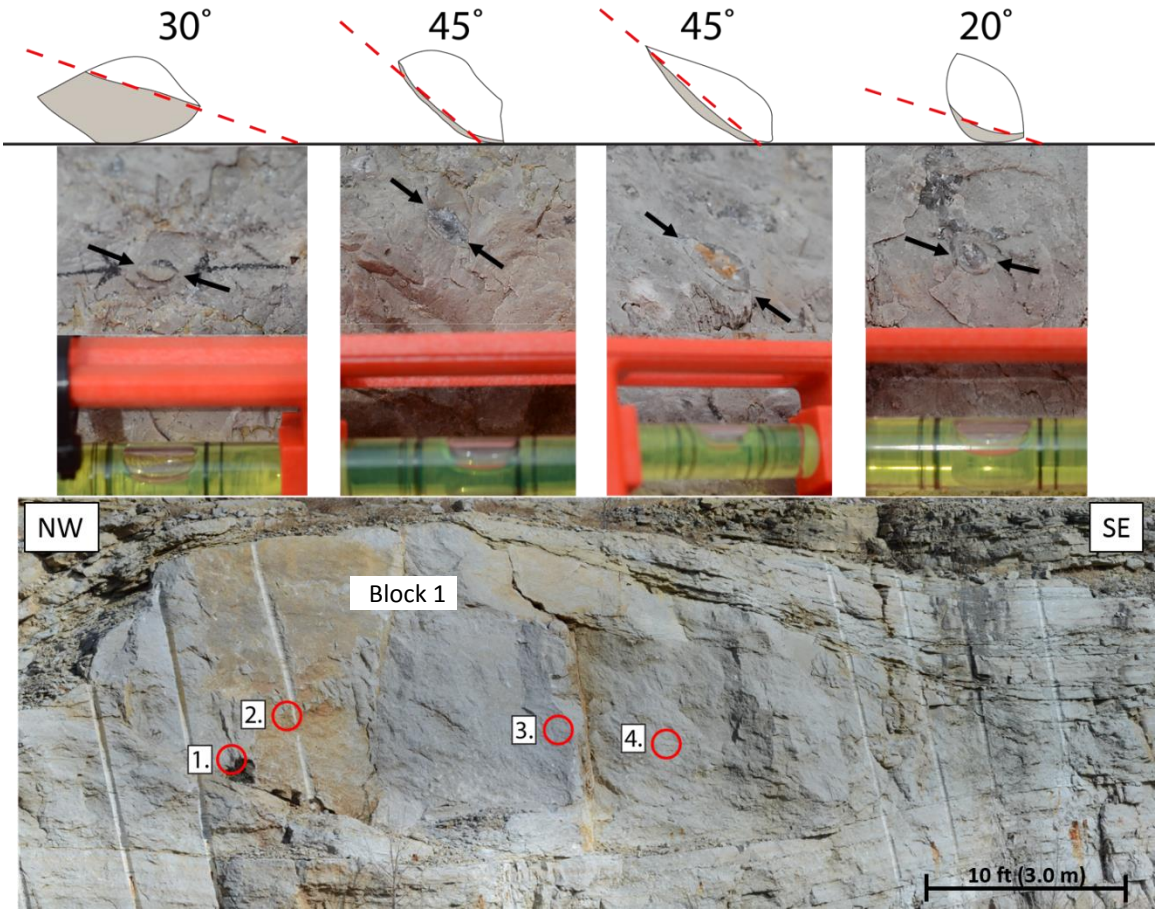

Figure 38: Location of four geopetal structures within Block 1. Magnified images of each geopetal are shown above the Gigapan image of Block 1. Enlarged drawings of each geopetal are shown above the magnified photographs and display the angle of rotation. If the block was *in situ*, the sediment within each of the geopetal structures would have been oriented in a horizontal direction. Since each geopetal was found within the same block at different angles of rotation, this suggests multiple phases of movement.

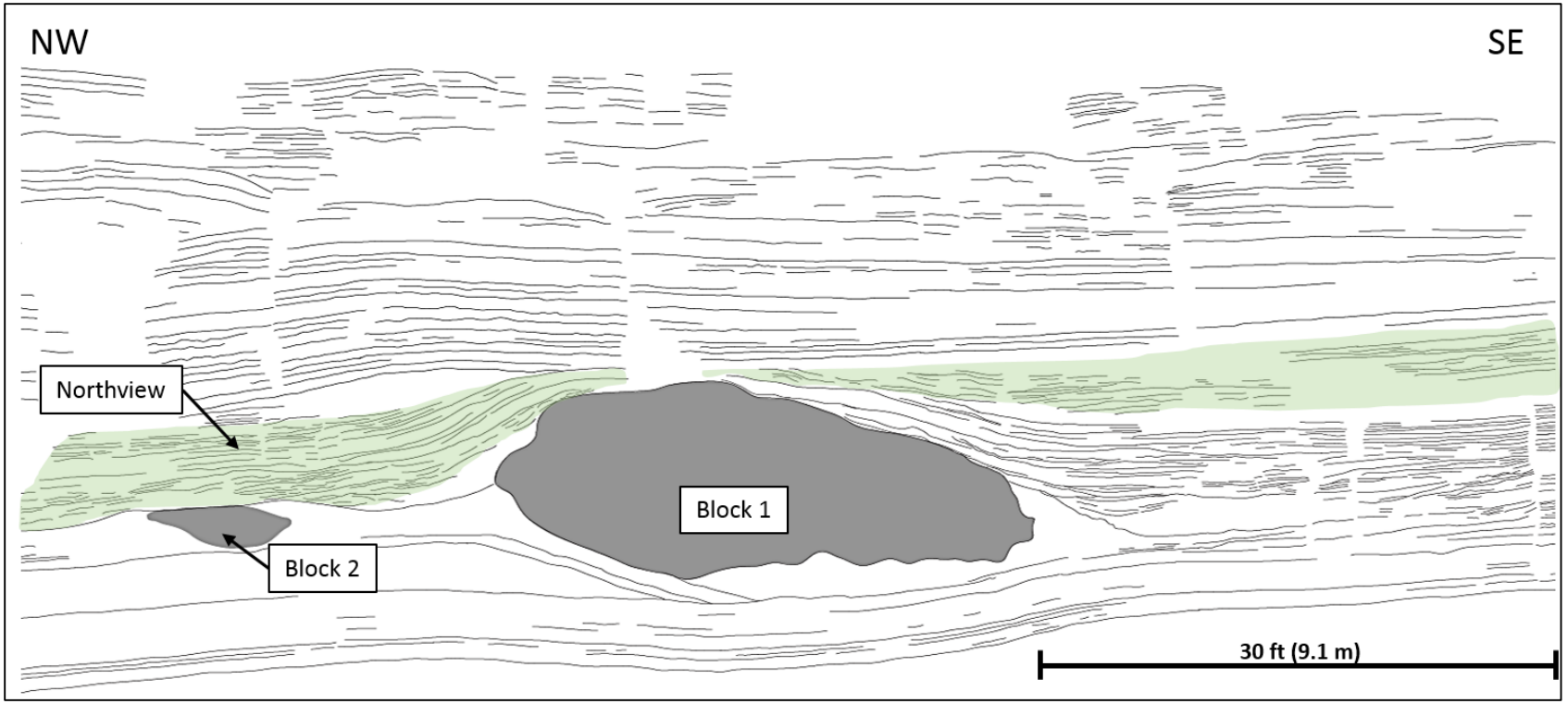

Figure 39: Compactional draping of the bedding within the Northview Formation (green) traced from the Gigapan photograph. A plausible explanation for the inclined Northview beds is sediments were compressed after being deposited on top of Block 1. This is also evidence the Blocks were originally sourced from within the Compton Formation further up-dip, as the Northview Formation represents a tidal flat environment. Once relative sea level fell during deposition of the Northview Formation, cementation would have affected the exposed sediments landward of the tidal flats, preventing any potential break-up of sediment (Shinn, 1983).

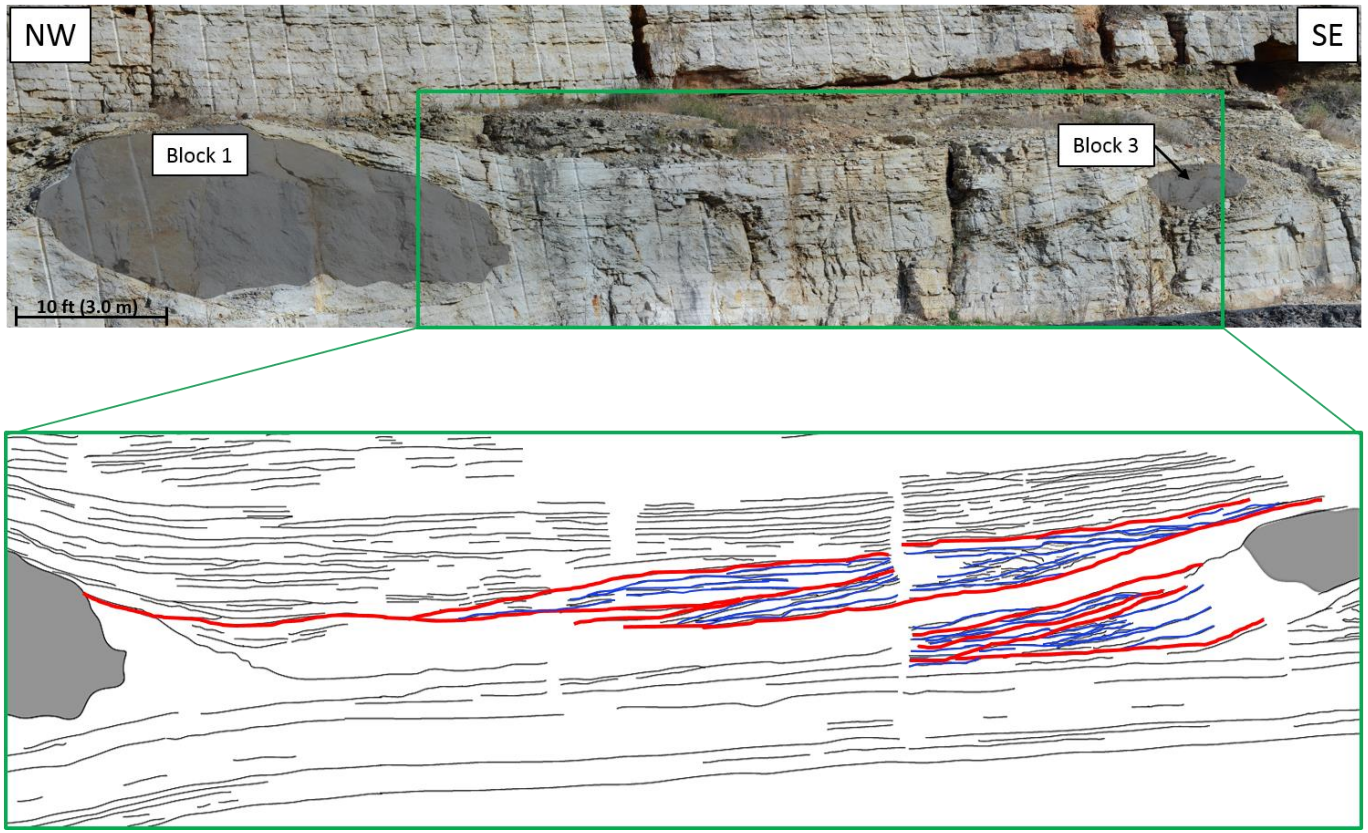

Figure 40: Intraformational truncation features located between Block 1 and Block 3, traced from the Gigapan photograph. Truncation surfaces are highlighted in red and truncated beds are highlighted in blue. Some of the truncated beds are parallel, suggesting no block movement occurred during deposition associated with each parallel bed. This evidence supports separate phases of movement for each block. Truncated bedding does not surround all blocks, which may be due to the small size of Blocks 2 – 6 (refer to Table 4 for block dimensions). Similar truncation surfaces have been observed within a base-of-slope carbonate apron (western Newfoundland) and are interpreted to represent deposition on an unstable sloping surface (Coniglio, 1985).

Thin Section Analysis – Thin section photomicrographs from Unrast's (2012) study document the core facies of Block 1 (Figure 41). Blocks 2-6 have been documented in this study and one thin section photomicrograph for each block is shown in Figures 42-47. Each block at the Jane outcrop is similar in composition and can be classified as a wackestone-packstone with localized skeletal grains primarily consisting of crinoids and bryozoans with local trilobites and ostracods. All blocks contain similar facies and skeletal components, indicating each block likely originated from the Compton Formation at a location further up-dip on the ramp. Additionally, thin section photomicrographs of the debris flow show clasts ranging in grain size from very coarse sand to very coarse pebbles (2μ – 2.5 in) supported by a mud matrix, confirming the deposit surrounding each outrunner block is a debris flow (Figure 48).

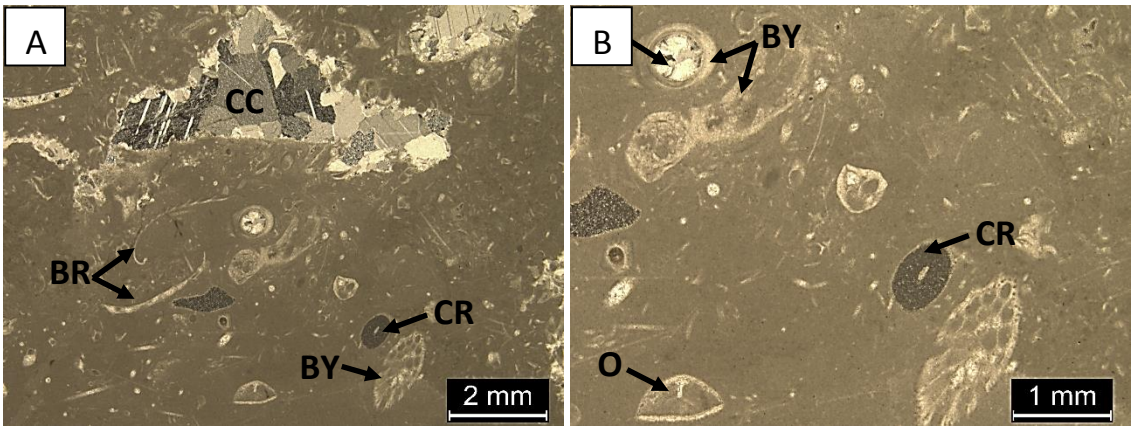

Figure 41: Thin section photomicrographs of sample JC1, sampled from Block 1 of Figure 35 to show its composition relative to the other blocks and the debris flow bed. **A.** Magnification at 25x. **B.** Magnification at 50x. This facies is Skeletal wackestone, fine to very coarse grained, poorly sorted. Contains 15% skeletal grains, 82% micrite matrix, and 3% blocky calcite cement (visual estimation). Grain types include crinoids (200 – 1mm), bryozoans (125µ – 2mm), brachiopods (600µ – 2mm), and ostracods (500µ – 800µ).

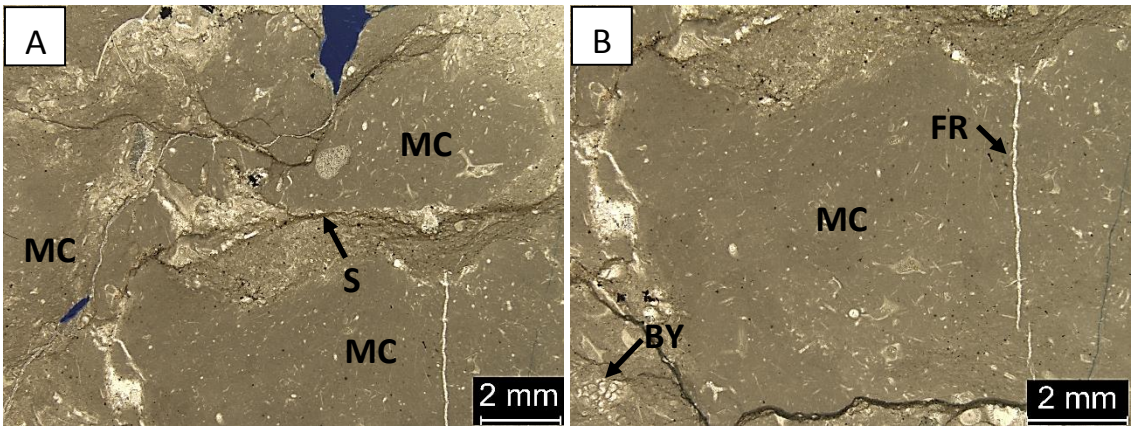

Figure 42: Thin section photomicrographs from Block 2 of Figure 35 to show its composition relative to the other blocks and the debris flow bed. **A.** Magnification at 25x shows the upper half of the thin section in CPL. **B.** Magnification at 25x shows the lower half of the thin section in CPL. This facies is a skeletal wackestone containing mud clasts broken up within. The mud clasts range in size from very coarse sand to fine pebbles. Skeletal grains include crinoids (250µ – 2mm) and bryozoans (125µ – 2mm). Pyrite and calcite cement have filled in fractures and void spaces within the micrite matrix. Stylolites have been filled with dolomite.

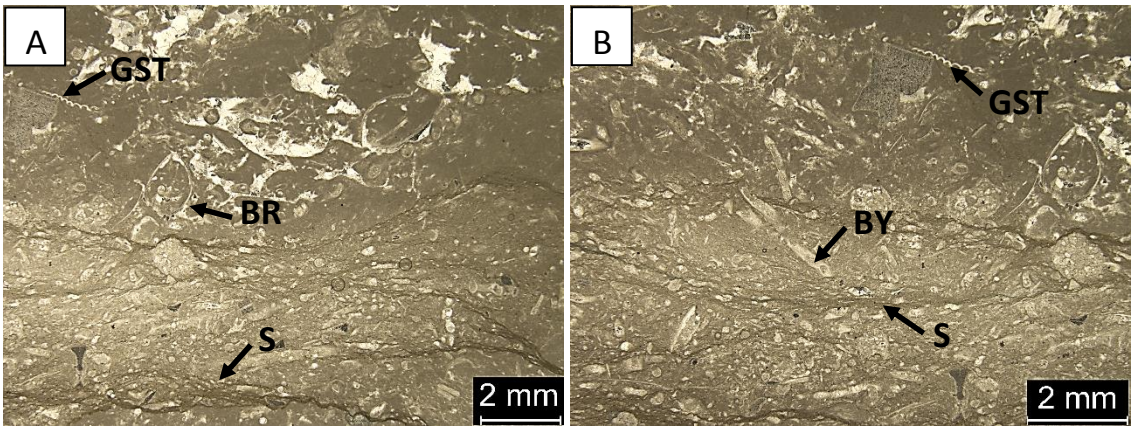

Figure 43: Thin section photomicrographs from Block 3 of Figure 35 to show its composition relative to the other blocks and the debris flow bed. **A.** Magnification at 25x shows the upper half of the thin section in CPL. **B.** Magnification at 25x shows the lower half of the thin section in CPL. This facies is a skeletal wackestone, grain size ranges from fine sand to very fine pebbles, poorly sorted. Contains crinoids (500µ – 2mm), bryozoans (125µ – 1mm), brachiopods (500µ – 2mm), ostracods (125µ – 450µ), and gastropods (750µ – 2mm). Wispy stylolites filled with dolomite occur throughout the lower half of the thin section (B).

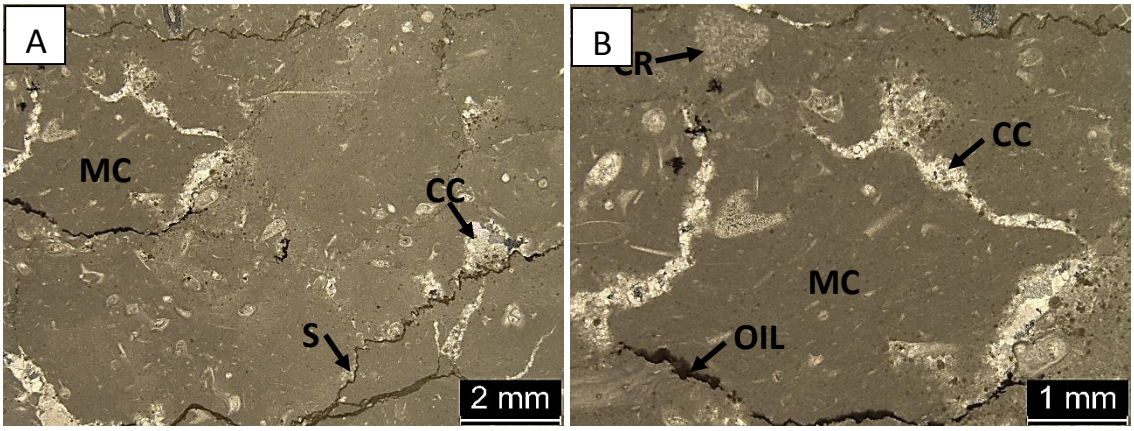

Figure 44: Thin section photomicrographs from Block 4 of Figure 35 to show its composition relative to the other blocks and the debris flow bed. **A.** Magnification at 25x. **B.** Magnification at 50x. This facies is a wackestone, very fine to coarse grained, moderately sorted. Contains crinoids (250µ – 1mm), bryozoans (62.5µ – 400µ), and brachiopods (400µ – 750µ). Pyrite and dead oil occur throughout. Calcite cement has filled in some skeletal grains and surrounded mud clasts.

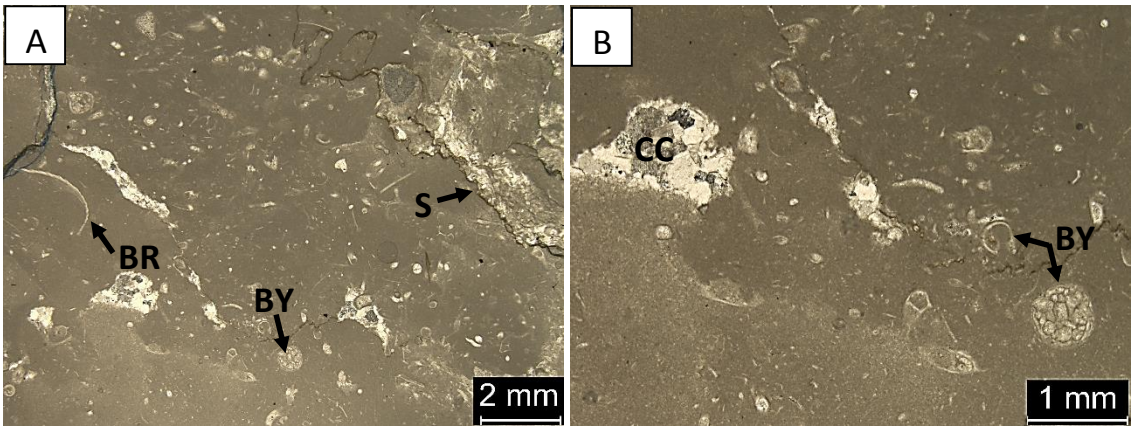

Figure 45: Thin section photomicrographs from Block 5 of Figure 35 to show its composition relative to the other blocks and the debris flow bed. **A.** Magnification at 25x. **B.** Magnification at 50x. This facies is a wackestone, fine to very coarse grained, poorly sorted. Contains 20% skeletal grains, 75% micrite matrix, and 5% calcite cement (visual estimation). Skeletal grains include crinoids (250µ – 1mm), brachiopods (750µ – 2mm), and bryozoans (125µ – 750µ).

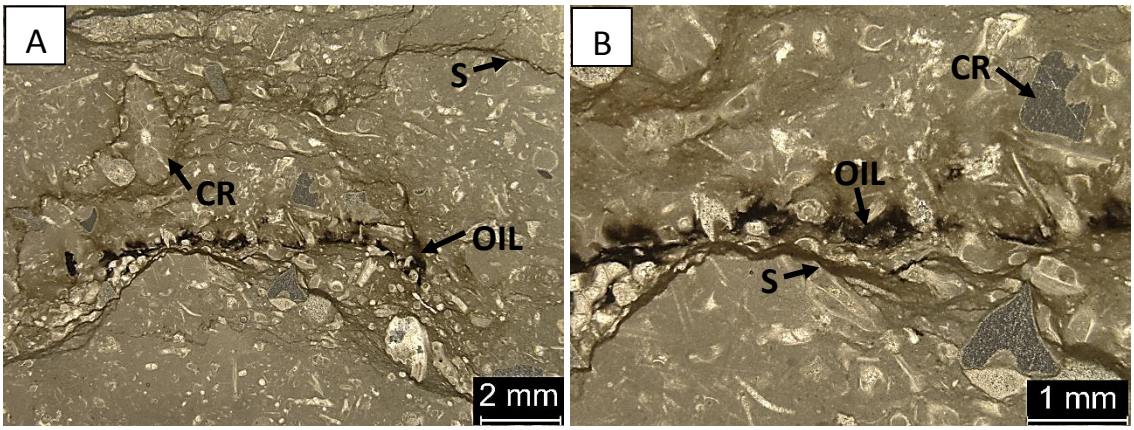

Figure 46: Thin section photomicrographs from Block 6 of Figure 35 to show its composition relative to the other blocks and the debris flow bed. **A.** Magnification at 25x. **B.** Magnification at 50x. This facies is a skeletal wackestone, very fine to very coarse grained, and poorly sorted. Contains 25% skeletal grains, 65% micrite matrix, 4% dead oil, and 6% blocky calcite cement (visual estimation). Skeletal grains include brachiopods (400µ – 750µ), crinoids (62.5µ – 1mm), bryozoans (62.5µ – 2mm). Dead oil can be seen along the stylolites.

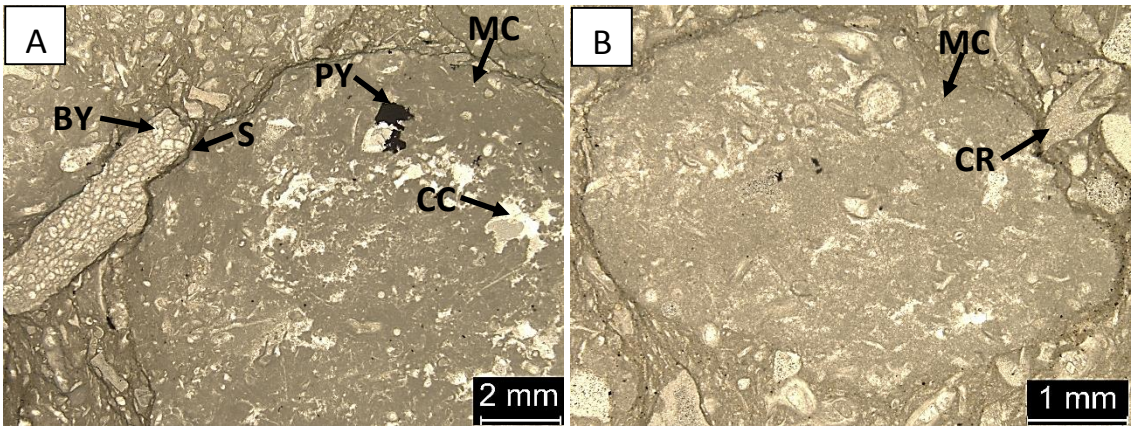

Figure 47: Thin section photomicrographs from the debris flow bed to show its composition relative to each of the blocks. **A.** Magnification at 25x. **B.** Magnification at 50x. This facies is a wackestone-packstone from the debris flow unit within the Compton Formation. Contains mudstone clasts ranging in size from very coarse sand to very coarse pebbles. The mudstone clasts are surrounded by a matrix of fine to coarse grained bryozoans (125 μ – 1mm), brachiopods (400 μ – 700 μ), and crinoids (125 μ – 2mm). These skeletal components are also contained within the mud clasts. Wispy stylolites, calcite cement, and pyrite can also be seen throughout.

Formation and flow mechanism: A plausible explanation for the development of the outrunner blocks found within the debris flow bed of the Compton Formation includes the activation of a slump. Tripsanas et al. (2008) defines a slump as a rotational slide characterized by displacement of relatively intact blocks over curved or spoon-like slip surfaces with limited downdip transport. Debris flows are often produced from a slump as broken clasts supported by a mud matrix (Tripsanas et al., 2008; De Blasio et al., 2006). Often associated with the slump rotation and debris flow are outrunner blocks, defined by De Blasio et al. (2006) as nearly intact pieces of debris that detach from a slowing-down submarine slide and flow ahead of the front. Development of the blocks is due to hydroplaning, acceleration, and final detachment of the head of submarine landslides and debris flows (Tripsanas et al., 2008; Ilstad et al., 2004). Elements stimulating the movement of the block include gravity, velocity, shape, surface roughness, and block orientation (De Blasio et al., 2006).

A diagram illustrating the processes involved during formation and flow of outrunner blocks is shown in Figure 48. In the initial detachment phase of an outrunner block, the block must be lubricated by hydroplaning. Lubrication occurs if the blocks move fast enough to induce pressure build-up in front of the debris flow, causing the head to lift off the seabed. Once the head is lifted off the seabed, this allows for intrusion of a water layer underneath the head. The block then builds up momentum and accelerates enough for final detachment (Ilstad et al., 2004). After detachment, it is possible for outrunner blocks to travel long distances (up to a km) on very low inclinations (less than 2˚), such as distally steepened ramps (Ilstad et al., 2004). The

hydroplaning block may leave a faintly visible track with linear patches of sediment along the track edges. A possible glide track of this type can be seen at the Jane outcrop just behind Block 1 in Figure 49 (Ilstad et al., 2004).

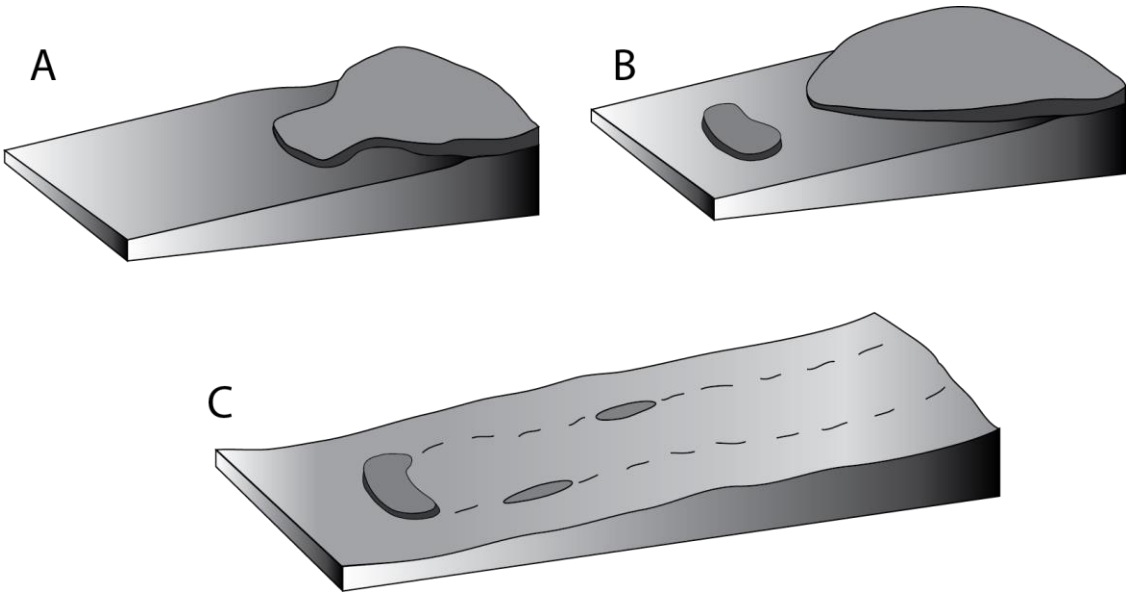

Figure 48: Diagram illustrating the formation and flow of outrunner blocks. A.) Detachment phase with lubricating front. B.) Outrunner block is formed and flows away from the main slide. C.) Hydroplaning block leaving a faintly visible track with linear patches of sediment along the track edges (Ilstad et al., 2004).

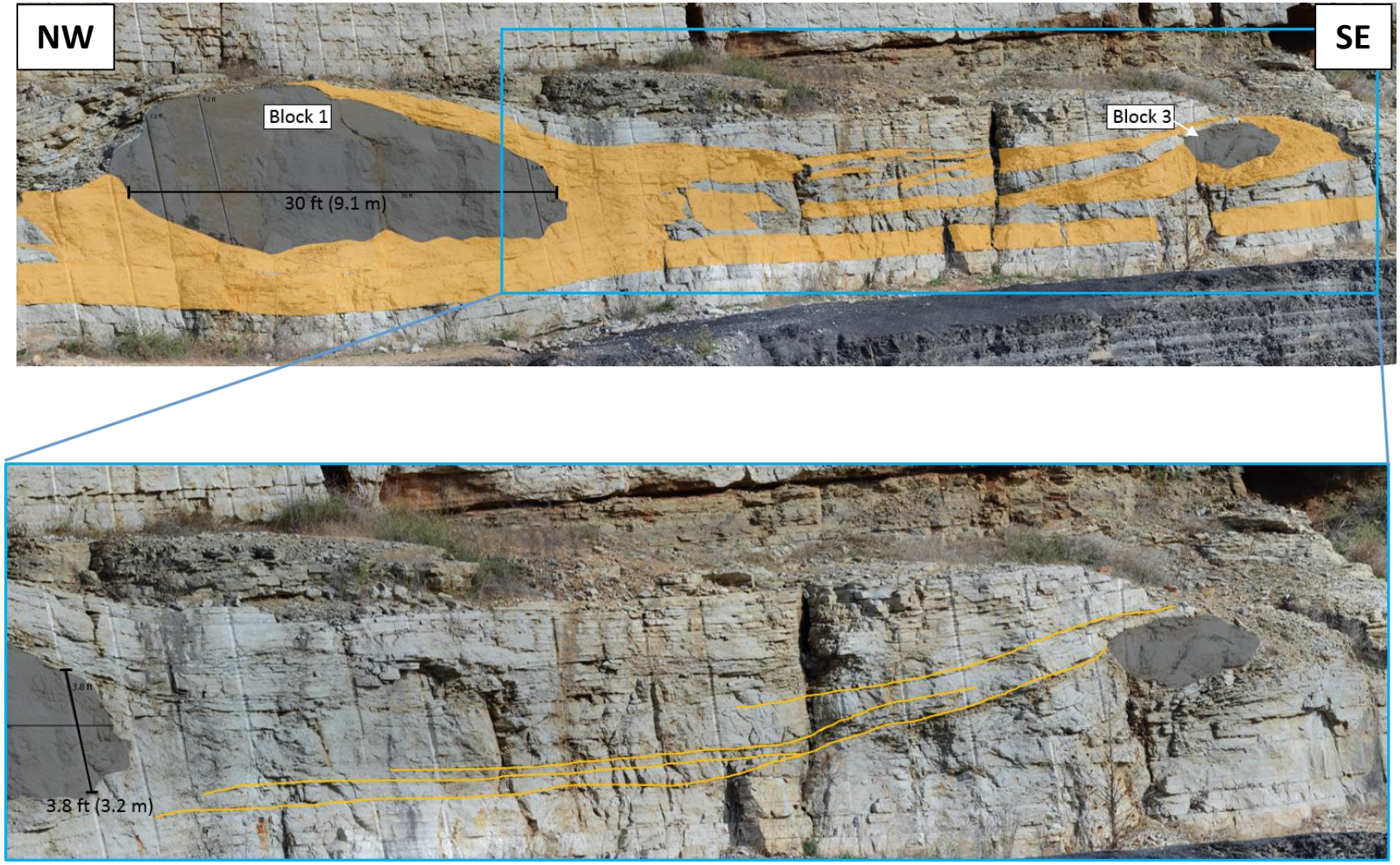

Figure 49: Top Gigapan photograph shows Block 1 and Block 3 (gray) and surrounding debris flow (orange). The lower Gigapan photograph shows possible glide tracks (orange lines) left behind by Block 1 as it moved down the distally steepened ramp to the northwest.

Triggering mechanism: The primary processes likely involved with initiating block movement include sediment loading (Schlager, 2005; Coniglio, 1986) and regional tectonism (Boardman, 2013; Heubeck, 1992; Gawthorpe and Clemmey, 1985; Moore, 1976). Autochthonous micrite in the form of layers, lenses, or mounds serves as an *in-situ* growth of a rigid body and adds additional weight to the slope or ramp (Schlager, 2005; Wolf, 1965). The mounds act as a rigid weight and represent localized loads capable of triggering slides and slumps (Schlager, 2005; Figure 50A). Coniglio (1986) describes a similar form of sediment loading within the Cow Head Group, a base-of-slope carbonate apron. In this case, synsedimentary shear zones in the form of brecciation, truncation surfaces, and slide zones represent deposition on an unstable sloping surface that eventually gives way to sediment failure.

The alternative explanation for triggering block movement is regional and/or local tectonism (Figure 50B; Boardman, 2013; Evans et al., 2011; Heubeck, 1992; Gawthorpe and Clemmey, 1985; Moore, 1976). Boardman (2013) provided evidence for active syndepositional tectonism throughout Kinderhookian and Osagean using conodont biostratigraphy and identifying unconformities throughout the Mid-Continent region. Evans et al. (2011) described regional tectonic behavior in southwestern Missouri as being made up of northwest-southeast trending transpressional faults that would have effected sedimentation during the Late Devonian and Early Mississippian. According to the Evans et al. (2011) model, flexure, loading, and tectonic subsidence were associated with the northwest-southeast regional faults. Resulting tectonic adjustments could have initiated movement of the outrunner blocks within the

Compton (Figure 50B). Based on evidence from Boardman (2013) and Evans et al. (2011), syndepositional tectonism is the favored mechanism for block movement in this study.

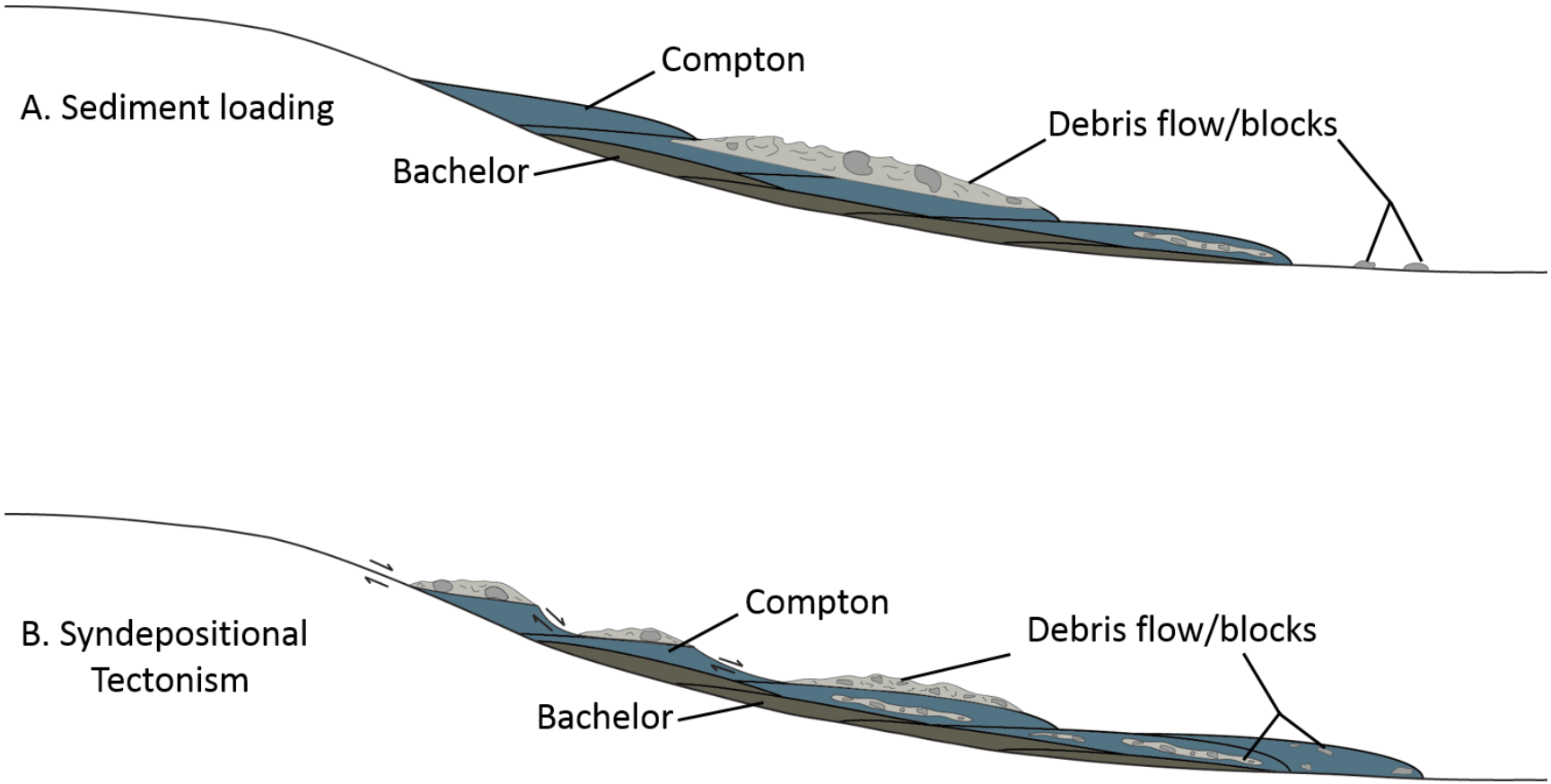

Figure 50: Mechanisms for initiation of block movement on a distally steepened ramp. **A.** Block movement initiated by sediment loading involves buildup of automicrite, which forms a rigid body and acts as extra weight on the ramp triggering a slide. **B.** Block movement initiated by syndepositional tectonism. Syndepositional tectonism was active during the Early Mississippian in the form of compressional and strike-slip fault movements and is the favored mechanism for initiation of block movement (Boardman, 2013; Evans et al., 2011). Modified from (Schlager, 2005; Coniglio, 1986; Gawthorpe and Clemmey, 1985).

Outside of the local study area, additional explanations are cited in support of tectonics triggering movement of submarine slides in the form of olistostromes and olistoliths (Heubeck, 1992; Moore et al., 1976). Olistostrome refers to the entire slide mass, which contains multiple olistoliths. Olistoliths are defined as coherent blocks, or megaclasts, of stratified sediment. Olistoliths commonly range from a few to less than ten kilometers in length and a few to hundreds of meters thick (Heubeck, 1992; Moore et al., 1976). Although there is a large size discrepancy between olistoliths and the blocks found at the Jane outcrop, it should be noted that the blocks continue to break up and travel tens of kilometers down the ramp from the line source they originated from (Ilstad et al., 2004).

Heubeck (1992) explains strike-slip faulting paired with rapid buildup of pore pressure from cyclic loading of seismic waves as a triggering mechanism for olistolith movement. Moore et al. (1976) explain a slide triggered by a seismically induced earthquake in combination with rapid sediment loading during the Late Quaternary glacial low sea level (Moore et al., 1976). An additional example is given by Gawthorpe and Clemmey (1985), involving slides and debris flows related to synsedimentary tectonic activity. Since tectonism was active during the Kinderhookian through Osagean time in the form of transpressional faults, the tectonic models explained by Heubeck (1992), Gawthorpe and Clemmey (1985), and Moore et al. (1976) are likely explanations behind the initiation of outrunner blocks (Evans, 2011; Wilhite et al., 2011).

Outrunner Block Example

Finneidfjord Slide: Outrunner blocks that have been previously documented in literature range in size from tens to hundreds of meters and can travel up to a kilometer on very gentle slopes of 1-2˚ (Tripsanas et al., 2008; De Blasio et al., 2006; Ilstad et al., 2004). Ilstad et al. (2004) document a recent example from the Finneidfjord slide that occurred in Norway on June 20, 1996. This slope failure occurred after detachment along a weak layer, which caused excess pore pressure and triggered the clay slide. The slide was examined in the field and in laboratory experiments to better understand the geometry and depositional patterns of the outrunner blocks. Based on a combination of side scan sonar and swath bathymetry mapping tools, the morphology of the subaqueous mass flow was divided into four different zones (Figure 51). Zone A contains the main bulk of sediment deposited into a lobe at 2.86˚. At Zone B, deposition becomes more scattered and individual blocks start to detach and spread out further downslope. These blocks are elongated, 131-230 ft (40-70 m) long, 33-66 ft (10-20 m) wide, and 3-7 ft (1-2 m) thick. Smaller blocks were deposited along Zone C and may be blocks in the same path or breakoffs from the largest block seen in Zone D. The blocks in Zone C are likely similar to the outrunner blocks within the Compton Formation at the Jane outcrop. Other recent examples of outrunner blocks associated with debris flows have been investigated in the Nigerian sea by Nissen et al. (1999) and in the Kitimat Arm of Canada by Prior et al. (1984).

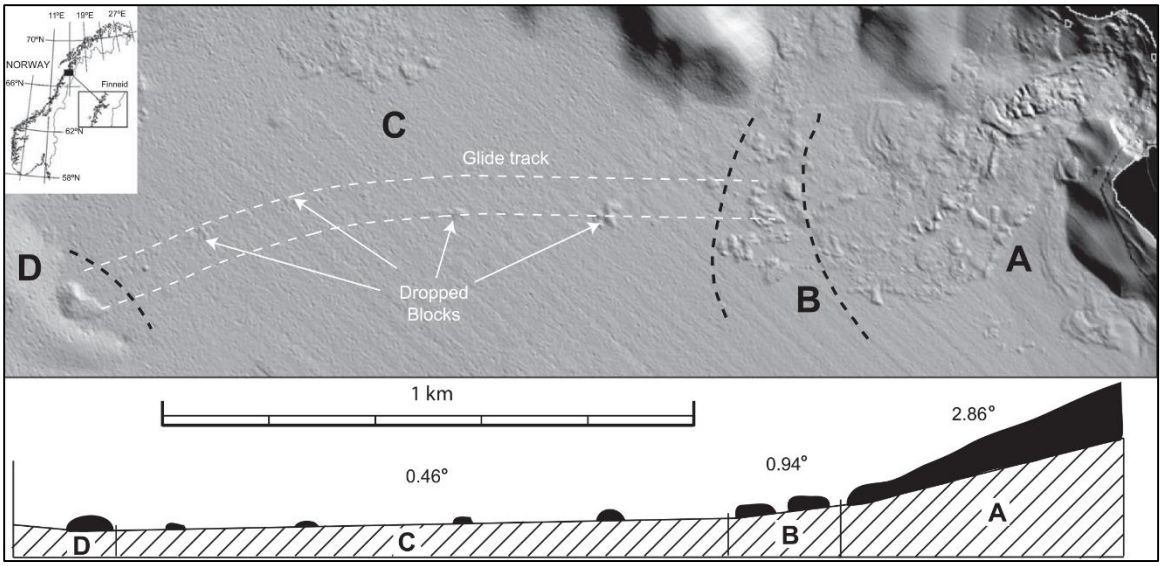

Figure 51: Finneidfjord slide with slide morphology divided into zones A: Main lobe. Zone B: Zone with scattered blocks. Zone C: Glide Zone. Zone D: Main outrunner block. Average slopes at each zone are shown in the lower panel. Although this specific example is not a distally steepened ramp, the lower panel resembles a similar profile to the distally steepened ramp. A likely location for the outrunner blocks within the Compton Formation at the Jane outcrop would be between Zone B and Zone C (Ilstad et al., 2004).

Depositional Model

Outrunner Blocks on a Distally Steepened Ramp: Based on the primary depositional facies present at the Jane outcrop, a distally steepened ramp model best represents the formations at the Jane outcrop. The primary facies types are dominated by mud-supported fabrics and were likely deposited in a more distal environment between storm wave base and fair weather wave base. Figure 532 is a model of a distally steepened ramp modified from Handford (1986), showing the distribution of depositional environments for the Jane outcrop formations outlined in the red box. The figure also includes localized mass transport deposits often associated with distally steepened ramps between fair weather wave base and storm wave base. The debris flow bed and multiple outrunner blocks seen at the study area would likely have taken place within the area outlined in a red circle in the lower portion of Figure 52. This schematic diagram demonstrates what a slump, debris flow, and outrunner blocks would look like in the context of a distally steepened ramp.

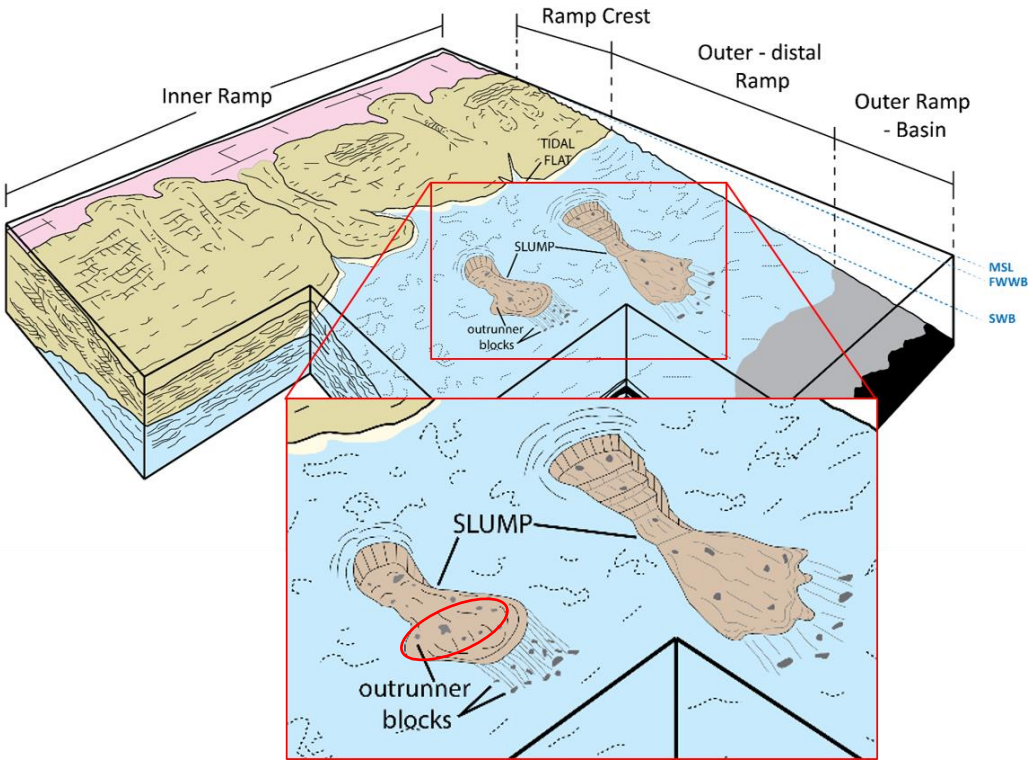

Figure 52: Schematic diagram illustrating the distribution of depositional environments for the Jane outcrop formations. Deposition of the Bachelor, Compton, Northview, and Pierson Formations occurred on the distally steepened ramp between fair weather wave base and storm wave base outlined by the red box. This portion of the ramp is magnified to show the slump features formed from displacement of intact blocks with limited downdip transport. The outrunner blocks associated with the slumps are also displayed. These features develop by hydroplaning, acceleration, and final detachment of the head of submarine slides and debris flows (Ilstad et al., 2004). Placement of the debris flow bed containing multiple outrunner blocks shown in the Gigapan image of Figure 35 likely would have taken place within the area circled in red (Modified from Handford, 1986).

Sequence Stratigraphy

Third order sequences have been constrained throughout the Mid-Continent using distinctive conodont types to recognize biostratigraphical correlations (Boardman, 2013). In this study, the biostratigraphic framework from Boardman (2013) was combined with the eustatic sea level curve from Haq and Schutter (2008) to identify two 3rd order sequences represented by the Kinderhookian and Osagean strata exposed at the study area. This sequence stratigraphic framework defined by biostratigraphy and eustatic sea level was refined to delineate 4th order high frequency sequences and 5th order high frequency cycles, identified by a combination of exposure horizons, flooding surfaces, and vertical stacking patterns. Understanding this hierarchy of cyclicity within the sequence stratigraphic architecture of the Jane outcrop reflects the distribution of vertical and lateral heterogeneity within the system (Grammer et al., 1996).

Based on Boardman's (2013) conodont zonations and the eustatic sea level curve from Haq and Schutter (2008), there are two 3rd order sequences represented by the Kinderhookian and Osagean strata exposed at the Jane outcrop. At the outcrop, the Compton Formation is primarily composed of bryozoan-crinoidal wackestones and packstones and represents the transgressive systems tract of the first 3rd order sequence. Superimposed on the transgressive leg of this 3rd order sequence are two probable 4th order high frequency sequences on the order of 2-5 m thick. Based on the sequence stratigraphic architecture of the Jane outcrop, the debris flow bed and associated outrunner blocks within the Compton Formation were likely deposited during

the transgressive systems tract of the second probable 4th order high frequency sequence. The debris flow and outrunner blocks are part of the thickest 4th order sequence at the outcrop (5 m thick), suggesting the blocks and debris flow filled the accommodation space provided during the transgressive leg of the succession. The debris flow bed was not uniformly deposited throughout the Compton Formation and multiple outrunner block movements occurred during deposition, adding elements of complexity to the sequence stratigraphic architecture of the system.

CHAPTER IV

SUMMARY AND CONCLUSIONS

Utilizing the 3rd order chronostatigraphy developed through a combination of conodont biostratigraphy (Boardman, 2013) and the established eustatic sea level curve (Haq and Schutter, 2008), this study has revealed a hierarchy of high frequency cyclicity within Lower and Middle Mississippian strata exposed at the Jane outcrop in southwest Missouri. In this study, detailed outcrop analysis has revealed the depositional environment is likely a distally steepened ramp rather than rimmed shelf, and has also provided an alternative model for the development of depositional features previously termed "*in situ* mud mounds" present throughout the Compton Formation. A distally steepened ramp depositional model more accurately displays the complex facies mosaics that may exist due to lateral migration of facies related to fluctuations in base level within the Kinderhookian and Osagian strata. The angle of slope for a carbonate ramp is generally less than 1˚, potentially resulting in significant shifts in facies during transitional icehouse/greenhouse periods of sea level change on the order of 20-70 m (Read, 1995; Burchette and Wright, 1992).

The outcrop-based data from this study was applied to the distally steepened ramp model of Mississippian-age strata in the Mid-Continent to produce updated

paleo-depositional maps, leading to a better understanding of overall shifts in depositional facies. The complex facies mosaics that exist across the distally steepened ramp due to lateral migration of facies related to fluctuations in base level complicate the lithostratigraphic-based nomenclature used throughout the Mid-Continent. Determining how Mississippian lithofacies fit into the regional sequence stratigraphic framework will increase the accuracy of paleo-depositional maps used for modeling changes in facies mosaics.

Anomalous Stratigraphy – North and south of the study area anomalously thick Kinderhookian and Osagean strata has been defined by Wilhite et al. (2011), who explained its existence to be related to forebulge and backbulge structures associated with syndepositional tectonism (Morris and Mazzullo, 2013; Mazzullo et al., 2011; Wilhite et al., 2001). “Anomalous” in this context refers to the abnormal thickness of the Compton, Northview, and Pierson Formations in areas surrounding the Jane outcrop (Figure 53). The anomalous Northview is located 100 miles north of the study area and is described by WIlhite et al. (2011) as a 50-80 ft (15.2-24.3 m) thick unit composed of siltstones and shaly siltstones of shallow-marine nearshore origin. The study area is located within the bounds of the anomalously thick Compton and Pierson Formations. In the Wilhite et al. (2011) model, these anomalously thick areas may have formed along submarine forebulge highs that vacillated north and south. Shallow subsiding backbulge basins formed immediately ahead of forebulge highs and migrated over time (Morris and Mazzullo, 2013). According to this model, the anomalous Northview in Figure 53 is a

part of the backbulge basin and shelf, while the anomalous Pierson and Compton are part of the forebulge province (Wilhite et al., 2011).

An alternative model to Wilhite's (2011) forebulge/backbulge model was derived from a sequence stratigraphic approach and includes modified paleo-depositional maps that better illustrate the complexity of shifting facies belts that likely occurred as a result of Milankovitch-scale sea level change. The modified maps are based on Gutschick and Sandberg's (1983) paleo-depositional model, which shows the study area as a "rimmed shelf." After detailed outcrop analysis, the "rimmed shelf" may actually be a slight break in the distally steepened ramp depositional model.

Sequence Stratigraphy – Based on conodont biostratigraphy from Boardman (2013), the eustatic sea level curve defined by Haq and Schutter (2008), and the depositional facies defined in this study, two 3rd order sequences occurred during deposition of the Kinderhookian and Osagean strata exposed at the Jane outcrop (Figure 54). The first 3rd order sequence is represented by the Bachelor, Compton, and Northview Formations. Deposition of the Bachelor Formation occurred during a transgressive systems tract (TST), depositing a calcareous shale facies at the base of the ramp (Figure 54, T1). The wackestones and packstones of the Compton Formation were also deposited during the transgressive leg of the first 3rd order sequence (Figure 54, T2). Tectonic failure triggered block movement and produced a debris flow within the Compton (Figure 54, T2.5). Deposition of the Northview Formation occurred during the highstand systems tract (HST) of the first 3rd order sequence and serves as the boundary

between the two 3rd order sequences (Figure 54, T3). As evidenced by the stacking patterns and subaerial exposure surfaces present at the outcrop, a flooding event occurred after deposition of the Northview Formation and was followed by deposition of the Pierson Foromation during the highstand systems tract (Figure 54, T4) included within the second 3rd order sequence.

Alternative Explanations – As an alternative explanation to the forebulge/backbulge model proposed by Wilhite et al. (2011), localized subsidence may have been present throughout the Mid-Continent area during deposition of the Northview Formation. The anomalous area may have been affected by more rapid subsidence than the study area during time of Northview deposition, resulting in increased aggradation of the Northview strata 100 miles north of the study area. Currently, no biostratigraphy has been completed on the anomalous Northview strata. Based on its description as shallow-marine, nearshore origin, it may be consistent with a tidal flat depositional environment similar to that seen at the Jane outcrop. If the depositional systems of the Jane and anomalous areas were similar during deposition of the Northview strata, a decrease in the level of rising sea level at the anomalous area would allow for tidal flat deposits to aggrade and "keep up" with base level, depositing an anomalously thick package. In contrast, sea level may have risen at a faster rate closer to the Jane outcrop, resulting in a much thinner (3-5 ft; 1-1.5 m) Northview package at the study area.

Additionally, the anomalously thick Northview Formation 100 miles north of the study area may have been deposited during a flooding event following the relative sea level fall and original deposition of the Northview strata at the study area. This flooding event would have resulted in the geometry of the Northview strata to backstep towards the anomalously thick area 100 miles north of the study area. This would result in the anomalous Northview deposited as part of the transgressive systems tract of the second 3rd order sequence, which would not have been captured at the Jane outcrop. During the flooding event that deposited the anomalously thick Northview 100 miles north, the study area may have caught the early part of high frequency transgressive systems tract, while the majority of the system was further north during the highstand systems tract.

As a result of this study, it is evident that each of the above explanations could have caused significant differences in Northview thickness at the study area versus that of the anomalous section 100 miles north of the study area. It may also be that a combination of localized subsidence and a decline in the rate of rising sea level resulted in a thicker package 100 miles north of the study area. Each of the alternative explanations may have also occurred during increased erosional conditions at the study area, causing the Northview strata at the Jane outcrop to thin at a faster rate than that of the anomalous Northview strata.

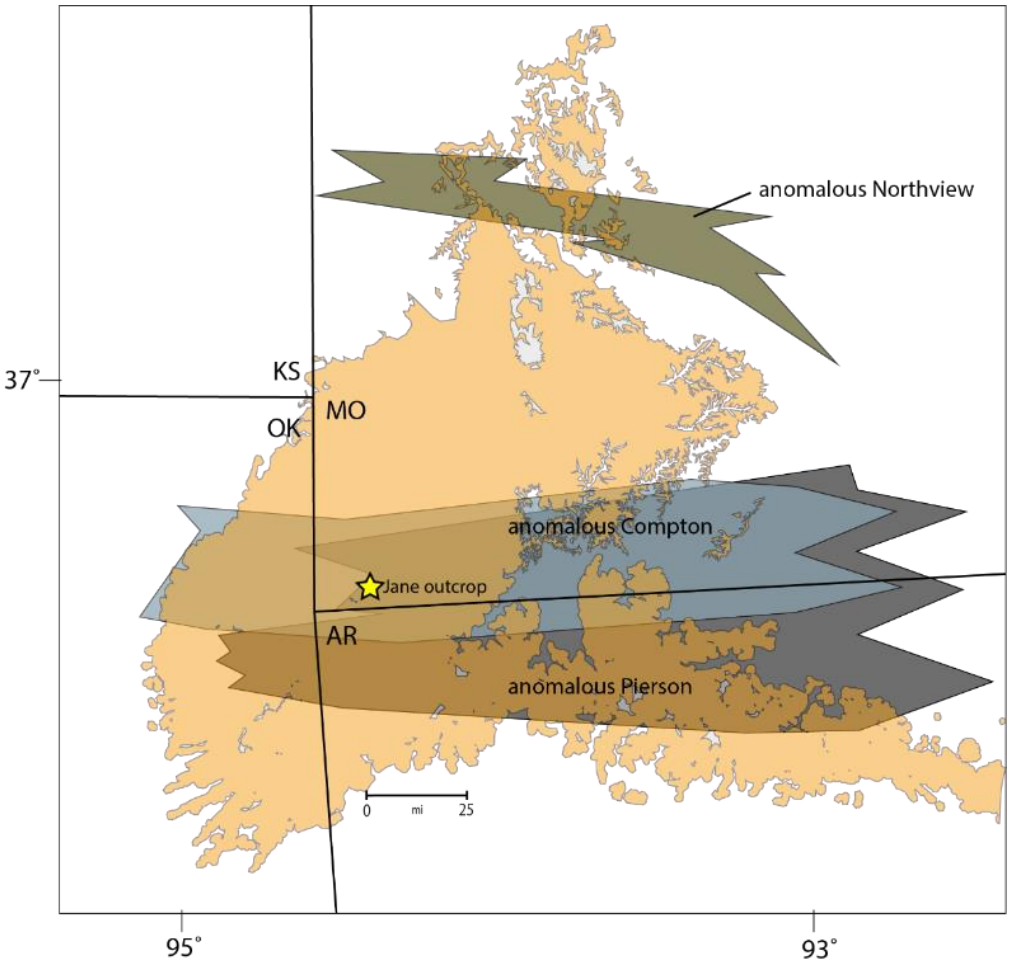

Figure 53: Distribution of Mississippian strata across the Mid-Continent region. The Mississippian outcrop belt is shown in orange and the Jane outcrop study area is located at the yellow star. The "anomalous stratigraphy" defined by Wilhite et al. (2011) includes the Compton (blue), Northview (green), and Pierson (gray) Formations. Alternative explanations for the deposition of the anomalous Northview strata include increased localized subsidence, a decrease in the rate of sea level rise 100 miles north of the Jane outcrop, and erosion (Modified from Wilhite et al., 2011).

Integrating this sequence stratigraphic approach with an understanding of the probable complexity of facies mosaics from modern analogs (Grammer et al., 2004) has led to a modified time-series of paleo-depositional maps that illustrate the dynamic facies model and associated shifts in facies belts related to Milankovitch-scale sea level

change (Figures 55 – 61). In each time slice, the shelf margin and shelf edge areas originally defined by Gutschick and Sandberg (1983) are subtly adjusted based on interpretations made from the integrated approach outlined in this study.

The Bachelor Formation is a calcareous shale unit and therefore likely represents a transgressive systems tract (Figure 55). With deposition of the Compton Formation, sea level gradually fell in conjunction with deposition of crinoidal-bryozoan wackestones and packstones (Figure 56). During this time, a tectonic failure along the ramp may have caused a slump feature responsible for deposition of a debris flow and multiple outrunner blocks (Figure 57). Relative sea level then fell, depositing the Northview Formation in a tidal flat environment as a part of the highstand systems tract (Figure 58). Deposition of the anomalous Northview is represented by Figure 59, which could possibly be due to localized subsidence and/or increased deposition in conjunction with sea level rise. Based upon the stacking patterns defined in this study and the subaerial exposure crust at the top of the Northview Formation, a flooding event likely occurred after deposition of the Northview Formation and before deposition of the Pierson Formation. The Pierson Formation was likely deposited during the transgressive systems tract (TST) and highstand systems tract (HST) of the second 3rd order sequence (Figure 60-61).

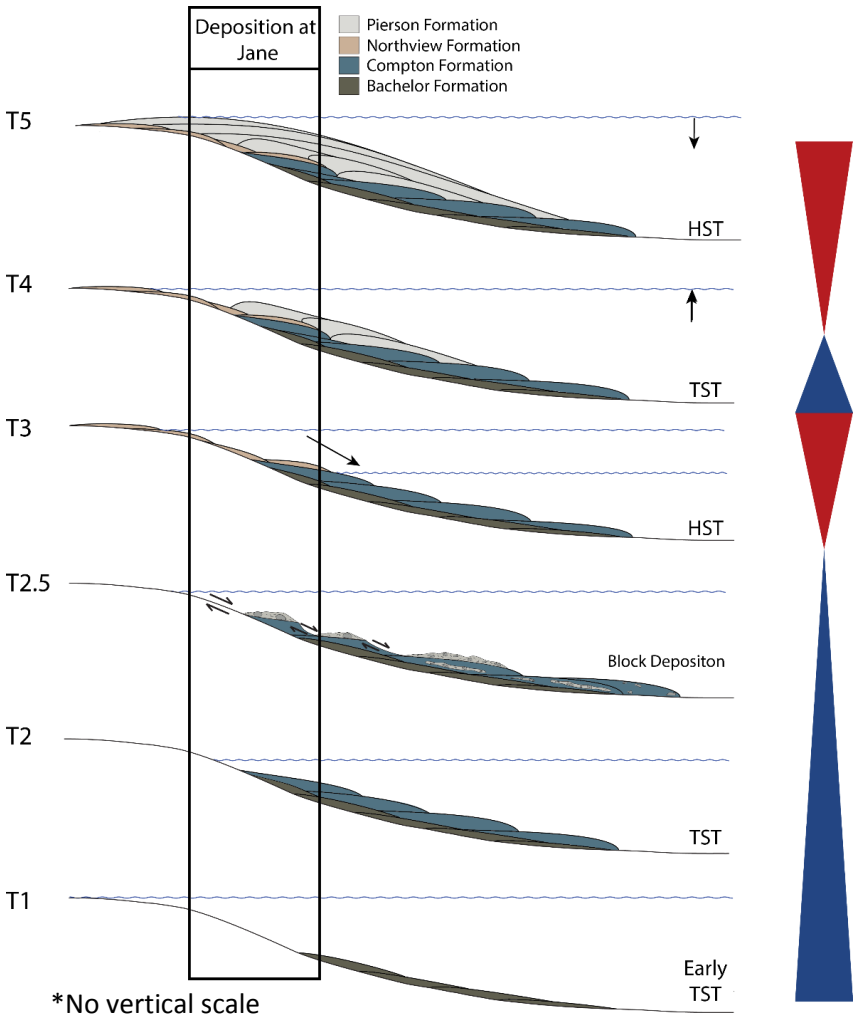

Figure 54: Cross-sectional distally steepened ramp models show deposition specific to each formation during sea level change throughout Mississippian time (T1 – T4) during the two 3rd order sequences defined by Boardman's (2013) conodont biostratigraphy and the eustatic sea level curve of Haq and Schutter (2008). Deposition of the Bachelor Formation (T1) occurred during a transgressive systems tract (TST), depositing a calcareous shale facies at the base of the ramp. The wackestones and packstones of the Compton Formation were also deposited during the transgressive leg of the first 3rd order sequence (T2). Tectonic failure triggered block movement and produced a debris flow within the Compton (T2.5). Deposition of the Northview Formation occurred during the highstand systems tract (HST) of the first 3rd order sequence and serves as the boundary between the two 3rd order sequences (T3). As evidenced by the stacking patterns and subaerial exposure surfaces present at the outcrop, a flooding event occurred after deposition of the Northview Formation and was followed by deposition of the Pierson Formation during the highstand systems tract (T4) that marks the second 3rd order sequence (Ramp profiles modified from Schlager, 2005).

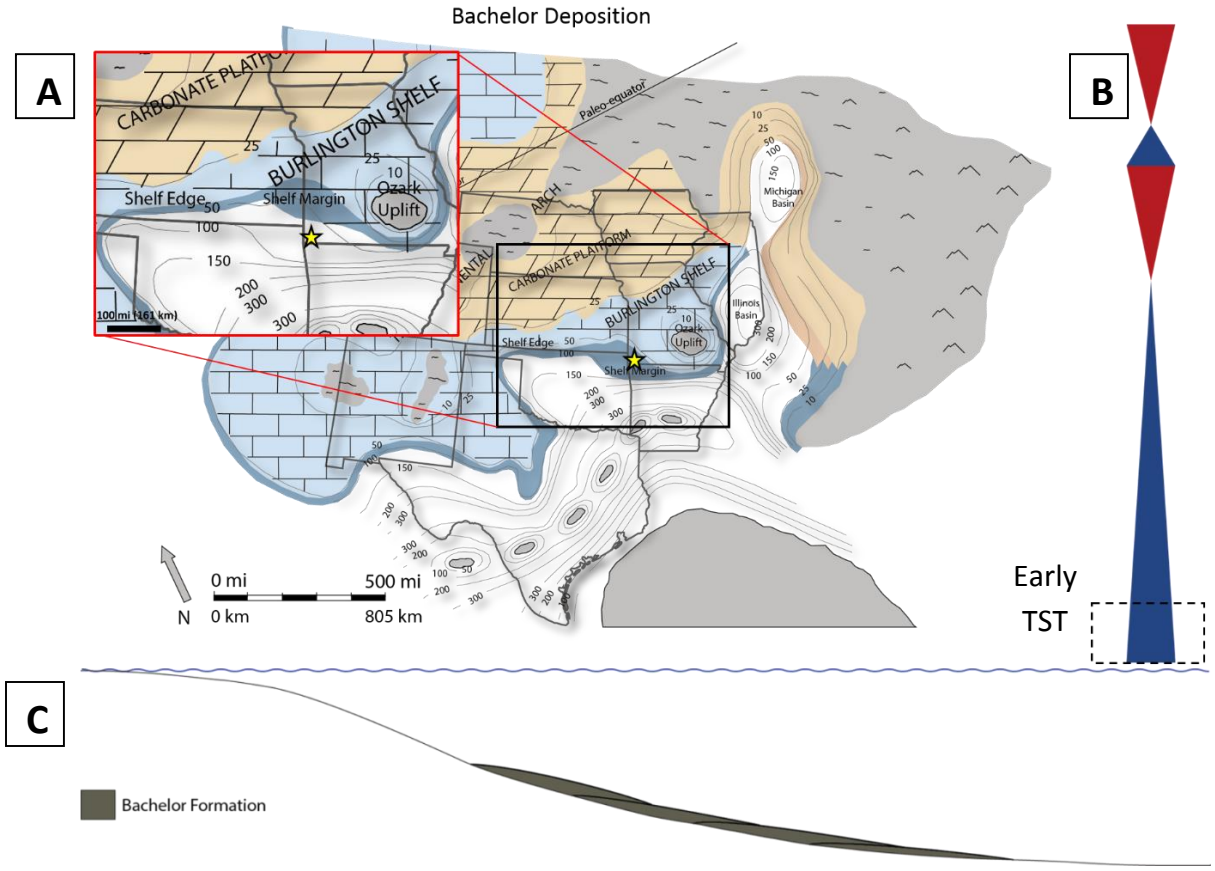

Figure 55: (A) Paleo-depositional map, (B) 3rd order sequences constrained by biostratigraphy (Boardman, 2013) and eustatic sea level (Haq and Schutter, 2008), and (C) ramp model during deposition of the Bachelor Formation at the Jane outcrop. The Bachelor is a thin, calcareous shale unit that represents the early part of the transgressive systems tract (TST). (A) Study location is at the yellow star. The larger view of the paleo-depositional map is the Gutschick and Sandberg (1983) version (black outline). Outlined in the red box is the version that has been edited in this study. Movement of the shelf margin and shelf edge areas have been adjusted to more accurately represent deposition of the Bachelor Formation. (B) Outlined box illustrates the part of the first 3rd order sequence the Bachelor Formation was deposited. (C) Ramp model showing the Bachelor Formation deposited on a distally steepened ramp during the transgressive leg of the first 3rd order sequence (Modified from Gutschick and Sandberg, 1983).

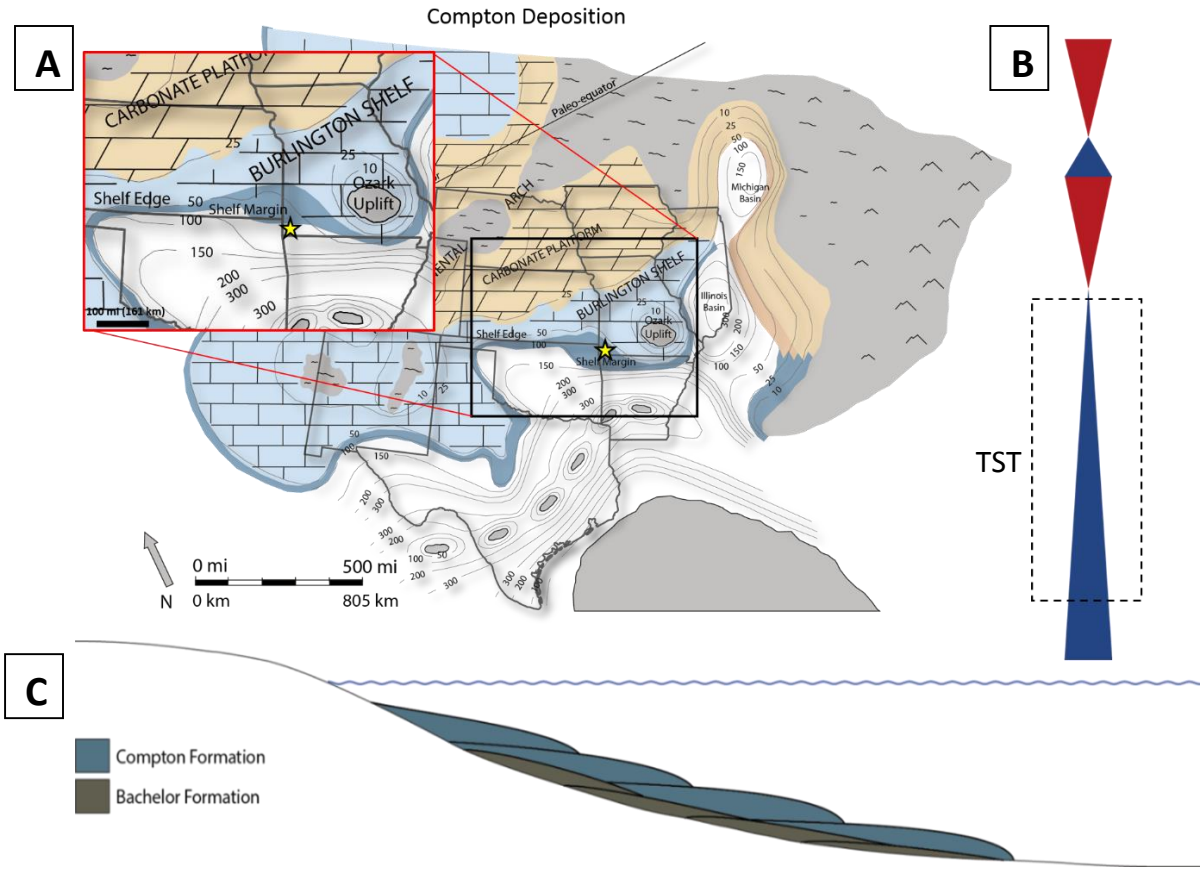

Figure 56: (A) Paleo-depositional map, (B) 3rd order sequences constrained by biostratigraphy (Boardman, 2013) and eustatic sea level (Haq and Schutter, 2008), and (C) ramp model during deposition of the Compton Formation at the Jane outcrop. The Compton is a gray, skeletal wackestone to packstone unit that represents the transgressive systems tract (TST) of the first 3rd order sequence. (A) Study location is at the yellow star. The larger view of the paleo-depositional map is the Gutschick and Sandberg (1983) version (black outline). Outlined in the red box is the version that has been edited in this study. Movement of the shelf margin and shelf edge areas have been adjusted to more accurately represent deposition of the Compton Formation during the transgressive systems tract. (B) Outlined box illustrates the part of the sequence the Compton Formation was deposited. (C) Ramp model showing the Compton Formation deposited on a distally steepened ramp during the TST of the first 3rd order sequence, after deposition of the Bachelor Formation (Modified from Gutschick and Sandberg, 1983).

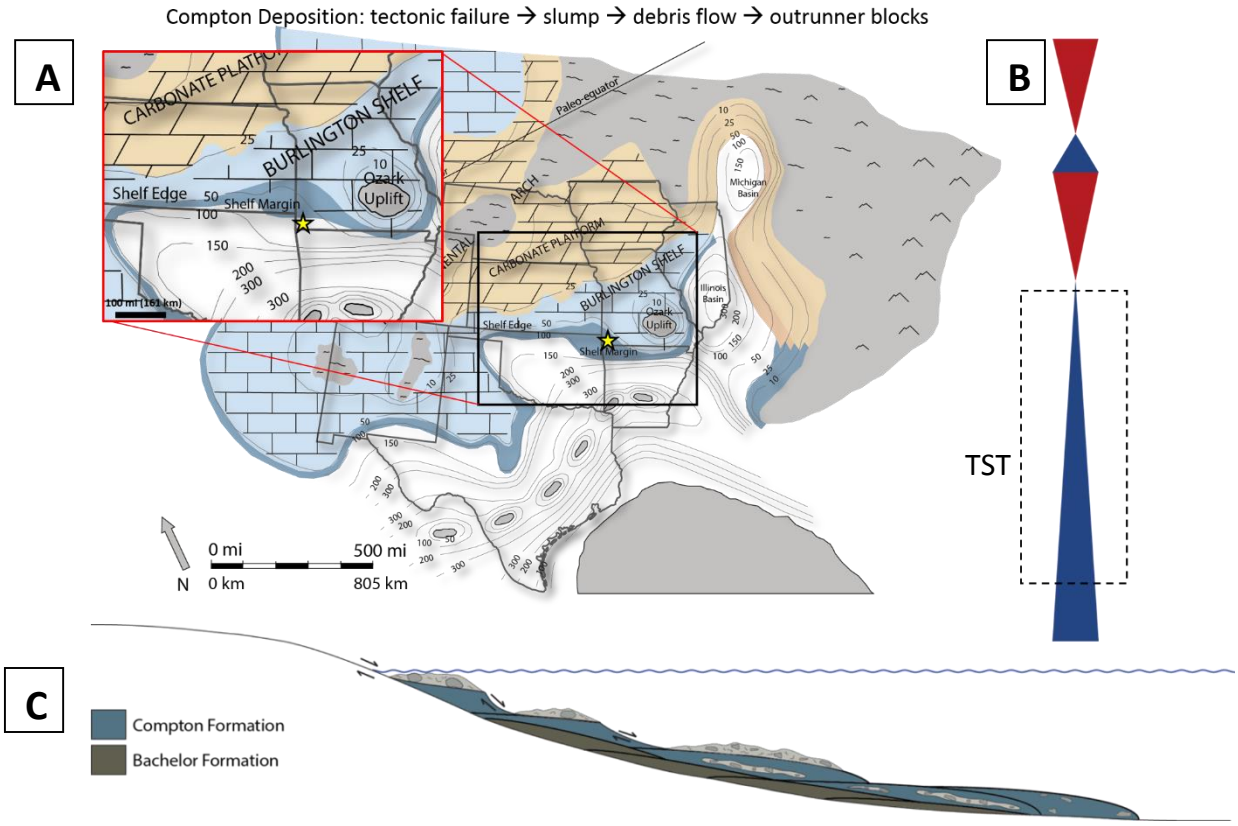

Figure 57: (A) Paleo-depositional map, (B) 3rd order sequences constrained by biostratigraphy (Boardman, 2013) and eustatic sea level (Haq and Schutter, 2008), and (C) ramp model during deposition of the blocks found within the Compton Formation at the Jane outcrop. The Compton is a gray, skeletal wackestone to packstone unit that represents the transgressive systems tract (TST) of the first 3rd order sequence. (A) The larger view of the paleo-depositional map is the Gutschick and Sandberg (1983) version (black outline). Outlined in the red box is the version that has been edited in this study. Movement of the shelf margin and shelf edge areas have been adjusted to more accurately represent deposition of the Compton Formation during the TST. (B) Outlined box illustrates the part of the sequence the Compton Formation was deposited. (C) Ramp model showing block deposition within the Compton Formation on a distally steepened ramp during a transgression. Tectonic failure likely initiated slump movement, depositing a debris flow and outrunner blocks (Modified from Gutschick and Sandberg, 1983).

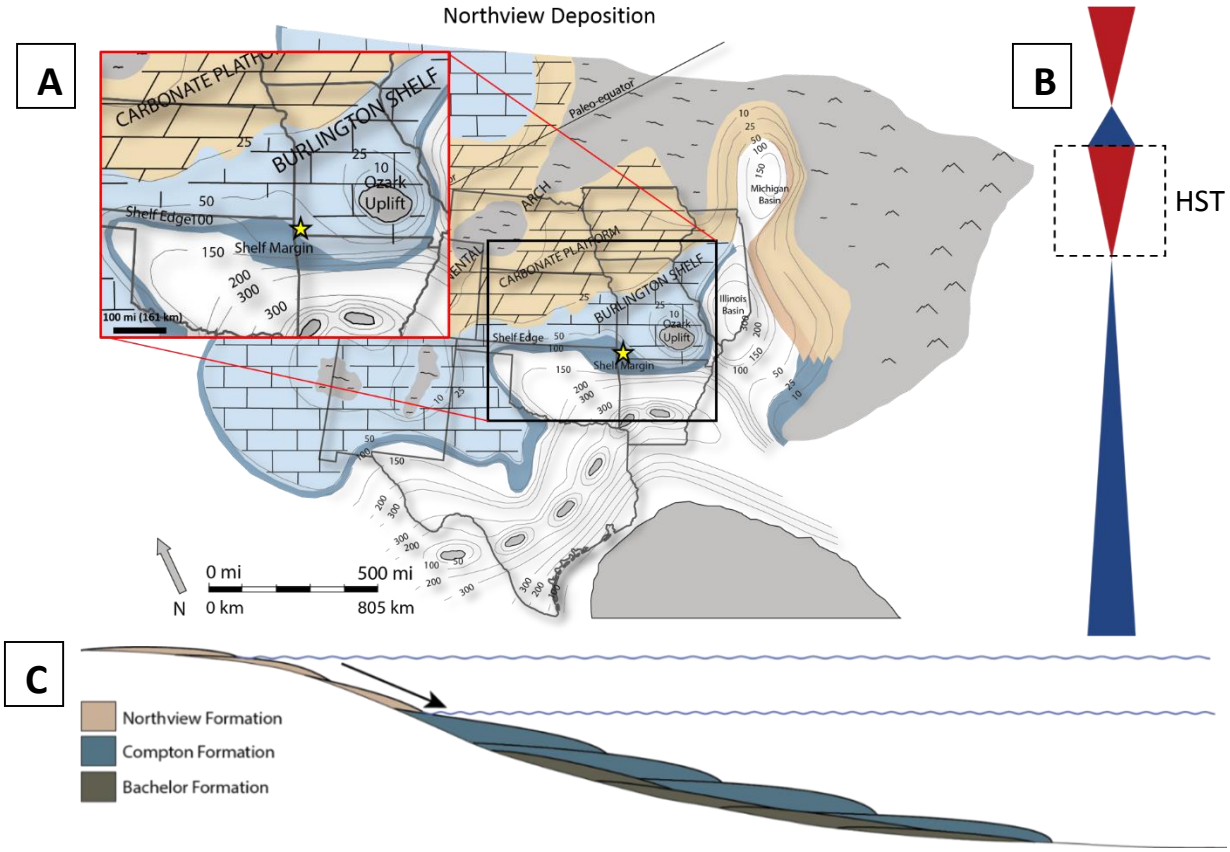

Figure 58: (A) Paleo-depositional map, (B) 3rd order sequences constrained by biostratigraphy (Boardman, 2013) and eustatic sea level (Haq and Schutter, 2008), and (C) ramp model during deposition of the Northview Formation at the Jane outcrop. The Northview is composed of wackestones, packstones, and grainstones deposited in a tidal flat environment that represents the highstand systems tract (HST) of the first 3rd order sequence. (A) Study location is at the yellow star. The larger view of the paleo-depositional map is the Gutschick and Sandberg (1983) version (black outline). Outlined in the red box is the version that has been edited in this study. Movement of the shelf margin and shelf edge areas have been adjusted to more accurately represent deposition of the Northview Formation during the HST. (B) Outlined box illustrates the part of the first 3rd order sequence the Northview Formation was deposited. (C) Ramp model showing the Northview Formation deposited on a distally steepened ramp during the HST of the first 3rd order sequence, after deposition of the Bachelor and Compton Formations (Modified from Gutschick and Sandberg, 1983).

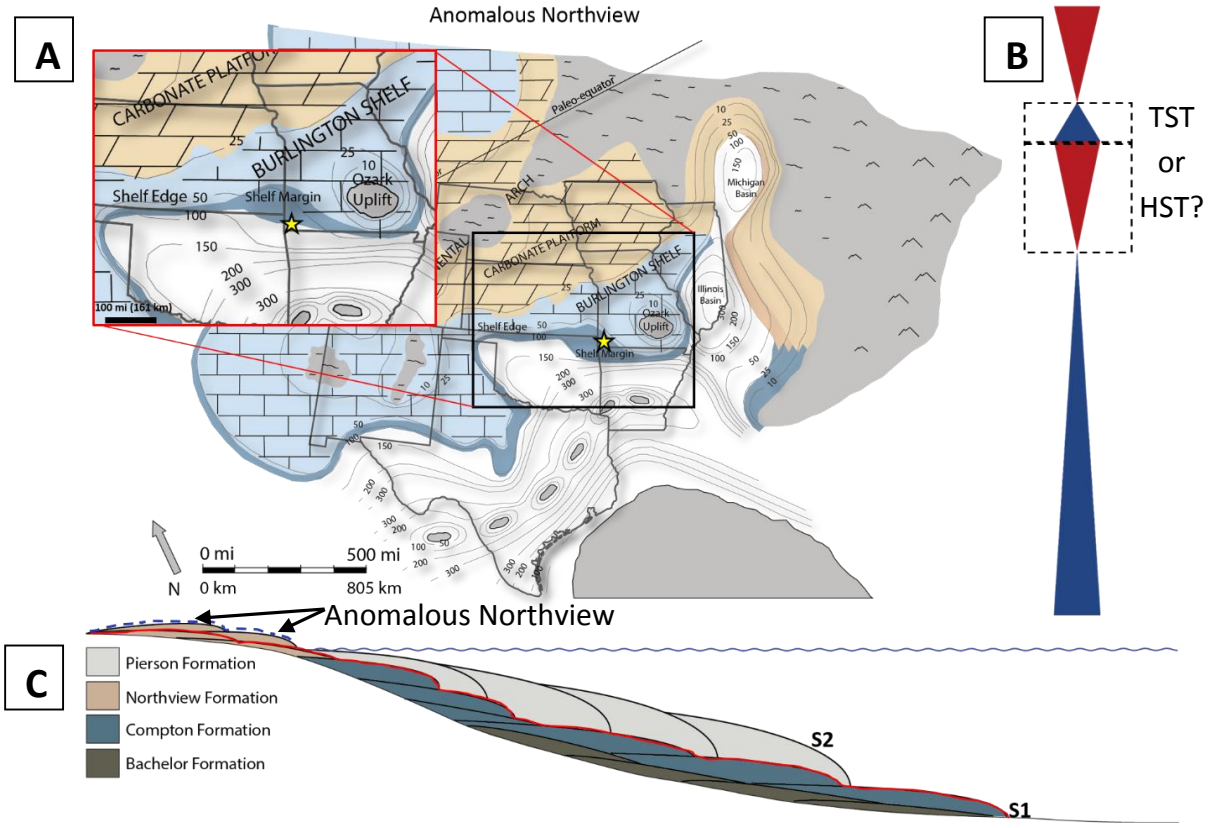

Figure 59: (A) Paleo-depositional map, (B) 3rd order sequences constrained by biostratigraphy (Boardman, 2013) and eustatic sea level (Haq and Schutter, 2008), and (C) ramp model during deposition of the anomalously thick Northview Formation 100 miles north of the Jane outcrop. At this location, the Northview is composed of siltstones and shaly stilstones of a nearshore origin. Explanations for the anomalous thickness include increased subsidence and/or increased deposition with sea level rise. (A) Study location is at the yellow star. The larger view of the paleo-depositional map is the Gutschick and Sandberg (1983) version (black outline). Outlined in the red box is the version that has been edited in this study. Movement of the shelf margin and shelf edge areas have been adjusted to more accurately represent deposition of the Northview Formation during increased subsidence and/or increased deposition with sea level rise. (B) The two outlined boxes illustrate the part of the first or second 3rd order sequence the anomalous Northview strata could have been deposited in. If increased subsidence caused deposition of the anomalously thick Northview, this would likely correspond to deposition during the HST of the first 3rd order sequence. If increased deposition during sea level rise caused the anomalously thick Northview, this would likely correspong to deposition during the TST of the second 3rd order sequence. (C) Ramp model showing the Anomalous Northview deposited on a distally steepened ramp during either the HST of the first 3rd order sequence or the TST of the second 3rd order sequence (Modified from Gutschick and Sandberg, 1983).

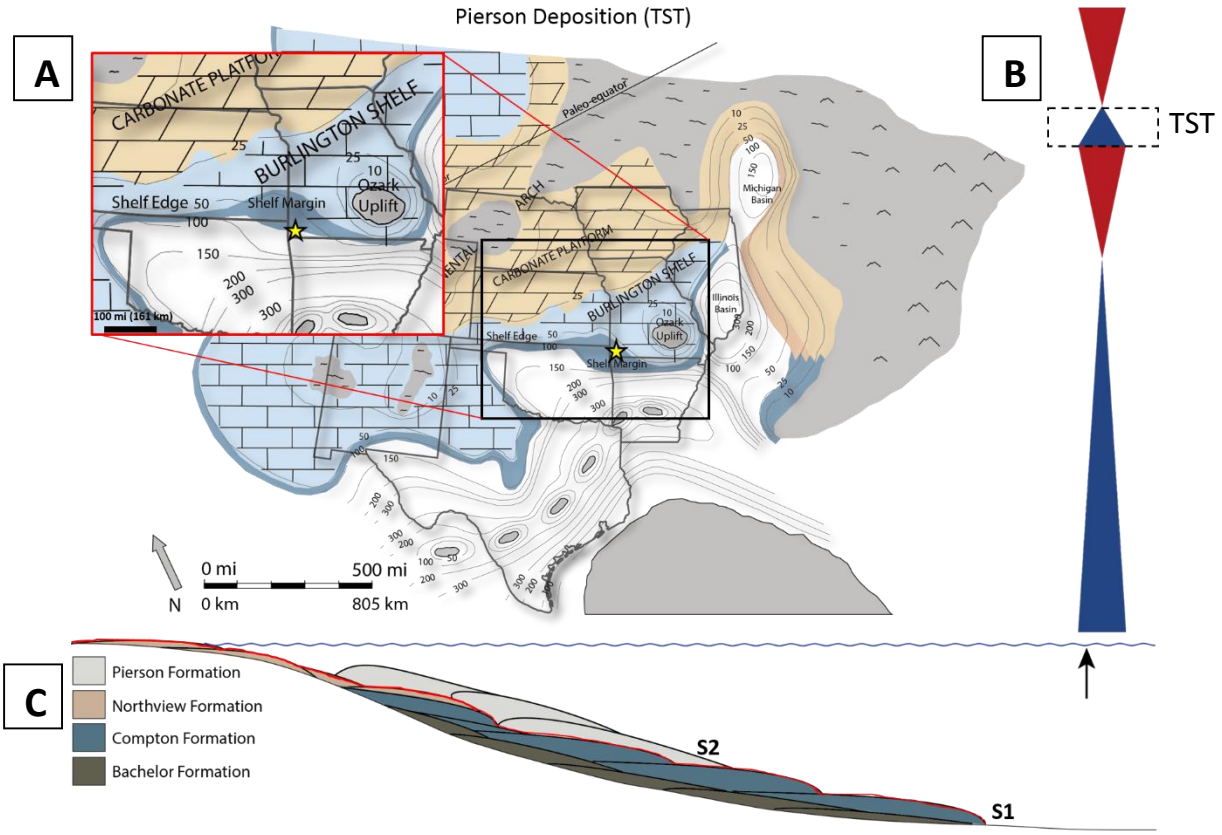

Figure 60: (A) Paleo-depositional map, (B) 3rd order sequences constrained by biostratigraphy (Boardman, 2013) and eustatic sea level (Haq and Schutter, 2008), and (C) ramp model during deposition of the Pierson Formation during the transgressive systems tract (TST) at the Jane outcrop. The Pierson Formation is composed of mud-lean packstones and grainstones deposited after a flood and during the second 3rd order sequence. (A) Study location is at the yellow star. The larger view of the paleo-depositional map is the Gutschick and Sandberg (1983) version (black outline). Outlined in the red box is the version that has been edited in this study. Movement of the shelf margin and shelf edge areas have been adjusted to more accurately represent deposition of the Pierson Formation during a TST. (B) Outlined box illustrates the part of the second 3rd order sequence the Pierson Formation was deposited. (C) Ramp model showing the Pierson Formation deposited on a distally steepened ramp during the TST of the second 3rd order sequence, after deposition of the Bachelor, Compton, and Northview Formations (Modified from Gutschick and Sandberg, 1983).

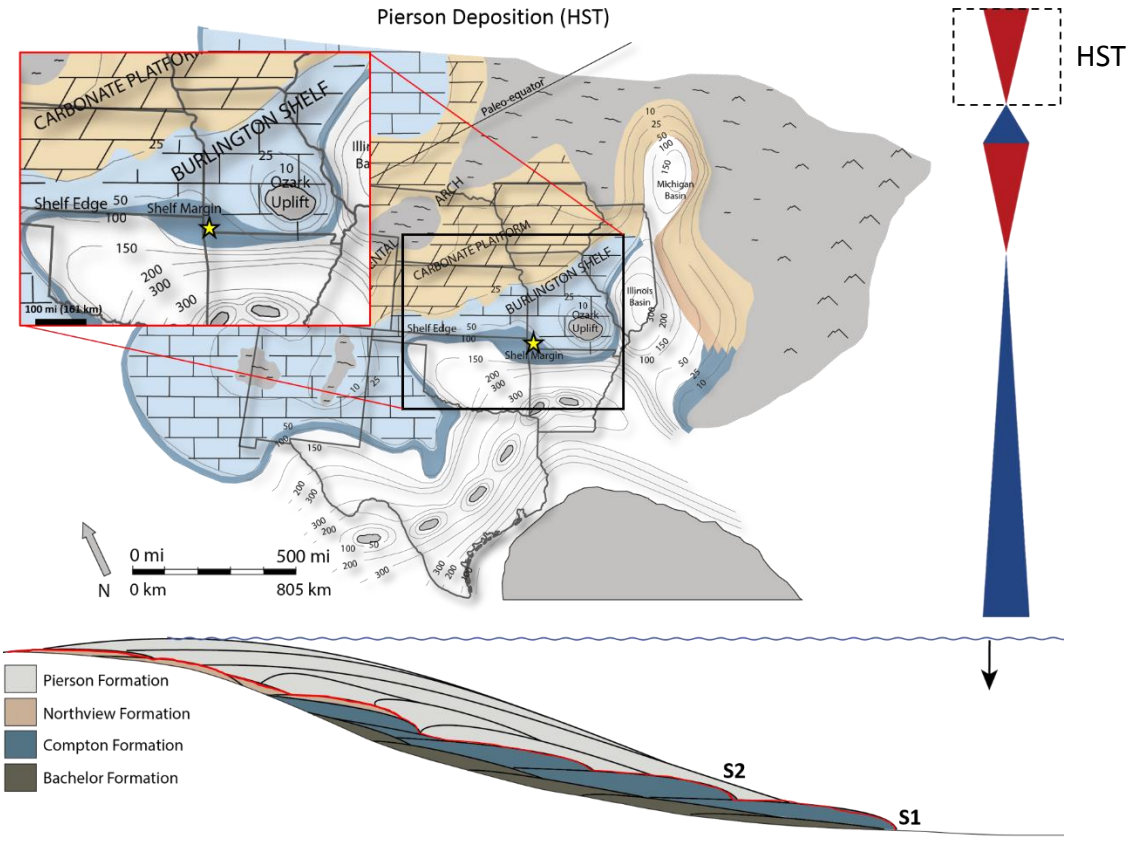

Figure 61: (A) Paleo-depositional map, (B) 3rd order sequences constrained by biostratigraphy (Boardman, 2013) and eustatic sea level (Haq and Schutter, 2008), and (C) ramp model during deposition of the Pierson Formation at the Jane outcrop. The Pierson Formation is dominated by mud-lean packstones and grainstones deposited after a flood and during the second 3rd order sequence. (A) Study location is at the yellow star. The larger view of the paleo-depositional map is the Gutschick and Sandberg (1983) version (black outline). Outlined in the red box is the version that has been edited in this study. Movement of the shelf margin and shelf edge areas have been adjusted to more accurately represent deposition of the Pierson Formation during a HST. (B) Outlined box illustrates the part of the second 3rd order sequence the Pierson Formation was deposited. (C) Ramp model showing the Pierson Formation deposited on a distally steepened ramp during the HST of the second 3rd order sequence, after deposition of the Pierson during the TST, Bachelor, Compton, and Northview Formations (Modified from Gutschick and Sandberg, 1983).

In addition to changes of the paleo-depositional maps, a conceptual diagram illustrates the dynamic shifts in facies that exist across the distally steepened ramp due to lateral migration of facies (Figure 62). This diagram illustrates deposition of Lower and Middle Mississippian-age formations across a distally steepened ramp. As sea level falls, each facies shifts in a seaward direction. During the ensuing transgression, the same facies shift once more, this time in a landward direction. As Milankovitch-scale sea level change controls facies distribution within the system, confusion easily arises as a result of applying lithologic names to Mid-Continent Mississippian formations. Without integration of sequence stratigraphy and shifts in complex facies mosaics, accurately distinguishing between Mississippian-age formations distributed throughout the Mid-Continent is impossible.

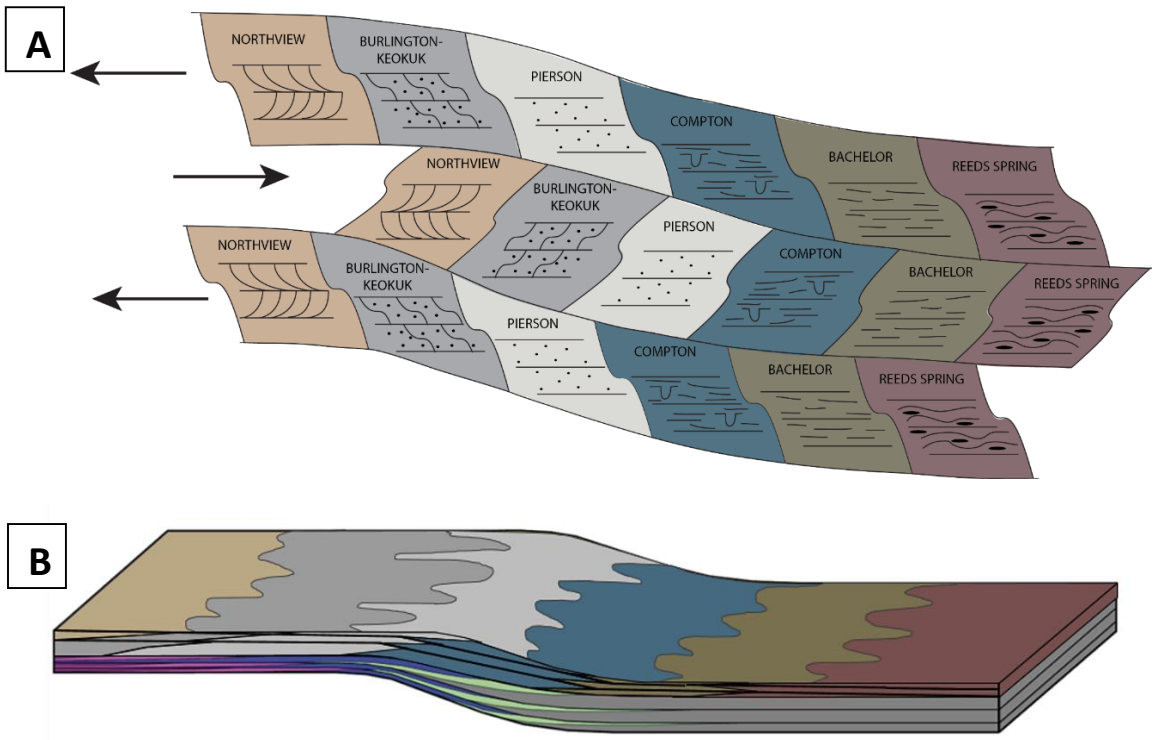

Figure 62: (A) Conceptual diagram that illustrates the range of Mississippian facies deposited in a transect across the distally steepened ramp from the most proximal position on the ramp (left) to the more distal portion of the ramp (right). This figure demonstrates shifts in facies associated with Mississippian-age formations as a result of changes in base level (arrows), and as such does not necessarily follow the lithostratigraphically defined "formation" succession. This model helps explain the discrepancy between lithologically-based nomenclature and sequence stratigraphy used throughout the Mid-Continent. It should be noted that this model only applies under the assumption that all facies were deposited and preserved. All facies may have been present at any one time during deposition, but may have not been equally developed in all places, in which case this conceptual model would need to be adjusted to accommodate missing facies. (B) Two dimensional view illustrates complex stacking patterns formed from dynamic shifts in facies related to Milankovitch-scale sea level change. Lateral migration of facies within the Mississippian depositional regime would result in this type of facies complexity (Modified from Harris et al., 2011).

This study used an integrated approach to determine the high resolution sequence stratigraphic architecture of a Mississippian-age outcrop in Jane, Missouri. Gigapan imagery, primary facies, depositional environments, gamma ray, thin section analysis, and scanning electron microscopy were combined in an effort to delineate the vertical and lateral heterogeneity within the high resolution sequence stratigraphic framework of the Lower and Middle Mississippian-age strata at the Jane outcrop. Key conclusions from this study are:

1. Sequence stratigraphic architecture is responsible for controlling reservoir distribution. This architecture is controlled by Milankovitch-related sea level changes, which often produce complex facies mosaics and compartmentalize reservoir flow units.
2. Conodont biostratigraphy in combination with the eustatic sea level curve has constrained 3rd order sequences within the Mississippian-age strata throughout the Mid-Continent region. Based on this outcrop study, a hierarchy of cyclicity is recognizable throughout the exposed Kinderhookian and Osagean strata. It is probable that these high frequency events are at the 4th and 5th order scales.
3. In this study, detailed outcrop analysis has revealed the depositional environment is consistent with a distally steepened ramp rather than rimmed shelf, and has also provided an alternative model for the development of depositional features previously termed *in situ* Waulsortian-type mud mounds present throughout the Compton Formation.

4. The anomalous features distributed throughout the Compton Formation at the study area are not *in situ* features, but are outrunner blocks set within a debris flow. These mass transport deposits are common in the distally steepened ramp setting and were likely initiated by syndepositional tectonism known to exist throughout the Mississippian-age strata of the Mid-Continent.
5. The Northview Formation was deposited in a tidal flat environment, rather than the previous interpretation that it represented a deeper water facies. Outcrop evidence supporting deposition of the Northview Formation in a tidal flat environment includes bi-directional ripples, multiple subaerial exposure surfaces, and flaser bedding.
6. Based on conodont biostratigraphy, the eustatic sea level curve for the Mississippian, and detailed outcrop analysis, there are two 3rd order sequences represented by the Kinderhookian and Osagean strata at the Jane outcrop. The Bachelor and Compton Formations form the transgressive systems tract of the first 3rd order sequence. The Northview Formation is part of the highstand systems tract of first 3rd order sequence, as it is considered to be deposited in a tidal flat environment. The second 3rd order sequence is represented by the Pierson Formation, deposited after a flooding event during the following highstand.
7. The high resolution sequence stratigraphic architecture created as a result of this study reveals the vertical and lateral heterogeneity of the system that is

controlled by Milankovitch-scale cyclicity. Based on thin section analyses and SEM imaging, the skeletal mud-lean packstone to grainstone facies within the Northview Formation contains the most porosity and is likely the best reservoir facies. The stratigraphic architecture delineates the continuity of the reservoir facies and shows the complexity of the reservoir architecture across the outcrop.

8. Integrating a sequence stratigraphic approach with an understanding of the probable complexity of facies mosaics from modern analogs has led to a modified time-series of paleo-depositional maps that better illustrate the complexity of shifting facies belts that are associated with Milankovitch-scale sea level change. Determining how Mississippian lithofacies fit into the regional sequence stratigraphic framework will increase the accuracy of paleo-depositional maps used for modeling shifts in facies belts.

REFERENCES

Alsharhan, A.S. and Sadd, J.L., 2000, Stylolites in Lower Cretaceous carbonate reservoirs, U.A.E.: SEPM Special Publication No. 69, p. 185-207.

Asmus, J.J. and Grammer, G.M., 2013, Characterization of deepwater carbonate turbidites and mass-transport deposits utilizing high-resolution electrical borehole image logs: Upper Leonardian (Lower Permian) Upper Bone Spring Limestone, Delaware Basin, Southeast New Mexico and West Texas: Gulf Coast Association of Geological Societies Transactions, v. 63, p. 27-65.

Blakey, R.C., 2013, Early Mississippian Paleogeography of North America: <http://www2.nau.edu/rcb7/nam.html>, Northern Arizona University, Accessed May 22, 2013.

Boardman, D.R., 2013, High resolution conodont zonation for Kinderhookian (Middle Tournaisian) and Osagean (Upper Tournaisian-Lower Visean) strata of the western edge of the Ozark Plateau, North America: Shale Shaker Digest, v. 64, p. 86-151.

Boardman, D.R., II, and Nestell, M.K., 1993, Glacial-Eustatic sea level fluctuation curve for Carboniferous-Permian boundary strata based on outcrops in the North American Midcontinent and north-central Texas: Fort Worth Geological Society, Southwest Section, AAPG Convention, p. 15-25.

Buggisch, W., Joachimski, M.M., Sevastopulo, G., Morrow, J.R., 2008: Mississippian $\delta^{13}C_{carb}$ and conodont apatite $\delta^{18}O$ records – Their relation to the Late Palaeozoic Glaciation: Palaeogeography, Palaeoclimatology, Palaeoecology, v. 268, pp.273 292.

Burchette, T.P. and Wright, V.P., 1992, Carbonate ramp depositional systems: Sedimentary Geology, v. 79, p. 3-57.

Camp, W.K., 2013, Enhancing SEM grayscale images through pseudocolor conversion: Examples from Eagle Ford, Haynesville, and Marcellus shales: URTEC 1598427.

Coniglio, M., 1986, Synsedimentary submarine slope failure and tectonic deformation in deep water carbonates, Cow Head Group, western Newfoundland: Department of Earth Sciences, Memorial University, St. John's Nfld., Canada, v. 23, p. 476 490.

Cook, H.E. and Mullins, H.T., 1983, Basin Margin Environment, *in* P.A. Scholle, D.G. Bebout, and C.H. Moore, eds., Carbonate depositional environments: AAPG Memoir 33, Tulsa, Oklahoma, p. 449-617.

De Blasio, F.V., Engvik, L.E., Elverhoi, A., 2006, Sliding of outrunner blocks from submarine landslides: Geophysical research letters, v. 33, 4 p.

Doveton, J.H., 1994, The spectral gamma-ray log: The Society for Sedimentary Geology (SEPM): Geologic Log Interpretation (SC29), p. 36-52.

Drummond, C.N. and Wilkinson, B.H., 1993, Carbonate cycle stacking patterns and hierarchies of orbitally forced eustatic sea level change: Journal of Sedimentary Petrology, v. 63, no. 3, p. 369-377.

Dunham, R.J., 1962, Classification of carbonate rocks according to depositional texture, *in* Ham, W.E., ed., Classification of Carbonate Rocks: AAPG Memoir, v. 1, p. 108 121.

Eberli, G.P., and Grammer, G.M., 2004, Distribution and geometry of potential reservoir facies, Great Bahama Bank *in* Eberli G.P., Grammer, G.M., Harris, P.M, eds., AAPG Field Guide, p. 1-250.

Ehrenberg, S.N. and Svana, T.A., 2001, Use of spectral gamma-ray signature to interpret stratigraphic surfaces in carbonate strata: An example from the Finnmark carbonate platform (Carboniferous-Permian), Barents Sea: AAPG Bulletin, v. 85, p. 295-308.

Elebiju, O.O., Matson, S., Keller, G.R., Marfurt, K.J., 2011, Integrated geophysical studies of the basement structures, the Mississippi chert, and the Arbuckle Group of Osage County region, Oklahoma: AAPG Bulletin, v. 95, p. 371-393.

Elrick, M. and Read, J.F., 1991, Cyclic ramp-to-basin carbonate deposits, Lower Mississippian, Wyoming and Montana: A combined field and computer modeling study: Journal of Sedimentary Petrology, v. 61, p. 1194-1224.

Ettensohn, F.R., 1993, Possible flexural controls on the origins of extensive, ooid-rich, carbonate environments in the Mississippian of the United States: Chapter 2 *in* Keith, B.D. and Zuppann, C.W., eds., Mississippian Oolites and Modern Analogs, p. 13-30.

Evans, K.R., Jackson, J.S., Mickus, K.L., Miller, J.F., and Cruz, D., 2011, Enigmas and Anomalies of the Lower Mississippian subsystem in southwestern Missouri: Search and Discovery Article #50406, p. 1-47.

Fischer, A.G., D' Argenio, B., Silva, I.P., Weissert, H., Ferreri, V., 2004, Cyclostratigraphic approach to earth's history: An introduction: SEPM, Special Publication No. 81, p. 513.

Fischer, A.G. and Bottjer, D.J., 1991, Orbital Forcing and Sedimentary sequences: Journal of Sedimentary Petrology, v. 61, p. 1063-1069.

Friesenhahn, T.C., 2010, Reservoir characterization and outcrop analog: The Osagean Reeds Spring Formation (Lower Boone), western Osage and eastern Kay County, Oklahoma: ProQuest Dissertations and Theses, University of Arkansas, p. 1-98.

Gawthorpe, R.L. and Clemmey, H., 1985, Geometry of submarine slides in the Bowland Basin (Dinantian) and their relation to debris flows: Journal of the Geological Society of London, v. 142, p. 555-565.

Glover, P., 2012, The Spectral Gamma Ray Log, *in* Petrophysics MSc Course Notes, p. 111-120.

Google Earth Image, June 8, 2012, Jane Outcrop, 36°32'43.18" N 94°19'57.65" W, June 18, 2013.

Grammer, G.M., Harris, P.M., Eberli, G.P., 2004, Integration of outcrop and modern analogs in reservoir modeling: Overview with examples from the Bahamas *in* Grammer, G.M., Harris, P.M., Eberli, G.P., eds., Integration of Outcrop and Modern Analogs in Reservoir Modeling, AAPG Memoir 80, p. 1-22.

Grammer, G.M., Eberli, G.P., Buchem, Frans, S.P., Stevenson, G.M., Homewood, P.W., 2000, Application of high resolution sequence stratigraphy in developing an exploration and production strategy for a mixed carbonate/siliciclastic system, (Carboniferous) Paradox Basin, Utah, USA *in* Homewood P.W. & Eberli, G.P., eds., Genetic stratigraphy on the exploration and the production scales: Bulletin of Center of Research, Elf Aquitaine Memoir 24, p. 30-69.

Grammer, G.M., Eberli, G.P., Van Buchem, F.S.P., Stevenson, G.M., Homewood, P., 1996, Application of high resolution sequence stratigraphy to evaluate lateral variability in outcrop and subsurface: Desert Creek and Ismay Intervals, Paradox Basin *in* M.W. Longman and M.D. Sonnenfeld, eds., 1996, Paleozoic Systems of Rocky Mountain Region, Rocky Mountain Section: SEPM, p. 235-266.

Gutschick, R.C. and Sandberg, C.A., 1983, Mississippian continental margins of the conterminous United States: The Society of Economic Paleontologists and Mineralogists, No. 33, p. 79-96.

Handford, C.R., 1986, Facies and bedding sequences in shelf-storm-deposited carbonates Fayetteville shale and Pitkin Limestone (Mississippian), Arkansas: Journal of sedimentary petrology, v. 56, p. 123-137.

Harris, P.M., Kenter, J., Playton, T., Andres, M., Jones, G., Levy, M., 2011, Enhancing subsurface reservoir models – An integrated approach using outcrop analogs, modern analogs, and forward stratigraphic models: Search and Discovery Article #50418, AAPG Annual Convention and Exhibition, Houston, TX, April, 2011, p. 1 39.

Harris, S.A., 1987, Hydrocarbon Accumulation in "Meramec-Osage" (Mississippian) Rocks, Sooner Trend, Northwest- Central Oklahoma, Tulsa Geological Society, Special Publication No. 3: Petroleum Geology of the Mid-Continent.

Haq, B.U. and Schutter, S.R., 2008, A chronology of Paleozoic sea-level changes: *Science*, v. 322, p. 64-68.

Heinzelmann, G.M., Jr., 1964, Mississippian Rocks in the Stillwater-Chandler Area: Shale Shaker Digest V, v. 15-17, p. 195-206.

Heubeck, C., 1992, Sedimentology of large olistoliths, Southern Cordillera Central, Hispaniola: Journal of Sedimentary Petrology, v. 62, p. 474-482.

Honjo, S., Fischer, A.G., Garrison, R., 1965, Geopetal pyrite in fine-grained limestones: Journal of Sedimentary Petrology, v. 35, p. 480-488.

Huffman, G.G., 1960, Geology of the Oklahoma Ozark region: North-Eastern Oklahoma: Guidebook, 25th Field Conference, p. 82-109.

Ilstad, T., Elverhoi, A., Issler, D., Marr, J.G., 2004, Subaqueous debris flow behavior and its dependence on the sand/clay ratio: a laboratory study using particle tracking: Marine Geology, v. 213, p. 415-438.

Ilstad, T., De Blasio, F.V., Elverhoi A., Harbitz, C.B., Engvik, L., Longva, O., Marr, J.G., 2004, On the frontal dynamics and morphology of submarine debris flows: Marine Geology, v. 213, p. 481-497.

Joshi, S.D., 1991, Overview of Well Technology *in* Horizontal Well Technology: Pennwell Publishing Company, Tulsa, Oklahoma, p. 1-32.

Kerans, C., 1995, Use of one- and two-dimensional cycle analysis in establishing high frequency sequence frameworks, part 2: SEPM (SC 35), p. 1-20.

Kerans, C. and Tinker, S.W., 1997, Sequence stratigraphy and characterization of carbonate reservoirs: SEPM, short course notes no. 40, p. 1-130.

Kerans, C., Lucia, F.J., and Senger, R.K., 1994, Integrated characterization of carbonate ramp reservoirs using Permian San Andres Formation outcrop analogs: AAPG Bulletin, v. 78, p. 181-216.

Kreman, D.M., 2011, Characterization of Kinderhookian and Osagean strata of northeast Oklahoma: University of Southern Illinois, unpublished M.S. thesis, p. 1-160.

Krueger, R.C., 1965, Subsurface study of the Mississippian rocks in the Tulsa area: The Shale Shaker Digest V, v. 15-17, p. 217-239.

Lane, H.R., 1978, The Burlington Shelf (Mississippian, north-central United States): Geologica et palaeontologica, p. 165-176.

Lane, H.R. and De Keyser, T.L., 1980, Paleogeography of the Late Early Mississippian (Tournaisian 3) in the central and southwestern United States: Rocky Mountain Section, SEPM, Paleozoic paleogeography of west-central United States, p. 149 162.

Le Blanc, S., 2014, High resolution sequence stratigraphy and reservoir characterization of the "Mississippian Limestone" in north-central Oklahoma: Oklahoma State University, unpublished thesis, 418p.

Lerat, O., Buchem, F.V., Eschard, R., Grammer, G.M., Homewood, P.W., 2000, Facies distribution and control by accommodation within high-frequency cycles of the Upper Ismay interval (Pennsylvanian, Paradox Basin, Utah) *in* Homewood P.W. & Eberli, G.P., eds., Genetic stratigraphy on the exploration and the production scales: Bulletin of Center of Research, Elf Aquitaine Memoir 24, p. 71-91.

Lisle, B.A., 1983, Short Creek Oolite (Lower Mississippian) deposition, War Eagle Quarry, Madison County, Arkansas: Arkansas Academy of Science Proceeding, v. 37, p. 47-49.

Loucks, R.G., Reed, R.M., Ruppel, S.C., Hammes, U., 2012, Spectrum of pore types and networks in mudrocks and a descriptive classification for matrix-related mudrock pores: AAPG Bulletin, v. 96, p. 1071-1098.

Lowe, D.R., 1982, Sediment Gravity Flows II: Depositional models with special reference to the deposits of high-density turbidity currents: Journal of Sedimentary Petrology, v. 52, p. 279-297.

Lowe, D.R., 1979, Sediment Gravity Flows: Their classification and some problems of application to natural flows and deposits: Society of Economic Paleontologists and Mineralogists, SEPM Special Publication No. 27, p. 75-82.

Manger, W.L. and Shanks, J.L., 1976, Lower Mississippian Lithostratigraphy, Northern Arkansas: Arkansas Academy of Science Proceedings, v. 30, p. 78-80.

Manger, W.L. and Thompson, T.L., 1982, Regional depositional setting of lower Mississippian Waulsortian mound facies, southern Mid-Continent, Arkansas, Missouri, and Oklahoma: Symposium on the Paleoenvironmental Setting and Distribution of the Waulsortian Facies, p. 43-50.

Mazzullo, S.J., 2013, Boardman, D.R., II, Wilhite, B.W., Morris, B.T., 2013 Revisions of outcrop lithostratigraphic nomenclature in the Lower to Middle Mississippian Subsystem (Kinderhookian to Basal Meramecian Series) along the shelf-edge in southwest Missouri, northwest Arkansas, and northeast Oklahoma: Shale Shaker Digest, v. 63, p. 414-454.

Mazzullo, S.J., 2011, Mississippian oil reservoirs in the southern Mid-Continent: New exploration concepts for a mature reservoir objective: Search and Discovery Article # 10373, p. 1-34.

Mazzullo, S.J., Wilhite, B.W., Boardman, D.R., II, 2011, Lithostratigraphic architecture of the Mississippian Reeds Spring Formation (Middle Osagean) in southwest Missouri, northwest Arkansas, and northeast Oklahoma: Outcrop analog of subsurface petroleum reservoirs: Shale Shake, v. 61, No. 5, p. 254-269.

Mazzullo, S.J. Wilhite, B.W., Woolsey, I.W., 2009, Petroleum reservoirs within a spiculite dominated depositional sequence: Cowley Formation (Mississippian: Lower Carboniferous), south-central Kansas: AAPG Bulletin, v. 93, p. 1649-1689.

McDuffie, R., 1964, Mississippian rocks in the subsurface of Garfield and Western Noble Counties, Oklahoma: Shale Shaker Digest IV, v. XII-XIV, p. 129-144.

McGraw-Hill Science & Technology Dictionary, <http://www.answers.com/topic/olistolith>, olistolith: 2013 Answers Corporation, Accessed July 2, 2013.

Mehl, M.G., 1961, Basal relationships of the Mississippian in northeastern Missouri: KGS, 2006 Northeastern Missouri and West Central Illinois: Guidebook, 26th Annual Field Conference in cooperation with the Missouri Geol. Survey and the Illinois Geol. Survey, 1961, p. 89-94.

Mii, H.S., Grossman, E.L., Yancey, T.E., 1999, Carboniferous isotope stratigraphies of North America: Implications for Carboniferous paleoceanography and Mississippian glaciation: GSA Bulletin, v. 111, p. 960-973.

Mitchum, R.M. Jr., and J.C. Van Wagoner, 1991, High-frequency sequences and their stacking patterns: Sequence-stratigraphic evidence of high-frequency eustatic cycles: Sedimentary Geology, v. 70, p. 131-160.

Moore, D.G., Curray, J.R., Emmel, F.J., 1976, Large submarine slide (olistostrome) associated with Suna Arc subduction zone, northeast Indian Ocean: Marine Geology, v. 21, p. 211 226.

Morris, B.T. and Mazzullo, S.J., 2013, Sedimentology, biota, and diagenesis of 'reefs' in Lower Mississippian (Kinderhookian to Basal Osagean: Lower Carboniferous) strata in the St. Joe Group in the western Ozark area: Shale Shaker, v. 64, p. 194 204.

Mulder, T. and Alexander, J, 2001, The physical character of subaqueous sedimentary density flows and their deposits: Sedimentology, v. 48, p. 269-299.

Plint, A.G., Eyles, N., Eyles, C.H., Walker, R.G., 1992, Controls on sea level changes *in* Walker, R.J. and James, N.P. (eds.), *Facies Models: Response to Sea Level Change*: Geological Association of Canada, St. John's Newfoundland, p. 15-25.

Rankey, E.C., 2003, Internal architecture and sequence stratigraphy of Middle Mississippian (Visean) grainstones, eastern Missouri: AAPG Search and Discovery Article #90013.

Rankey, E.C., 2002, Spatial patterns of sediment accumulation on a Holocene carbonate tidal flat, northwest Andros Island, Bahamas: Journal of Sedimentary Research, v. 72, p. 591-601.

Read, J.F., 1995, Overview of carbonate platform sequences, cycle stratigraphy and reservoirs in greenhouse and ice-house worlds, part 1: SEPM (SC35), p. 1-12.

Read, J.F., and Horbury, A.D., 1993, Eustatic and Tectonic Controls on Porosity Evolution Beneath Sequence-Bounding Unconformities and Parasequence Disconformities on Carbonate Platforms, *in* A.D. Horbury and A.G. Robinson, eds., Diagenesis and basin development: AAPG Studies in Geology 36, p. 155-197.

Rogers, S.M., 2001, Deposition and diagenesis of Mississippian chat reservoirs, north central Oklahoma: AAPG Bulletin, v. 85, p. 115-129.

Rogers, J.P., Longman, M.W., Lloyd, R.M., 1996, Spiculitic chert reservoir in Glick Field, south central Kansas: Transactions of the 1995 Mid-Continent Section Meeting, 31 p.

Roundtree, R., Wright, J., Miskimins, J., 2010, Unconventional resource recovery improvement using conventional reservoir engineering strategies: Search and Discovery Article #80088, 15 p.

Seale, R. and Snyder, D., 2011, Optimization of completions in unconventional reservoirs for ultimate recovery: Search and Discovery Article #80142, 25 p.

Schlager, W., 2005, Chapter 7: Sequence stratigraphy of the T factory, *in* Schlager, W., ed., Carbonate Sedimentology and Sequence Stratigraphy: SEPM Concepts in Sedimentology and Paleontology #8, p. 105-146.

Shinn, E.A., 1983, Tidal Flat Environment, *in* Scholle, P.A., Bebout, D.G., Moore, C.H. eds., Carbonate Depositional Environments: AAPG Memoir 33, p. 171-200.

Shoeia, O.K., 2012, High resolution stratigraphy of Lower Mississippian strata near Jane, Missouri: Oklahoma State University, unpublished M.S. thesis, 262p.

Smith, L.B., Jr., Eberli, G.P., Sonnenfeld, M., 2004, Sequence-stratigraphic and paleogeographic distribution of reservoir-quality dolomite, Madison Formation, Wyoming and Montana *in* G.M. Grammer, P.M. "Mitch" Harris, and G.P. Eberli, eds., Integration of outcrop and modern analogs in reservoir modeling: AAPG Memoir 80, p. 67-92.

Sonnenfeld, M.D., 1996, Sequence evolution and hierarchy within the Lower Mississippian Madison Limestone of Wyoming, *in* M.W. Longman and M.D. Sonnenfeld, eds., Paleozoic systems of the Rocky Mountain region: Rocky Mountain Section SEPM, p. 165 192.

Spreng, A.C., 1952, The Lower Pierson fauna of west-central Missouri: West-Central and Southwestern Missouri: Guidebook, 16th Regional Field Conference, p. 81-86.

Tennyson, R., Terry, J., Brahana, V., Hays, P., Pollock, E., 2008, Tectonic control of hypogene speleogenesis in the southern Ozarks: Implications for NAWQA and beyond: U.S. Geological Survey Scientific Investigations Report 2008, p. 37-46.

Thompson, T.L. and Fellows, L.D., 1970, Stratigraphy and conodont biostratigraphy of Kinderhookian and Osagean (Lower Mississippian) rocks of southwestern Missouri and adjacent areas: Missouri Geological Survey and Water Resources, Investigation No. 45, p. 1-263.

Tripsanas, E.K., Piper, D.J.W., Jenner, K.A., Bryant, W.R., 2008, Submarine mass transport facies: new perspectives on flow processes from cores on the eastern North American margin: Sedimentology, v. 55, p. 97-136.

Unrast, M.A., 2013, Composition and classification of Mississippian carbonate mounds in the Ozark region, North America: Shale Shaker, v. 63, p. 254-273.

Unrast, M.A., 2012, Composition of Mississippian Carbonate mounds in the Ozark region, North America and Ireland: Oklahoma State University, unpublished thesis, 120p.

Vail, P.R., Mitchum, R.M., and Thompson, S. III, 1977, Seismic stratigraphy and global changes of sea level, Part 3: Relative changes of sea level from coastal onlap *in* Payton, C.E., ed., Seismic stratigraphic application to hydrocarbon exploration: AAPG Memoir 26, p. 63-81.

Vanden Berg, B., Grammer, G.M., 2014, Combining sonic velocity and characterization of pore architecture to develop a proxy for reservoir permeability in unconventional carbonates: An example from the Mid-Continent Mississippian Limestone: URTEC Conference, DOI 10.15530, 8 p.

Van Wagoner, J.C., Posamentier, H.W., Mitchum, R.M., Vail, P.R., Sarg, J.F., Loutit, T.S., and Hardenbol, J., 1988, An Overview of the fundamentals of sequence stratigraphy and key definitions: SEPM, Special Publication No. 42, p. 39-45.

Watney, W.L., Guy, W.J., Byrnes, A.P., 2001, Characterization of the Mississippian chat in south central Kansas: AAPG Bulletin, v. 85, p. 85-113.

Westphal, H., Eberli, G.P., Smith, L.B., Grammer, G.M., Kislak, J., 2004, Reservoir characterization of the Mississippian Madison Formation, Wind River basin, Wyoming: AAPG Bulletin, v. 88, p. 405-432.

Wieczorek, J., 1979, Geopetal structures as indicators of top and bottom: Institute of Geological Sciences, Jagiellonian University, v. 30-063, p. 215-221.

Wilhite, B.W., Mazzullo, S.J., Morris, B.T., Boardman, D., II, 2011, Syndepositional tectonism and its effects on Mississippian (Kinderhookian to Osagean) lithostratigraphic architecture: Part 1 – Based on exposures in the Mid-Continent USA: Search and Discovery Article #30207, p. 1-43.

Wilson, W.B., Reef Definition: AAPG Bulletin, v. 34, p. 181.

Wolf, K.H., 1965, Gradational sedimentary products of calcareous algae: Sedimentology, v. 5, p. 1-37.

APPENDICES

THIN SECTION PHOTOMICROGRAPHS

Thin section photomicrographs show magnified views of samples taken from Vertical Section 1, Vertical Section 2, Vertical Section 3, and Blocks 1-6. All samples are oriented with the up direction at the top of the page. All samples are shown at three magnifications, increasing from left to right. The top row of each page is in cross polarized light, and the bottom row is the same image in plane polarized light. Each thin section is labeled using the thin section image labels in Table 6.

Thin Section Image Labels					
Feature Key				Porosity Key	
BR	brachiopod	MW	mud wisp	FR	fracture
BY	bryozoan	MC	mud clasts	IP	interparticle
C	coral	O	ostracod	IX	intercrystalline
CC	calcite cement	OIL	oil/dead oil	MO	moldic
CR	crinoid	PH	phosphate	VU	vug
D	dolomite	PY	pyrite	WP	intraparticle
FR	fracture	Q	quartz	WX	intracrystalline
GST	gastropod	S	stylolite		
L	lamination	SP	spicule		
M	mud/mudstone	T	trilobite		

Table 6: Thin section image labels.

Vertical Section 1

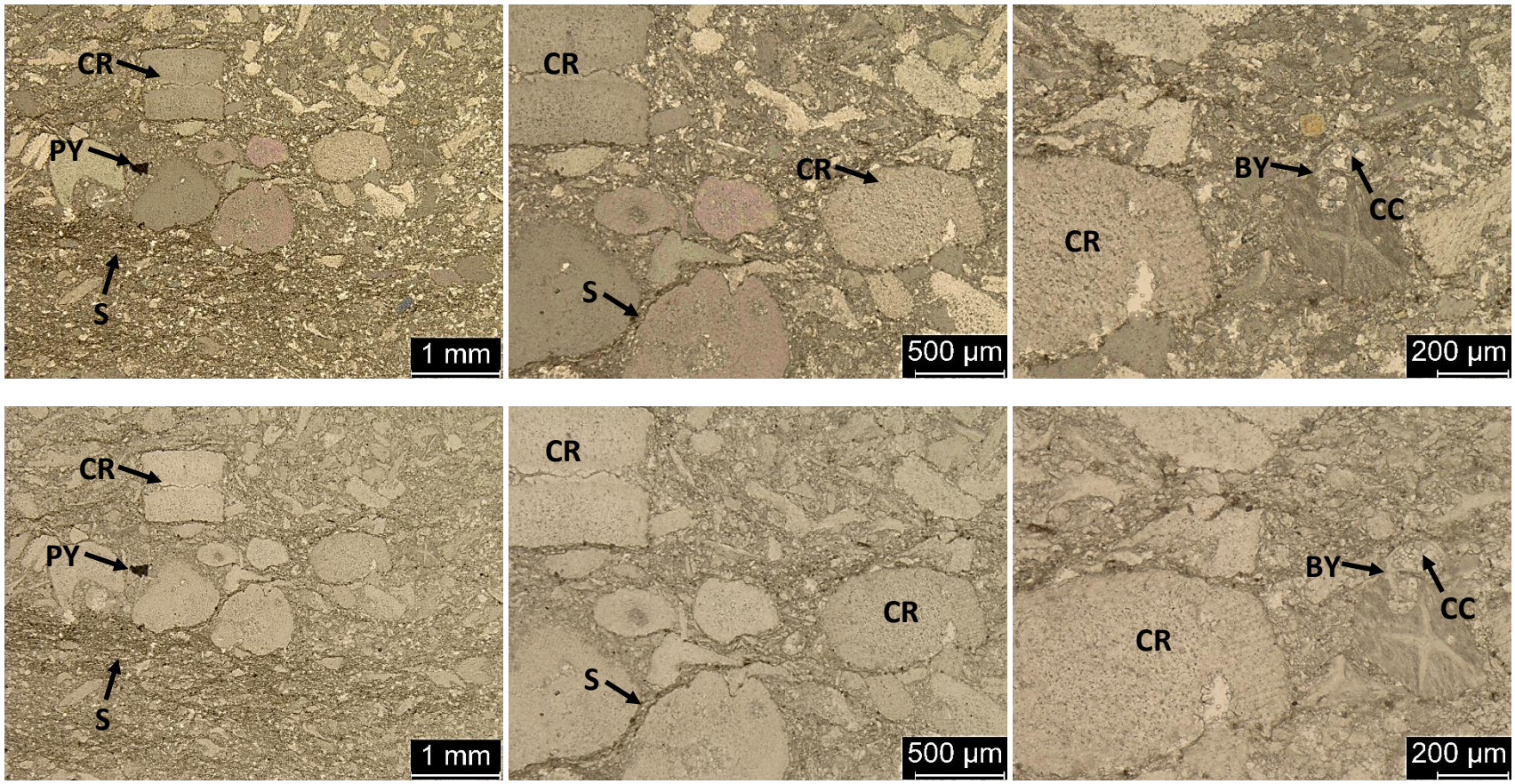

1c-1.0: Crinoidal wackestone to packstone, fine to coarse grained, very poorly sorted. Contains 50% skeletal grains, 49% micrite matrix, and 1% pyrite and cement (visual estimation). Grain types include crinoids and bryozoans. Crinoids range in size from 250µ-1mm and are the primary skeletal grain. Bryozoans range from 125µ – 250 µ. Muddy stylolites and calcite cement can also be seen.

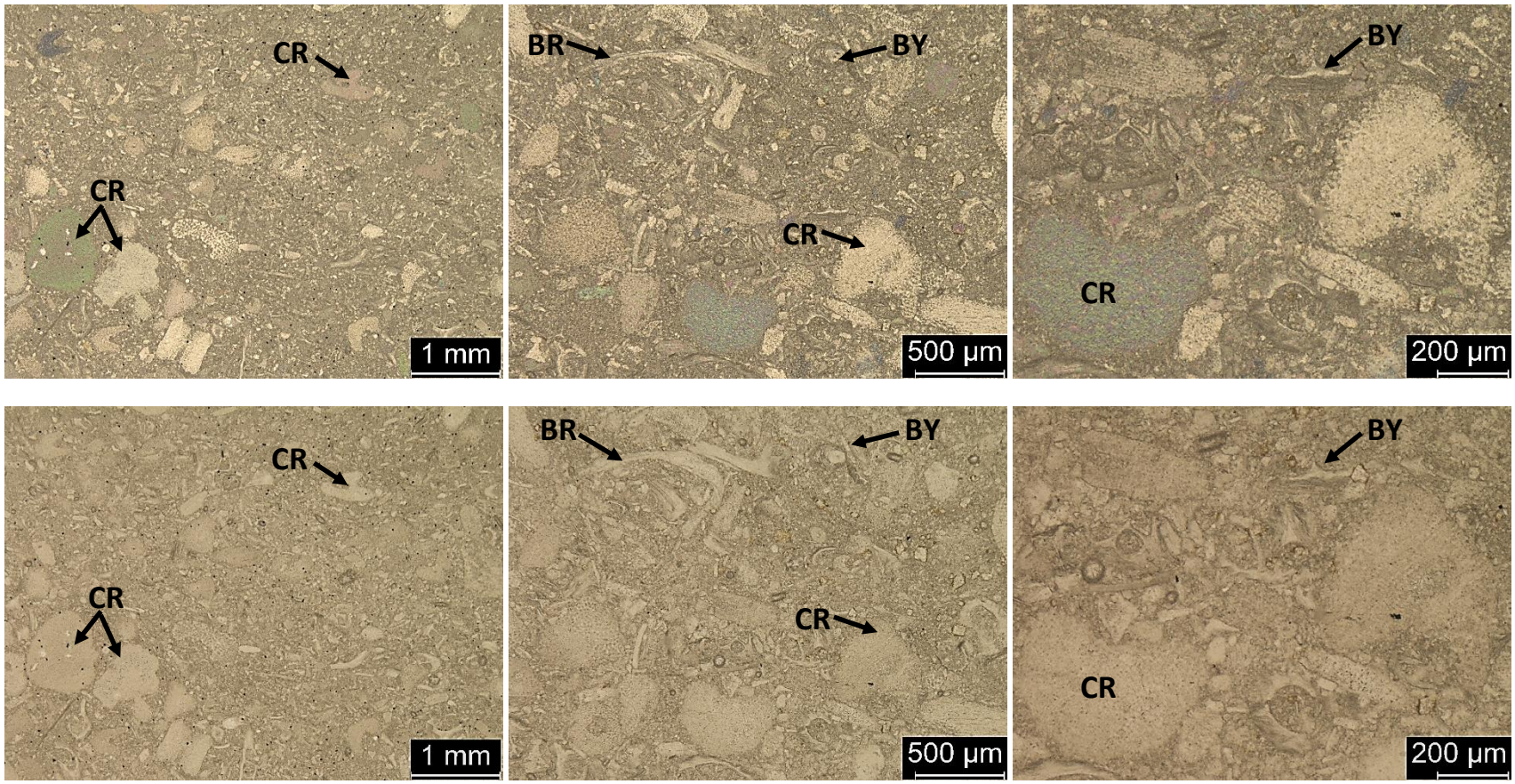

1c-1.5: Bryozoan-crinoidal wackestone, fine to medium grained, poorly sorted. Contains 35% skeletal grains, 64% micrite matrix, and 1% pyrite, dolomite, and calcite cement (visual estimation). Grain types include crinoids (125µ - 500µ), bryozoans (125µ - 200µ), and brachiopods (500µ - 750µ).

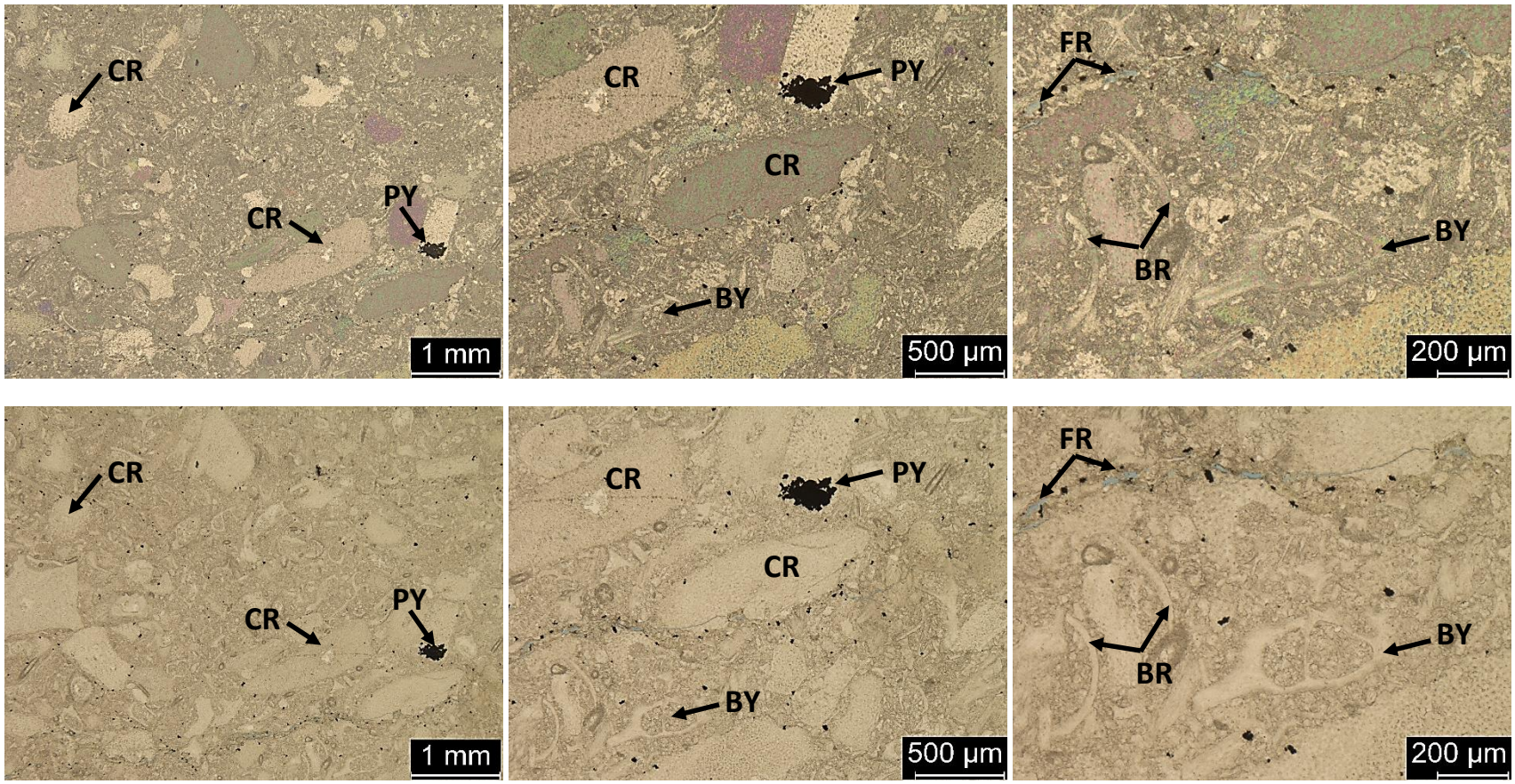

1c-2.25: Bryozoan-crinoidal wackestone, fine to coarse grained, poorly sorted. Contains 40% skeletal grains, 58% micrite matrix, and 2% pyrite and porosity (visual estimation). Grain types include crinoids (200µ - 1mm), bryozoans (200µ - 500µ), and brachiopods (500µ - 700µ). Pyrite has partially filled in a crinoid grain and fracture porosity can be seen at the highest magnification.

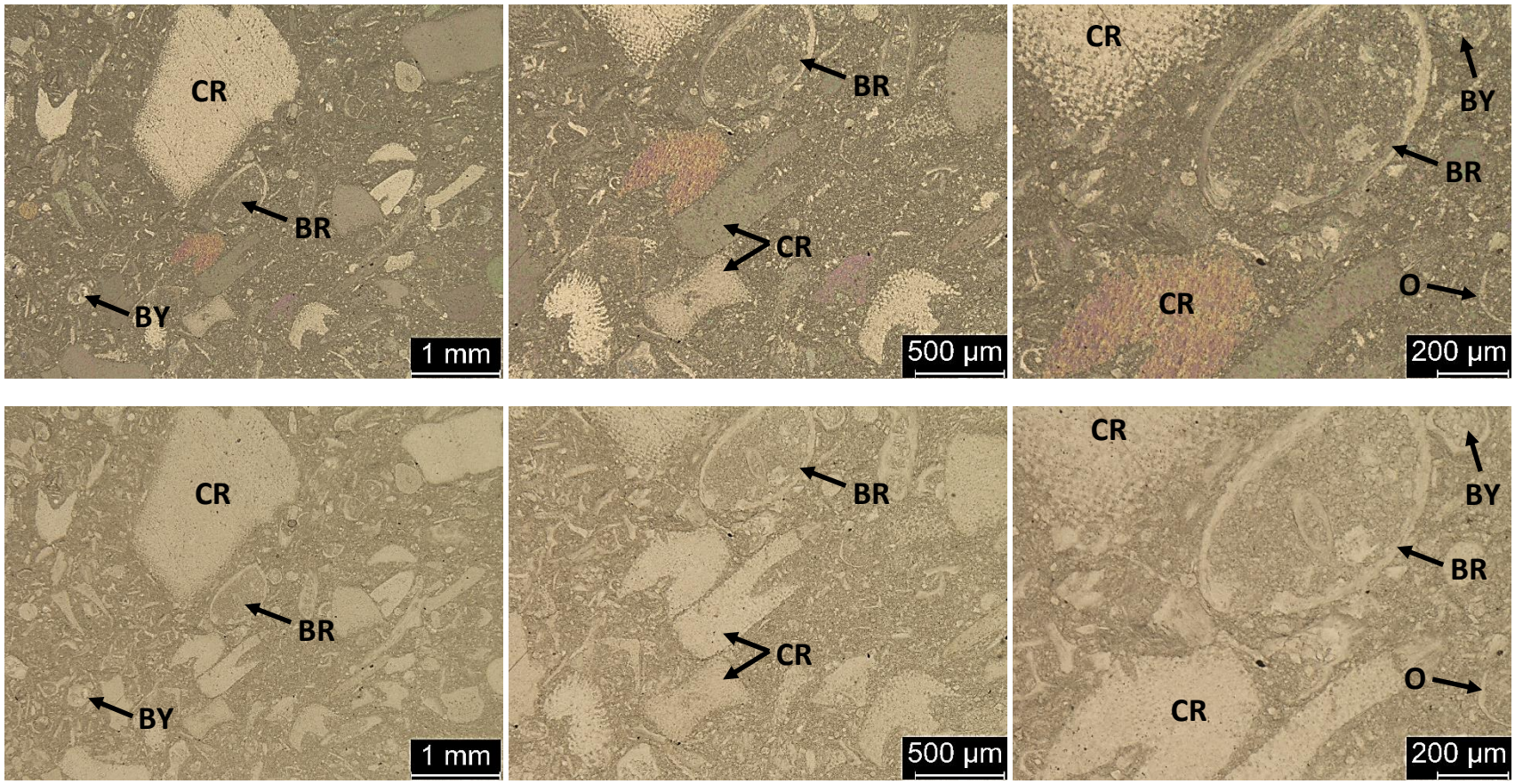

1c-4.0: Crinoidal wackestone, very fine to very coarse grained, poorly sorted. Contains 40% skeletal grains, 59% micrite matrix, and 1% pyrite (visual estimation). Grain types include crinoids (62.5µ - 2mm), bryozoans (62.5µ - 200µ), brachiopods (500µ - 750µ), and ostracods (125µ - 200µ).

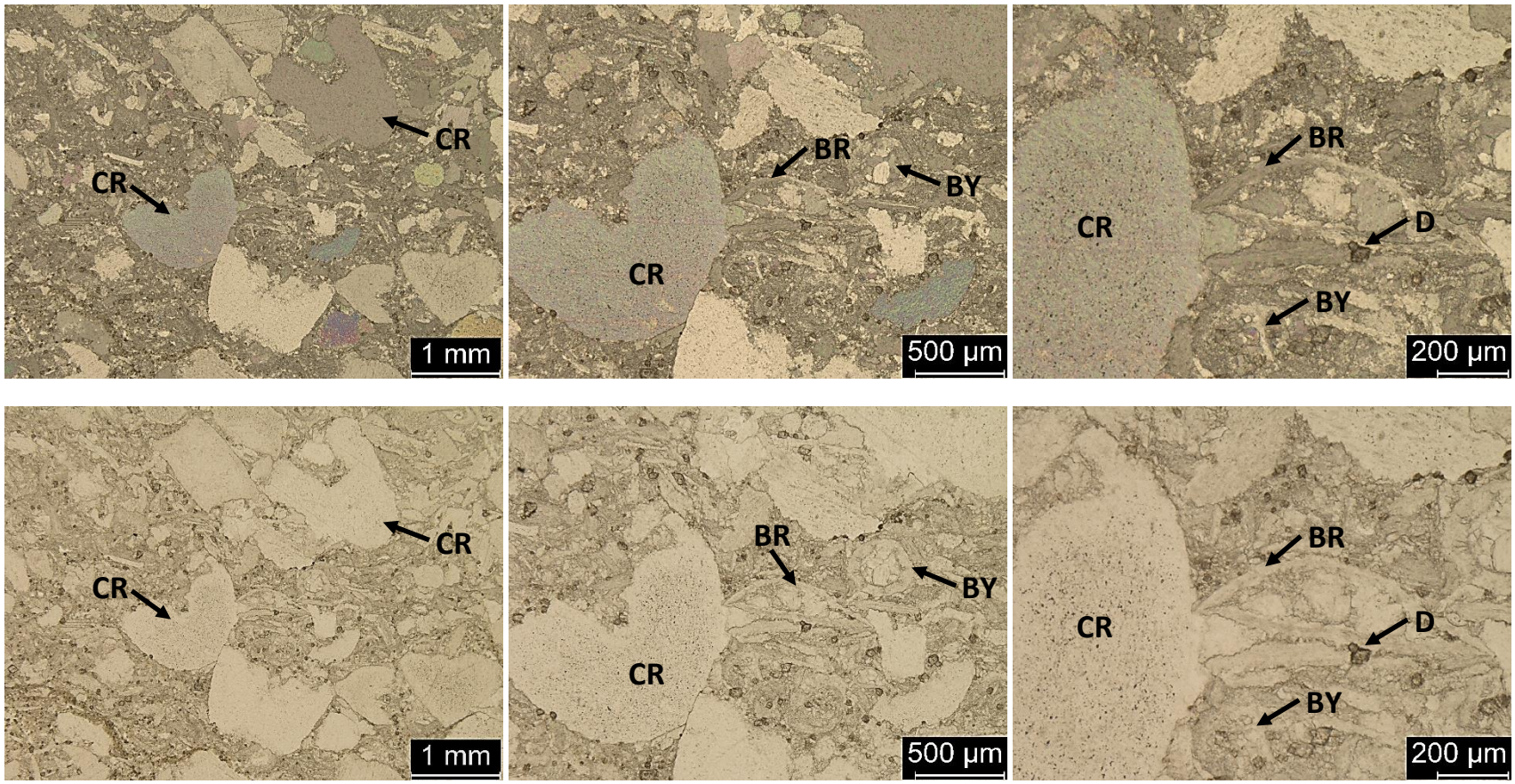

1c-4.5: Crinoidal packstone, fine to very coarse grained, poorly sorted. Contains 60% skeletal grains, 39% micrite matrix, 1% dolomite rhombs (visual estimation). Grain types include crinoids (125µ - 2mm), bryozoans (200µ - 300µ), and brachiopods (500µ - 750µ).

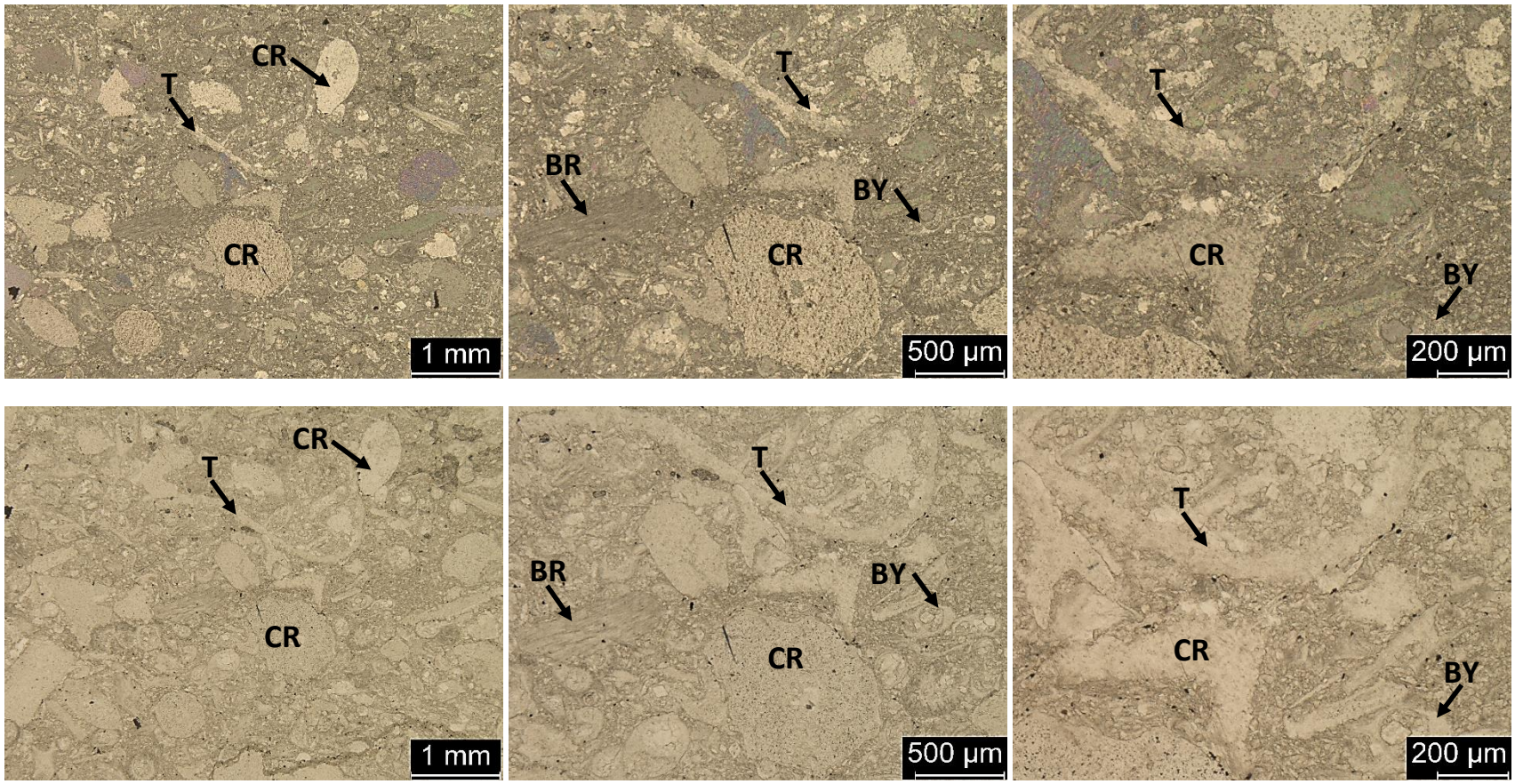

1c-5.5: Bryozoan packstone, fine to coarse grained, poorly sorted. Contains 50% skeletal grains, 49% micrite matrix, and 1% pyrite, calcite, dolomite rhombs (visual estimation). Grain types include crinoids (200µ - 1mm), bryozoans (125µ - 250µ), brachiopods (500µ - 750µ), and trilobites (500µ - 1mm). Calcite cement occurs within and around some of the skeletal grains. Pyrite fills in some of the crinoid grains and dolomite rhombs can be seen throughout.

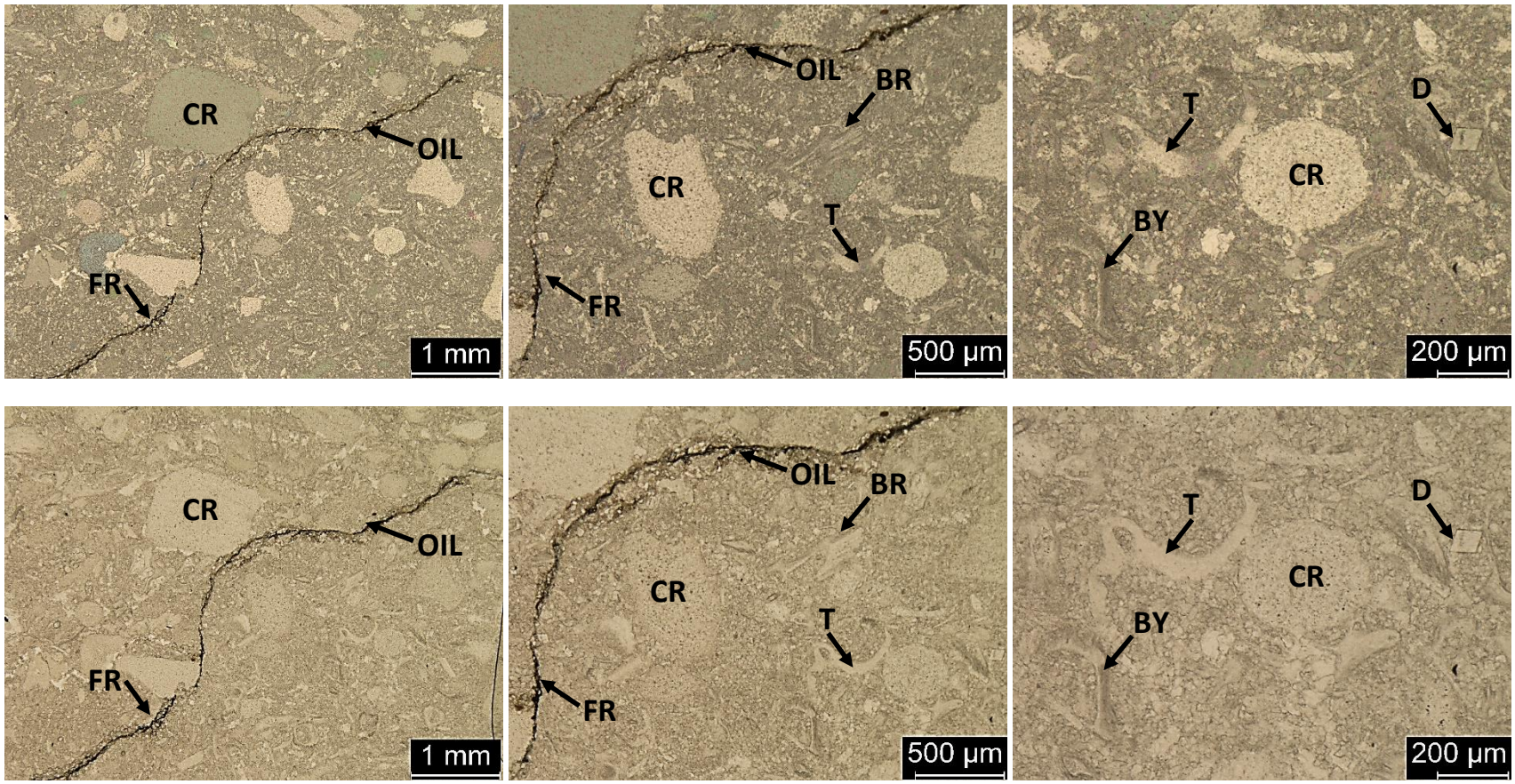

1c-7.0: Bryozoan wackestone to packstone, very fine to coarse grained, poorly sorted. Contains 45% skeletal grains, 53% micrite matrix, and 2% dead oil and dolomite rhombs (visual estimation). Grain types include crinoids (62.5µ – 1mm), bryozoans (62.5µ – 200µ), brachiopods (200µ – 500µ), and trilobites (200µ – 400 µ). Dead oil has filled a fracture and dolomite rhombs can be seen throughout.

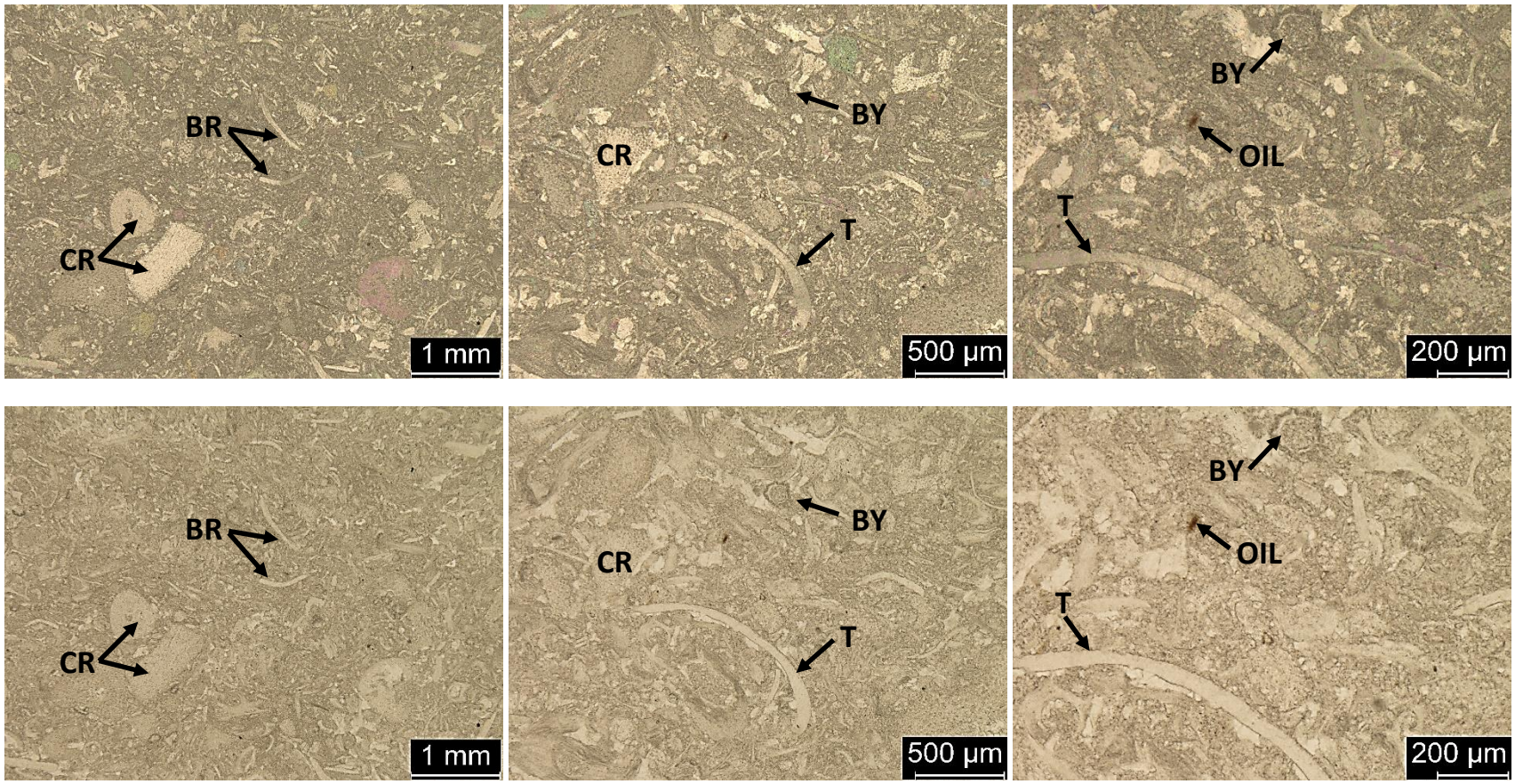

1c-7.25: Skeletal wackestone-packstone, very fine to coarse grained, poorly-moderately sorted. Contains 45% skeletal grains, 54% micrite matrix, and 1% pyrite and dolomite rhombs (visual estimation). Grain types include crinoids (62.5µ – 1mm), bryozoans (62.5µ – 400µ), brachiopods (300µ – 500µ), and trilobites (250µ – 1mm). Dead oil and dolomite rhombs occur throughout.

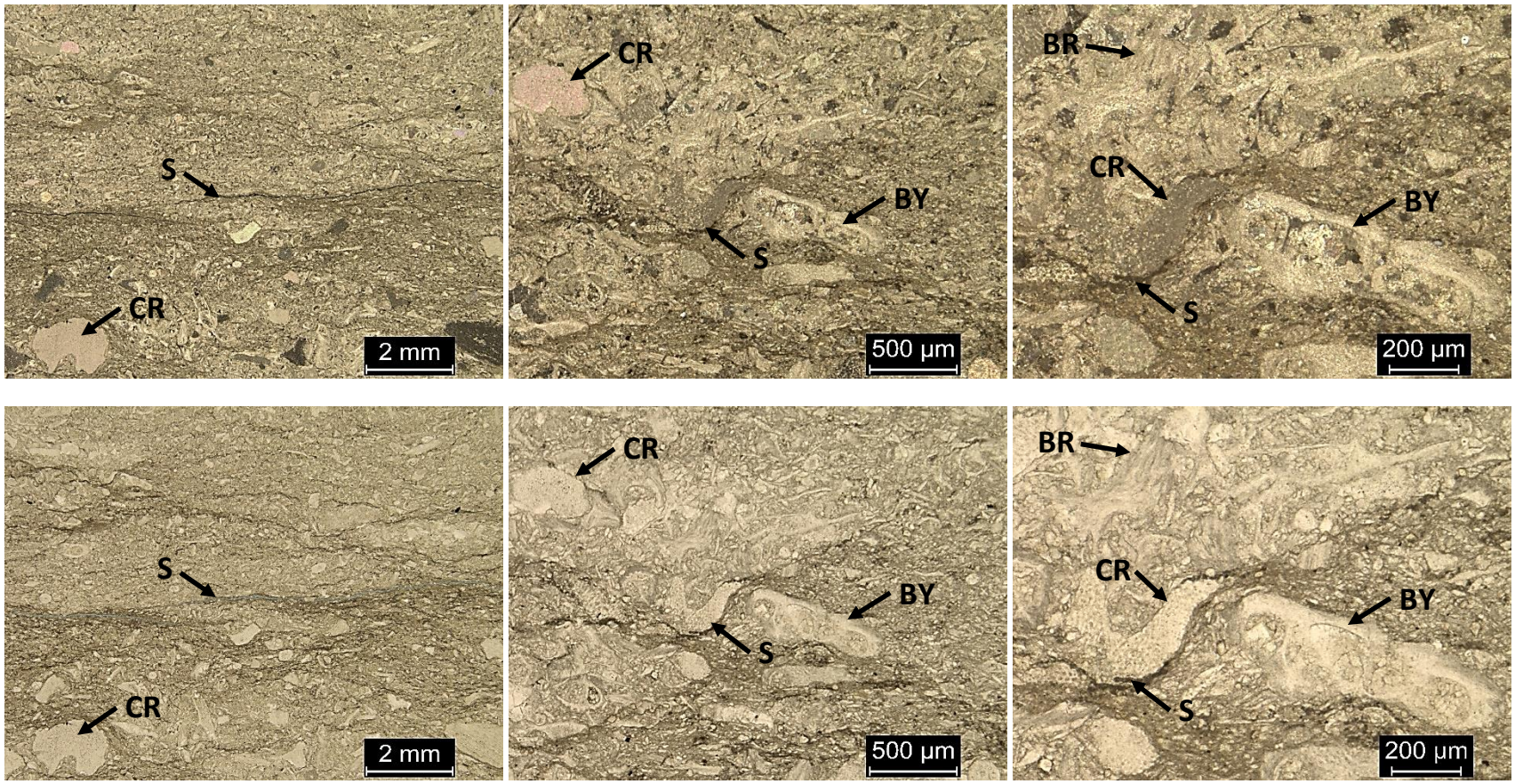

1nv-8.25: Skeletal wackestone, very fine to coarse grained, poorly sorted. Contains 30% skeletal grains and 70% micrite matrix (visual estimation). Grain types include crinoids (62.5µ – 1mm), bryozoans (62.5µ – 500µ), and brachiopods (250µ – 500µ). Muddy stylolites occur throughout.

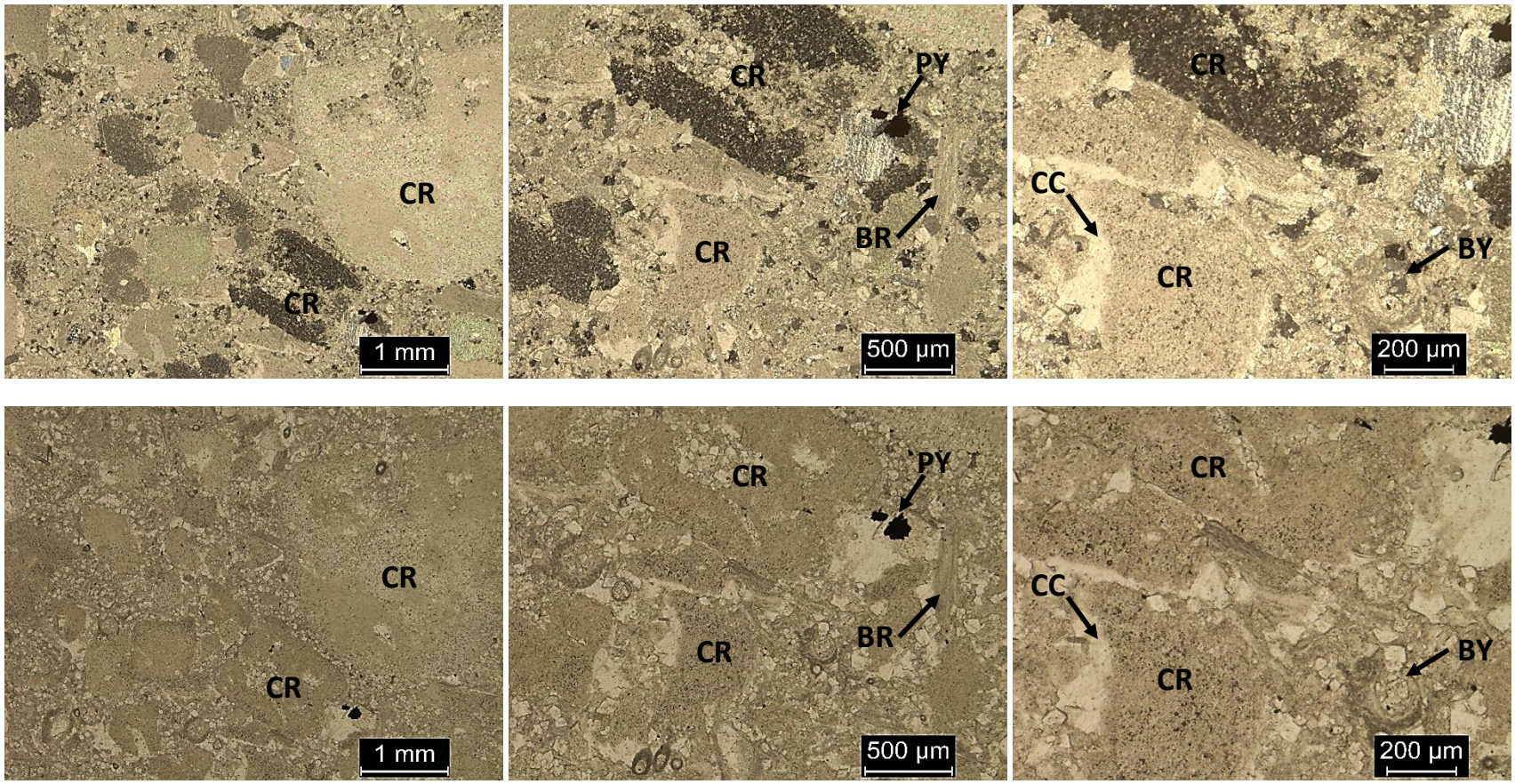

1nv-10.75: Crinoidal grainstone, medium to very coarse grained, very poorly sorted. Contains 95% skeletal grains, 4% blocky calcite cement, and 1% pyrite and dolomite (visual estimation). Grain types include crinoids (250µ – 2mm), bryozoans (250µ – 350µ), and brachiopods (400µ – 700µ). Blocky calcite cement surrounds and fills in skeletal grains. Dolomite rhombs and pyrite occur throughout.

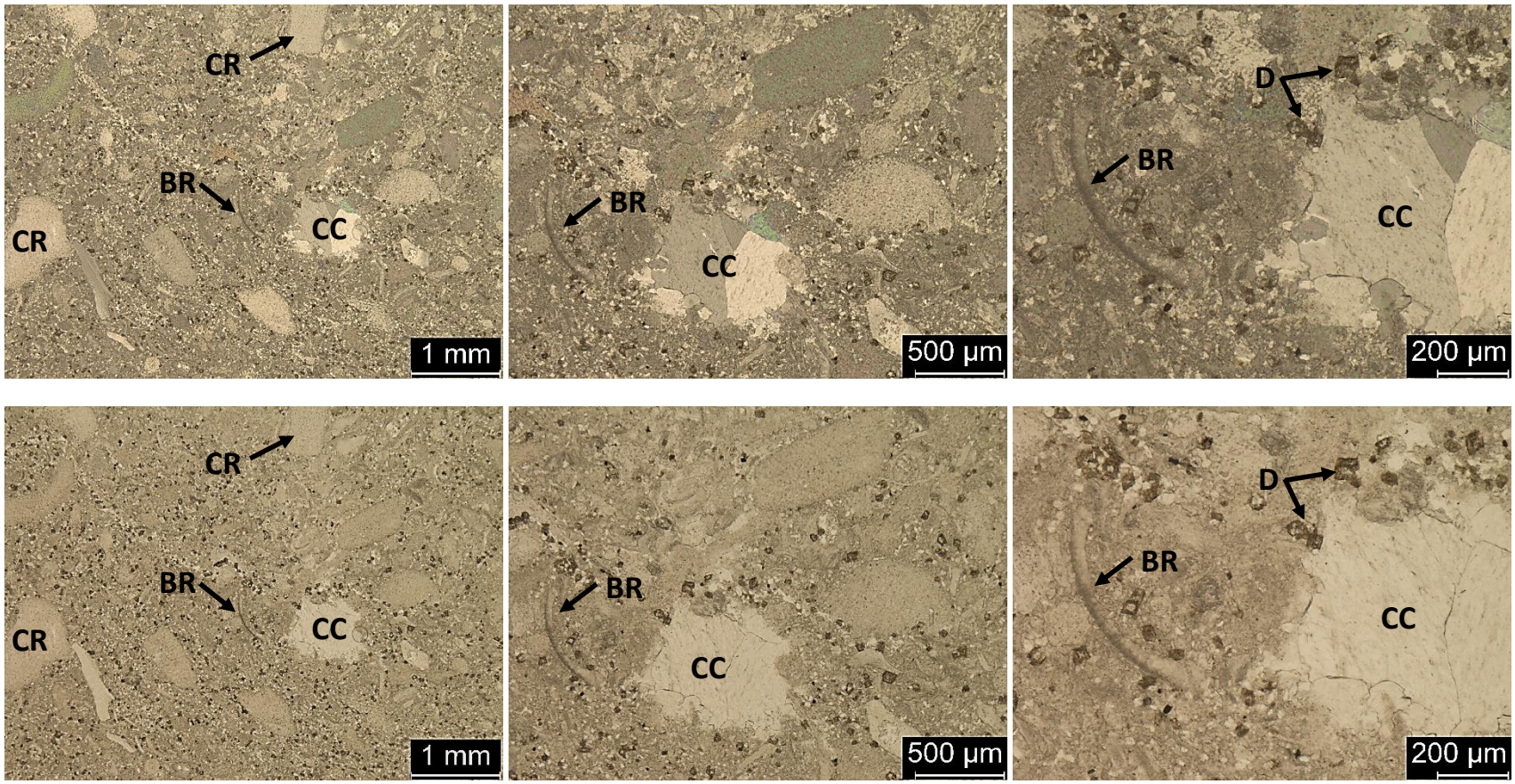

1p-11.75: Skeletal mud-lean packstone, fine to very coarse grained, poorly sorted. Contains 70% skeletal grains, 28% micrite matrix, and 2% blocky calcite cement and dolomite (visual estimation). Grain types include crinoids (250µ – 1mm), bryozoans (150µ – 200µ), and brachiopods (300µ – 500µ). This thin section contains the most dolomite rhombs and calcite cement relative to the thin sections from the other vertical sections.

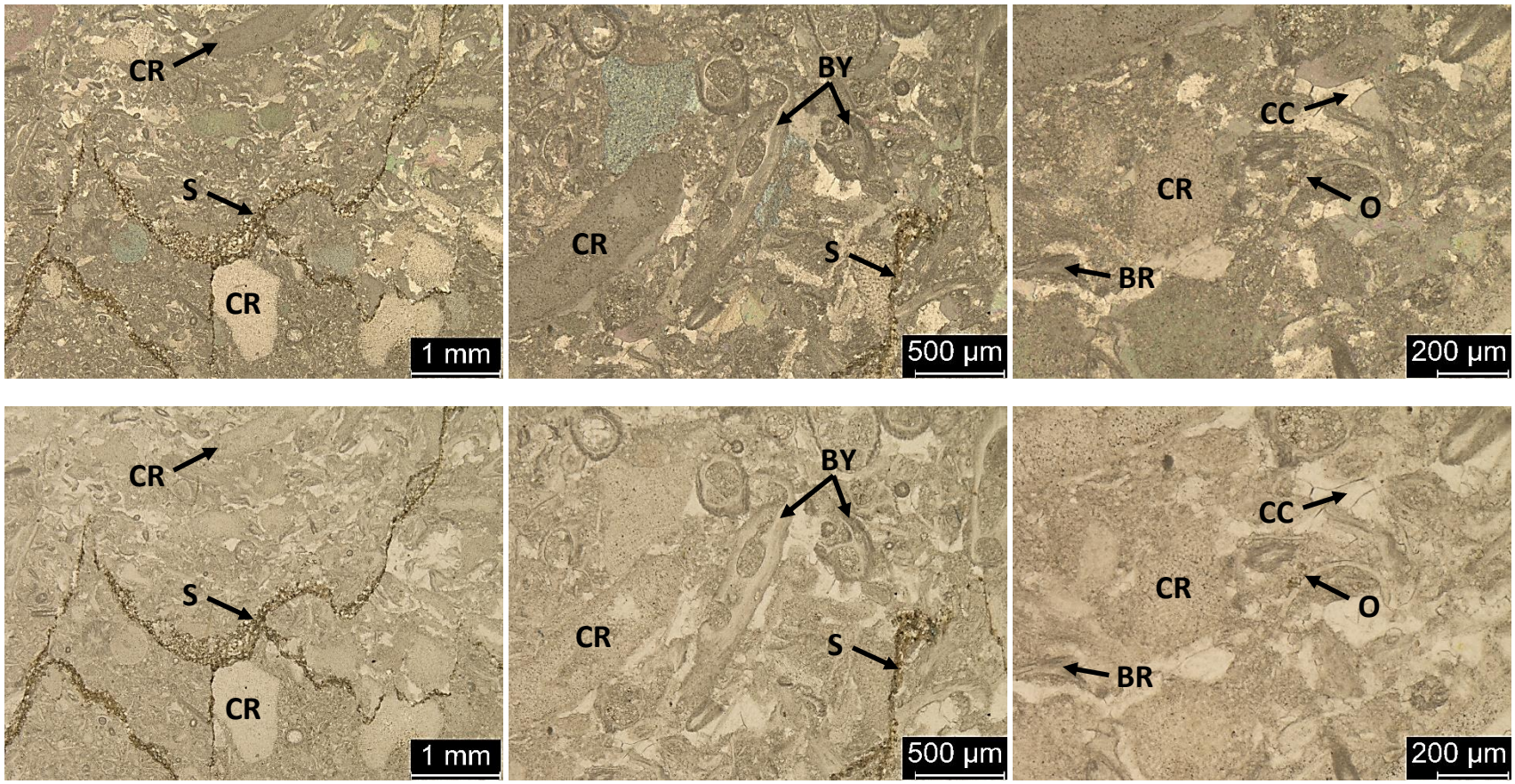

1p-12.25: Bryozoan-crinoidal packstone, fine to course grained, moderately-poorly sorted. Contains 55% skeletal grains, 41% micrite matrix, and 4% blocky calcite cement and dolomite (visual estimation). Grain types include bryozoans (125µ – 500µ), crinoids (125µ – 1mm), brachiopods (500µ – 700µ), and ostracods (125µ – 250µ). Dolomite rhombs and calcite cement have filled in a stylolite.

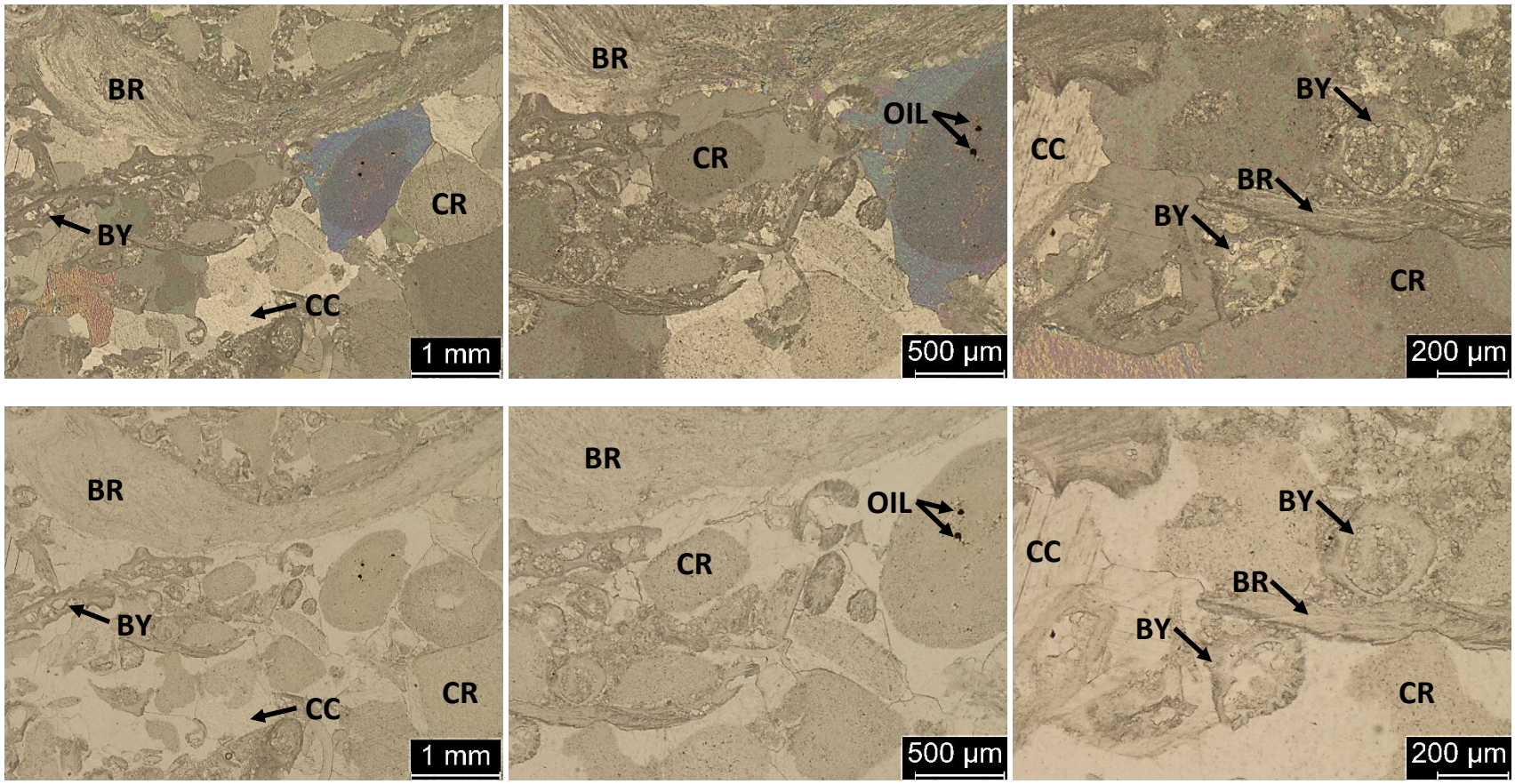

1p-14.5: Crinoidal grainstone, grain size ranges from fine sand to very fine pebbles, moderately to poorly sorted. Contains 90% skeletal grains and 9% blocky calcite cement, and <1% dead oil (visual estimation). Grain types include crinoids (150µ – 3mm), brachiopods (500µ – 4mm), bryozoans (150µ – 1mm), and trilobites (500µm – 1mm). Blocky calcite cement fills space in between and within skeletal grains. Dead oil can be seen within one of the crinoids.

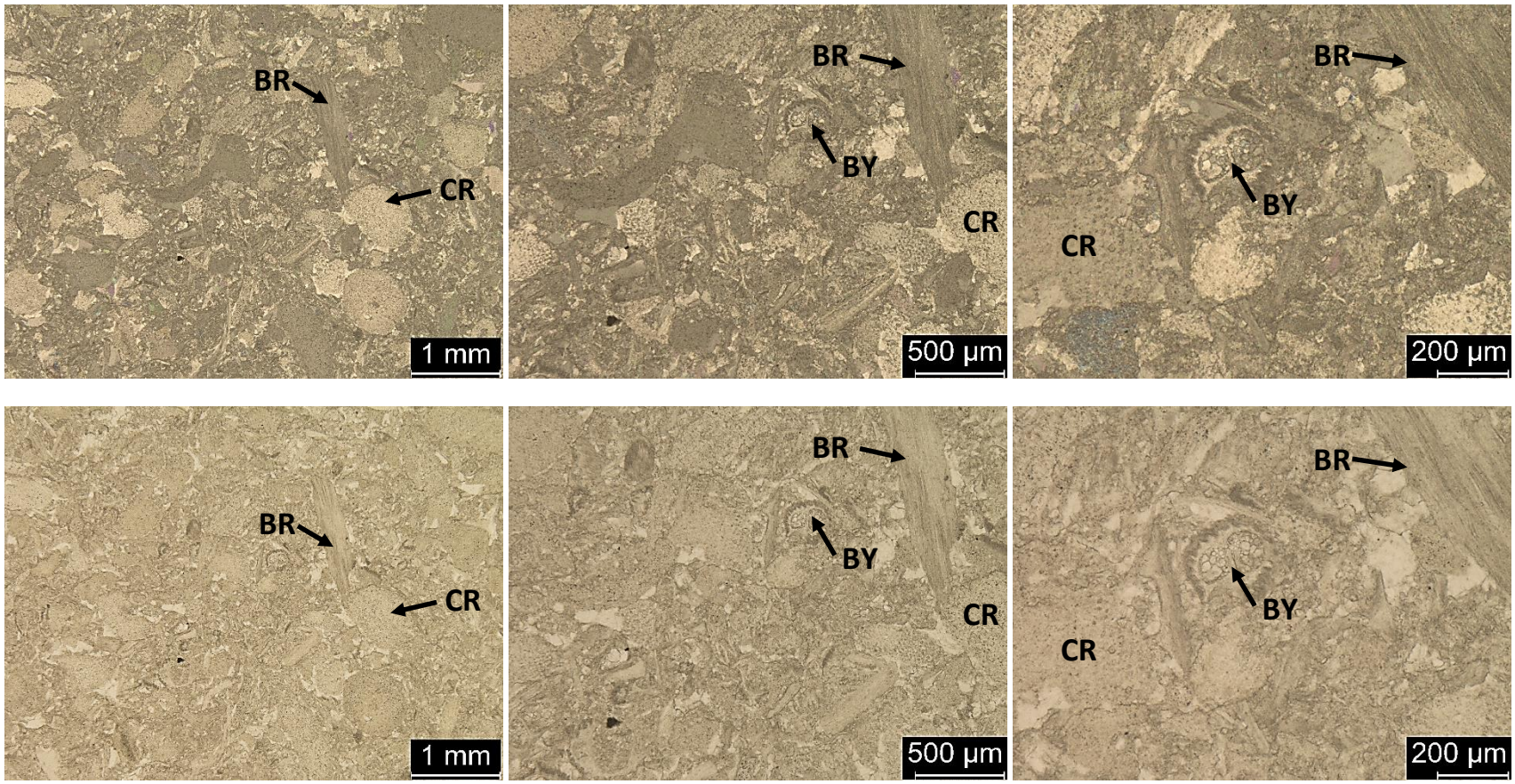

1p-16.5: Bryozoan-crinoidal packstone, very fine to course grained, moderately-poorly sorted. Contains 55% skeletal grains, 43% micrite matrix, and 2% calcite cement and pyrite (visual estimation). Grain types include crinoids (125µ – 1mm), bryozoans (62.5µ – 250µ), and brachiopods (500µ – 1mm). Pyrite and calcite cement occur throughout.

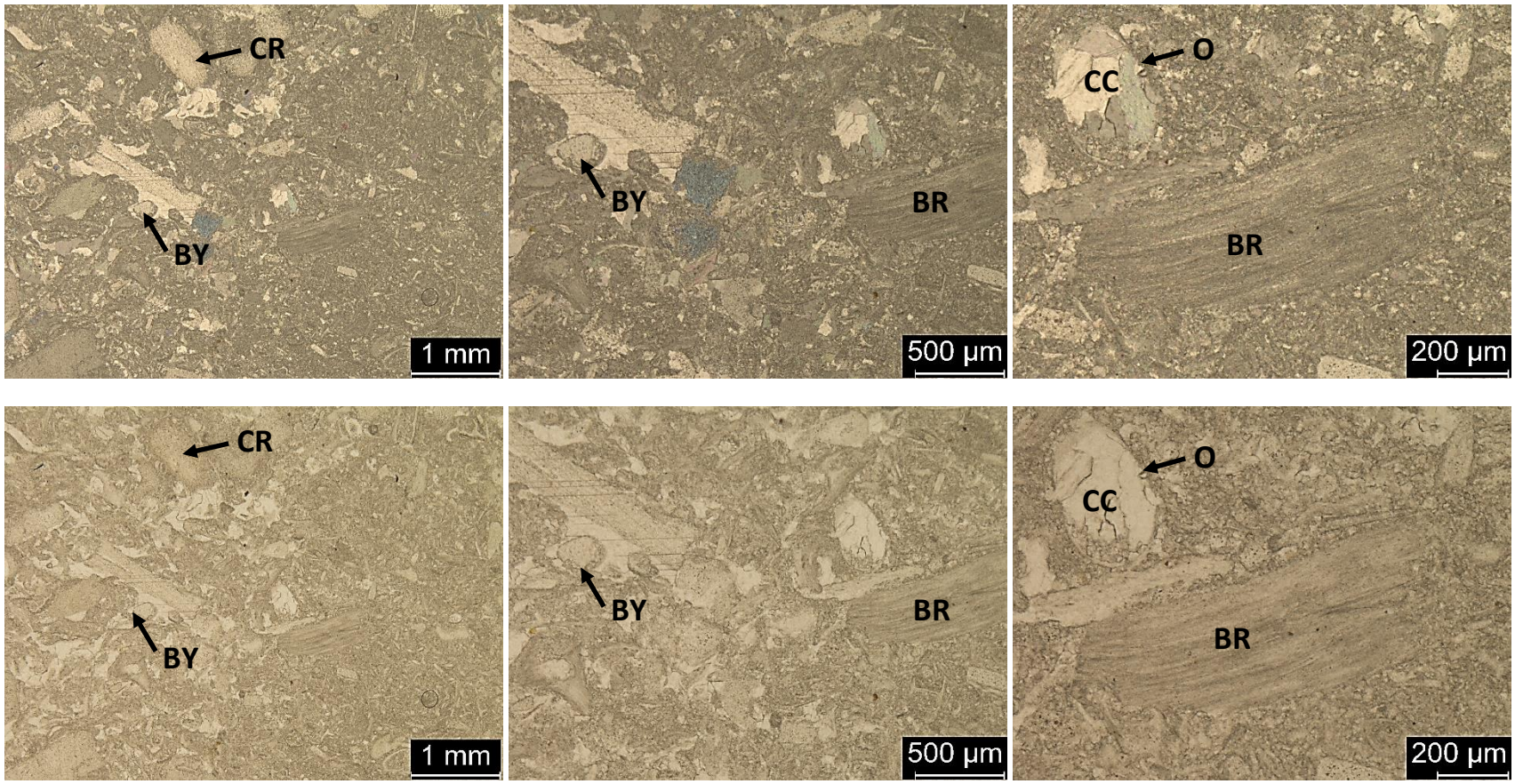

1p-19.75: Bryozoan-crinoidal wackestone-packstone, very fine to course grained, poorly sorted. Contains 35% skeletal grains, 64% micrite matrix, and 1% blocky calcite cement (visual estimation). Grain types include crinoids (200µ – 1mm), brachiopods (400µ – 750µ), bryozoans (250µ – 500µ), and ostracods (62.5µ – 200µ). Blocky calcite cement occurs within and between skeletal grains.

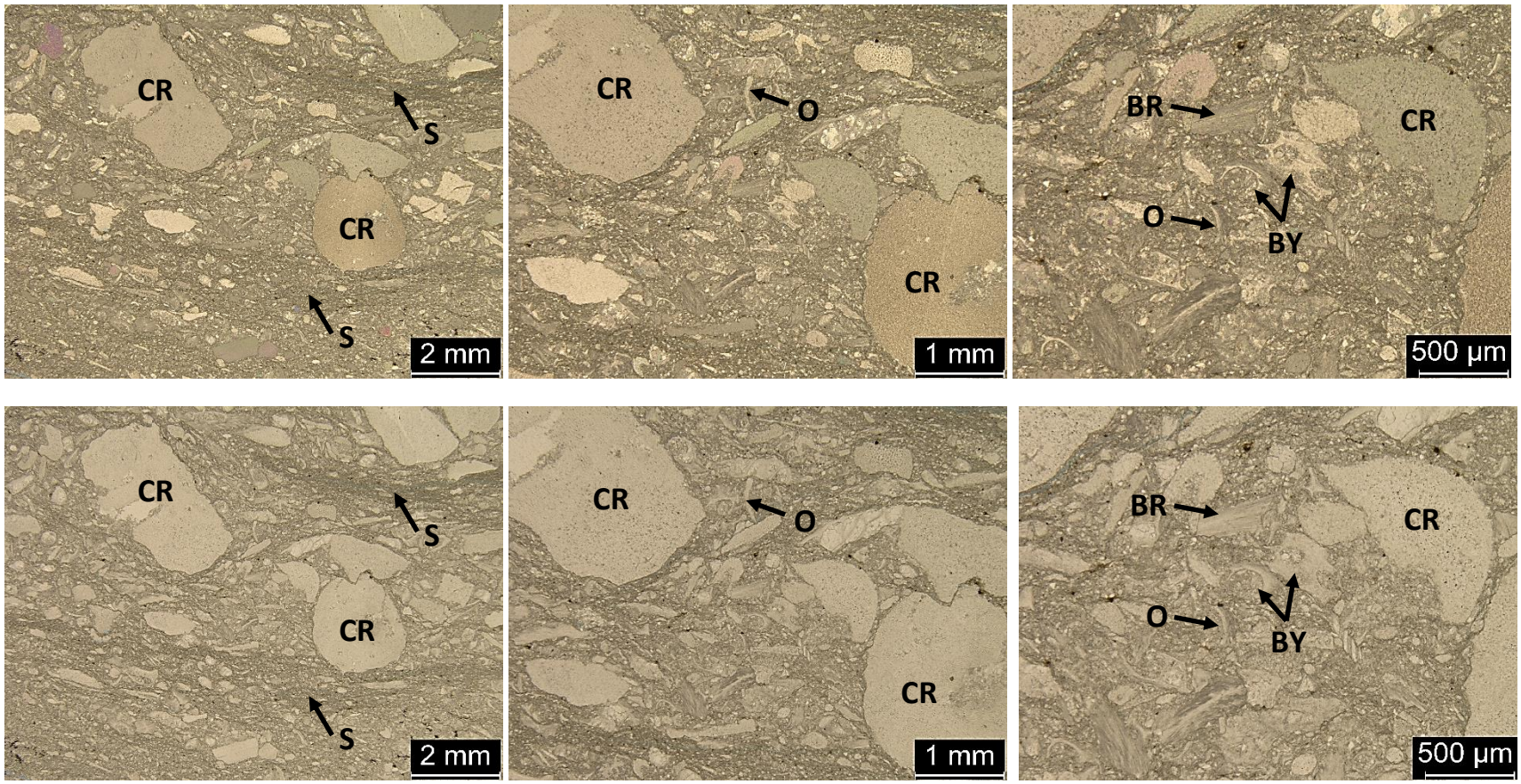

1p-20.75: Crinoidal wackestone, grain size ranges from fine sand to very fine pebbles, poorly sorted. Contains 35% skeletal grains, 64% micrite matrix, and 1% blocky calcite cement and pyrite (visual estimation). Grain types include crinoids (125µ – 3mm), bryozoans (125µ – 250µ), brachiopods (300µ – 500µ), and ostracods (125µ – 250µ). Muddy stylolites and dead oil can also be seen throughout.

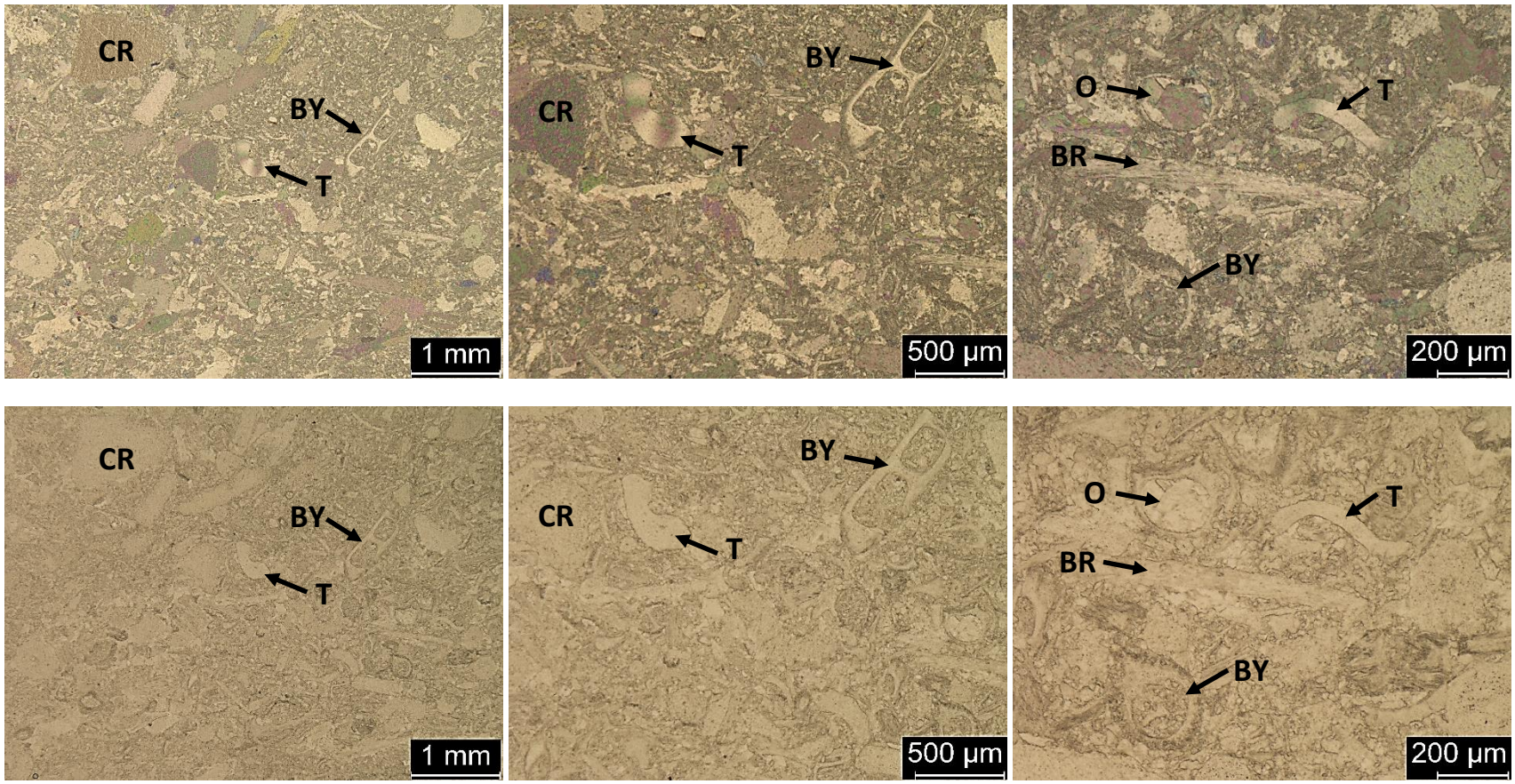

1p-22.0: Bryozoan mud-lean packstone, very fine to coarse grained, poorly sorted. Contains 55% skeletal grains, 43% micrite matrix, and 2% blocky calcite cement (visual estimation). Grain types include bryozoans (62.5µ – 500µ), crinoids (125µ – 1mm), brachiopods (500µ – 1mm), ostracods (62.5µ – 200µ), and trilobites (200µ – 500µ). Calcite cement occurs within and between skeletal grains.

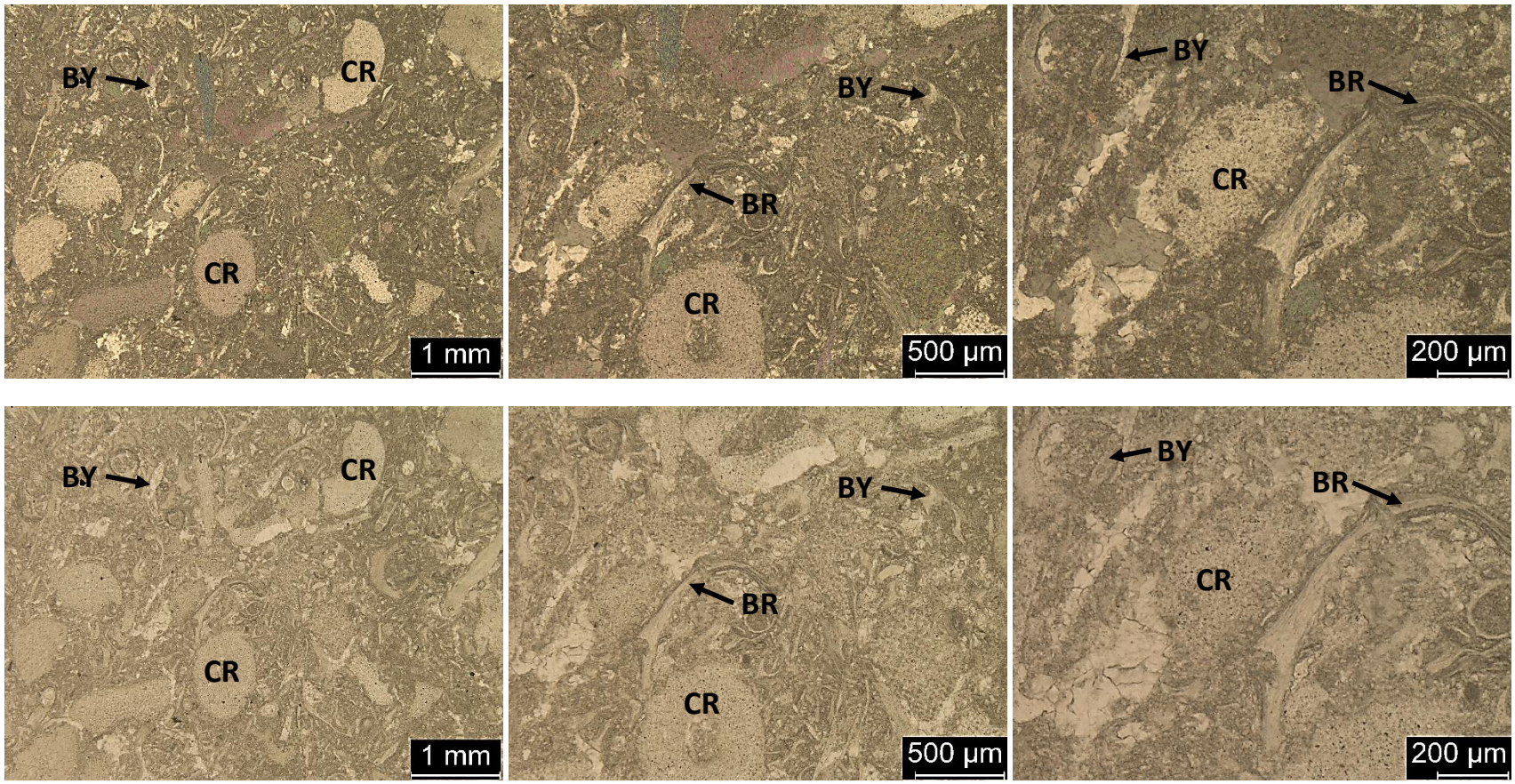

1p-23.75: Bryozoan-crinoidal wackestone, fine to coarse grained, poorly-moderately sorted. Contains 50% skeletal grains, 49% micrite matrix, and 1% blocky calcite cement (visual estimation). Grain types include bryozoans (125µ – 400µ), crinoids (250µ – 1mm), and brachiopods (400µ – 750µ). Calcite cement has filled within and between grains.

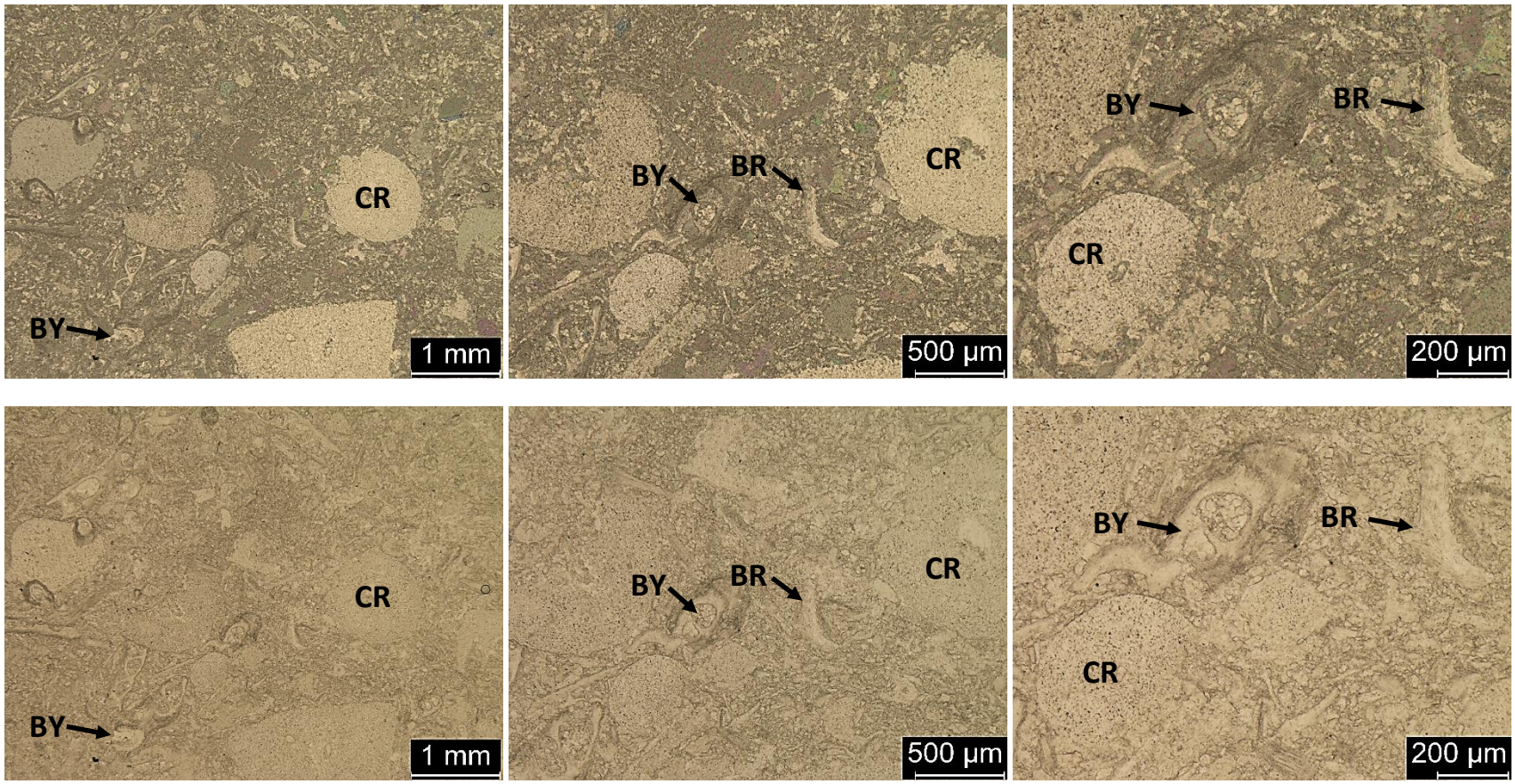

1p-24.5: Skeletal packstone, very fine to very coarse grained, poorly sorted. Contains 55% skeletal grains, 44% micrite matrix, and 1% blocky calcite cement (visual estimation). Grain types include crinoids (125µ – 2mm), bryozoans (200µ – 500µ), brachiopods (250µ – 500µ), and trilobites (600µ – 2mm). Calcite cement occurs throughout, between and within skeletal grains.

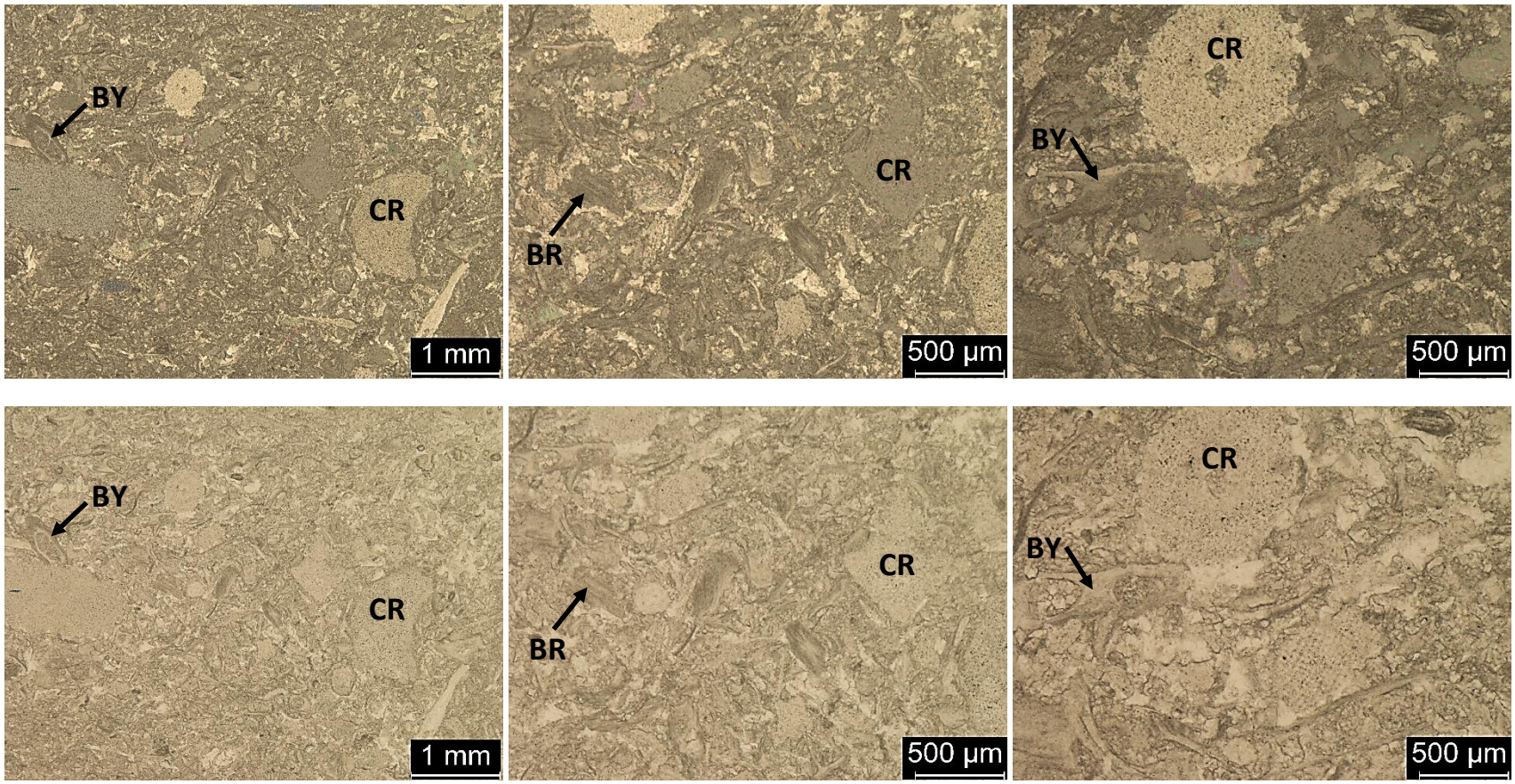

1p-25.0: Bryozoan wackestone-packstone, very fine to medium grained, poorly sorted. Contains 50% skeletal grains, 49% micrite matrix, and 1% calcite cement (visual estimation). Grain types include bryozoans (62.5µ – 500µ), crinoids (125µ – 500µ), and brachiopods (125µ – 400µ).

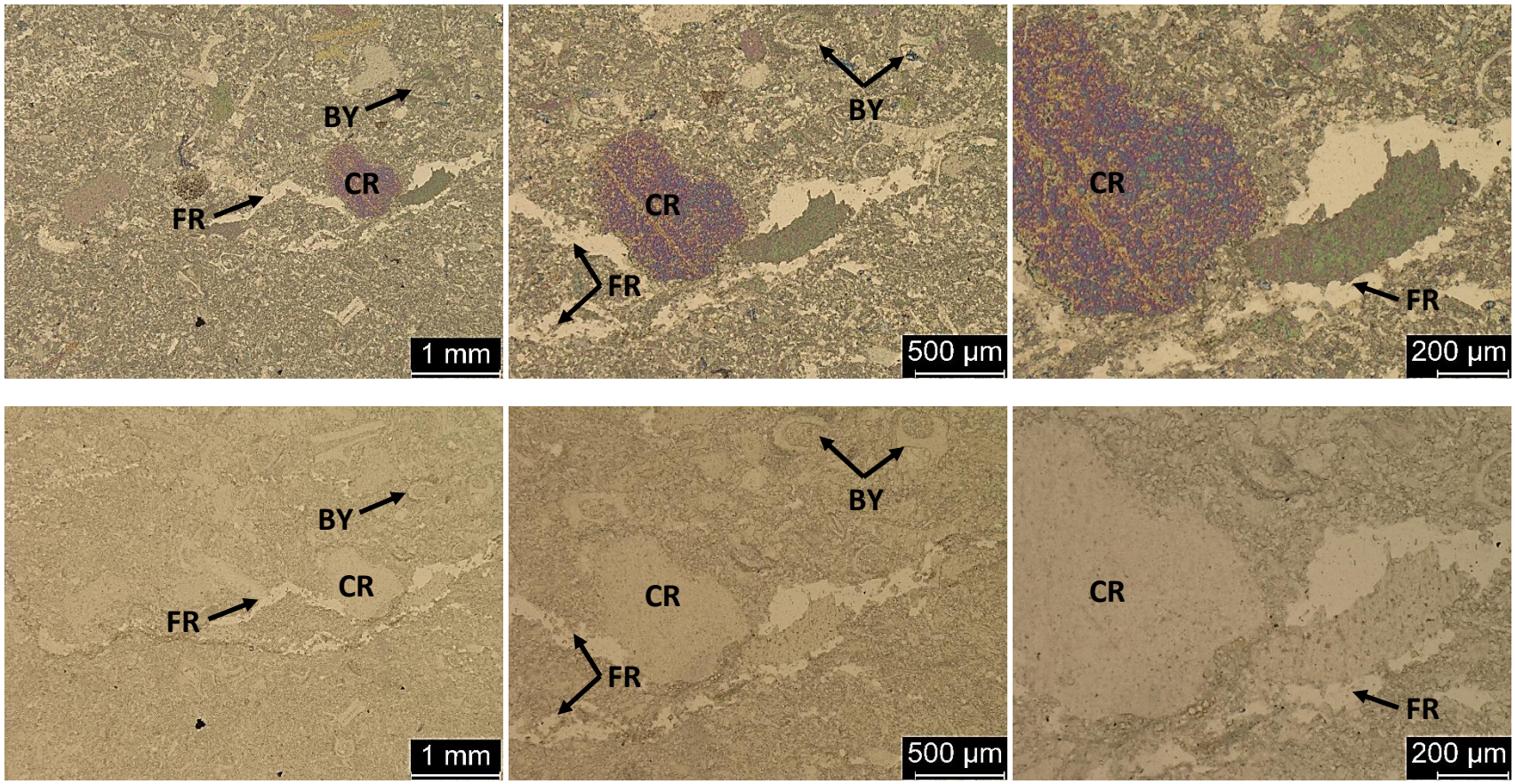

1p-25.75: Crinoidal-bryozoan wackestone-packstone, very fine to coarse grained, very poorly sorted. Contains 55% skeletal grains, 43% micrite matrix, and 2% calcite cement and fracture porosity (visual estimation). Grain types include crinoids (125µ – 1mm), bryozoans (62.5µ – 250µ), and ostracods (62.5µ – 125µ). Calcite cement and fracture porosity can be seen.

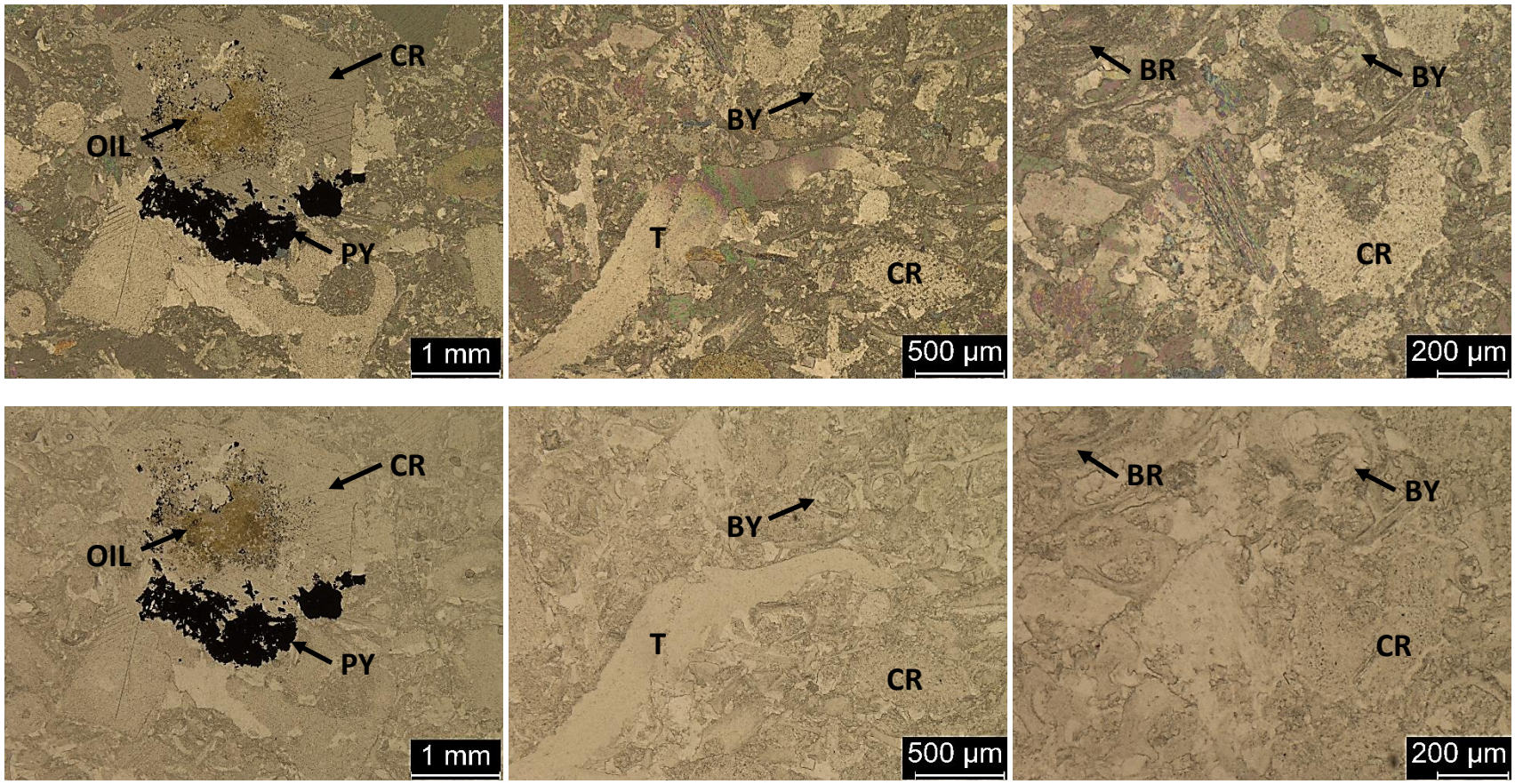

1p-29.0: Crinoidal-bryozoan mud-lean packstone to grainstone, fine to very coarse grained, poorly sorted. Contains 80% skeletal grains, 15% micrite matrix, and 5% pyrite, blocky calcite cement, and dead oil (visual estimation). Grain types include brachiopods (400µ – 700µ), crinoids (200µ – 2mm), bryozoans (125µ – 200µ), and trilobites (500µ – 2mmµ). Pyrite and dead oil are seen filling in a crinoid grain.

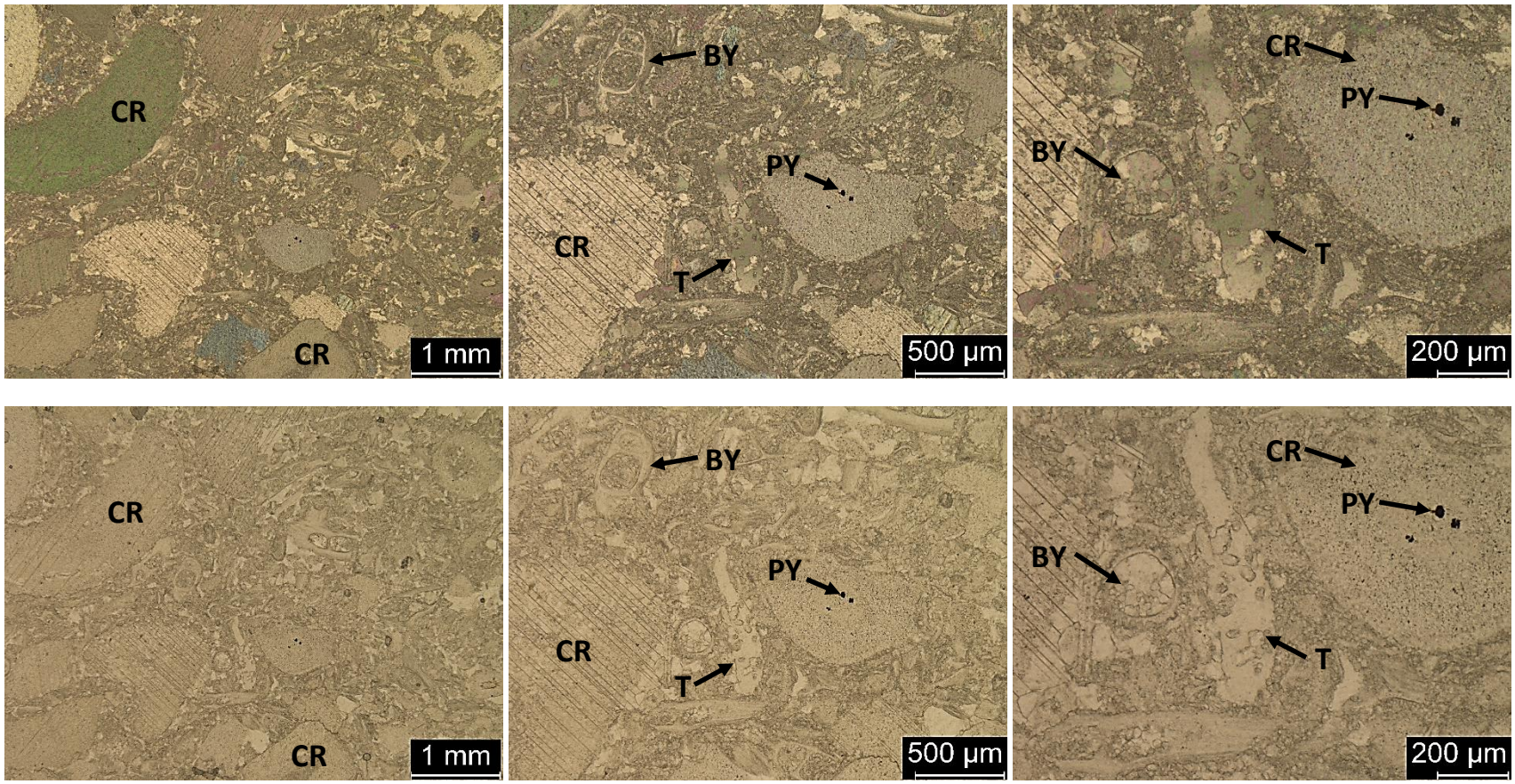

1p-30.0: Crinoidal-bryozoan mud-lean packstone, fine to very coarse grained, moderately to poorly sorted. Contains 65% skeletal grains, 32% micrite matrix, and 3% blocky calcite cement (visual estimation). Grain types include crinoids (125µ – 2mm), bryozoans (125µ – 500µ), trilobites (300µ – 600µ), and brachiopods (450µ – 650µ). Pyrite has formed on a crinoid grain.

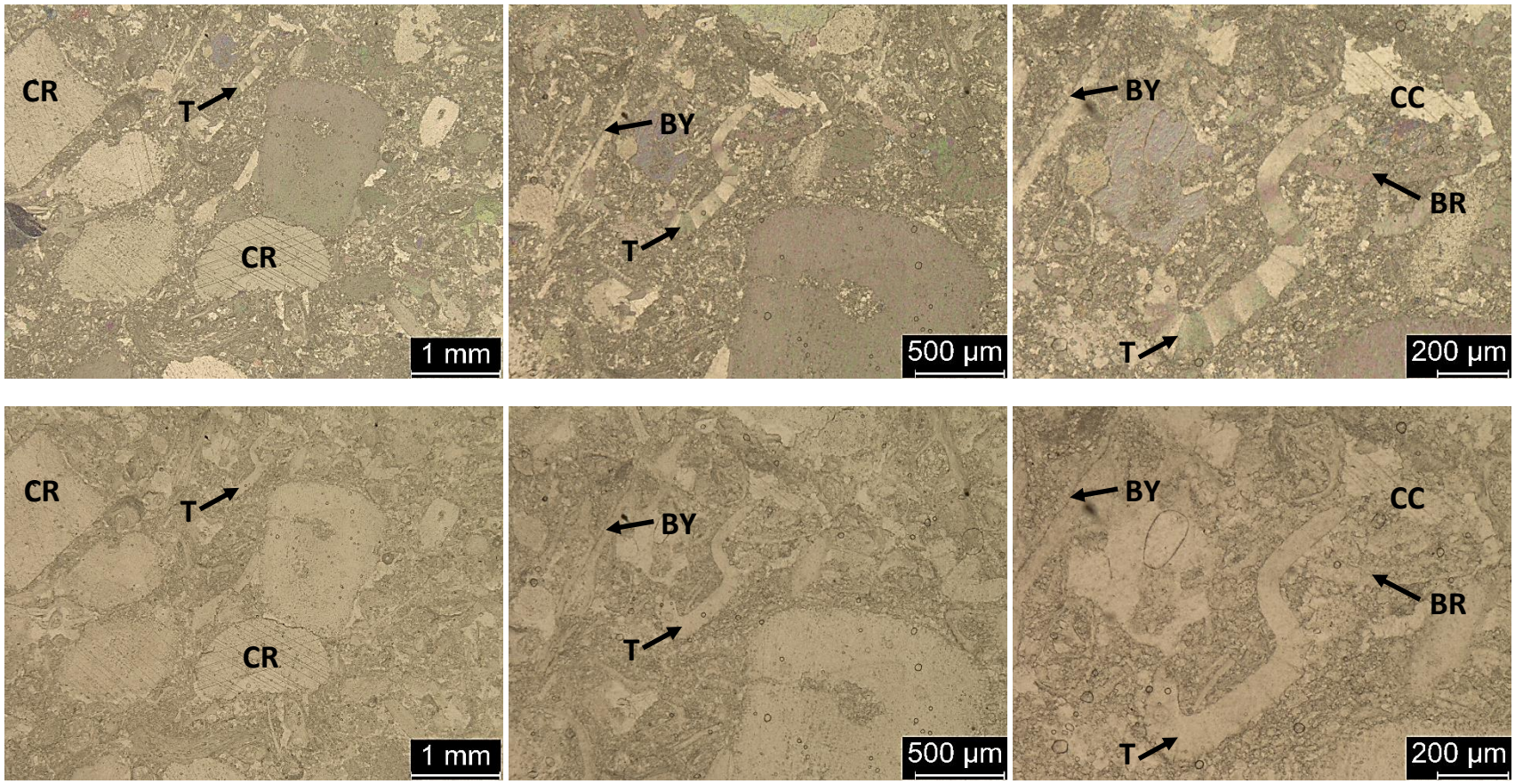

1p-30.5: Bryozoan-crinoidal wackestone to packstone, fine to very coarse grained, poorly sorted. Contains 60% skeletal grains, 37% micrite matrix, and 3% blocky calcite cement and pyrite (visual estimation). Grain types include bryozoans (125µ – 500 µ), brachiopods (500µ – 1mm), crinoids (250µ – 2mm), and trilobites (500µ – 1mm).

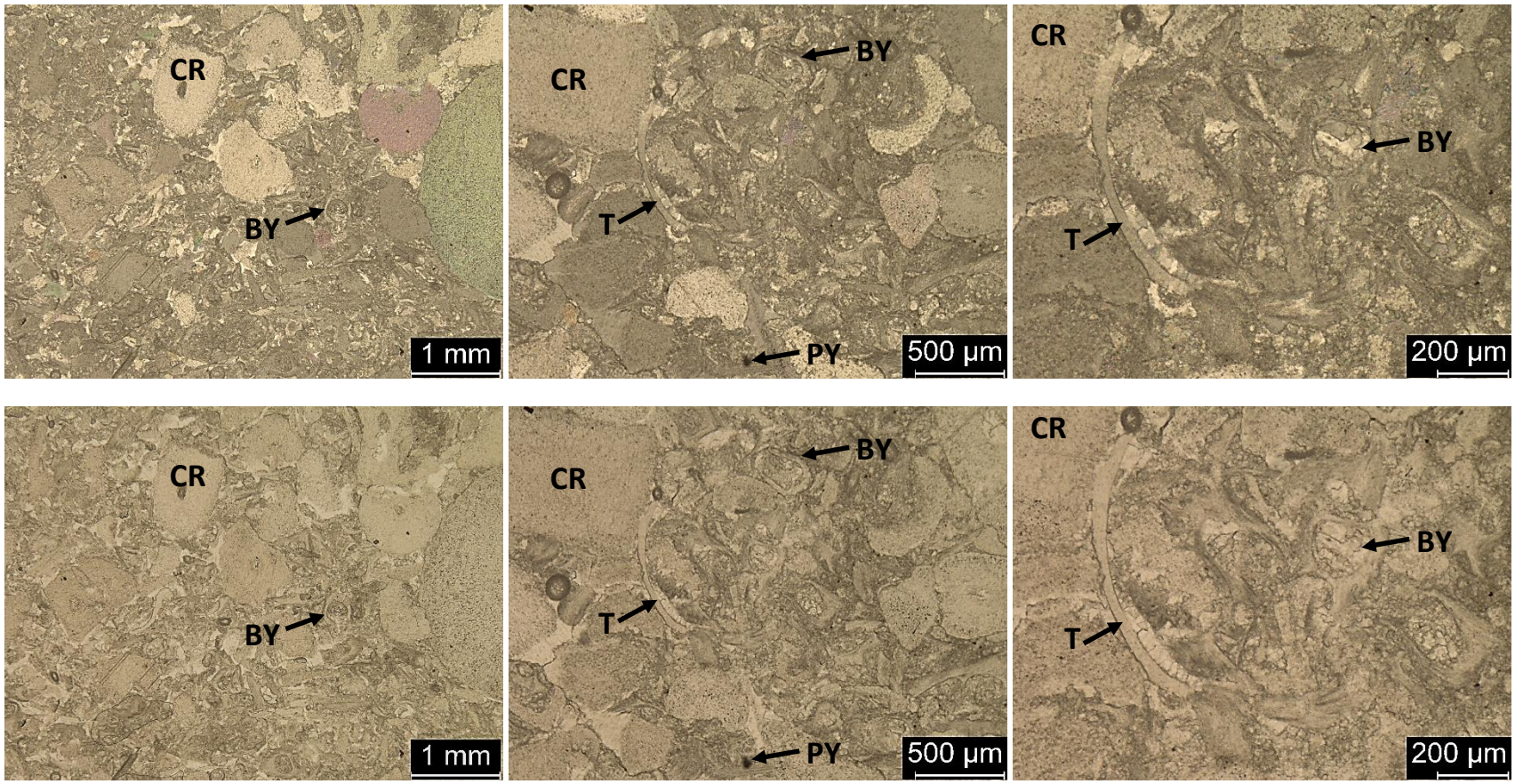

1p-32.0: Crinoidal mud-lean packstone-grainstone, medium to very coarse grained, moderately to poorly sorted. Contains 75% skeletal grains, 24% micrite matrix, and 1% blocky calcite cement and pyrite (visual estimation). Grain types include crinoids (250µ – 2mm), bryozoans (250µ – 300µ), brachiopods (300µ – 600µ), and trilobites (500µ – 1mm). Calcite cement and pyrite can also be seen.

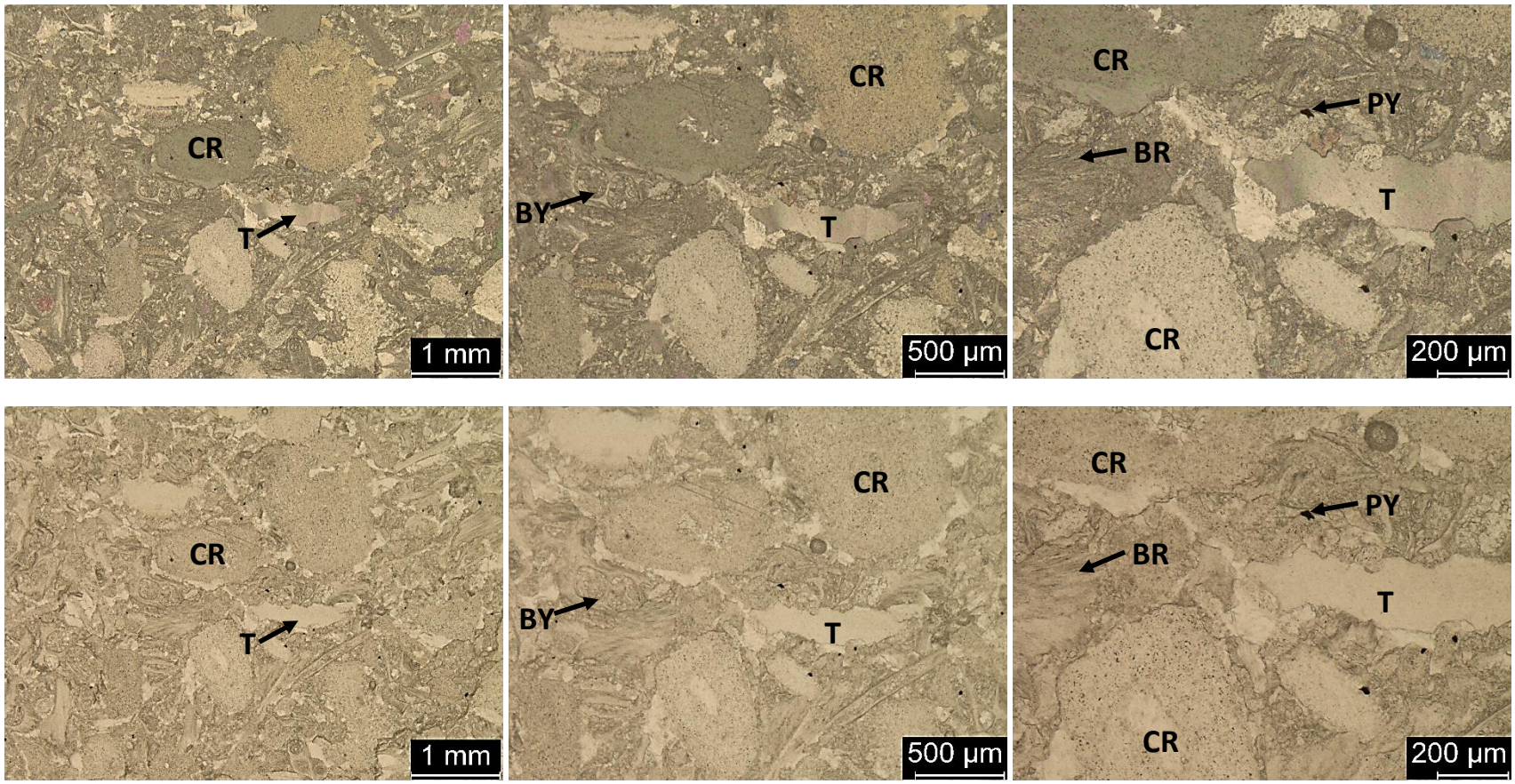

1p-33.25: Bryozoan-crinoidal mud-lean packstone-grainstone, fine to very coarse grained, poorly sorted. Contains 75% skeletal grains, 20% micrite matrix, and 5% pyrite and calcite cement (visual estimation). Grain types include crinoids (250µ – 2mm), bryozoans (125µ – 500µ), brachiopods (250µ – 600µ), ostracods (125µ – 200µ), and trilobites (500µ – 1mm).

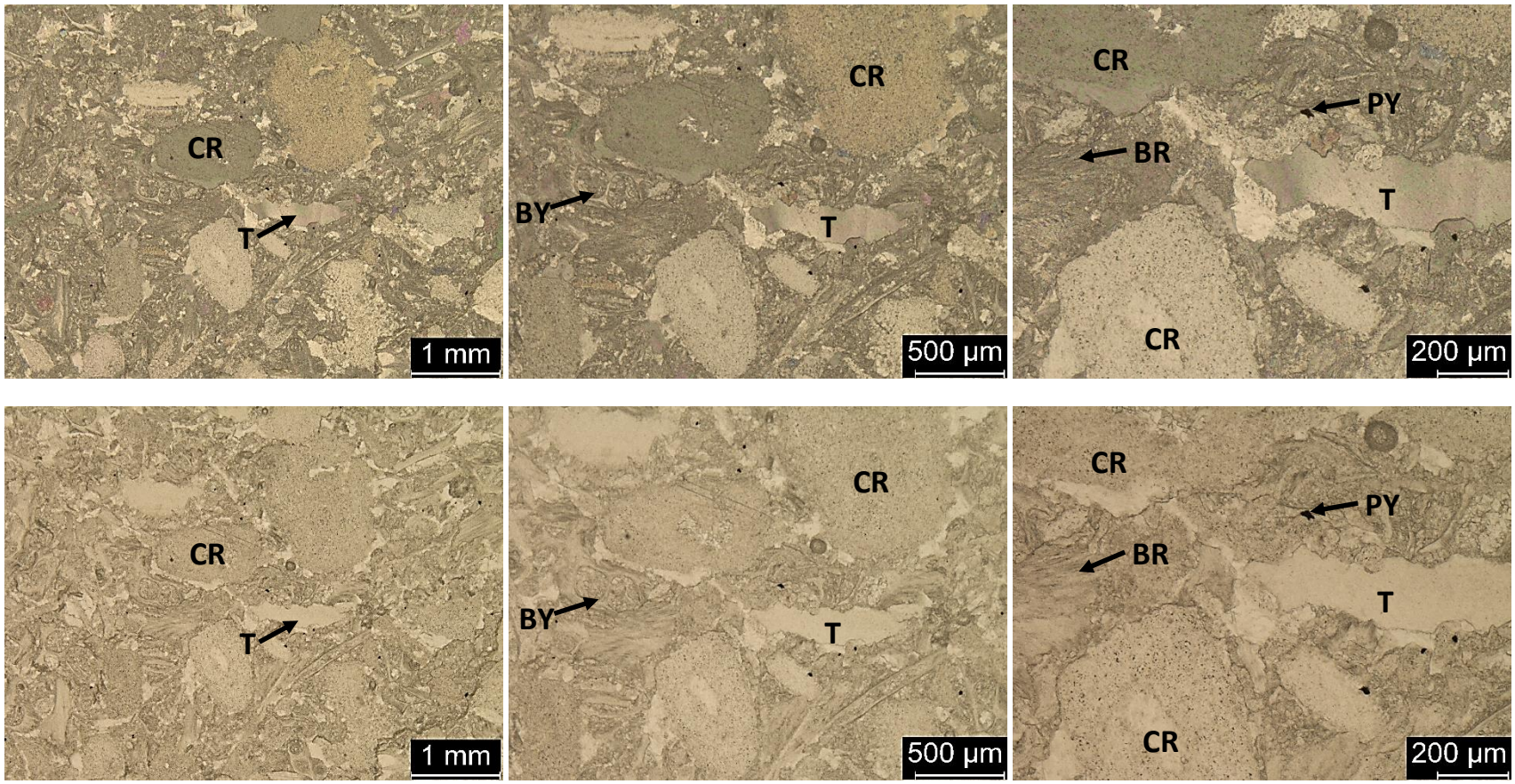

1p-33.25: Bryozoan-crinoidal mud-lean packstone-grainstone, fine to very coarse grained, poorly sorted. Contains 75% skeletal grains, 20% micrite matrix, and 5% pyrite and calcite cement (visual estimation). Grain types include crinoids (250µ – 2mm), bryozoans (125µ – 500µ), brachiopods (250µ – 600µ), ostracods (125µ – 200µ), and trilobites (500µ – 1mm).

Vertical Section 2

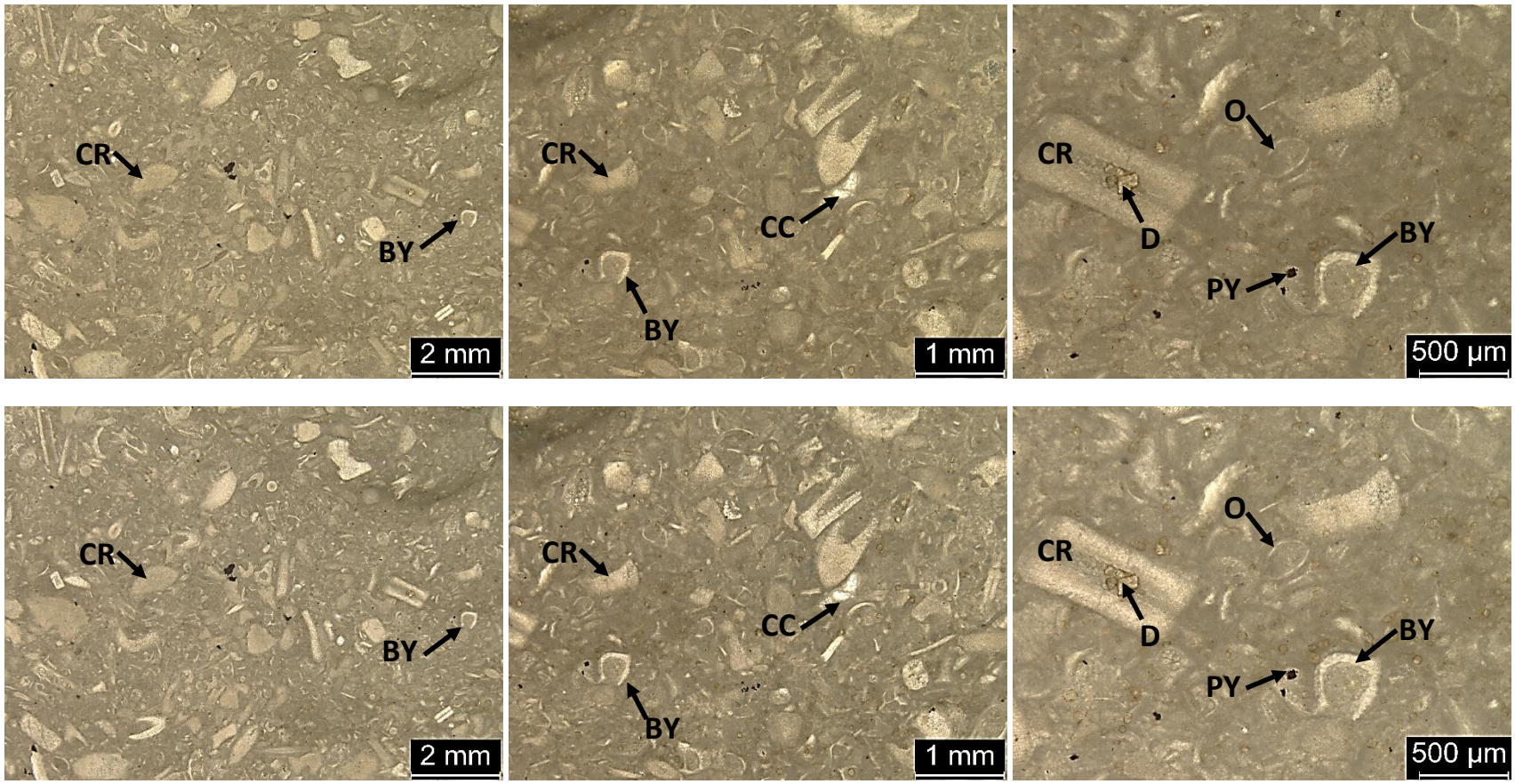

2c-1.25: Skeletal wackestone, very fine to coarse grained, poorly to moderately sorted. Contains 30% skeletal grians, 69% micrite matrix, and 1% pyrite and blocky calcte cement (visual estimation). Grain types include crinoids (62.5µ - 1mm), bryozoans (62.5µ – 250µ), and ostracods (125µ – 250µ).

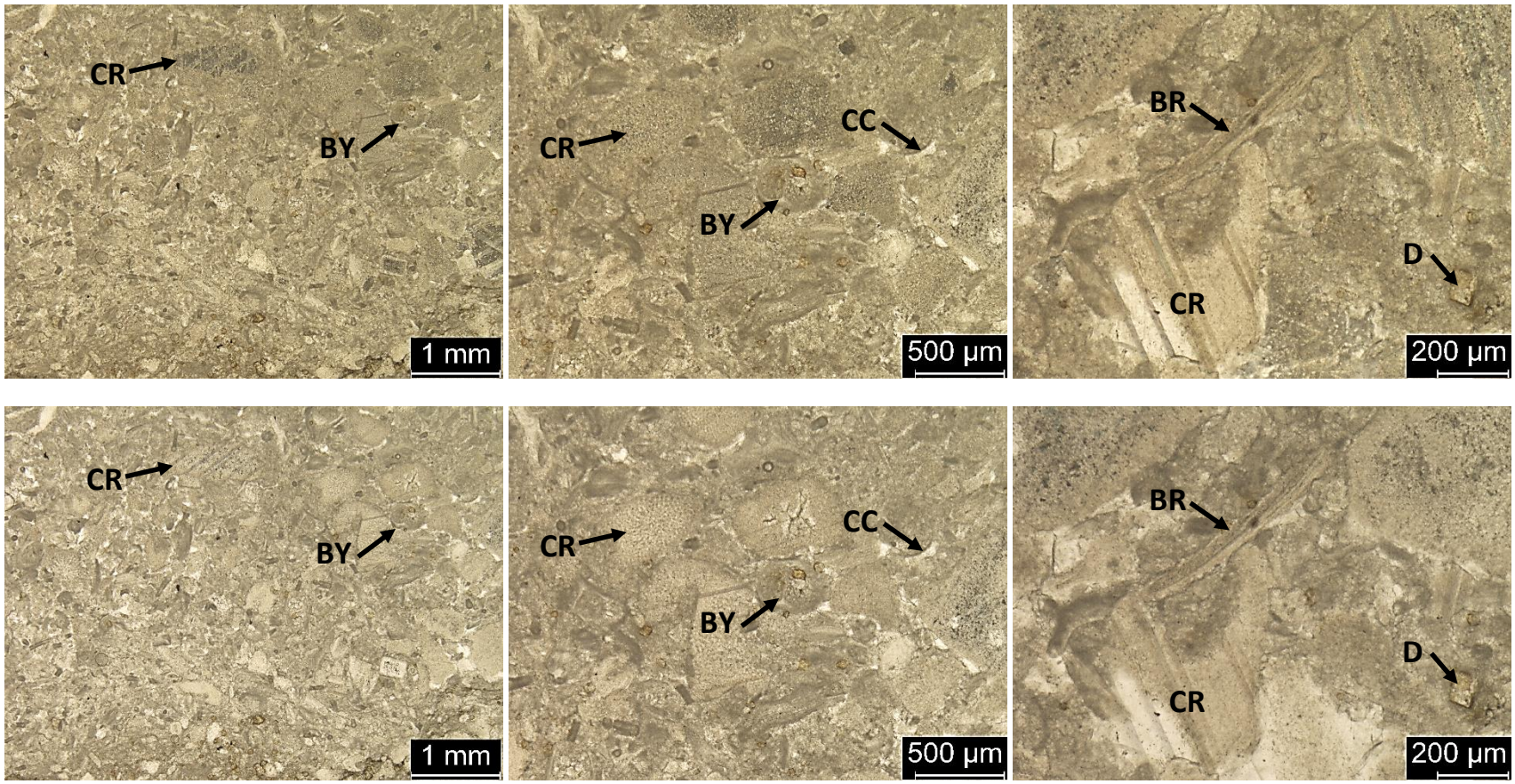

2c-2.5: Crinoidal grainstone to mud-lean packstone, fine to medium grained, moderatley sorted. Contains 80% skeletal grains, 19% calcite cement, and 1% dolomite and pyrite (visual estimation). Grain types include crinoids (125µ – 500µ), bryozoans (125µ – 400µ), and brachiopods (250µ – 500µ).

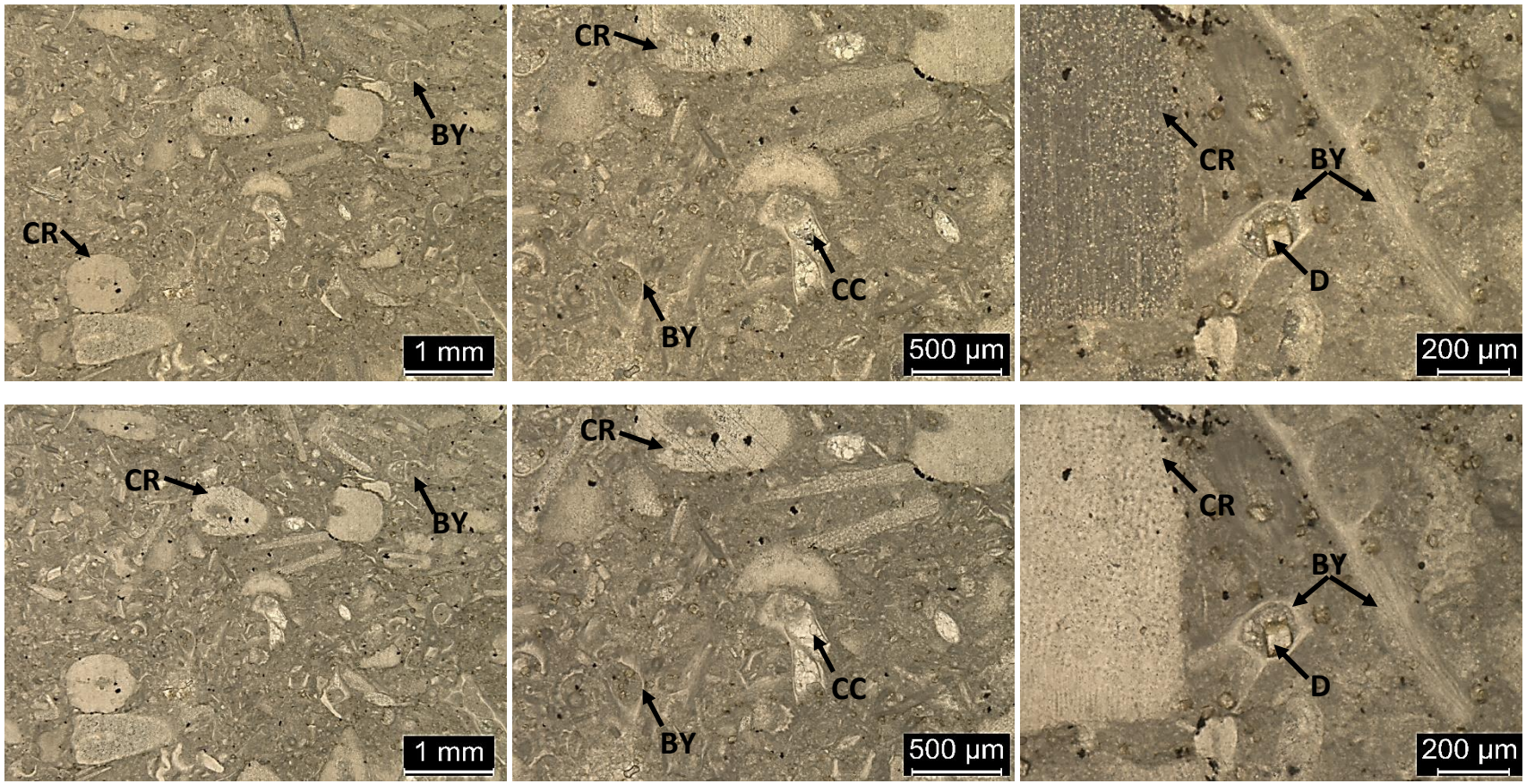

2c-3.0: Bryozoan-crinoidal wackestone to packstone, very fine to coarse grained, poorly sorted. Contains 40% skeletal grains, 56% micrite matrix, and 4% pyrite, blocky calcite cement, and dolomite (visual estimation). Grain types include crinoids (125µ - 1mm) and bryozoans (200µ - 500µ). Dolomite rhombs and calcite cement occur within some of the bryozoans.

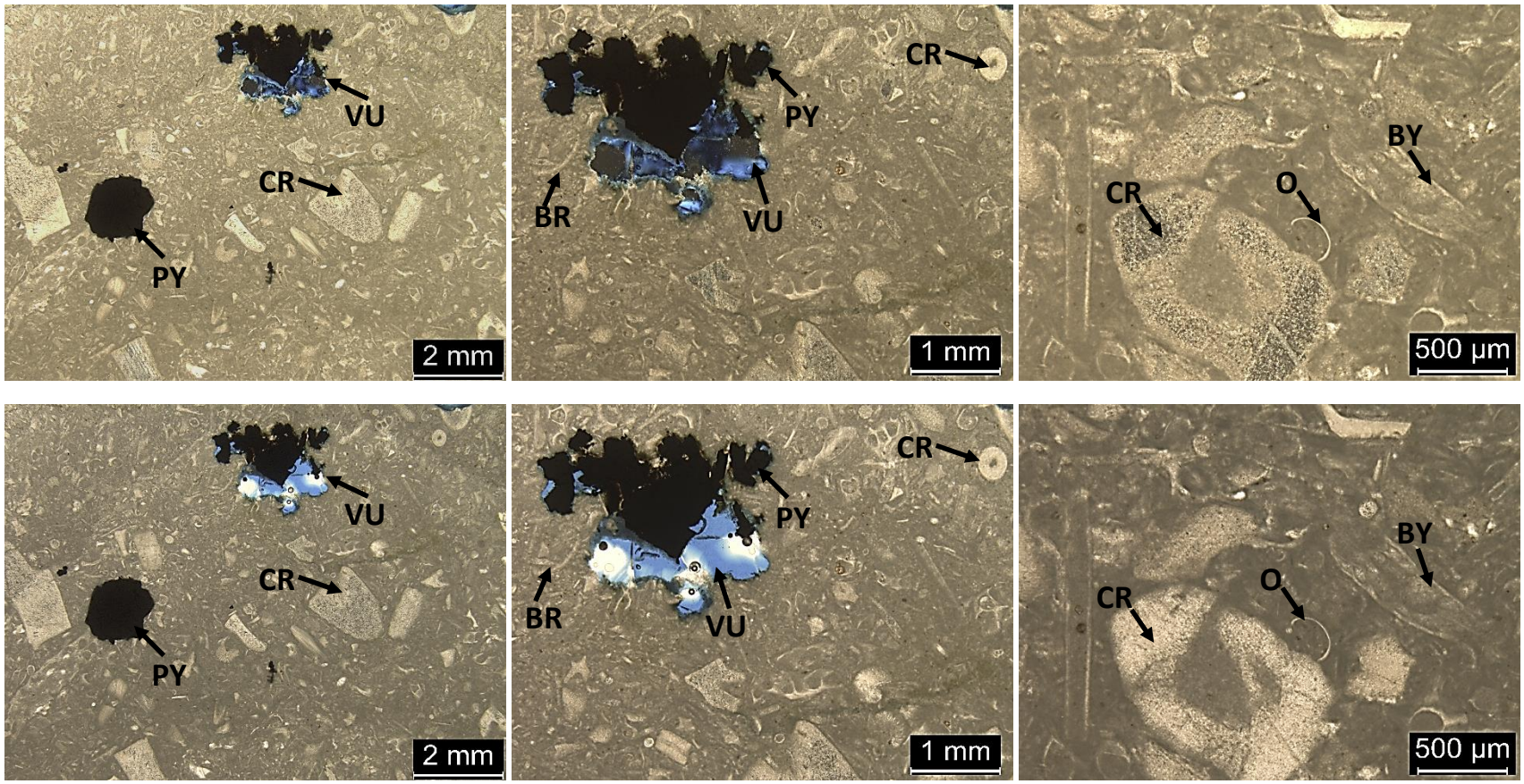

2c-5.0: Skeletal wackestone, very fine to coarse grained, poorly sorted. Contains 25% skeletal grains, 80% micrite matrix, 1% porosity, and 3% pyrite and calcite cement (visual estimation). Grain types include crinoids (250µ - 1mm), bryozoans (125µ - 250µ), ostracods (125µ - 250µ), and brachiopods (500µ - 750µ). A vug partially filled with pyrite can be seen at the left.

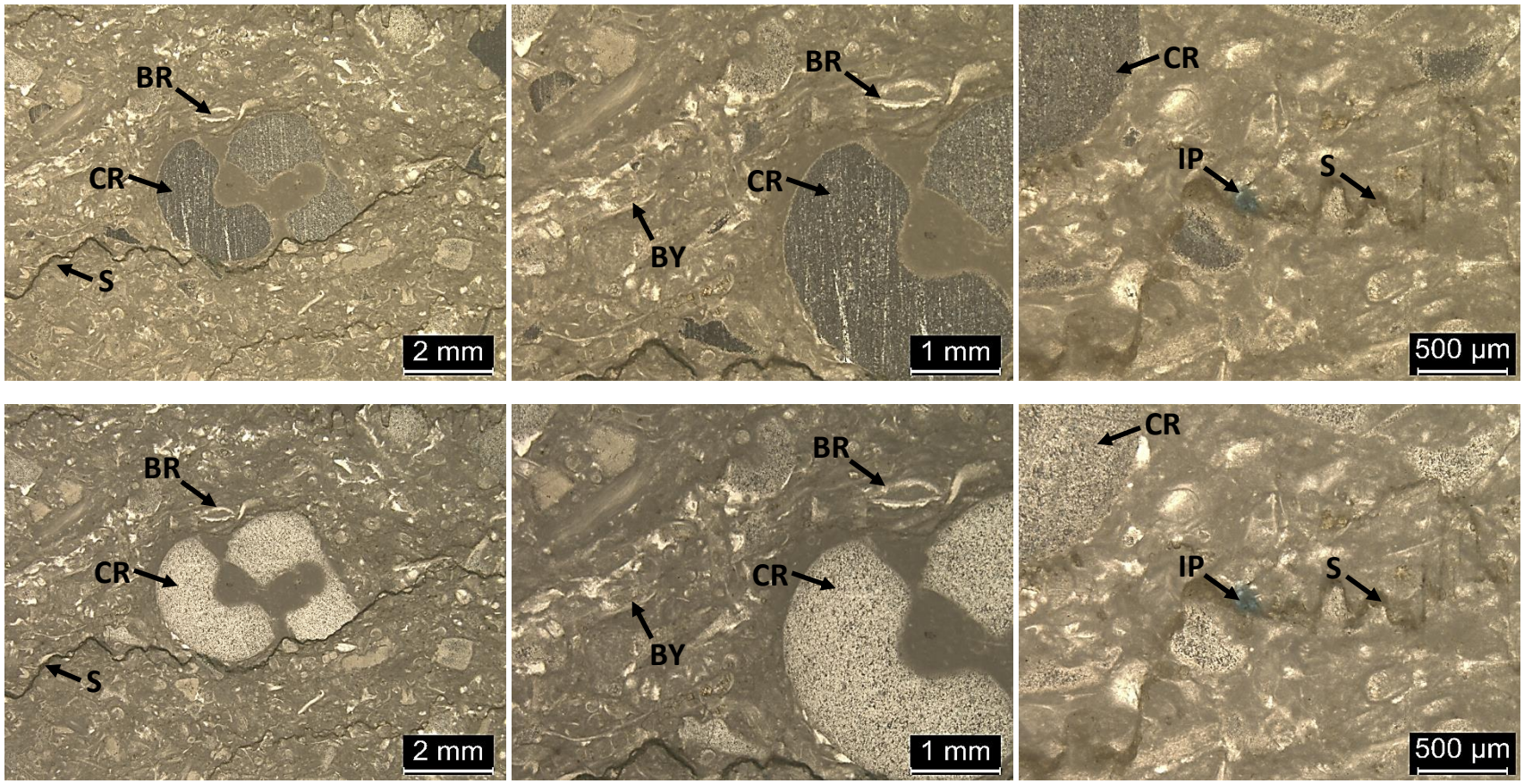

2c-6.0: Bryozoan wackestone, very fine to very coarse grained, poorly sorted. Contains 35% skeletal grains, 64% micrite matrix, and 1% pyrite, blocky calcite cement, and porosity. Grain types include crinoids (250µ - 2mm), brachiopods (500µ - 1mm), and bryozoans (125µ - 250µ). Interparticle porosity can be seen along a stylolite in the 500 µm-scale thin section photomicrograph.

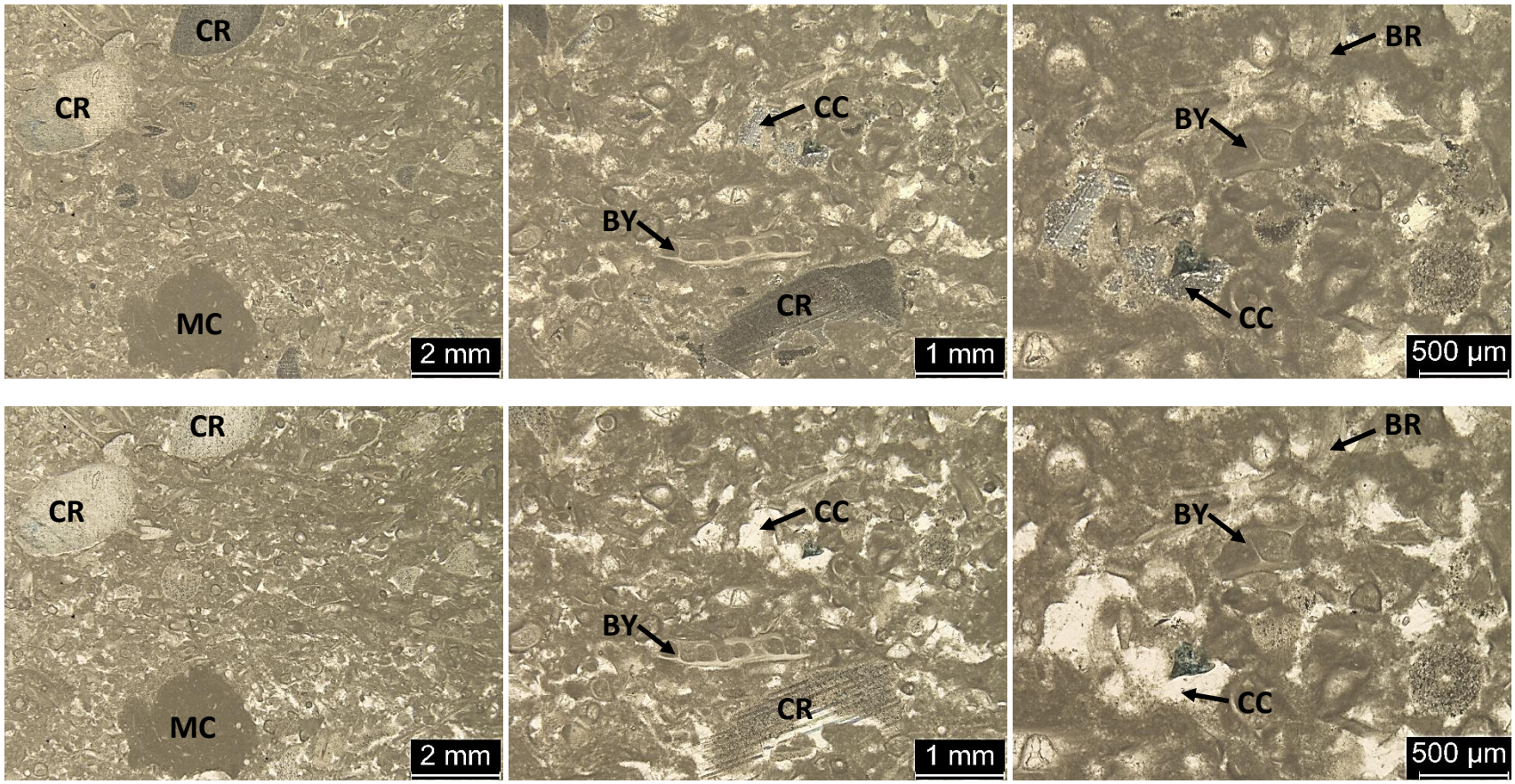

2c-6.2: Bryozoan-crinoidal wackestone to packstone, grain size ranges from fine sand to very fine pebbles, poorly sorted. Contains 40% skeletal grains, 50% micrite matrix, and 10% calcite cement (visual estimation). Grain types include crinoids (250µ – 3 mm) and bryozoans (125µ – 2mm). The sample location for this thin section is between Block 1 and 3, where bedding evidence suggests block movement. A mud clast (2mm wide) associated with this movement can be seen in the first thin section above.

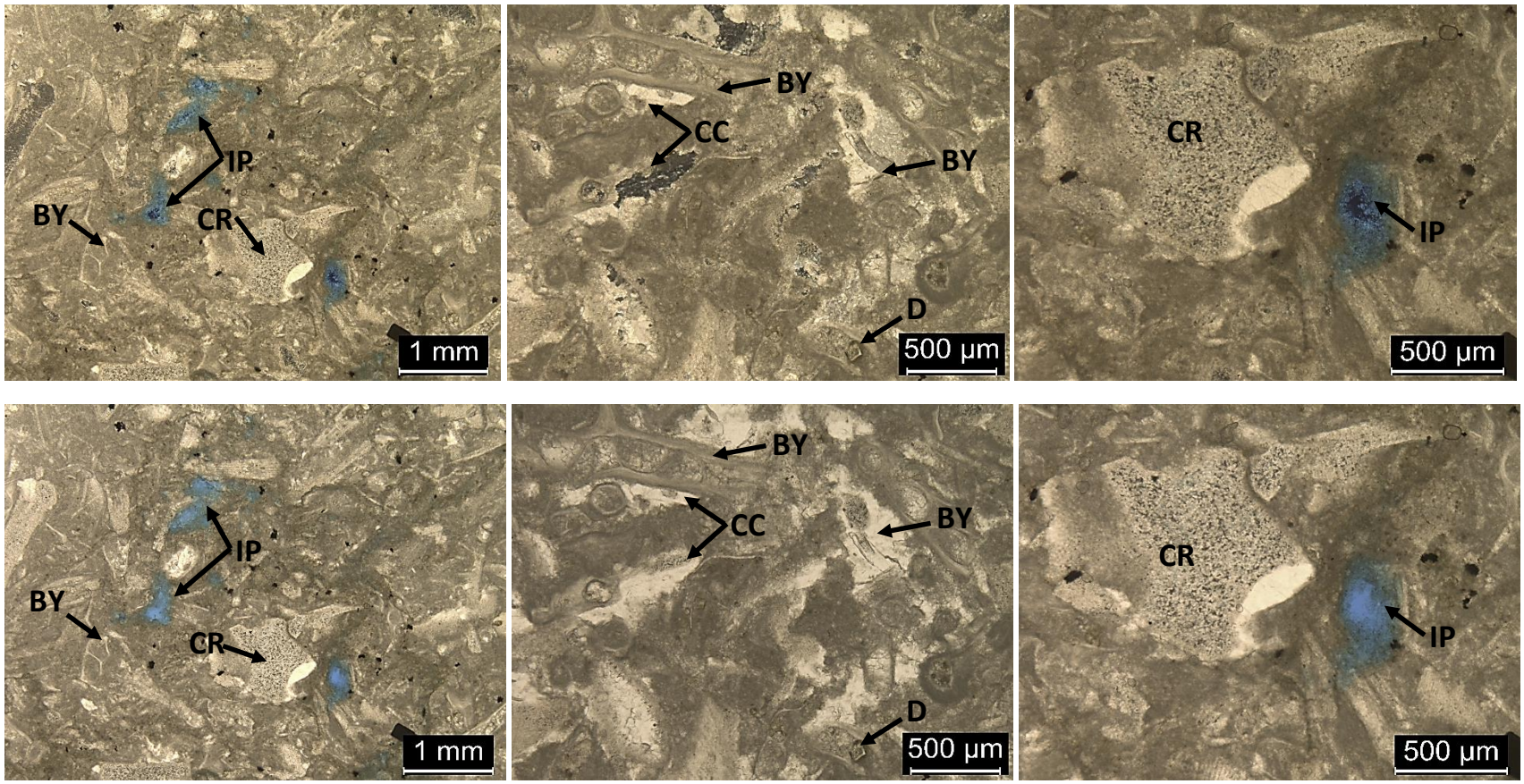

2c-7.0: Crinoidal-bryozoan skeletal wackestone, fine to coarse grained, moderately-poorly sorted. Contains 50% skeletal grains, 48% micrite matrix, and 2% calcite cement, pyrite, and porosity (visual estimation). Grain types include fenestrate bryozoans (250µ - 1mm), ostracods (125µ - 250µ), and brachiopods (250µ - 500µ).

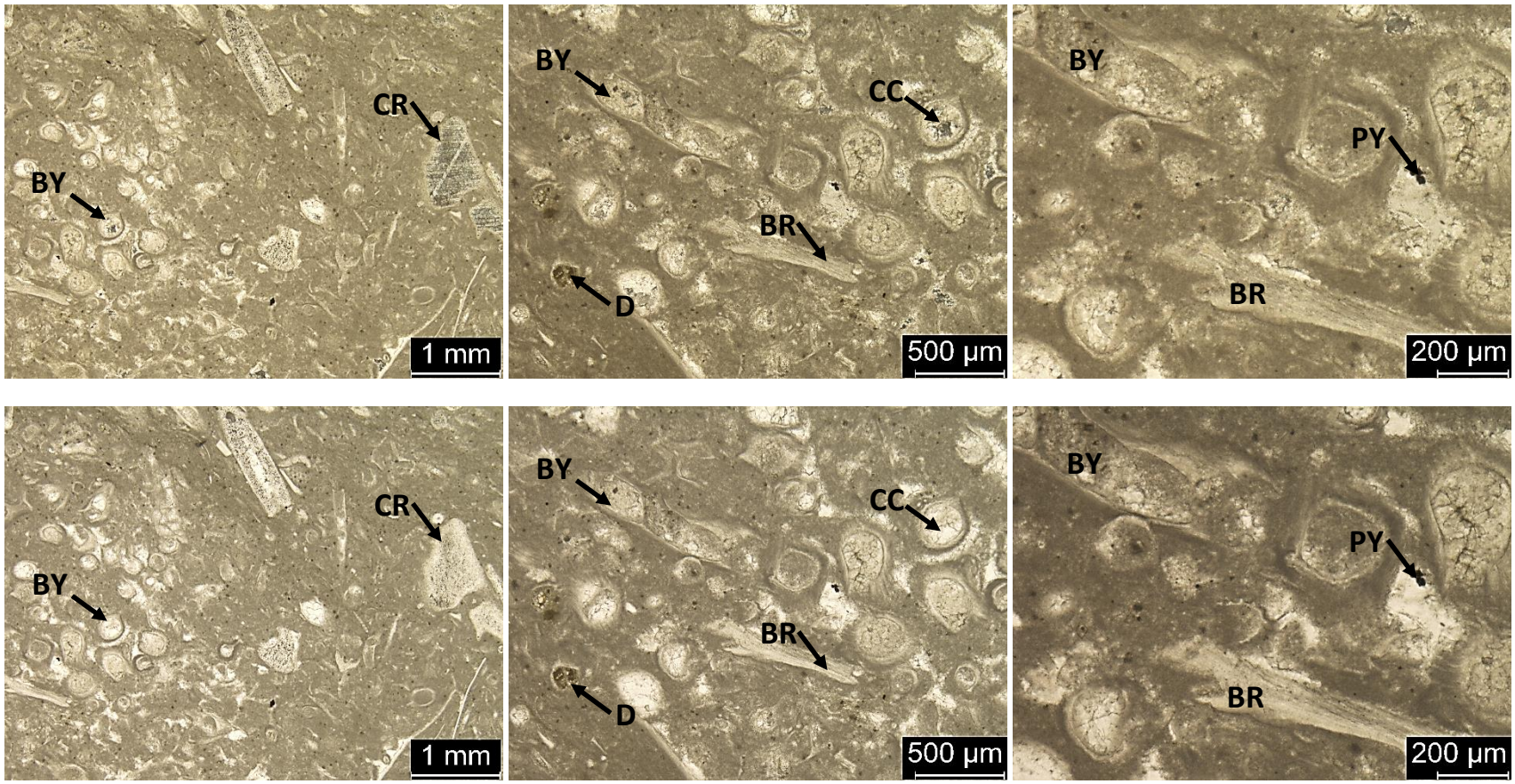

2c-7.5: Bryozoan wackestone, fine to coarse grained, poorly to moderately sorted. Contains 35% skeletal grains, 63% micrite matrix, and 2% blocky calcite cement and pyrite (visual estimation). Grain types include bryozoans (125µ – 1mm), crinoids (250µ – 1mm), and brachiopods (350µ – 600µ).

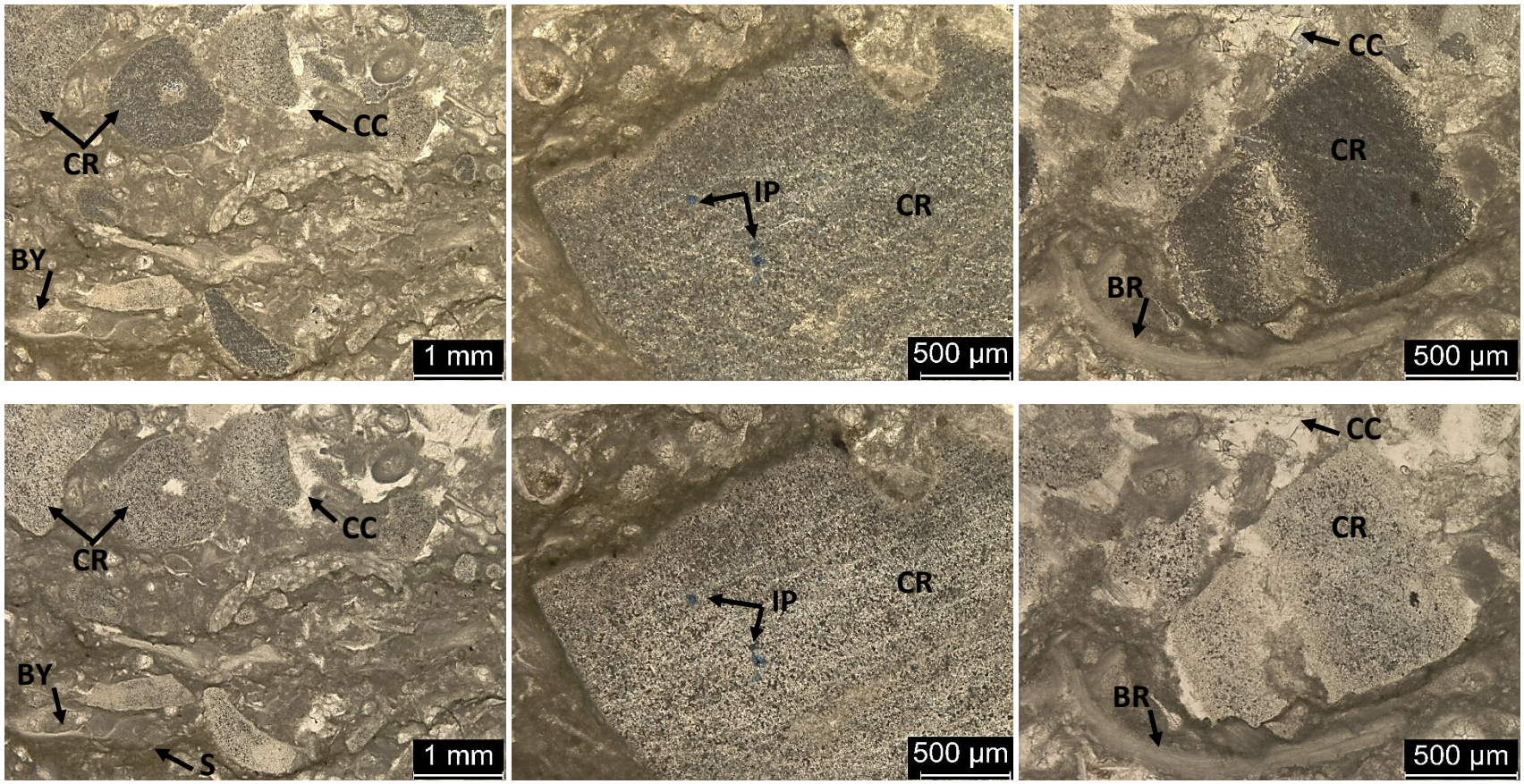

2c-9.5: Crinoidal wackestone, fine to very coarse grained, poorly sorted. Contains 40% skeletal grains, 56% micrite matrix, and 4% blocky calcite cement, porosity and pyrite (visual estimation). Grain types include crinoids (250µ - 2mm), bryozoans (250µ - 1mm), brachiopods (500µ - 1mm), and ostracods (125µ - 250µ).

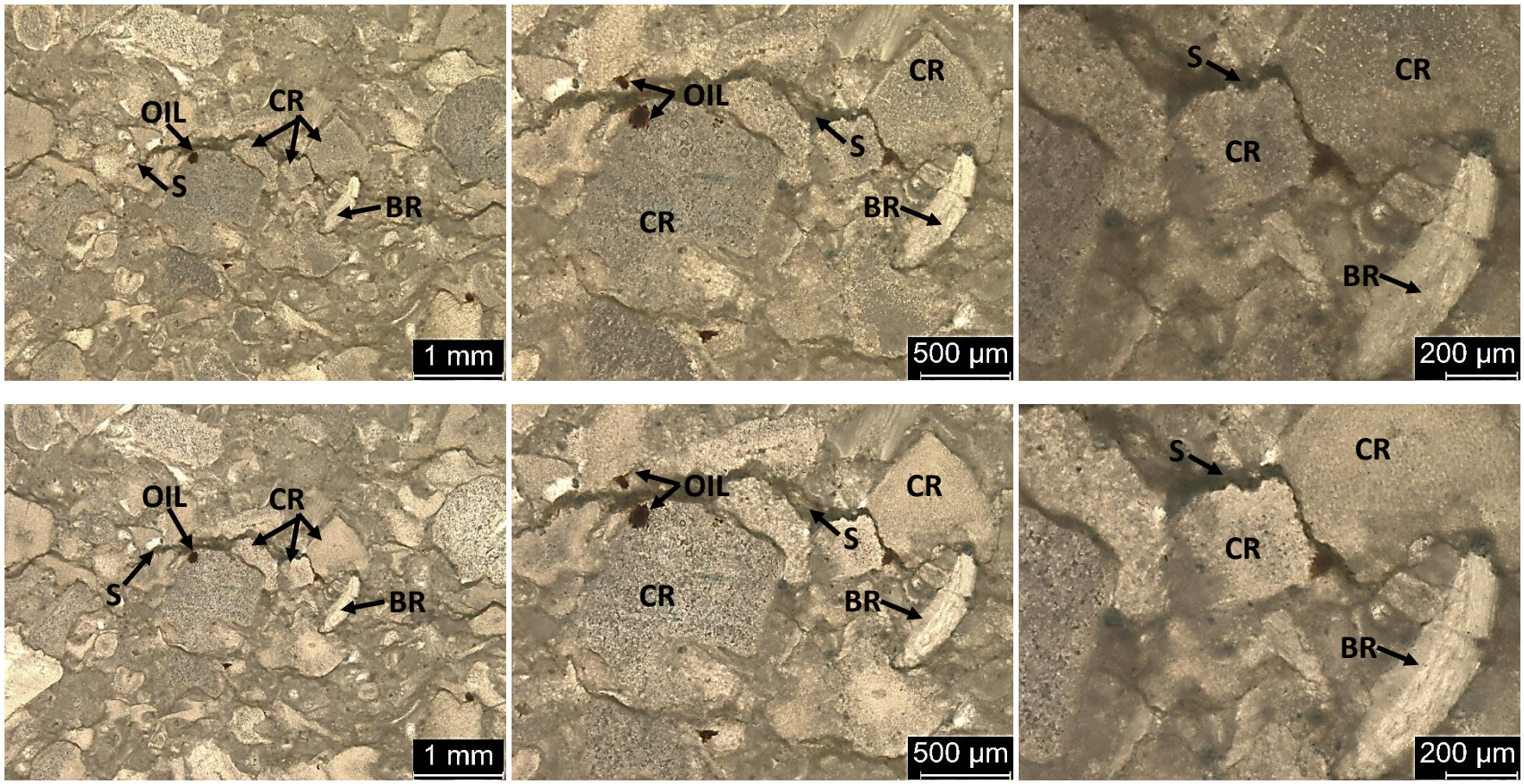

2nv-1.25: Crinoidal mud-lean packstone-grainstone, medium to coarse grained, moderately-poorly sorted. Contains 85% skeletal grains, 14% micrite matrix, and 1% calcite cement and dead oil (visual estimation). Grain types include crinoids (500µ - 1mm) and brachiopods (250µ - 500µ). Other features include muddy stylolites, calcite cement, and dead oil.

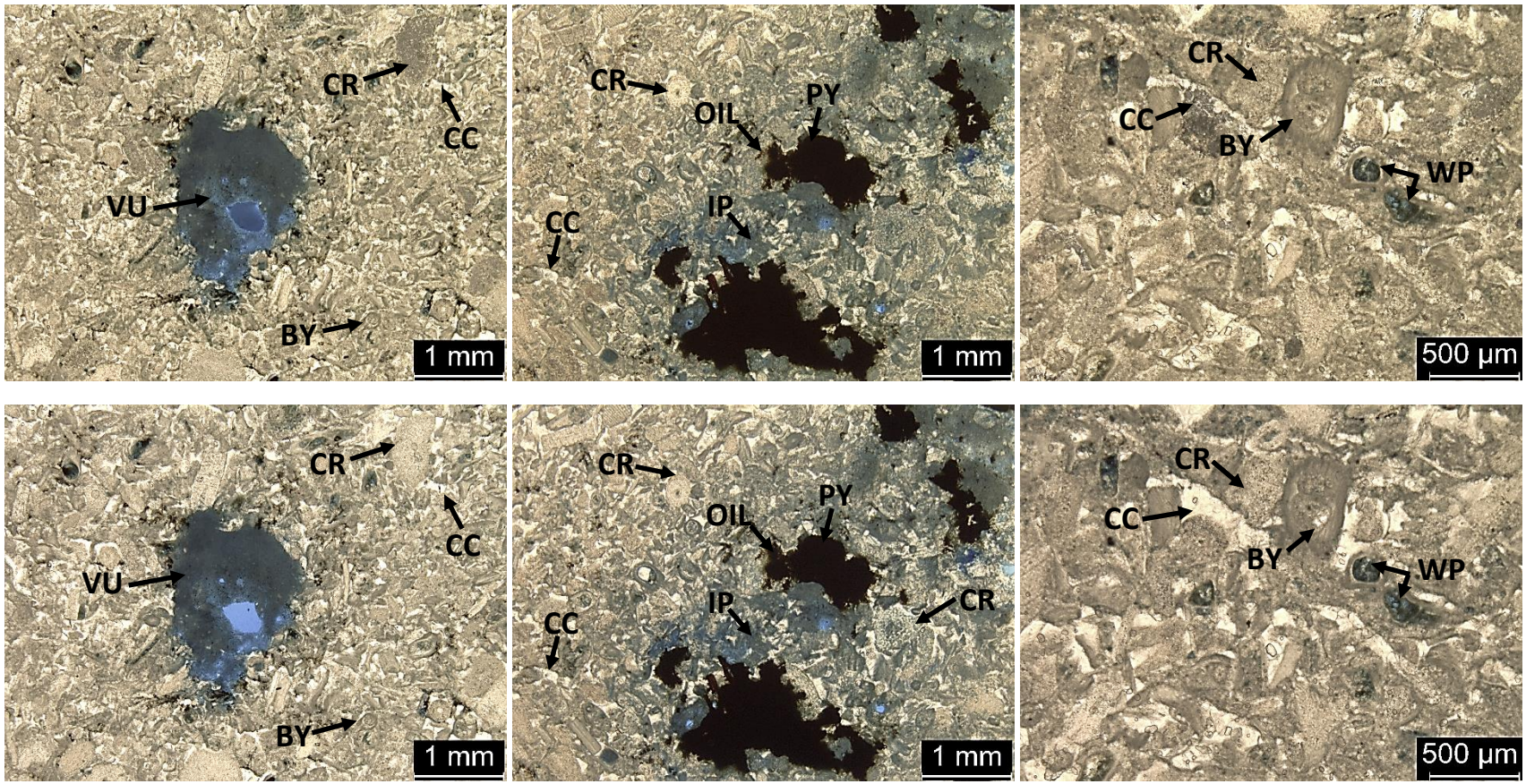

2p-0.5: Bryozoan grainstone to mud-lean packstone, very fine to medium grained, moderately-well sorted. Contains 85% skeletal grains, 5% micrite matrix, and 10% blocky calcite cement, pyrite, dead oil, and porosity (visual estimation). Primary grains include fenestrate bryozoans (125µ - 500µ) and crinoids (250µ - 500µ). A mixture of pyrite and dead oil can be seen filling in vugular porosity. Other types of porosity include intraparticle and interparticle. Calcite cement can be seen filling space in between the skeletal grains. Other pore tyes include interparticle and intraparticle

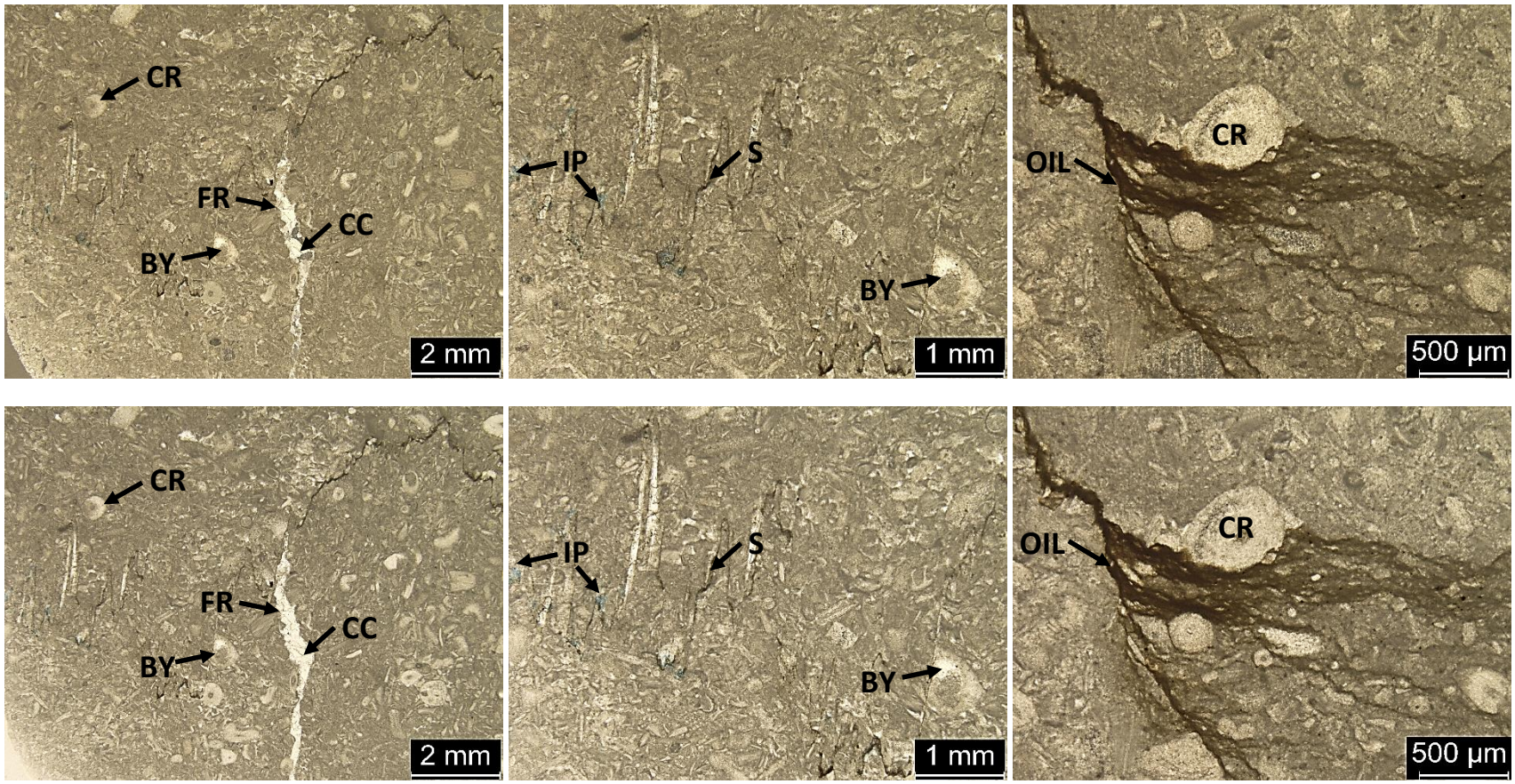

2p-2.6: Crinoidal packstone, very fine to medium grained, moderately sorted. Contains 40% skeletal grains, 59% micrite matrix, and 1% blocky calcite cement and dead oil (visual estimation). Skeletal grains include crinoids (62.5µ – 500µ) and bryozoans (62.5µ – 500µ). Blocky calcite cement has filled in the stylolite and within some of the skeletal grains. Dead oil occurs along fractures and interparticle porosity exists around the stylolite.

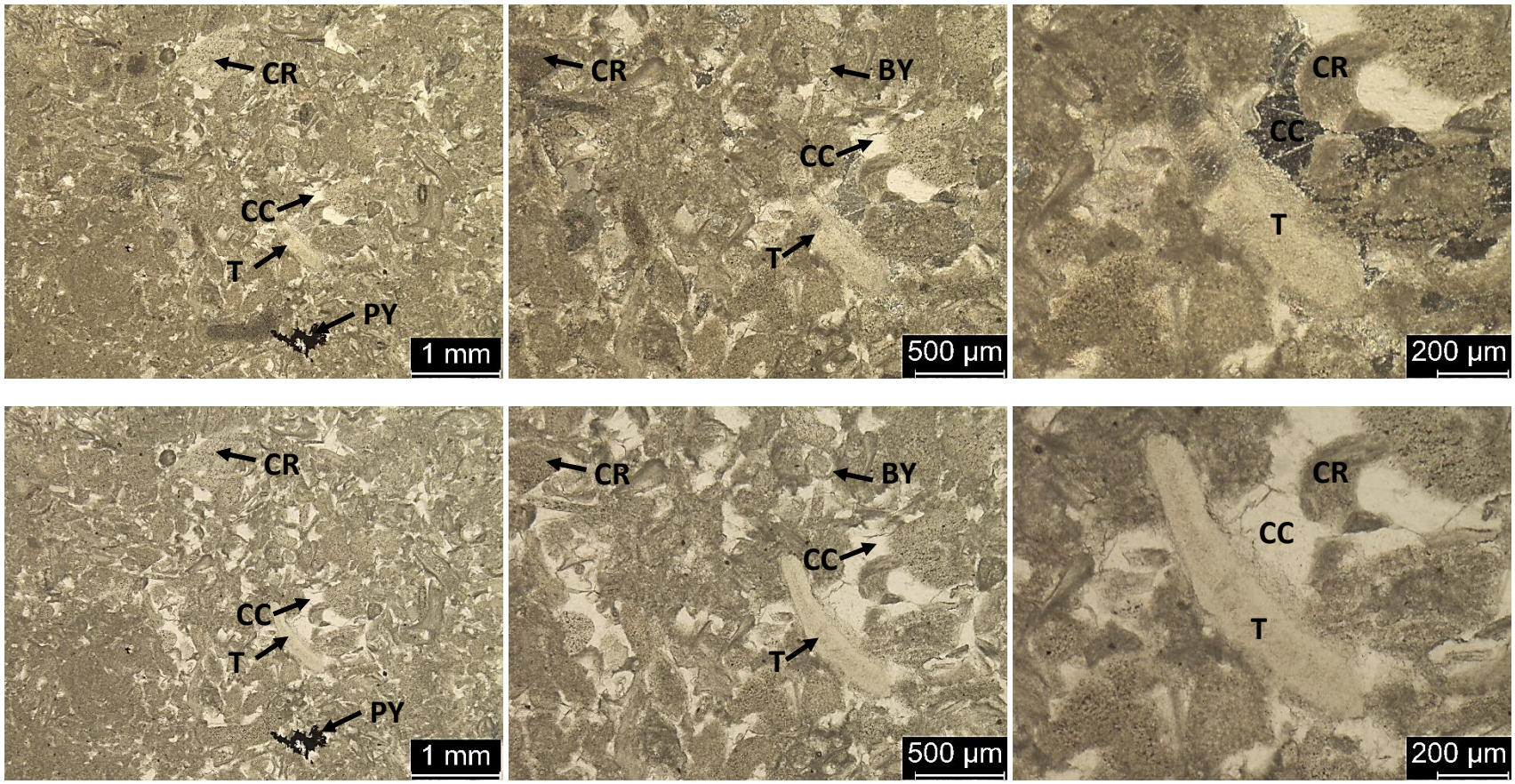

2p-2.7: Skeletal grainstone to mud-lean packstone, fine to coarse grained, moderately sorted. Contains 75% skeletal grains, 22% calcite cement, 3% micrite matrix and pyrite (visual estimation). Skeletal grains include crinoids (150µ – 1mm), bryozoans (125µ – 450µ), and trilobites (500µ – 1mm).

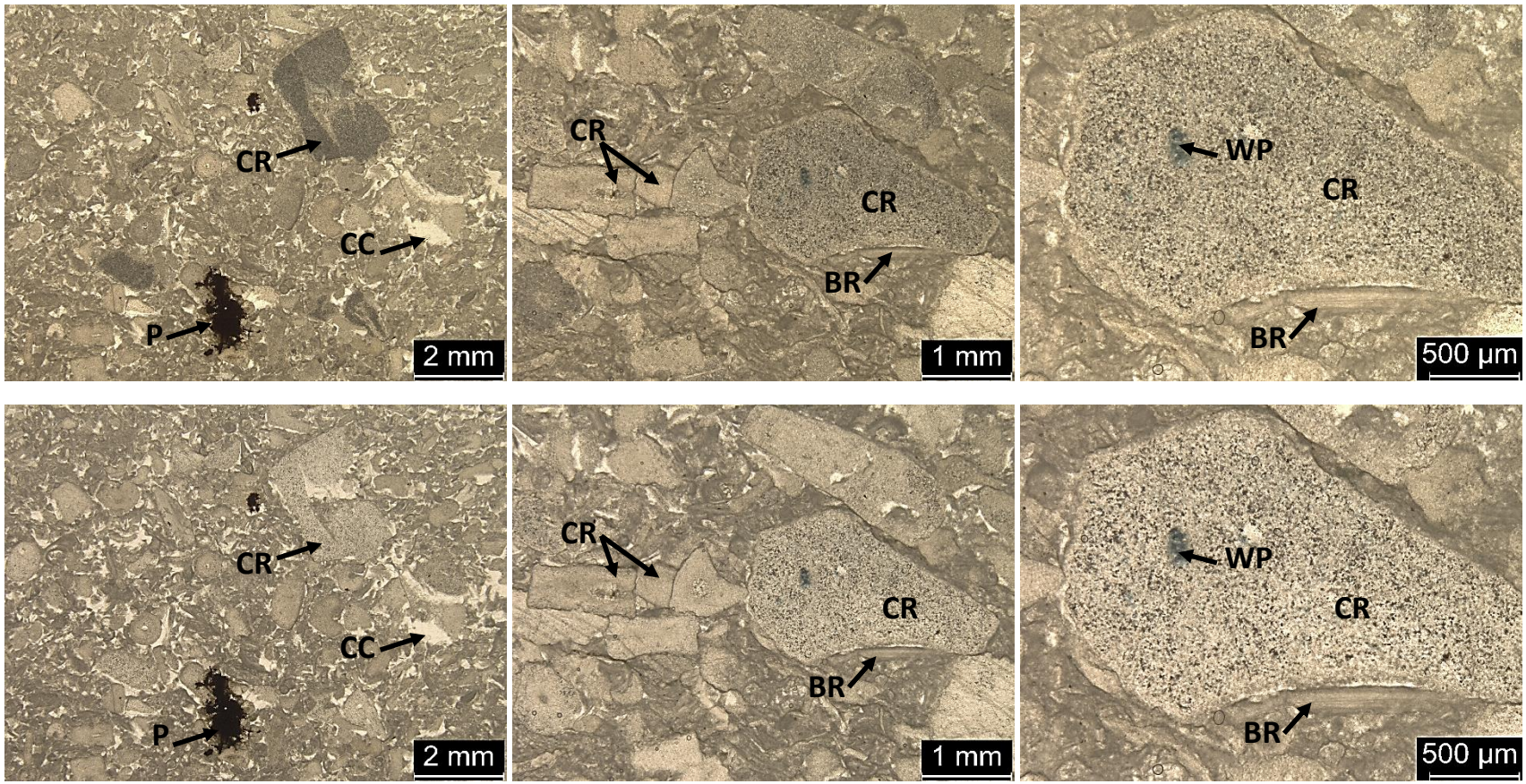

2p-3.0: Crinoidal grainstone, fine to very coarse grained, poorly to moderately sorted. Contains 85% skeletal grains, 10% blocky calcite cement, and porosity, and 5% micrite matrix (visual estimation). Skeletal grain types include crinoids (500µ - 2mm), and brachiopods (250µ - 500µ). Intraparticle porosity exists within a crinoid grain.

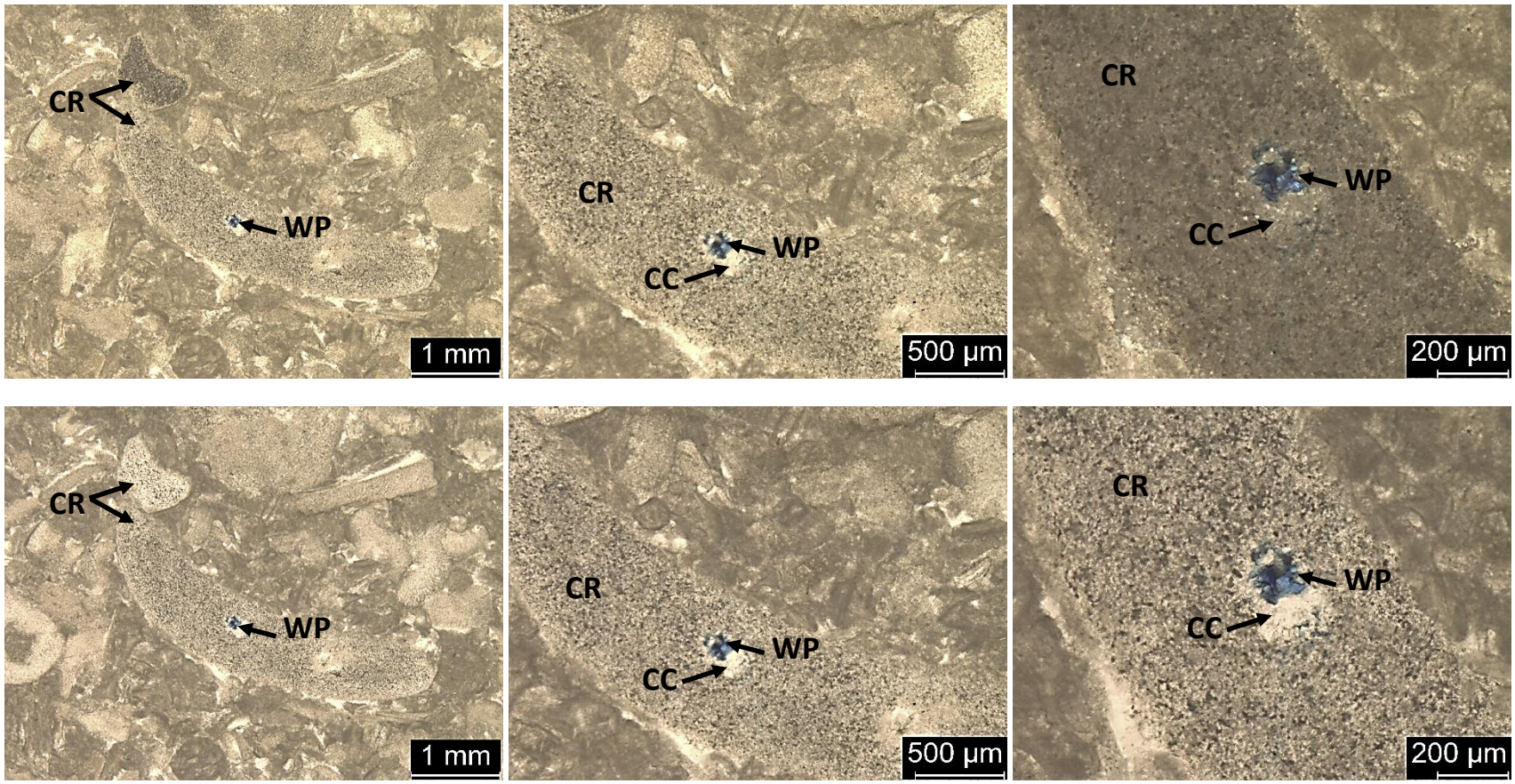

2p-5.5: Crinoidal wackestone, medium to very coarse grained, poorly sorted. Contains 40% skeletal grains, 58% micrite matrix, and 2% blocky calcite cement and porosity (visual estimation). Crinoids range in size from (500µ - 200µ). Intraparticle porosity and calcite cement are contained within a single crinoid grain.

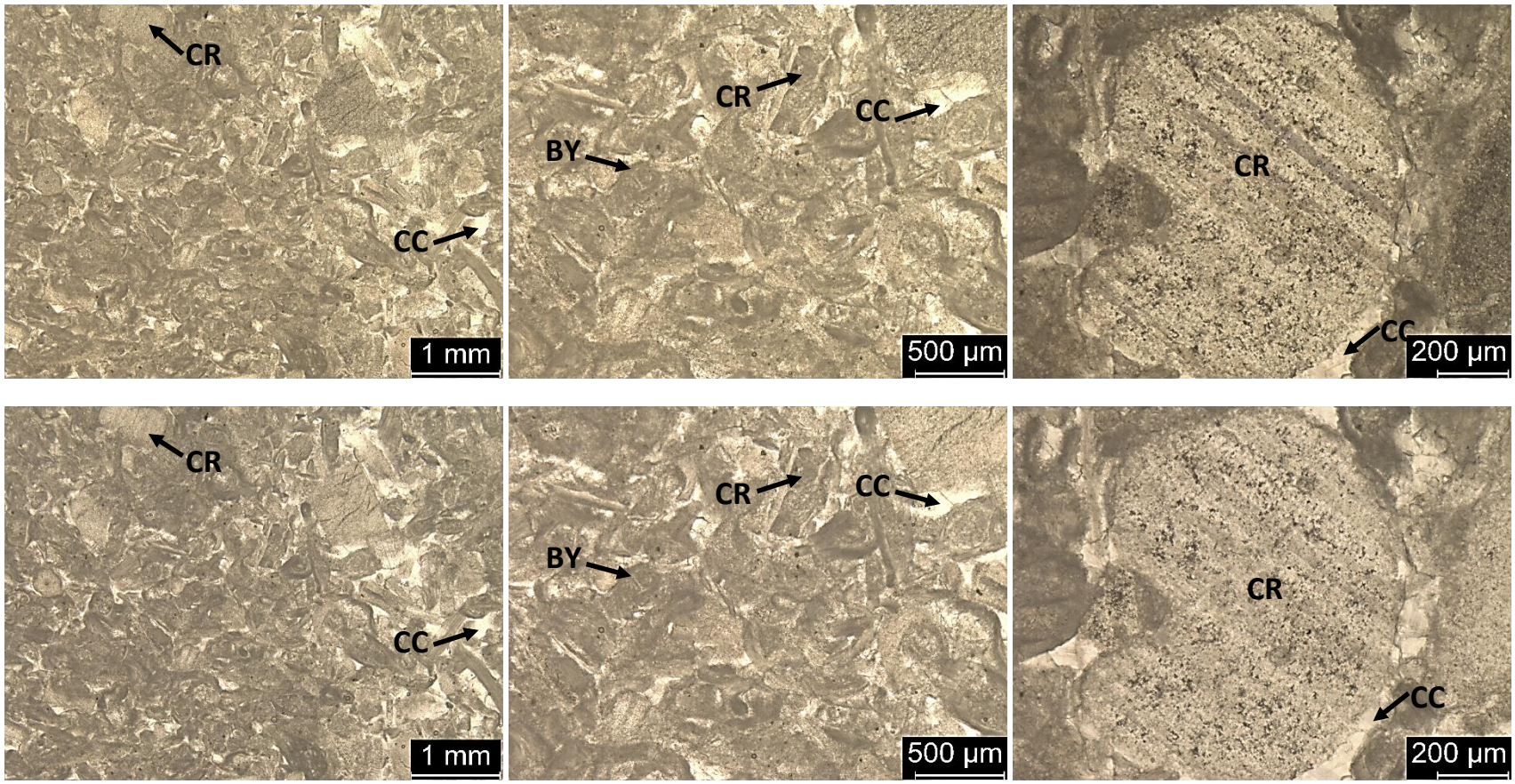

2p-7.5: Crinoidal-bryozoan grainstone, fine to coarse grained, poorly sorted. Contains 85% skeletal grains and 15% blocky calcite cement (visual estimation). Grain types include crinoids (250µ - 1mm) and bryozoans (125µ - 250µ). Calcite cement occurs between and within the skeletal grains throughout the thin section.

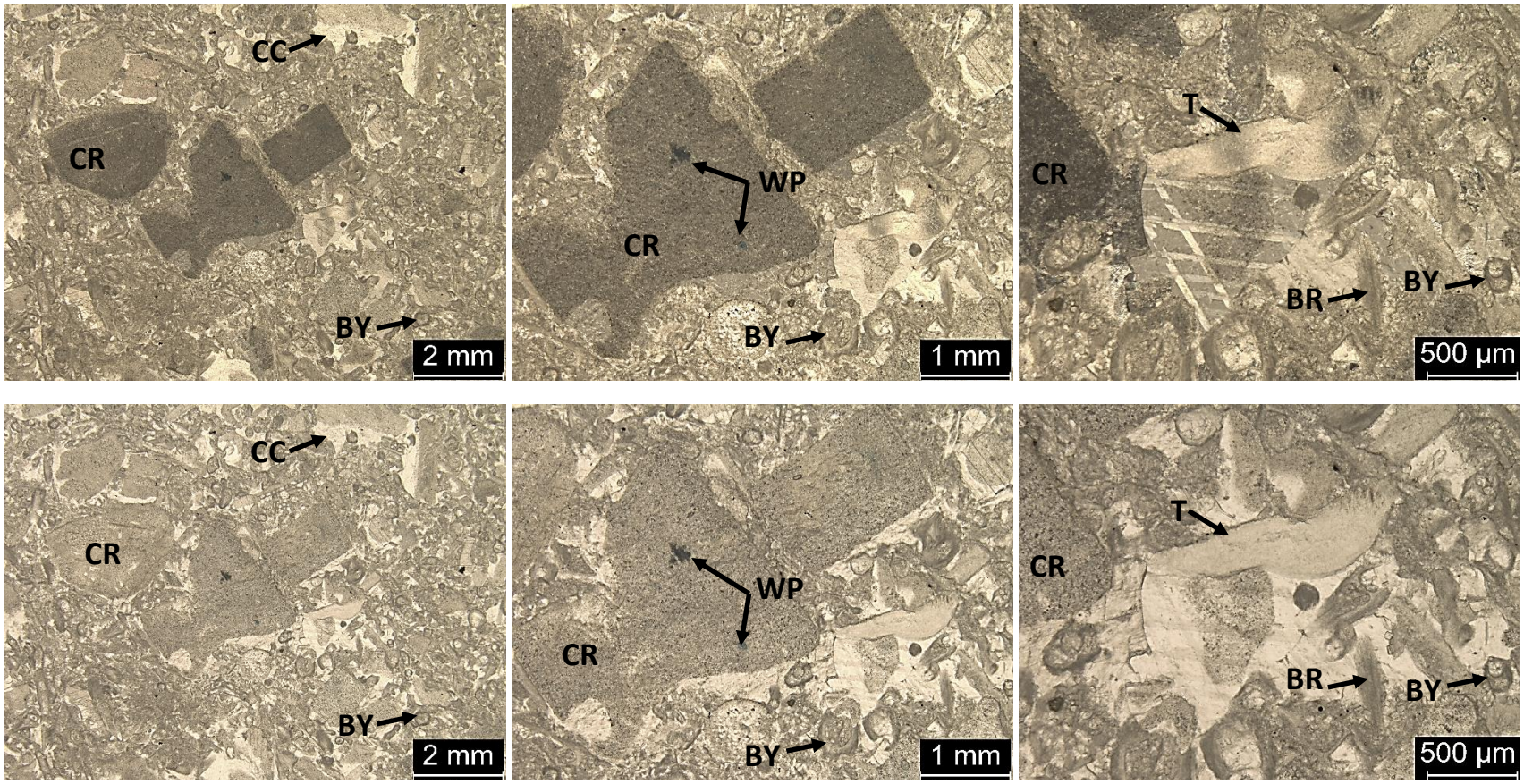

2p2-5.6: Skeletal mud-lean packstone, fine to very coarse grained, very poorly sorted. Contains 75% skeletal grains, 15% micrite matrix, and 5% blocky calcite cement (visual estimation). Grain types include crinoids(1mm – 2mm), bryozoans (125µ - 500µ), brachiopods (125µ - 250µ), and trilobites (1mm – 2mm). Intraparticle porosity occurrs within a crinoid grain.

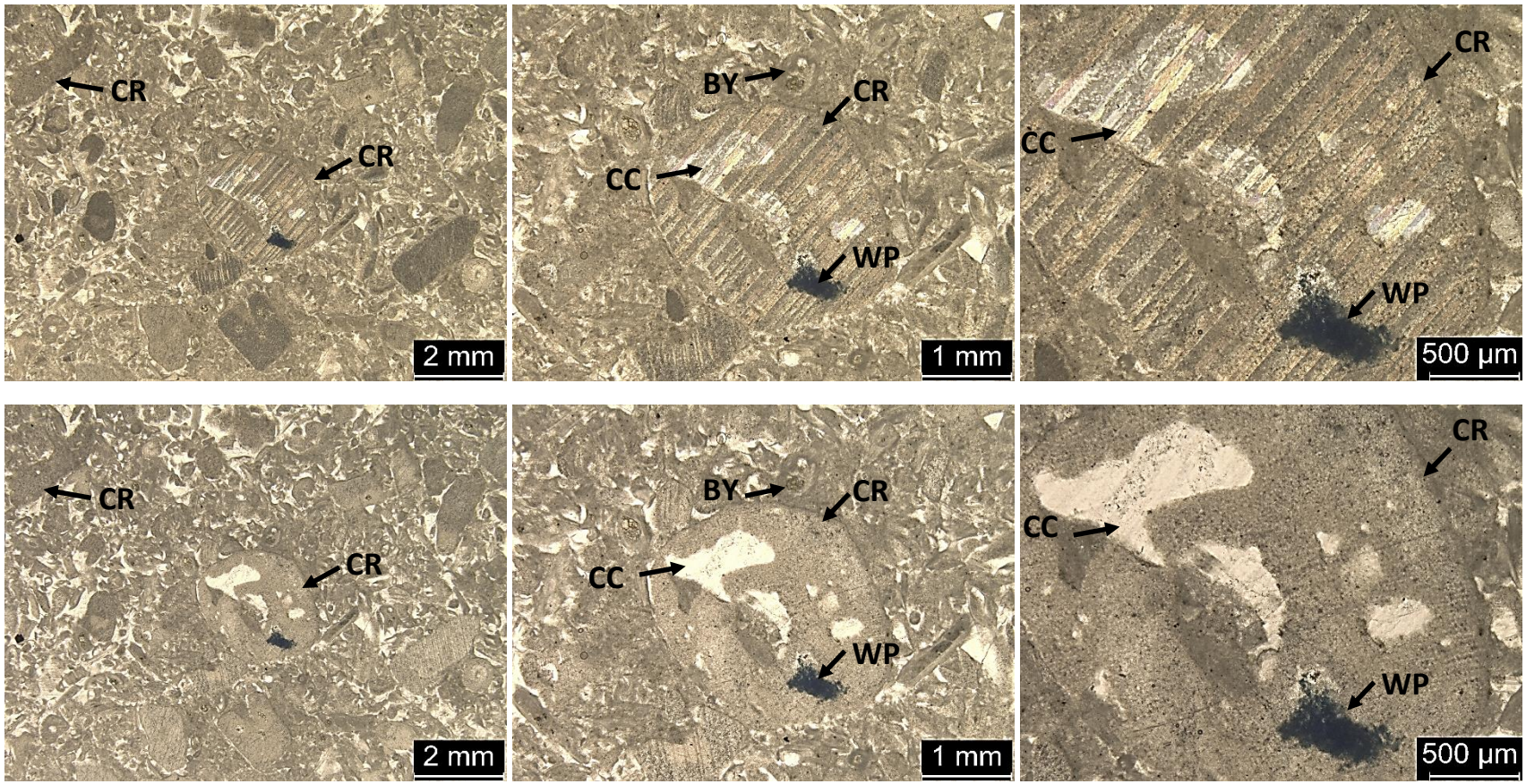

2p2-9.0: Crinoidal-bryozoan grainstone, fine to very coarse grained, poorly-very poorly sorted. Contains 85% skeletal grains, 14% blocky calcite cement, and <1% porosity (visual estimation). Primary grain types consist of crinoids (1mm – 2mm), bryozoans (125µ - 500µ), and brachiopods (250µ - 500µ). Calcite cement has filled in between and within the skeletal grains. Intraparticle porosity can be seen within a crinoid grain.

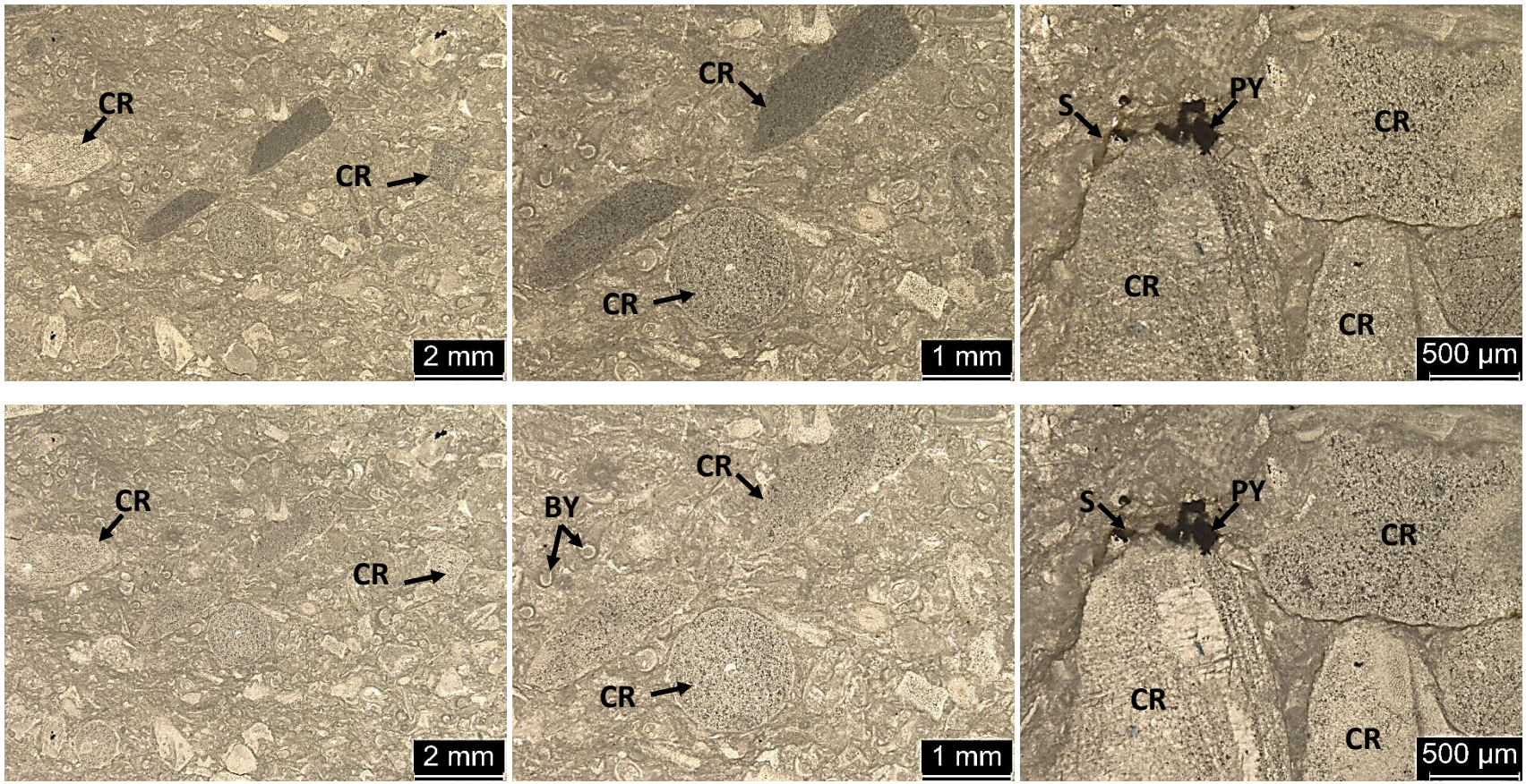

2p2-11.0: Crinoidal packstone to grainstone, very fine-very coarse grained, very poorly sorted. Contains 70% skeletal grains, 25% micrite matrix, and 5% blocky calcite cement and pyrite (visual estimation). Grain types include crinoids (500µ - 2mm), bryozoans (62.5µ - 125µ), and brachiopods (250µ - 500µ).

Vertical section 2-3c

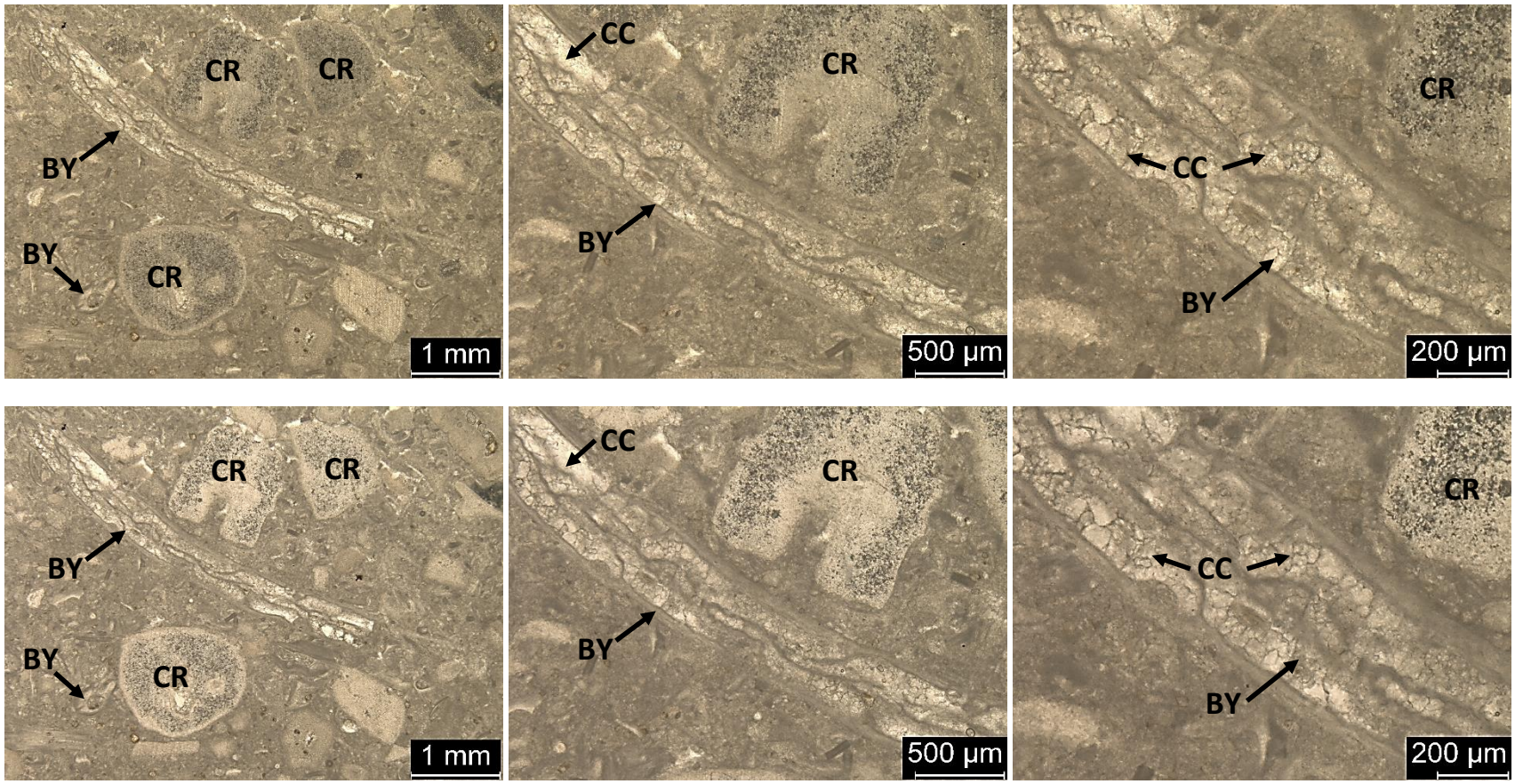

2-3c-3.25: Skeletal wackestone-packstone, grain size ranges from fine sand to very fine pebbles, poorly-moderately sorted. Contains 50% skeletal grains, 48% micrite matrix, and 2% blocky calcite cement, pyrite and dolomite (visual estimation). Grain types include crinoids (500µ - 1mm), fenestrate bryozoans (125µ - 2mm), and ostracods (125µ - 250µ). Calcite cement has filled in space surrounding and within the skeletal grains.

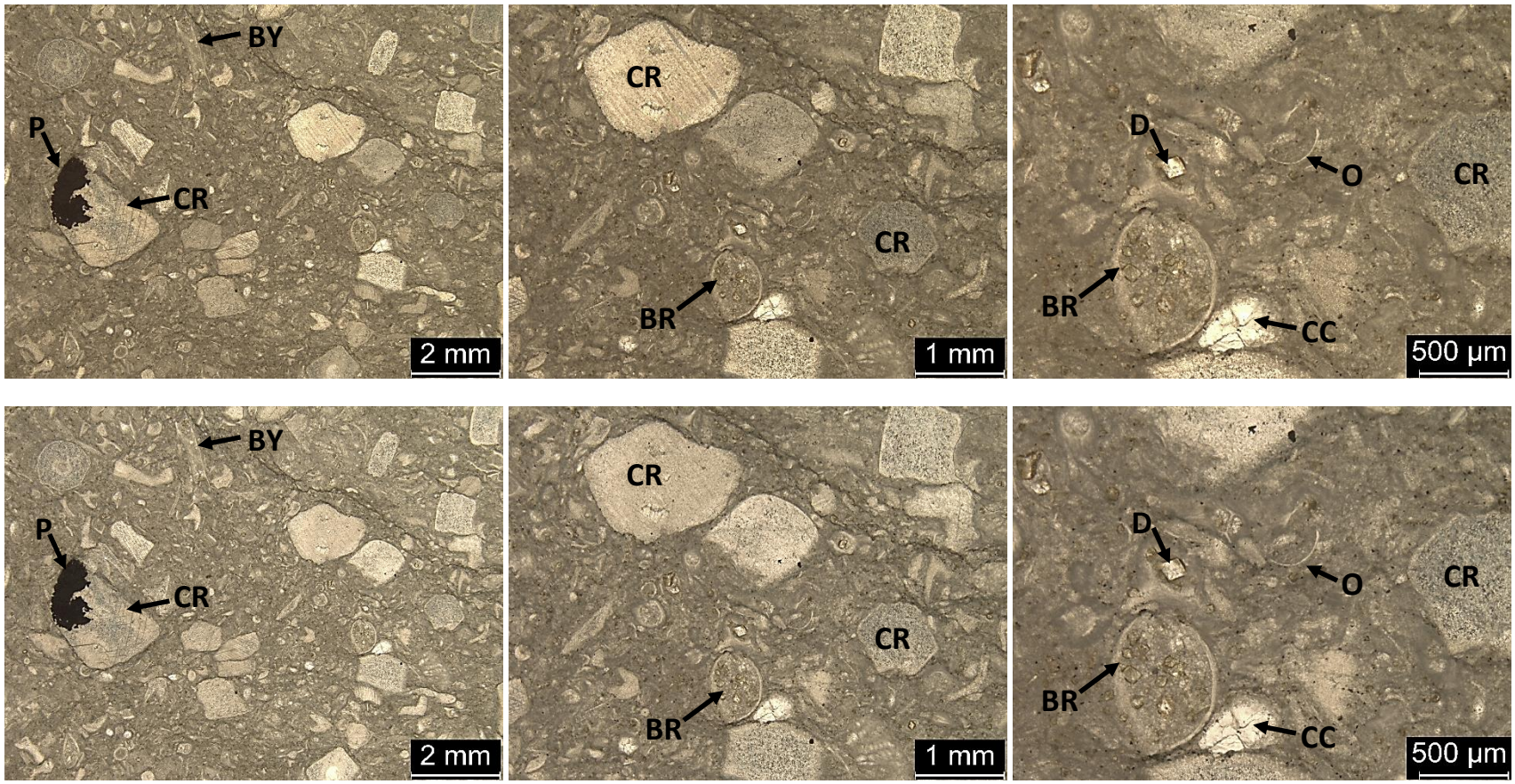

2-3c-5.2: Bryozoan-crinoidal wackestone, fine to very coarse grained, poorly sorted. Contains 40% skeletal grains, 57% micrite matrix, and 3% pyrite, calcite cement, and dolomite (visual estimation). Grain types include fenestrate bryozoans (250µ – 500µ), crinoids (500µ - 2mm), brachiopods (500µ - 1mm), and ostracods (125µ - 250µ). Other features include pyrite, dolomite rhombs and calcite cement.

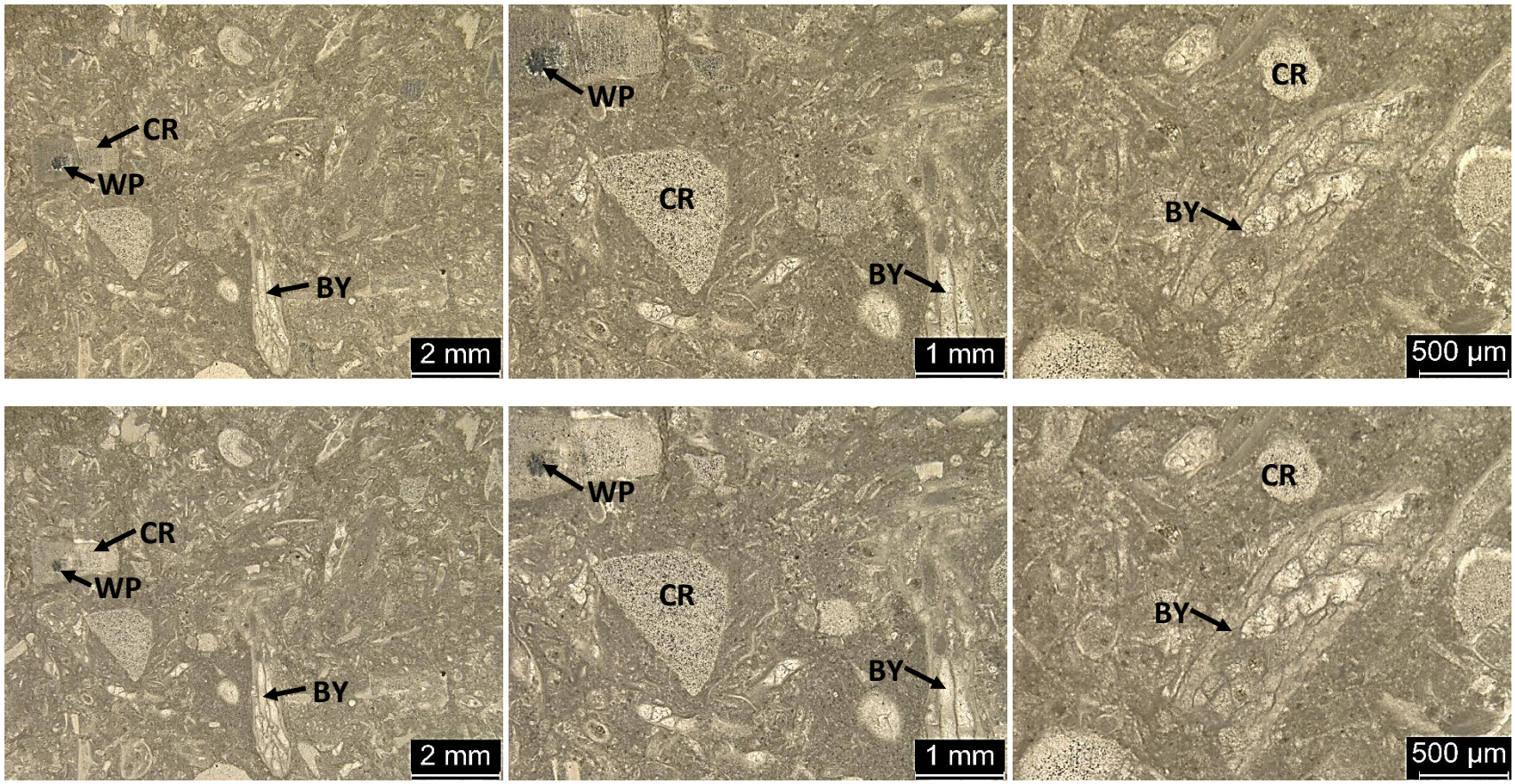

2-3c-7.8: Skeletal wackestone to packstone, very fine to very coarse grained, poorly sorted. Contains 40% skeletal grains, 58% micrite matrix, and 2% blocky calcite cement. Skeletal grains include crinoids (250µ – 2mm), bryozoans (62.5µ – 2mm), brachiopods (300µ - 650µ), and ostracods (125µ – 250µ).

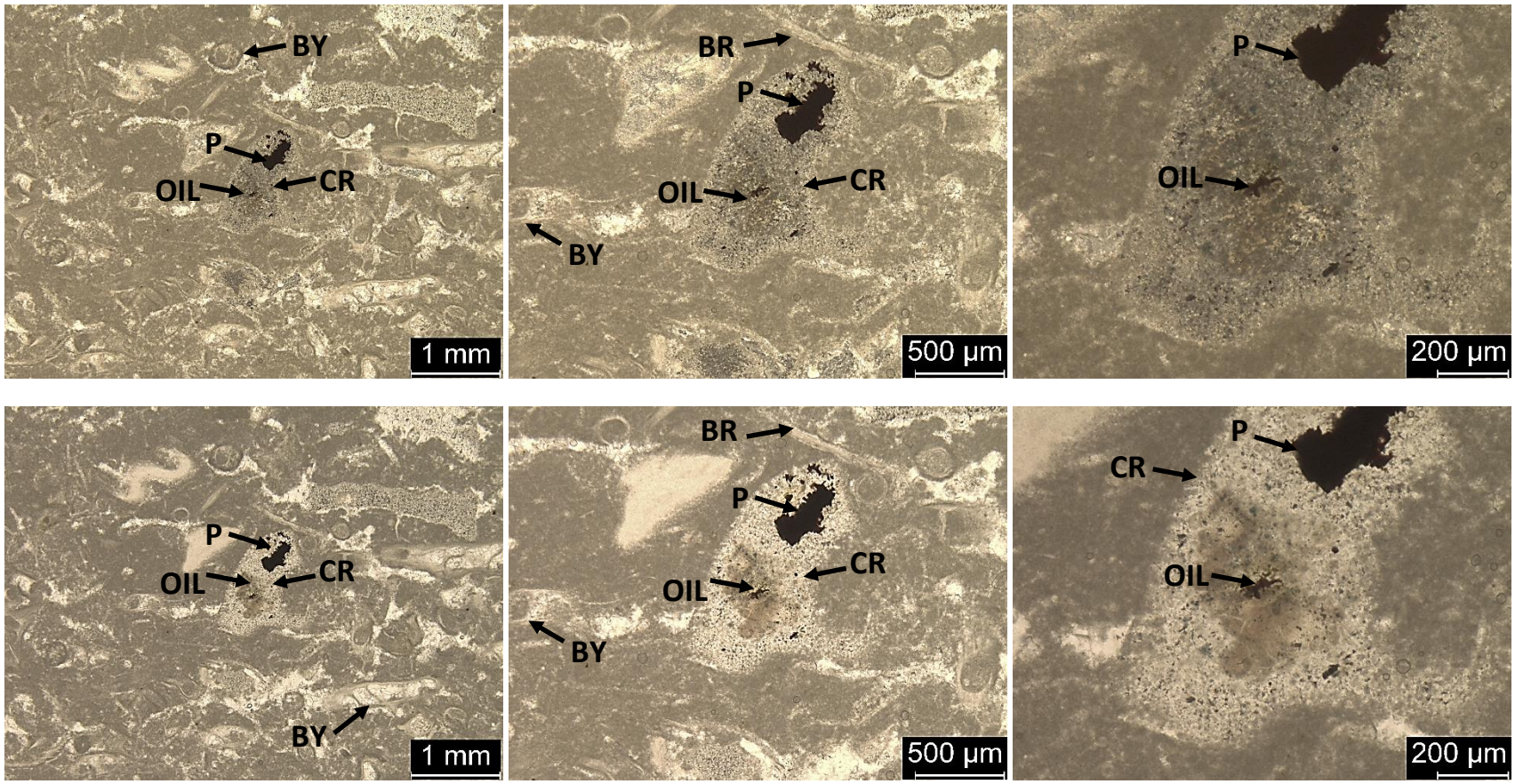

2-3c-9.8: Bryozoan wackestone, very fine to coarse grained, poorly sorted. Contains 30% skeletal grains, 65% micrite matrix, and 5% calcite cement, pyrite, and dead oil (visual estimation). Grain types include bryozoans (250µ - 1mm), crinoids (500µ - 2mm), and brachiopods (500µ - 1mm). Calcite cement cement has filled in spaces within the matrix and skeletal grains. Pyrite and dead oil can also be seen partially filling a crinoid grain.

Vertical Section 3

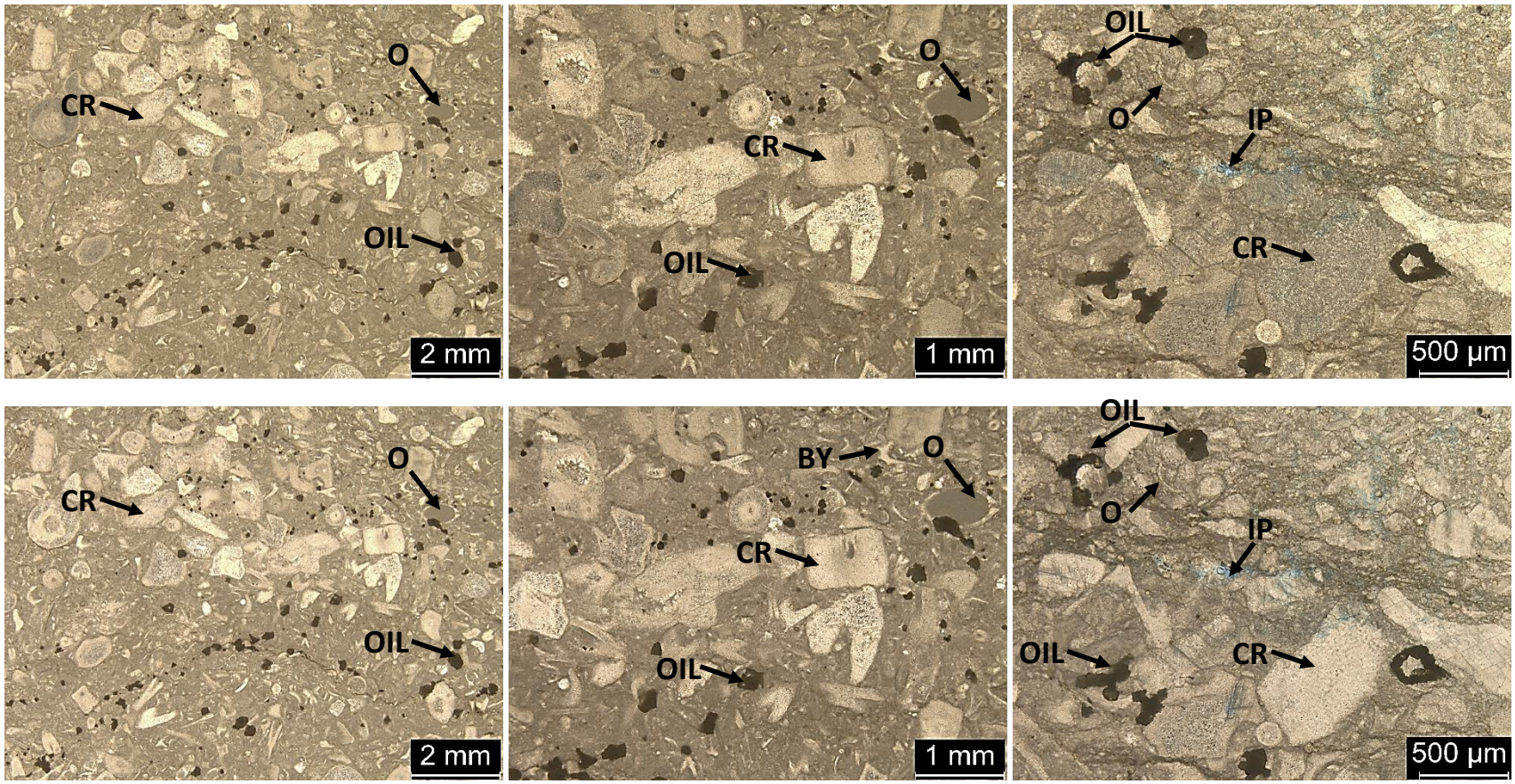

3c-0.0: Crinoidal wackestone, medium to very coarse grained, poorly to moderately sorted. Contains 40% skeletal grains, 57% micrite matrix, and 3% dead oil and porosity (visual estimation). Grain types include crinoids (250µ – 2mm), bryozoans (250µ – 300µ), and ostracods (250µ – 500µ). Dead oil and interparticle porosity can be seen throughout.

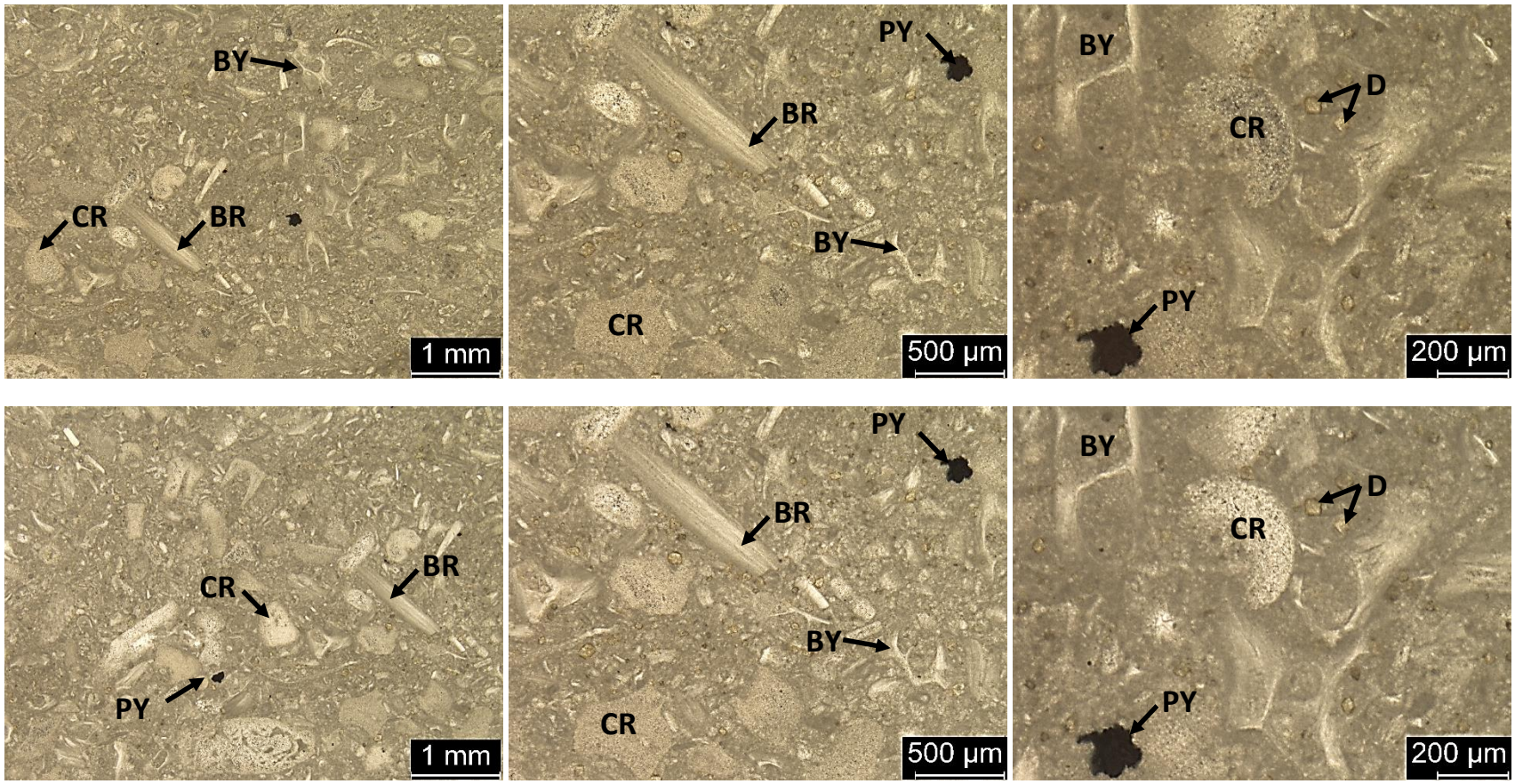

3c-2.25: Skeletal wackestone, very fine to very coarse grained, poorly to moderately sorted. Contains 35% skeletal grains, 63% micrite matrix, and 2% dolomite rhombs and pyrite (visual estimation). Skeletal grains include Crinoids (200µ – 700µ), brachiopods (350µ – 1mm), and bryozoans (125µ – 700µ).

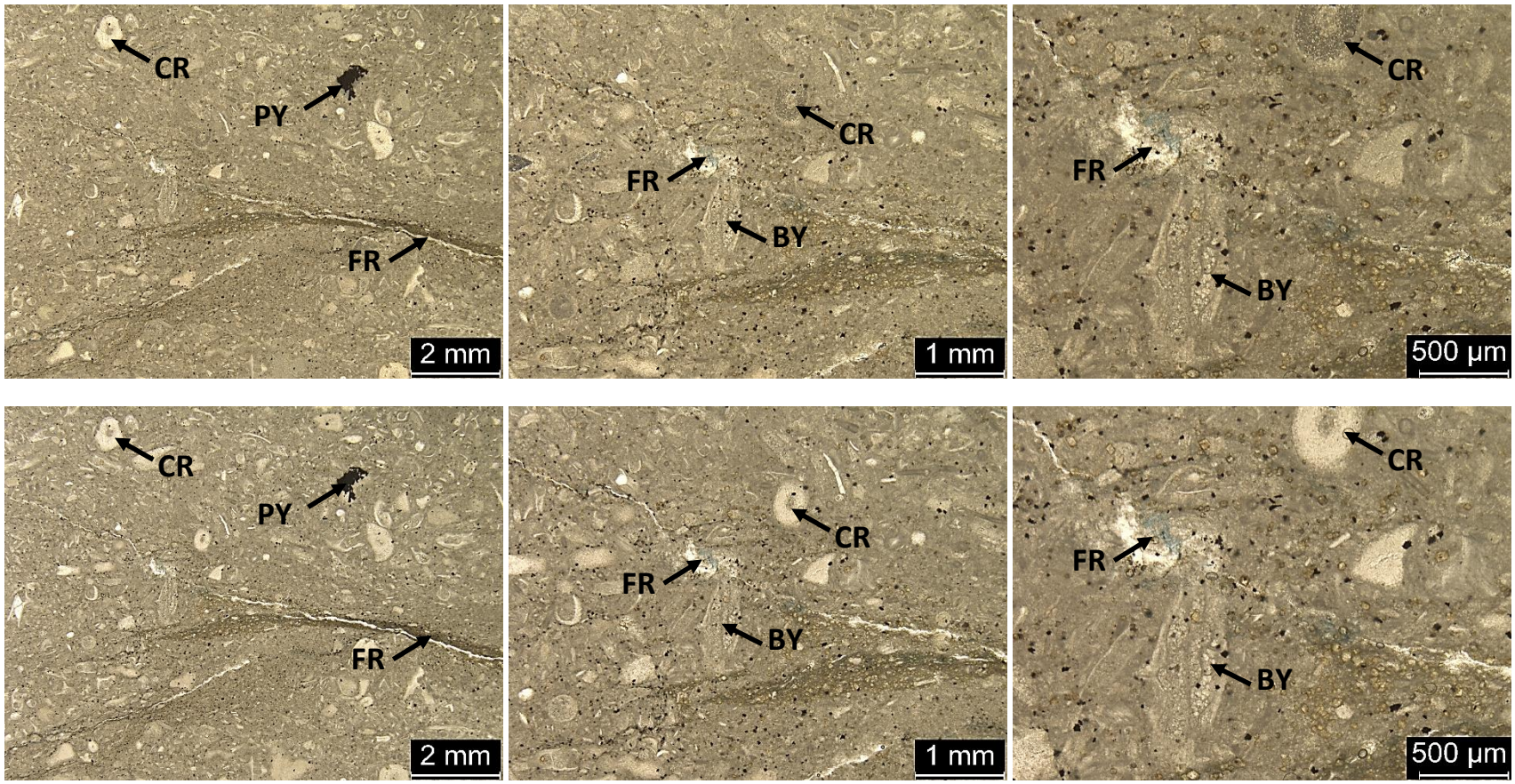

3c-4.0: Skeletal wackestone, very fine to medium grained, moderately sorted. Contains 30% skeletal grains, 68% micrite matrix, and 2% dolomite rhombs, calcite cement, and pyrite (visual estimation). Skeletal grains consist of crinoids (125µ – 500µ) and bryozoans (62.5µ – 500µ). Porosity occurs along a fracture that has been partially filled with calcite cement.

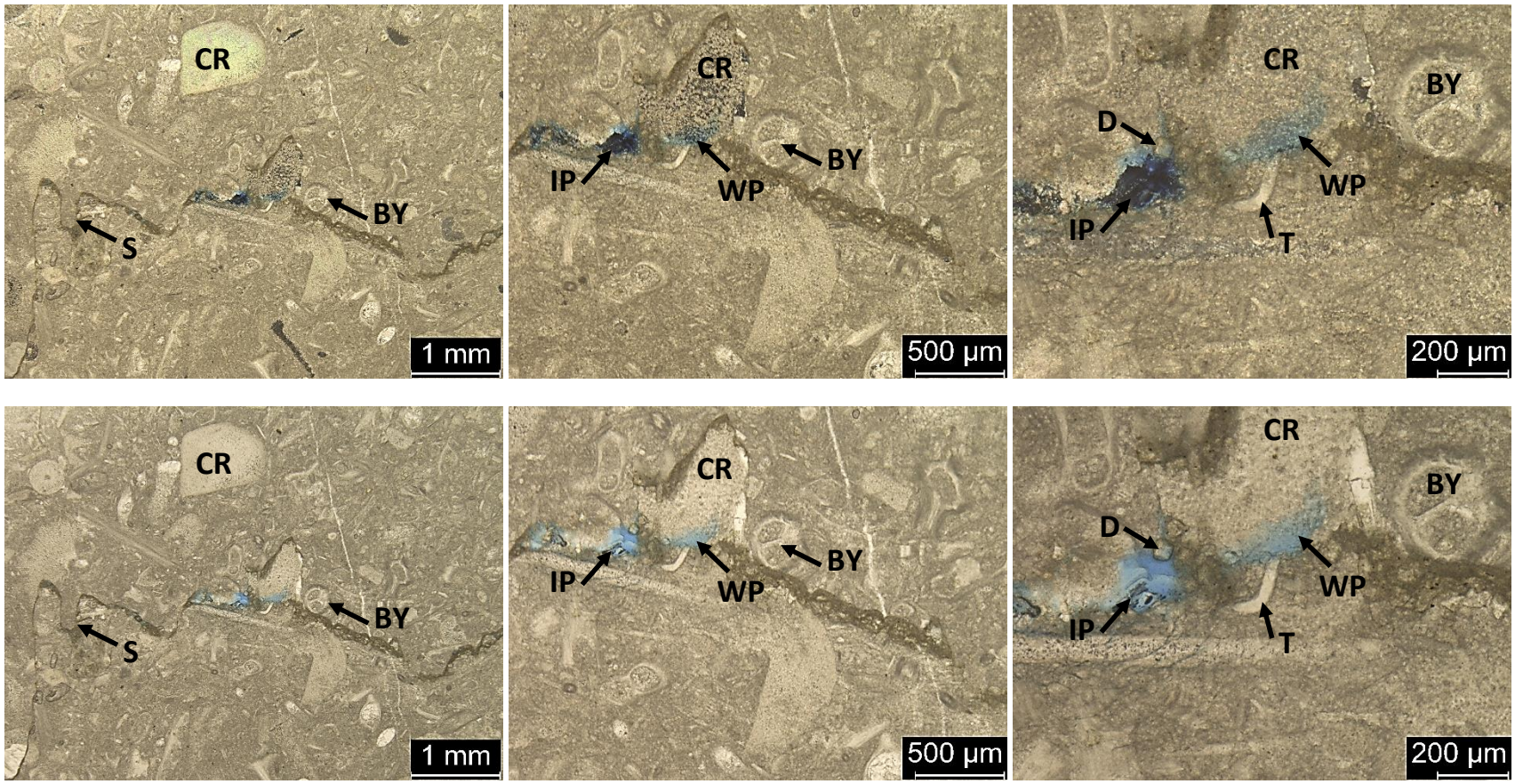

3c-5.5: Crinoidal-bryozoan wackestone, fine to coarse grained, poorly to moderately sorted. Contains 35% skeletal grains, 63% micrite matrix, and 2% dolomite and calcite cement (visual estimation). Skeletal grains include crinoids (250µ – 1mm), bryozoans (125µ – 400µ), brachiopods (700µ – 1.5mm), and trilobites (125µ – 200µ). Intraparticle and interparticle porosity occur near a stylolite.

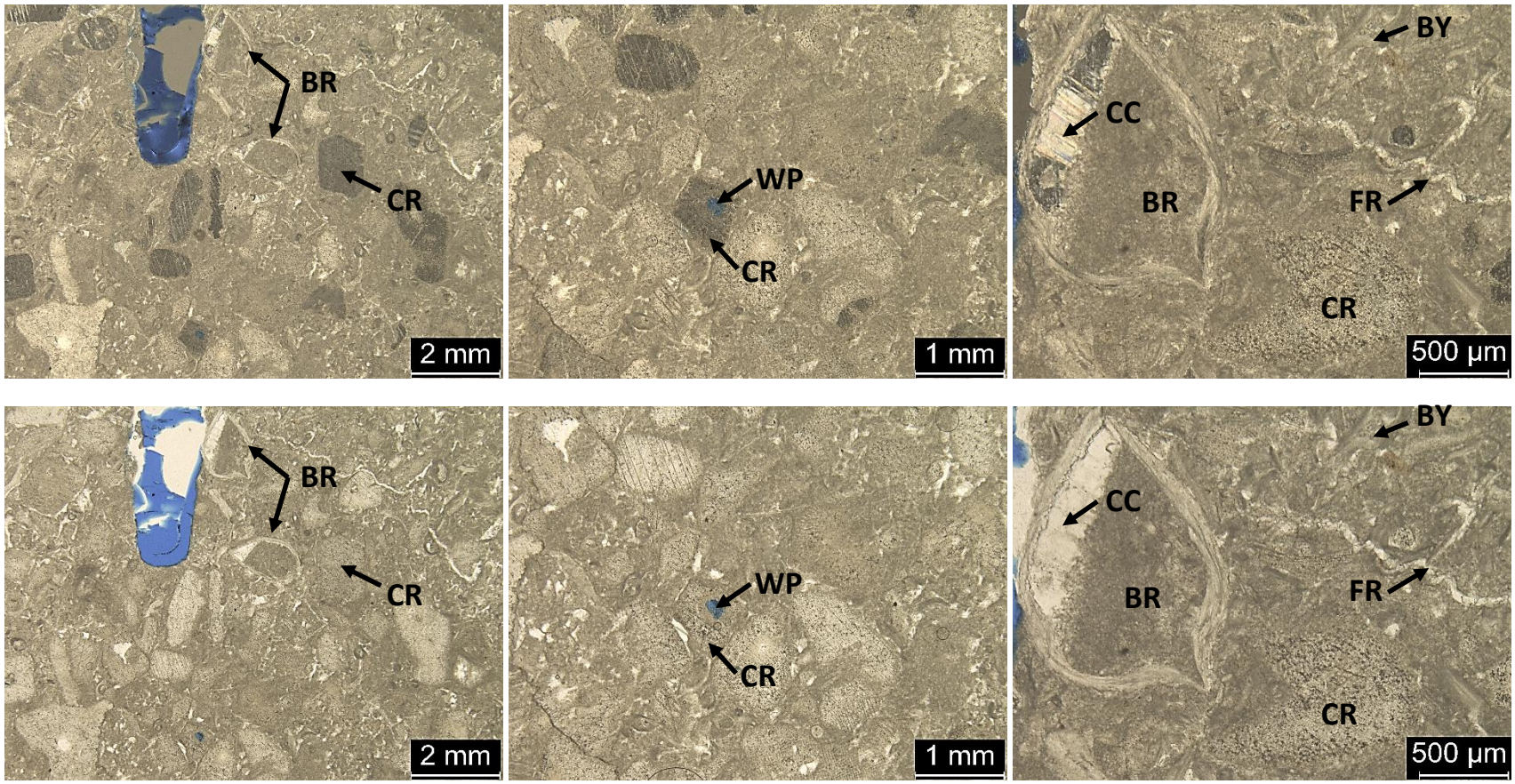

3c-6.0: Skeletal wackestone to packstone, fine to very coarse grained, poorly sorted. Contains 55% skeletal grains, 30% micrite matrix, and 15% calcite cement (visual estimation). Skeletal grains include crinoids (250µ – 1mm), brachiopods (700µ – 1.5mm), and bryozoans (125µ – 500µ). Note the blue epoxy in the first photomicrograph is showing through the notch that marks the top of the thin section. Intraparticle porosity can be seen in the middle thin section. The brachiopods have been filled with sediment and calcite cement and act as geopetals.

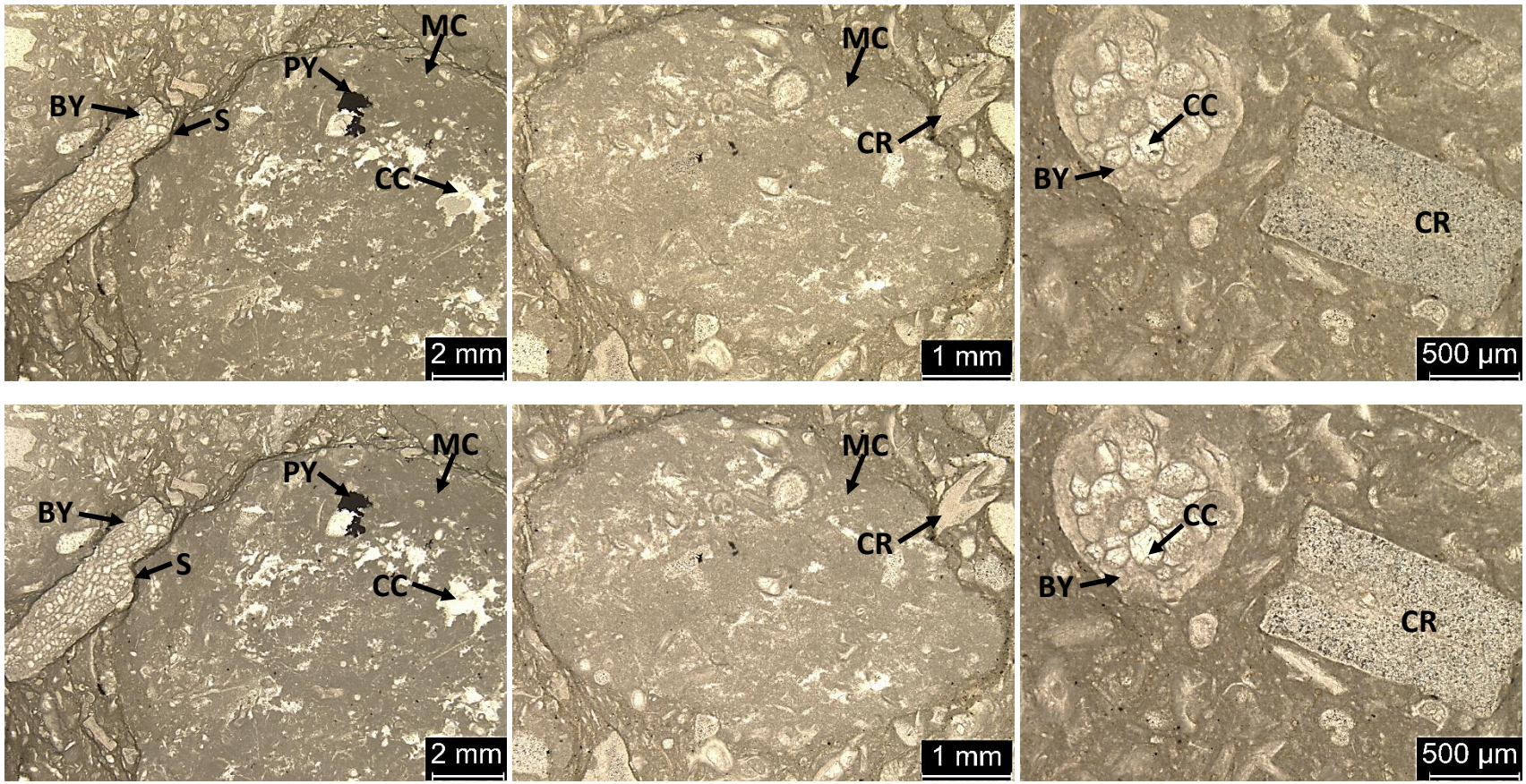

3c-6.5: Wackestone-packstone from the debris flow unit within the Compton Formation. Contains mudstone clasts ranging in size from very coarse sand to very coarse pebbles. The mudstone clasts are surrounded by a matrix of fine to coarse grained bryozoans (125 µ – 1mm), brachiopods (400 µ – 700 µ), and crinoids (125 µ – 2mm). These skeletal components are also contained within the mud clasts. Muddy stylolites, calcite cement, and pyrite can also be seen throughout.

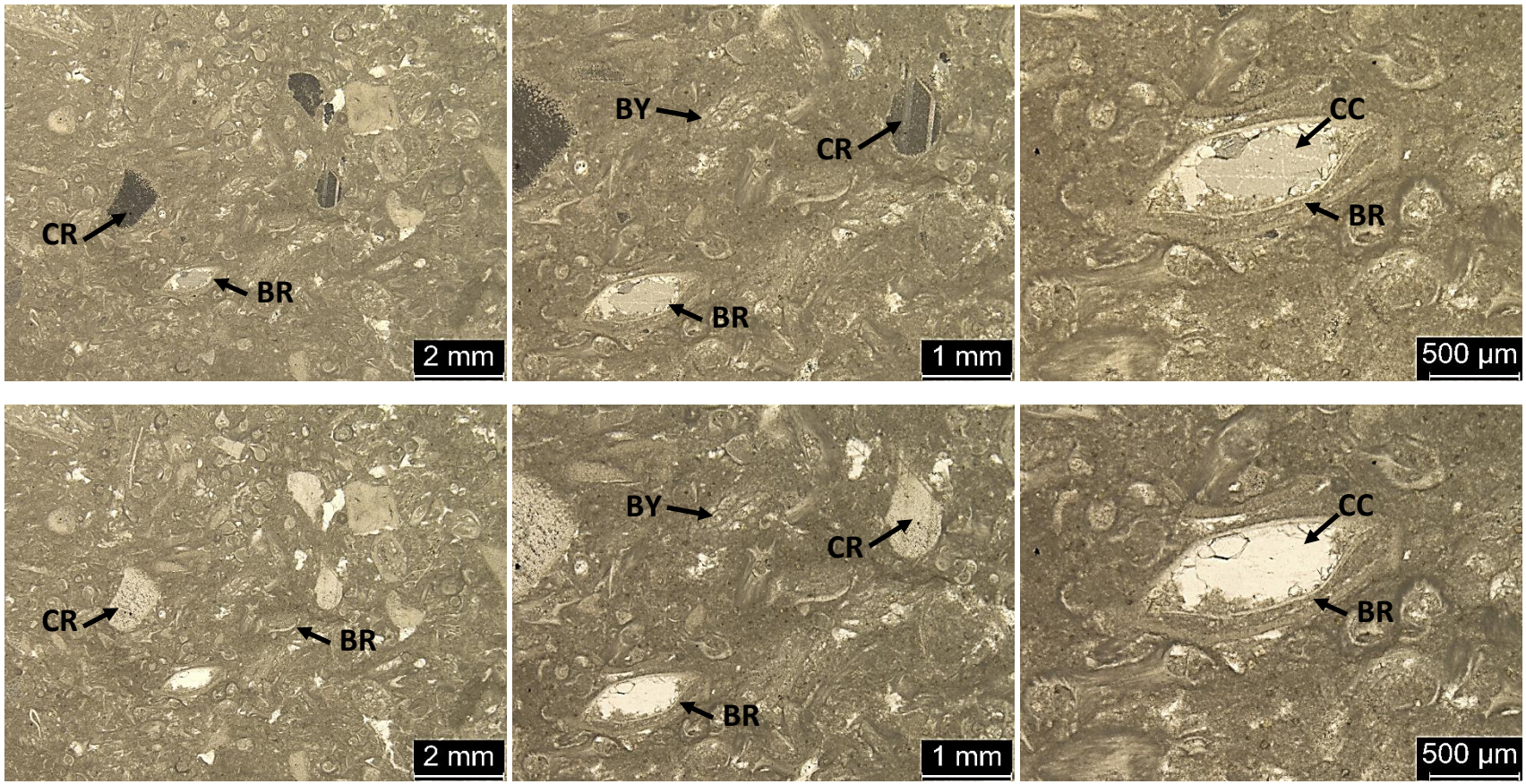

3c-10.5: Skeletal wackestone to packstone, fine to very coarse grained, poorly to moderately sorted. Contains 40% skeletal grains, 59% micrite matrix, 1% calcite cement (visual estimation). Skeletal grains consist of crinoids (500µ – 1.5mm), bryozoans (125µ – 700µ), and brachiopods (500µ – 1.5mm). A brachiopod grain has been filled in with sediment and blocky calcite cement and serves as a geopetal structure.

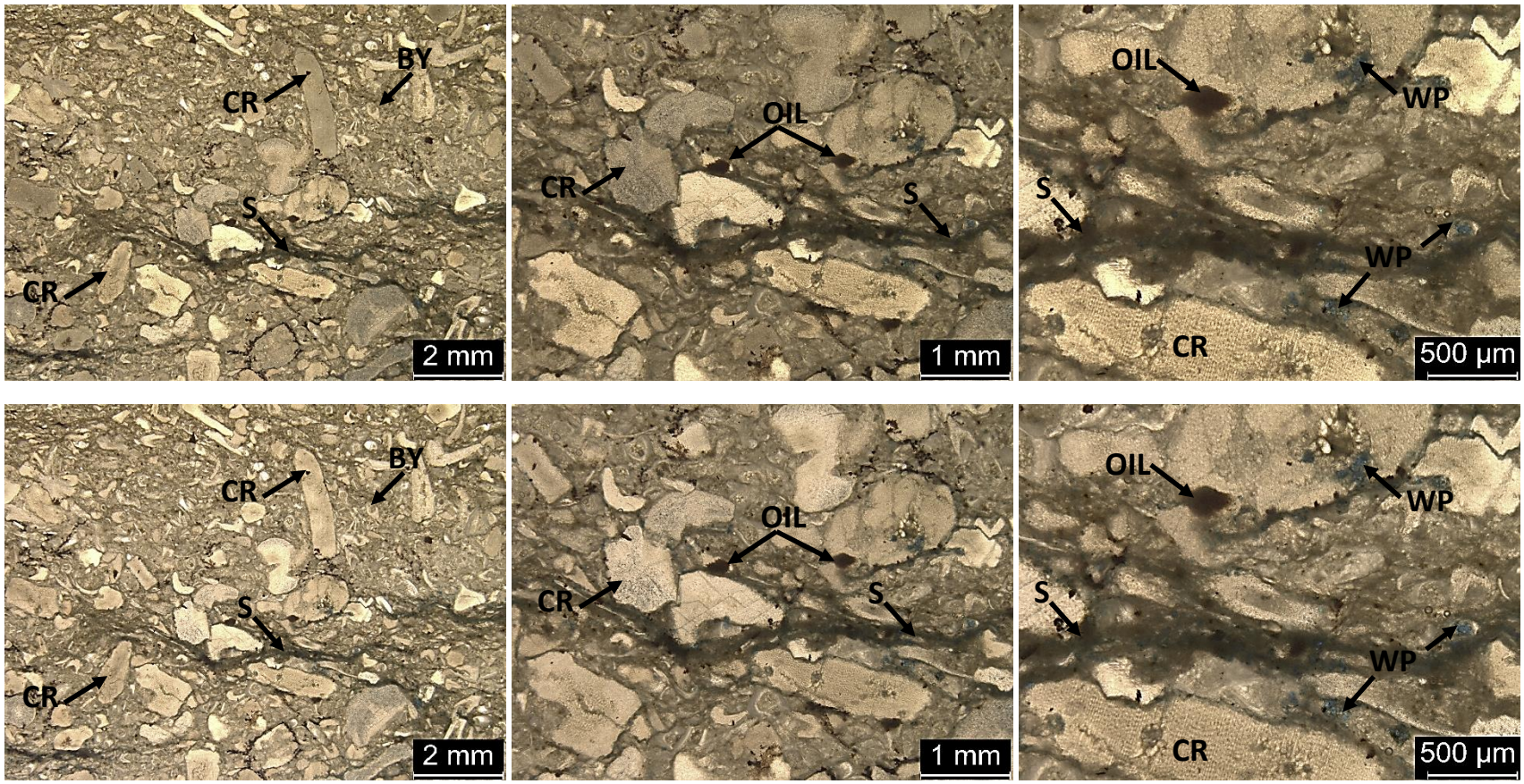

3nv-1.0: Crinoidal wackestone, fine to very coarse grained, poorly-moderately sorted. Contains 50% skeletal grains, 49% micrite matrix, and 1% dead oil, calcite cement and pyrite (visual estimation). Grain types include crinoids (125µ – 2mm) and bryozoans (125µ – 400µ). Muddy stylolites, dead oil, and intraparticle porosity can be seen throughout.

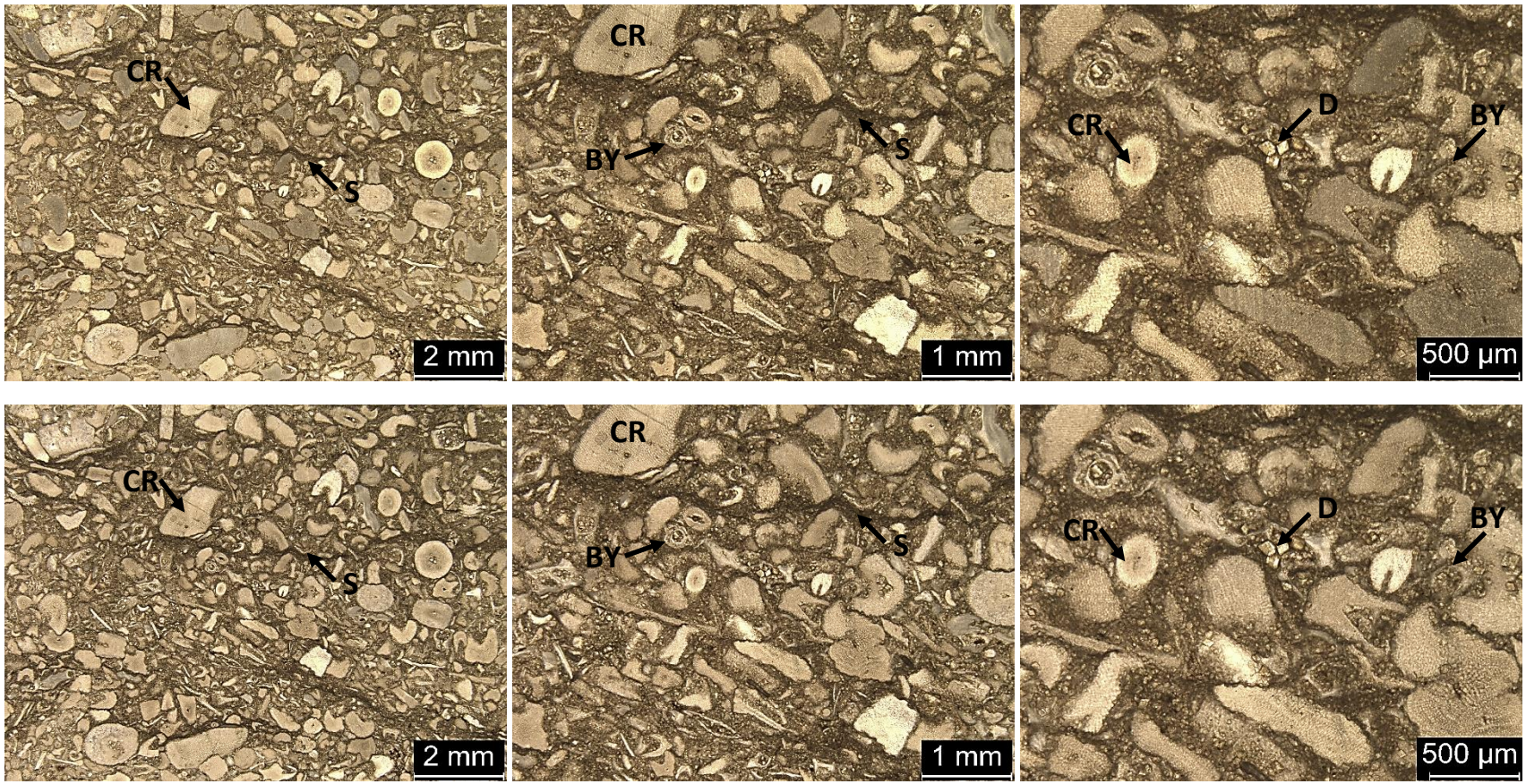

3nv-2.5: Crinoidal wackestone to packstone, medium to coarse grained, moderately to poorly sorted. Contains 50% skeletal grains, 45% micrite mud, and 5% dolomite rhombs (visual estimation). Grain types include crinoids (500 – 2mm) and bryozoans (250µ – 500µ).

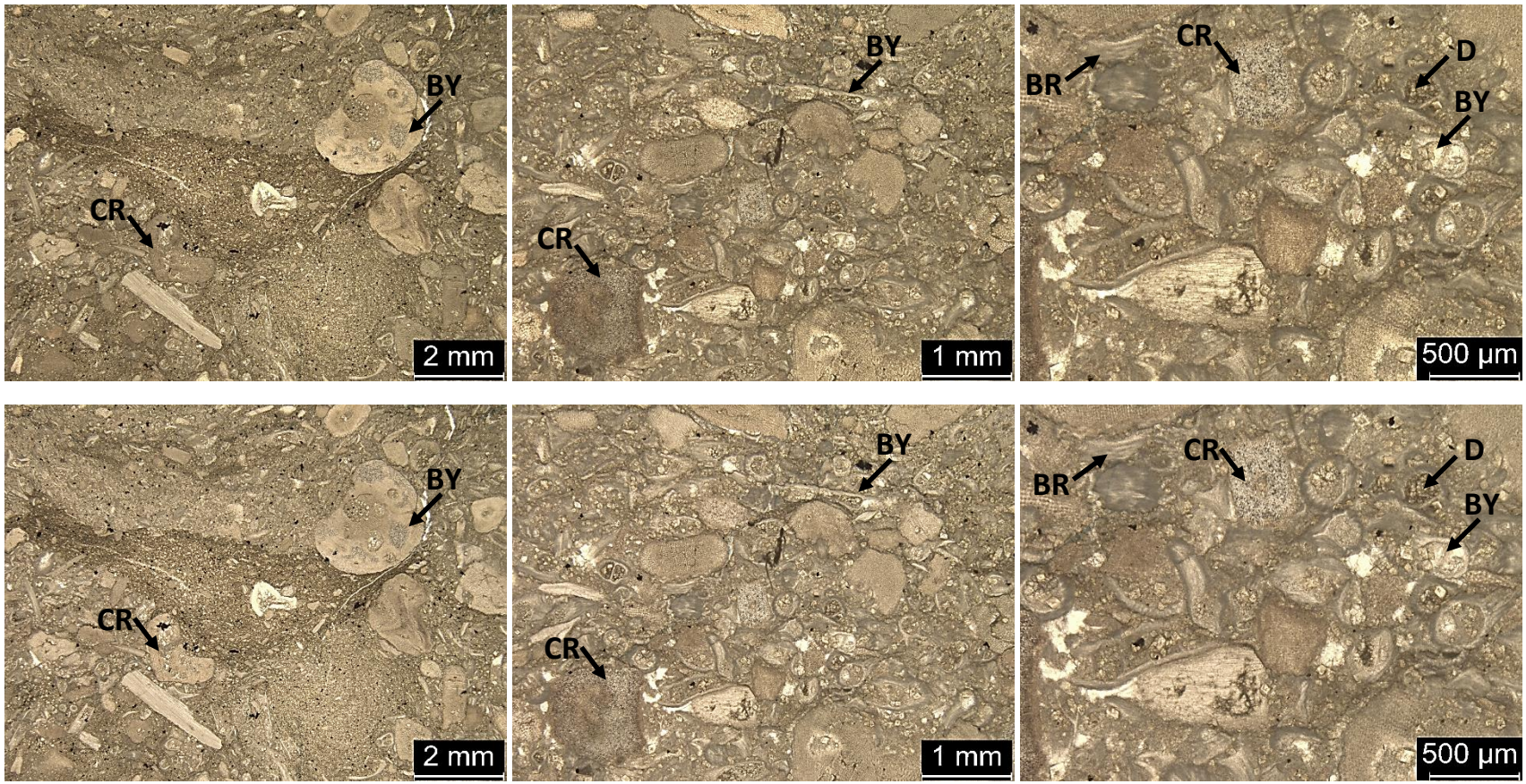

3nv-3.75: Crinoidal-bryozoan mud-lean packstone to grainstone, fine to coarse grained, moderately to poorly sorted. Contains 60% skeletal grains, 38% micrite matrix, and 2% blocky calcite cement and dolomite rhombs (visual estimation). Grain types include crinoids (250µ – 2mm), bryozoans (125µ – 500µ), and brachiopods (250µ – 400µ).

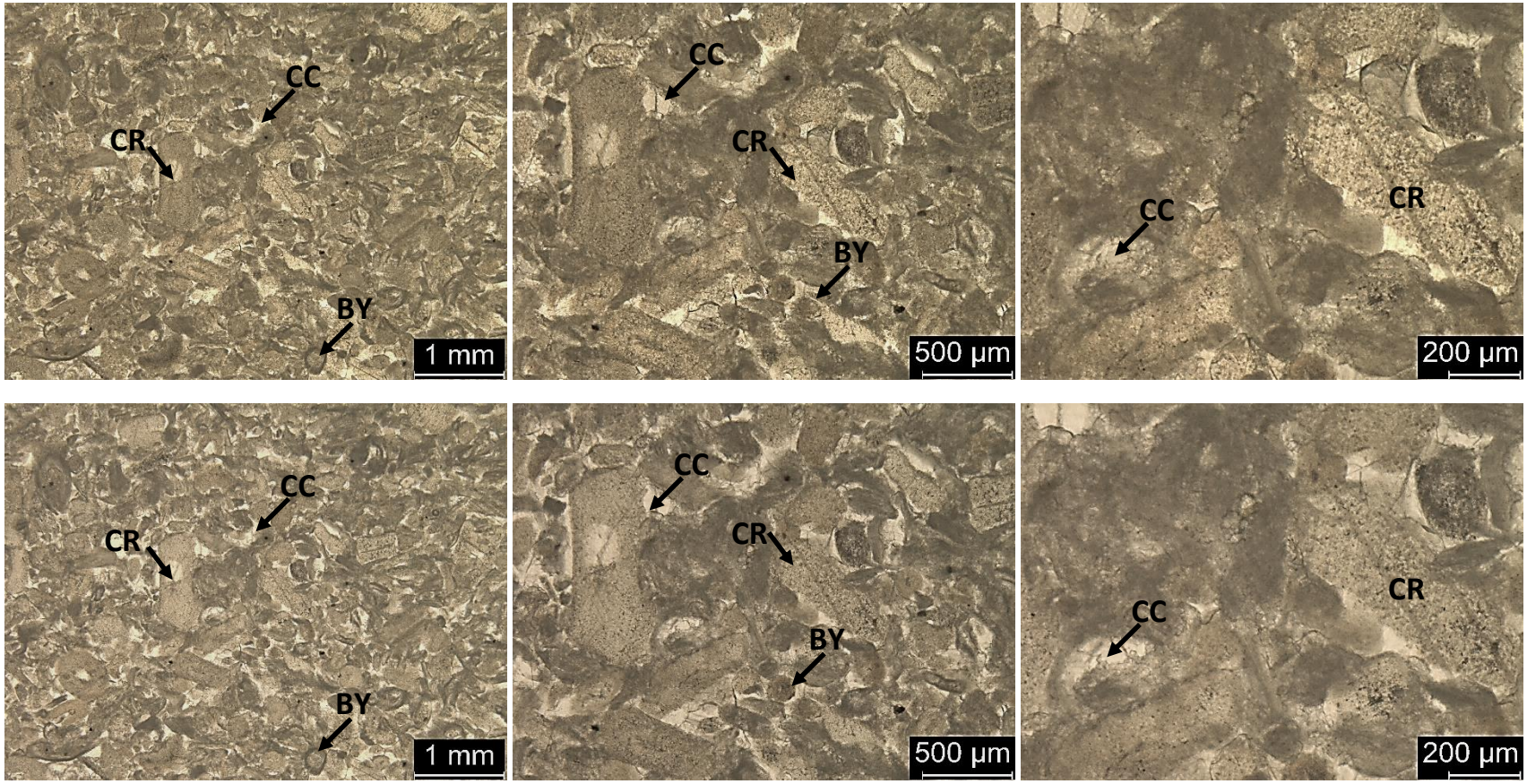

3p-1.0: Crinoidal grainstone, fine to coarse grained, moderately sorted. Consists of 80% skeletal grains and 20% blocky calcite cement (visual estimation). Primary grain types consist of crinoids (200µ – 1mm) and bryozoans (200µ – 300µ).

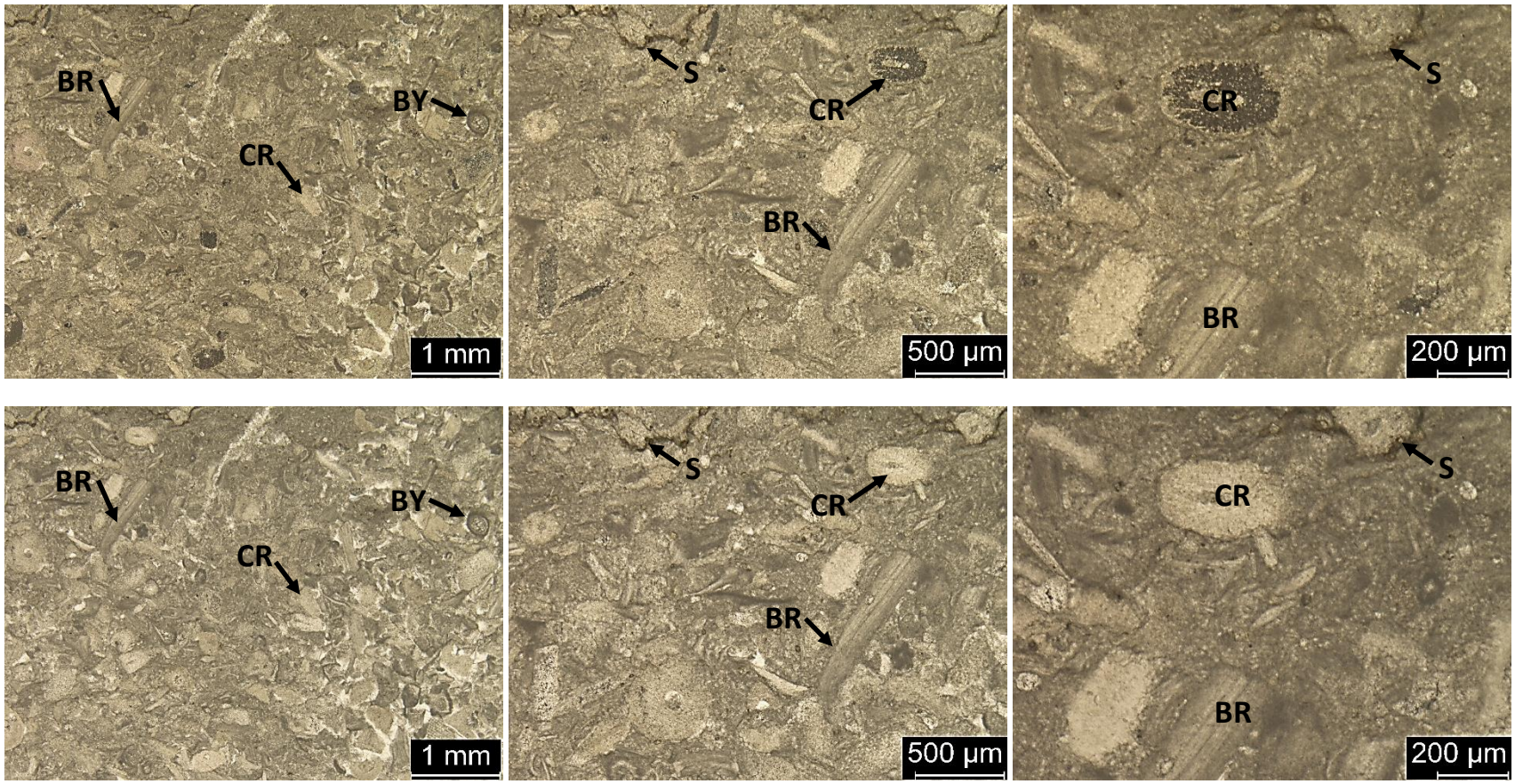

3p-3.5: Crinoidal mud-lean packstone to grainstone, fine to coarse grained, moderately to poorly sorted. Contains 70% skeletal grains, 14% calcite cement, 15% micrite matrix, and 1% dolomite and clay.

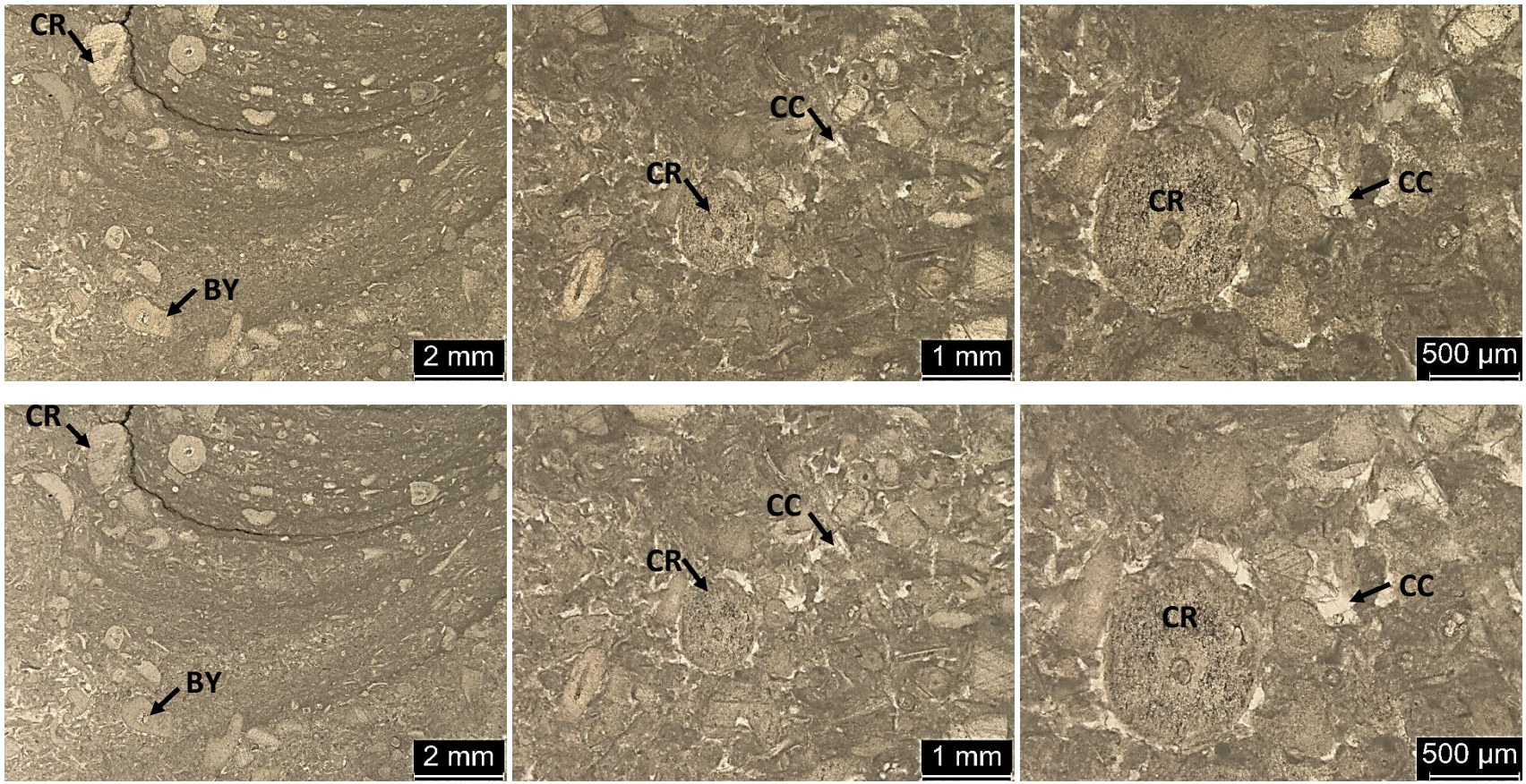

3p-5.0: Crinoidal mud-lean packstone, very fine to coarse grained, poorly sorted. Consists of 70% skeletal grains, 20% blocky calcite cement, and 10% micrite mud (visual estimation). Grain types include crinoids (250µ – 1mm), bryozoans (250µ – 500µ), and brachiopods (500µ – 700µ). Calcite cement surrounding the skeletal grains is extensive.

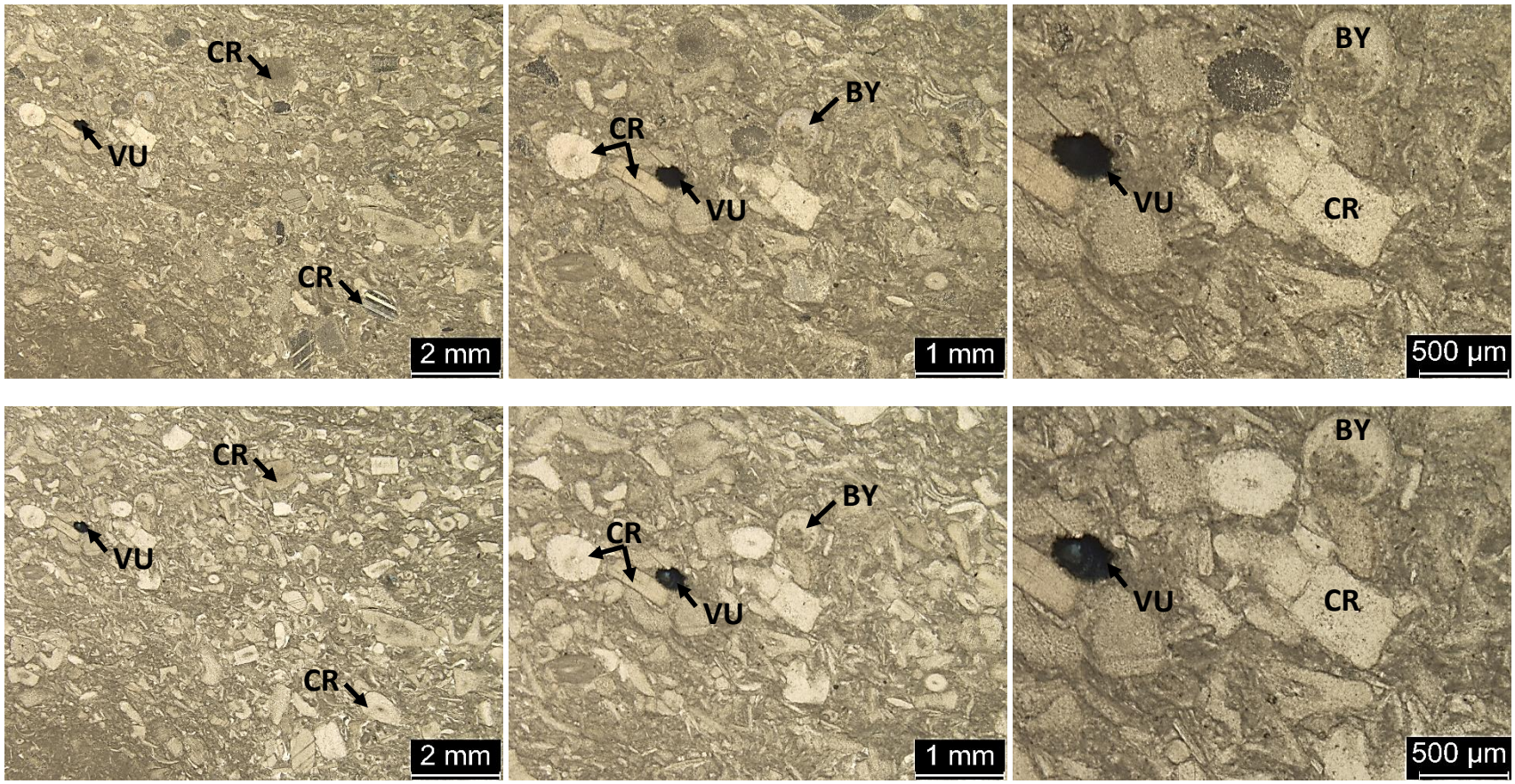

3p-8.0: Crinoidal packstone, very fine to coarse grained, moderately to well sorted. Contains 45% skeletal grains, 54% micrite matrix, and 1% calcite cement (visual estimation). Skeletal grains include crinoids (62.5µ – 750µ) and bryozoans (62.5µ – 500µ). Vugular porosity can also be seen.

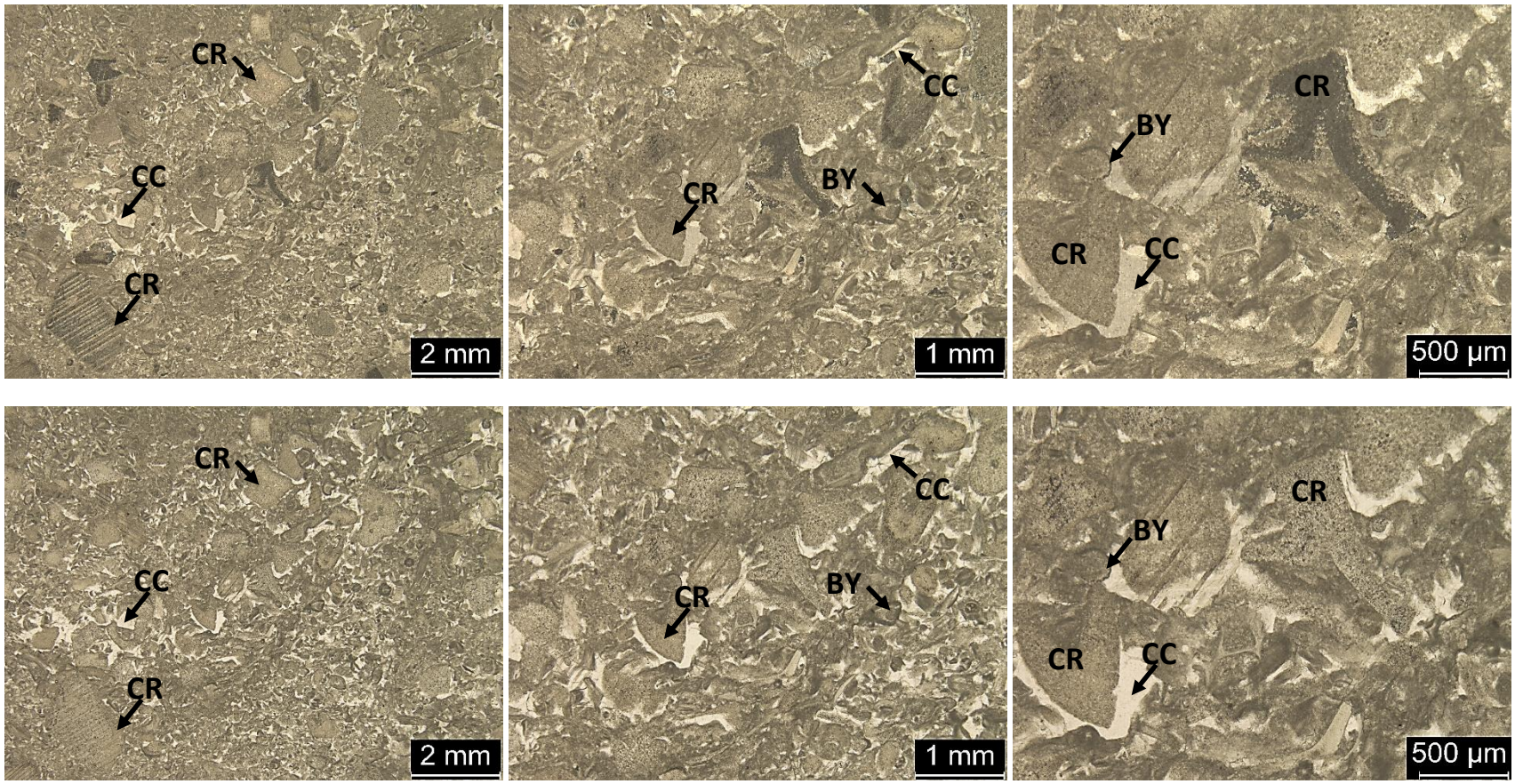

3p-9.0: Crinoidal grainstone, medium to very coarse grained, moderately to well sorted. Contains 75% skeletal grains and 25% calcite cement (visual estimation). Grain types include crinoids (250 – 2mm) and bryozoans (250 – 700).

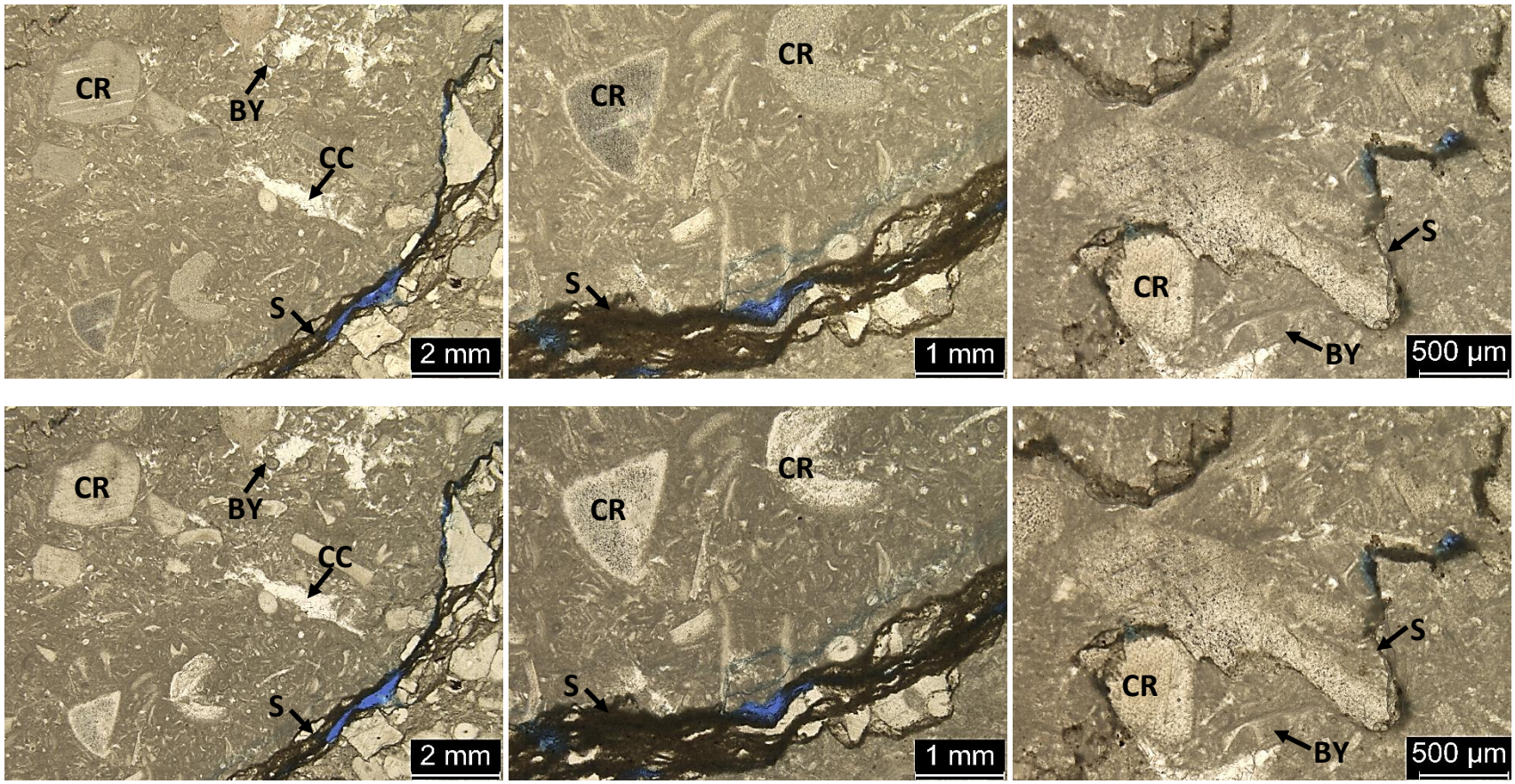

3p-12.0: Skeletal wackestone, very fine to very coarse grained, very poorly to poorly sorted. Contains 35% skeletal grains, 61% micrite matrix, and 4% calcite cement and clay (visual estimation). Grain types include crinoids (250 – 2mm) and bryozoans (62.5 – 500). Stylolitic porosity can be seen along the stylolite that is partially filled with clays.

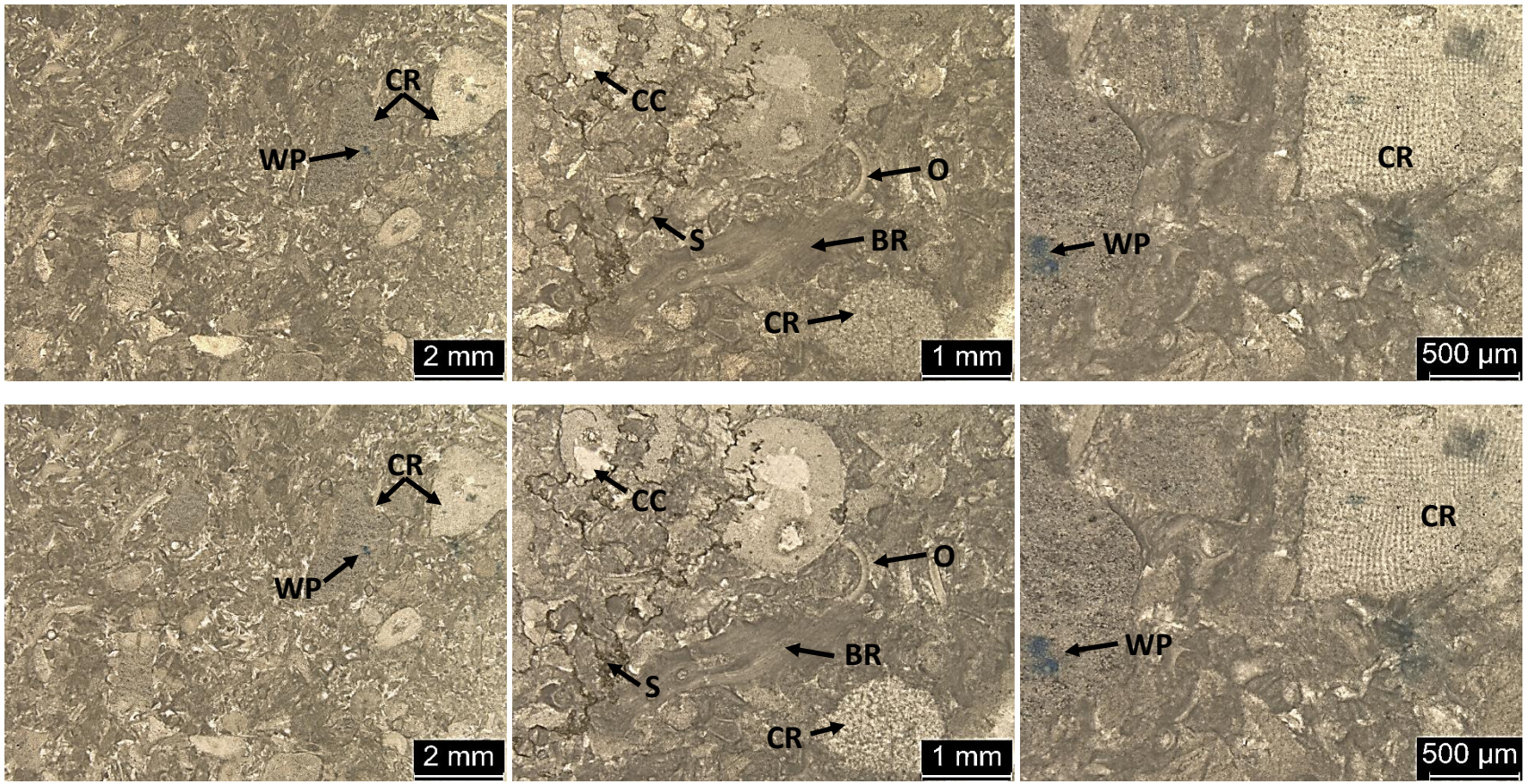

3p2-2.5: Crinoidal-bryozoan grainstone to mud-lean packstone, very fine to very coarse grained, poorly sorted. Contains 70% skeletal grains, 20% blocky calcite cement, and 10% micrite mud (visual estimation). Grain types consist of crinoids (250µ – 2mm), brachiopods (500µ – 700µ), bryozoans (125µ – 500µ), and ostracods (125µ – 400µ). Calcite cement, a muddy stylolite, and intraparticle porosity can also be seen.

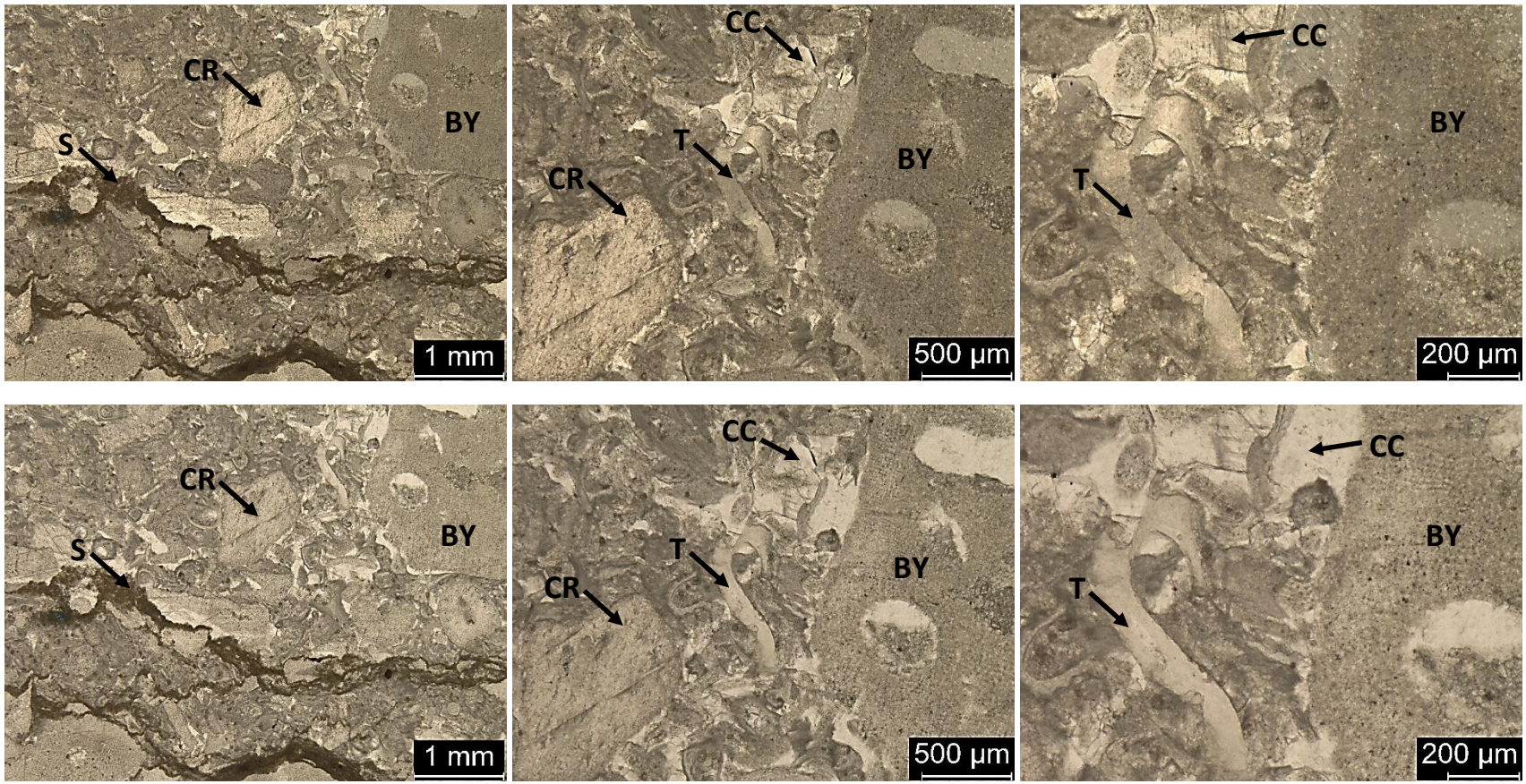

3p2-5.0: Bryozoan-crinoidal grainstone to mud-lean packstone, fine to very coarse grained, poorly sorted. Contains 65% skeletal grains, 35% blocky calcite cement, and 5% micrite matrix (visual estimation). Skeletal grains consist of crinoids (500µ – 2mm), bryozoans (125µ – 2mm), brachiopods (500µ – 700µ), and trilobites (500µ – 1mm).

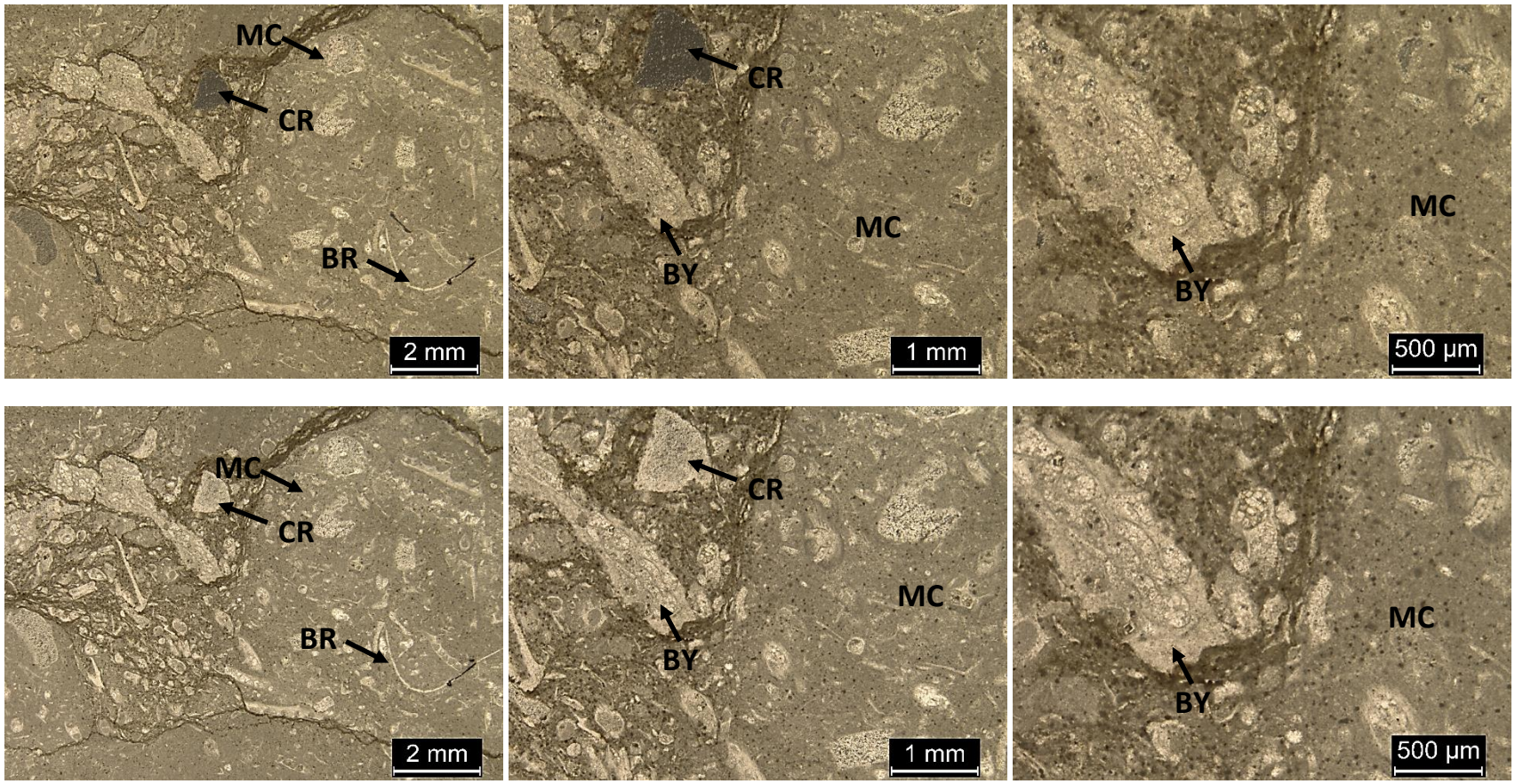

JS1 (Block 1): Crinoidal-bryozoan wackestone-packstone taken from the base of Block 1 and contains mud clasts that have been incorporated into the block from the underlying debris flow bed. Mudstone clasts range in size from very coarse sand to very coarse pebbles. The mudstone clasts are surrounded by a matrix of fine to coarse grained bryozoans (125 µ – 1mm), brachiopods (400 µ – 700 µ), and crinoids (125 µ – 2mm). Calcite cement has filled in voids within some of the skeletal grains.

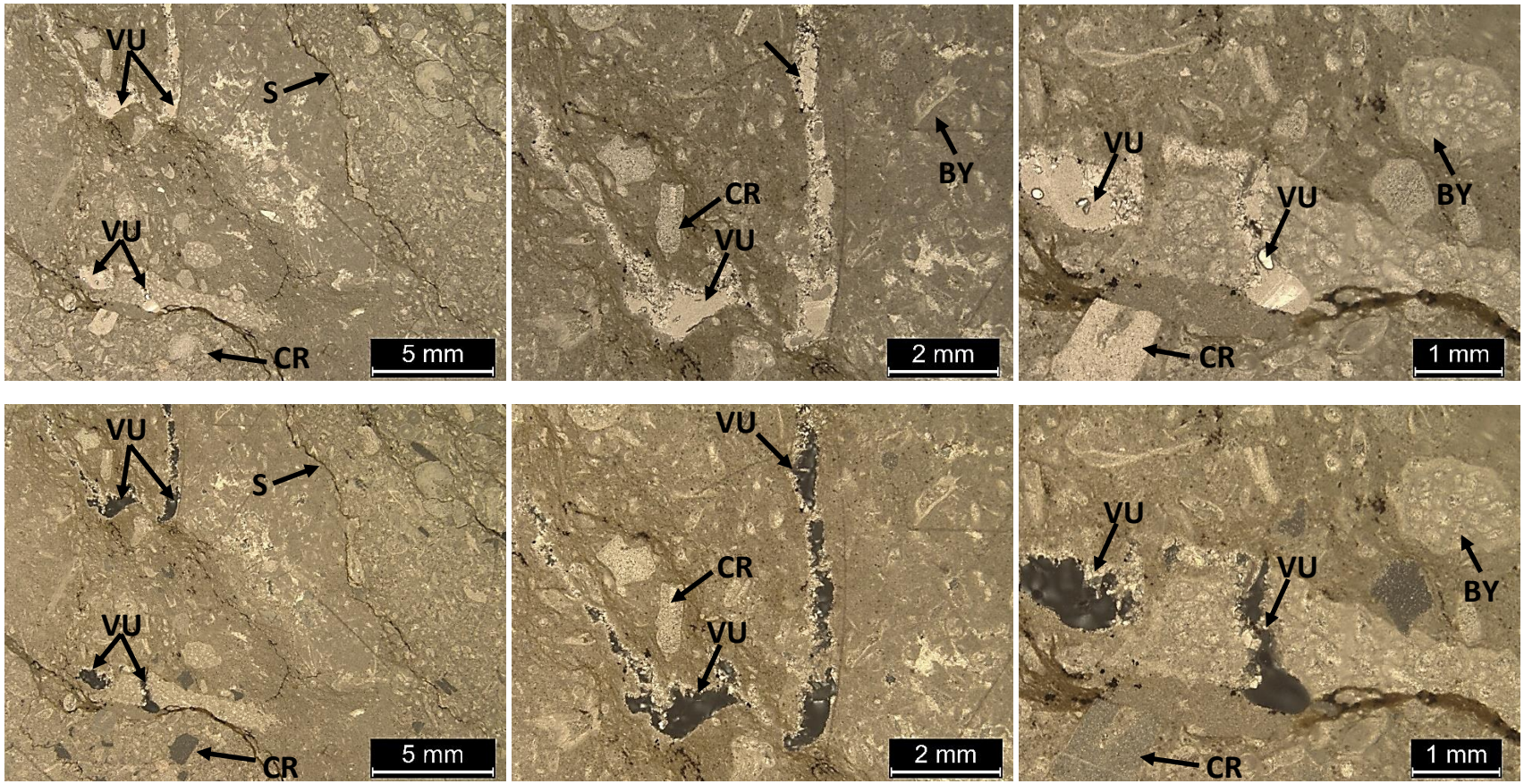

JS3 (Block 1): Crinoidal-bryozoan wackestone to packstone, poorly sorted, grain size ranges from fine sand to fine pebbles. Contains 35% skeletal grains, 62% micrite matrix, and 3% blocky calcite cement and porosity (visual estimation). Grain types include crinoids (250µ – 3mm) and bryozoans (125µ – 6mm). Vugular porosity and stylolites can also be seen throughout.

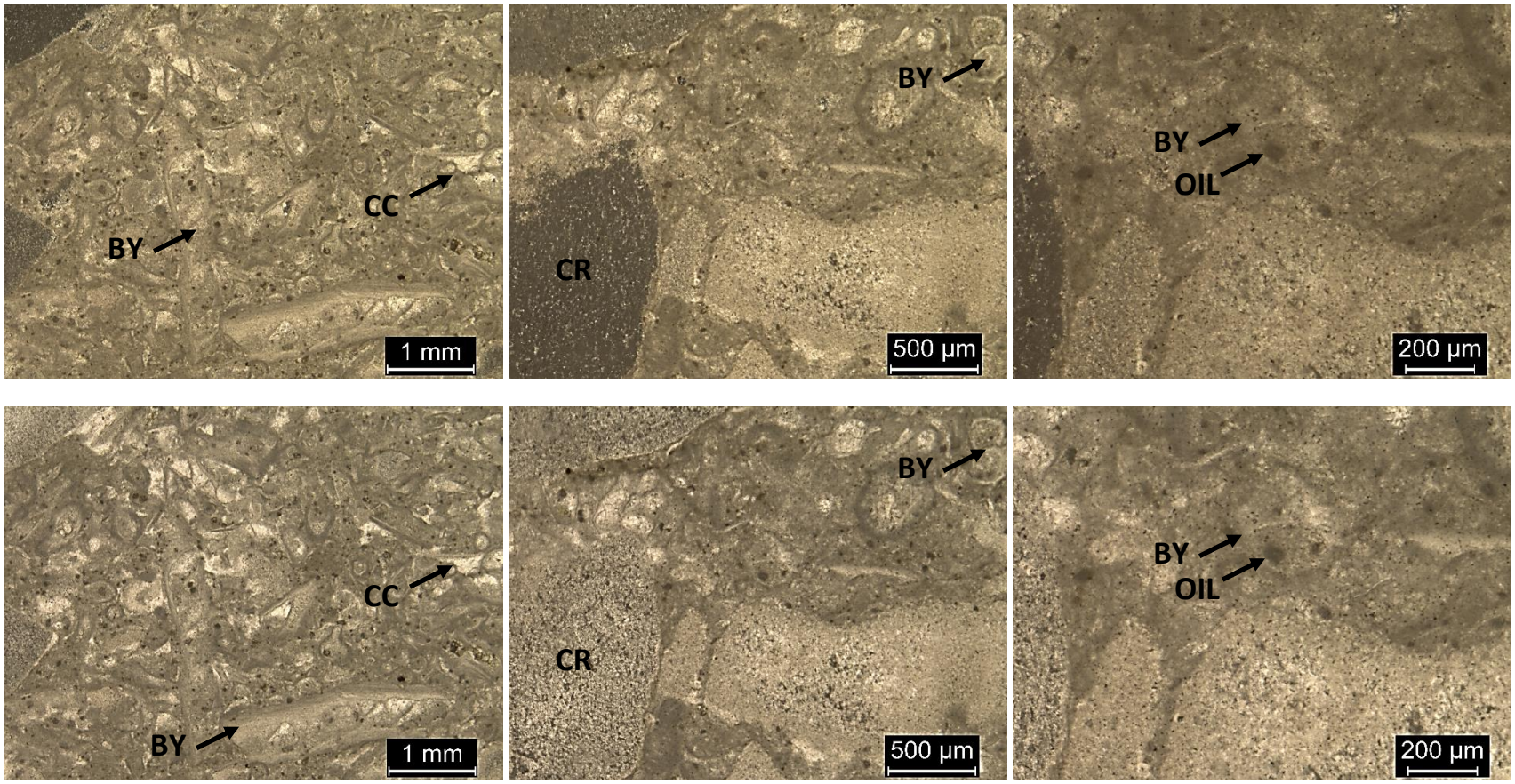

JS5.5 (Block 1): Bryozoan packstone, very fine to very coarse grained, poorly sorted. Contains 60% skeletal grains, 35% micrite matrix, and 5% blocky calcite cement and dead oil (visual estimation). Grain types include crinoids (62.5µ – 2mm) and bryozoans (62.5µ – 2mm). Calcite cement can be seen within and surrounding skeletal grains

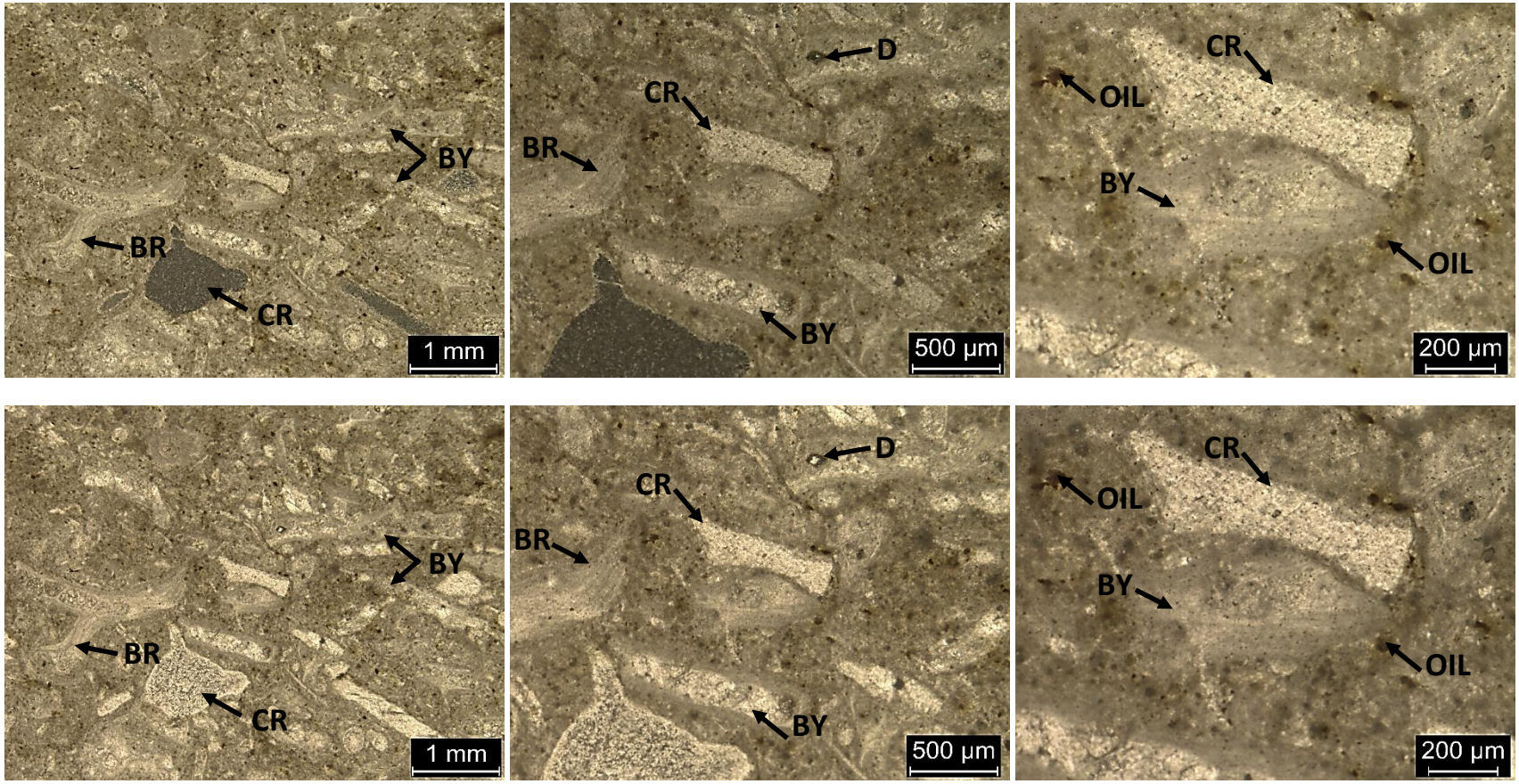

JS6 (Block 1): Crinoidal wacketstone, fine to very coarse grained, poorly sorted. Contains 40% skeletal grains, 57% micrite matrix, and 3% blocky calcite cement, dolomite, and dead oil (visual estimation). Grain types include crinoids (200µ – 1mm), bryozoans (125µ – 2mm), and brachiopods (500µ – 2mm).

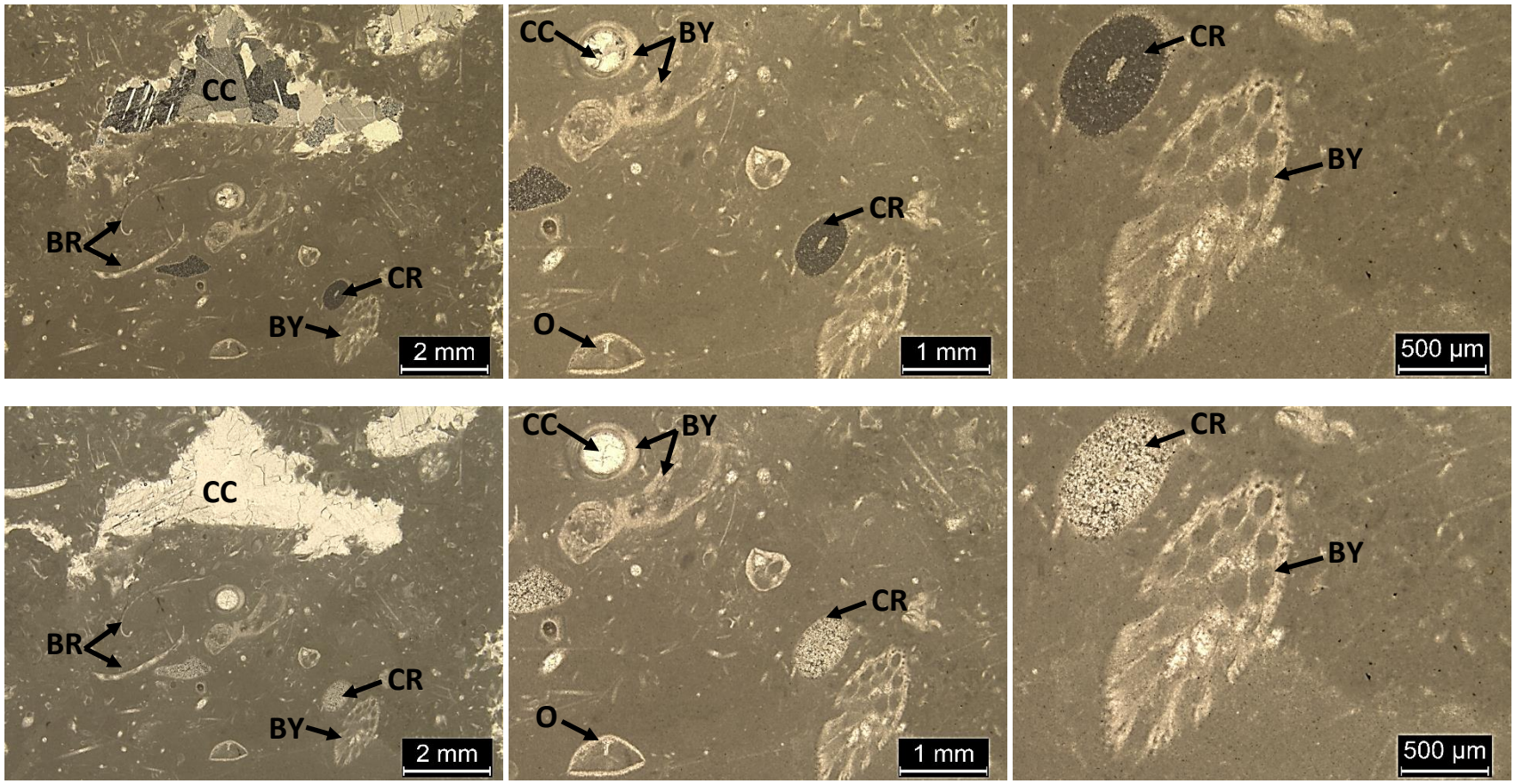

JC1 (Block 1): Skeletal wackestone, fine to very coarse grained, poorly sorted. Contains 15% skeletal grains, 82% micrite matrix, and 3% blocky calcite cement (visual estimation). Grain types include crinoids (200 – 1mm), bryozoans (125µ – 2mm), brachiopods (600µ – 2mm), and ostracods (500µ – 800µ).

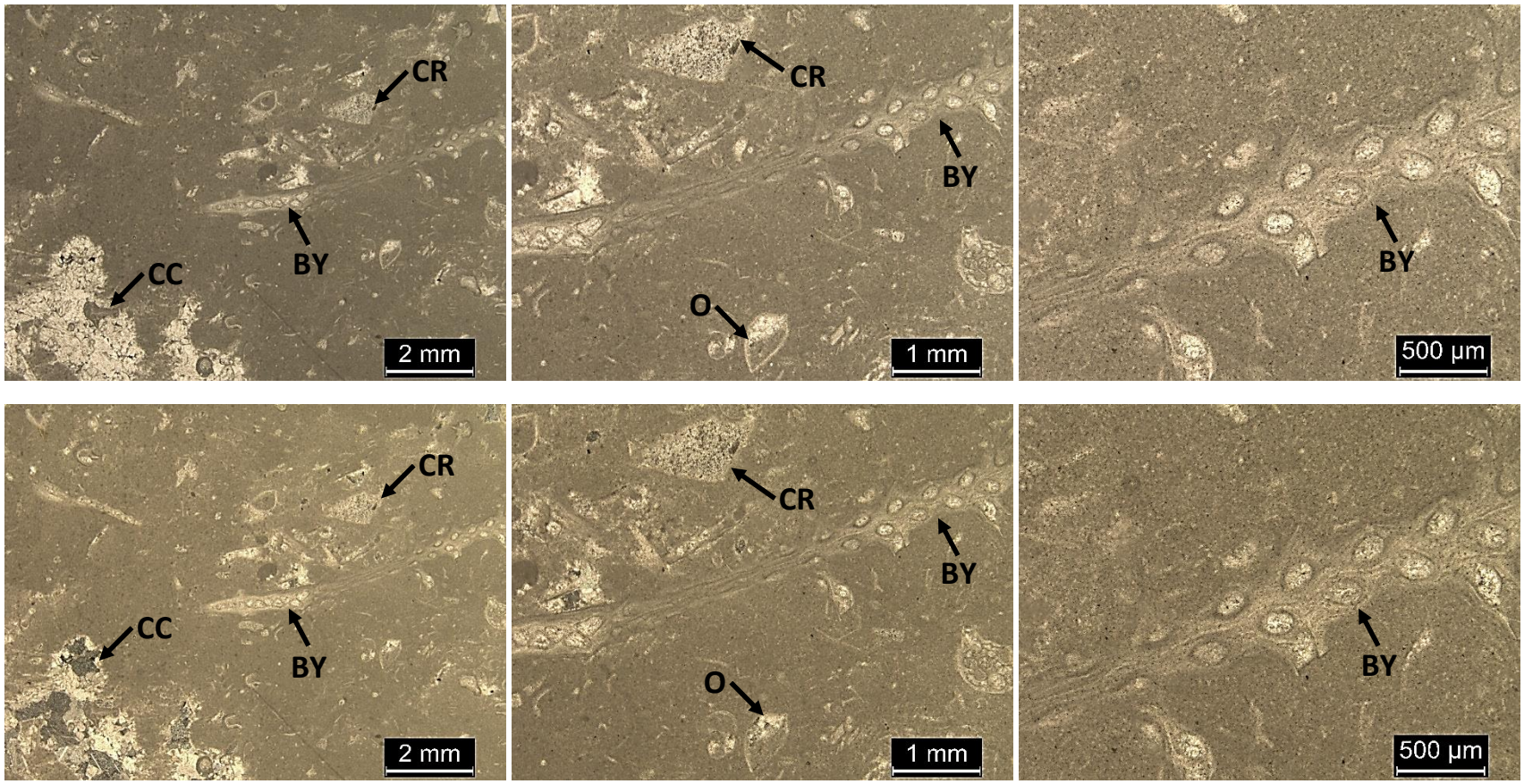

JC2 (Block 1): Bryozoan wackestone, poorly sorted, grain size ranges from fine sand to fine pebbles. Contains 25% skeletal grains, 73% micrite matrix, and 3% blockky calcite cement (visual estimation). Grain types include crinoids (125µ – 2mm), bryozoans (500µ – 6mm), ostracods (125µ – 500µ), and brachiopods (500µ – 1mm).

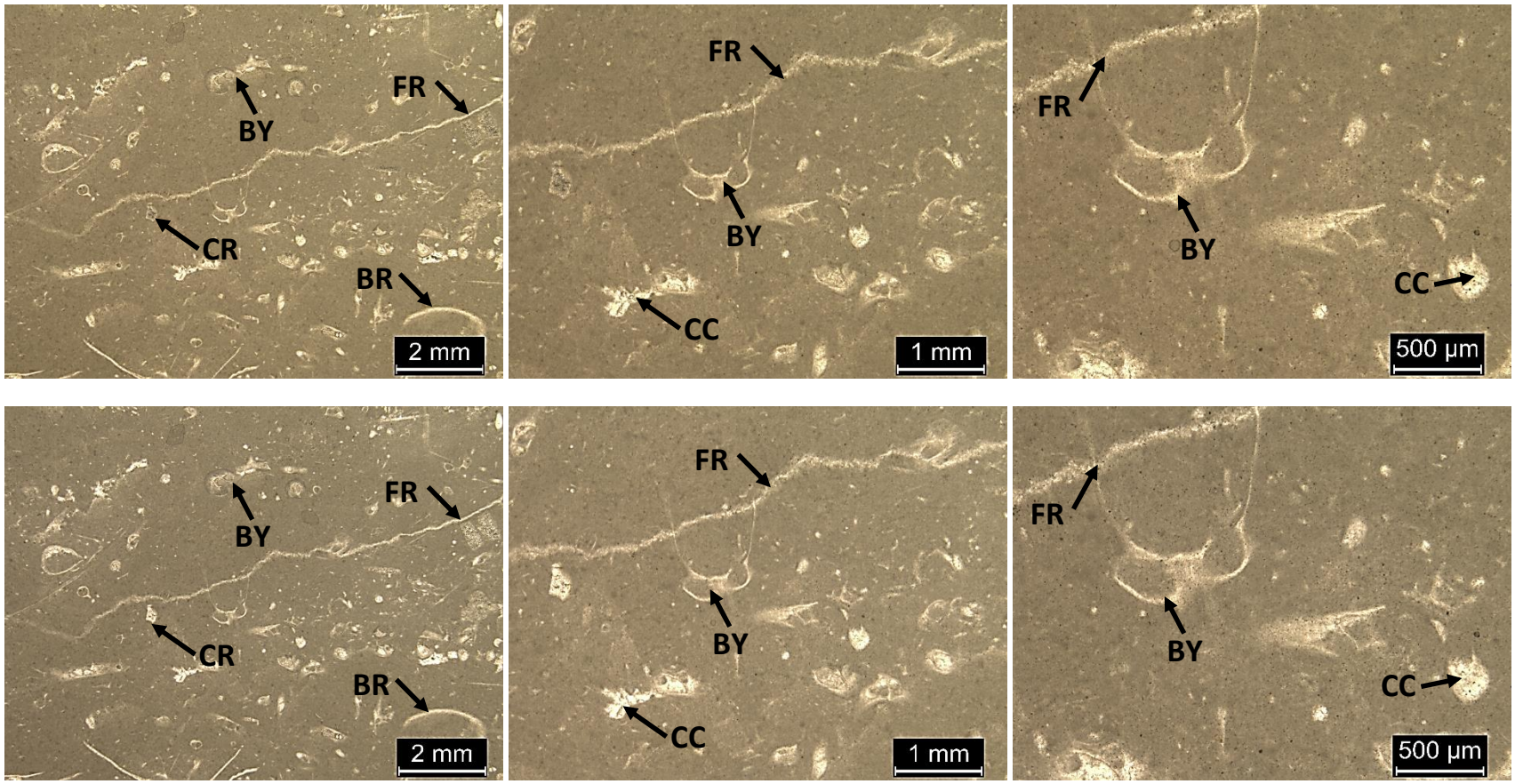

JC3 (Block 1): Skeletal wackestone, fine to coarse grained, poorly-moderately sorted. Contains 20% skeletal grains, 77% micrite matrix, and 3% calcite cement (visual estimation). Grain types include bryozoans (250µ – 1mm), brachiopods (500µ – 2mm), and crinoids (125µ – 200µ). Calcite cement fills in skeletal voids and fractures.

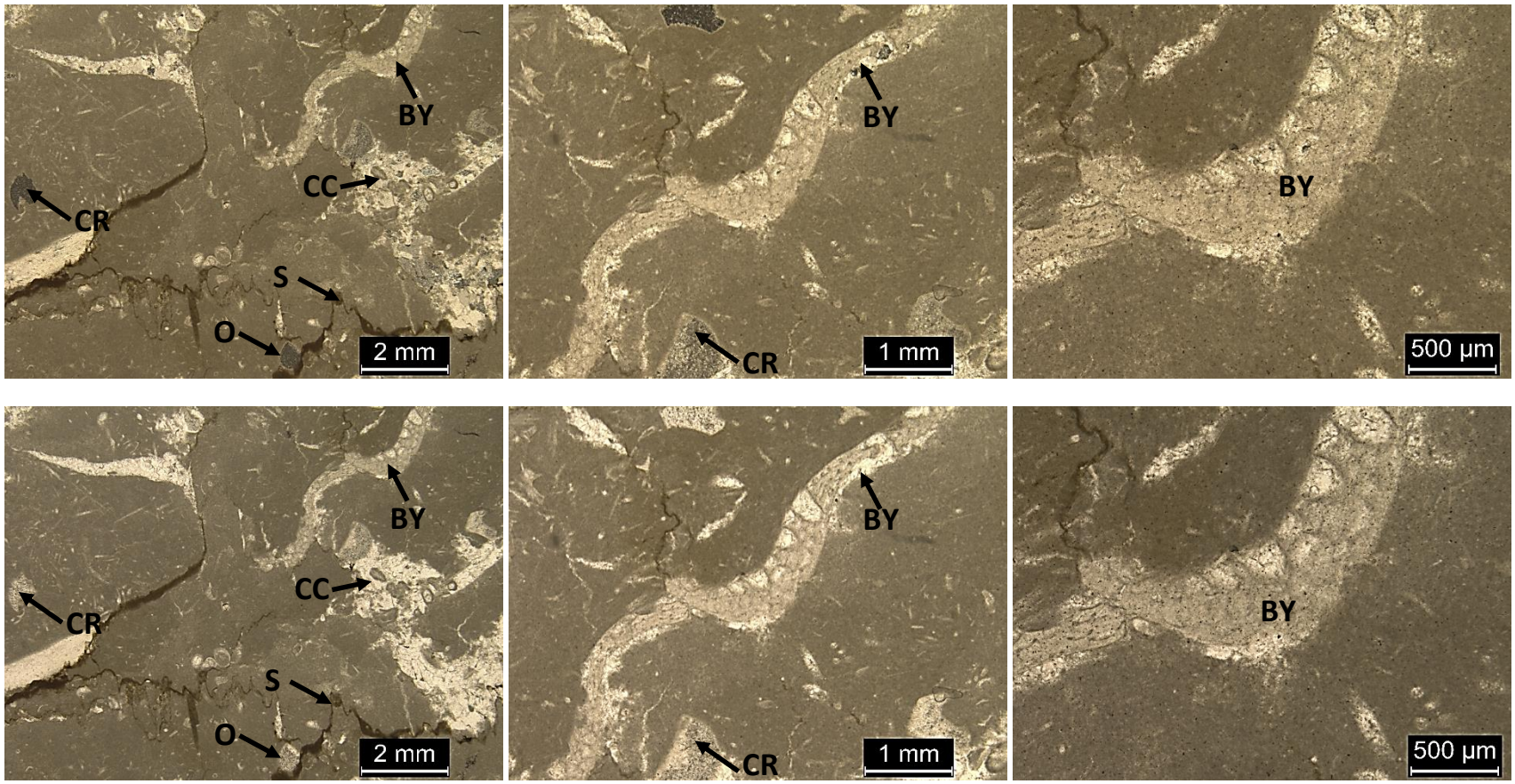

JC4 (Block 1): Skeletal wackestone, poorly sorted, grain size ranges from very fine sand to very fine pebbles. Contains 15% skeletal grains, 83% micrite matrix, and 2% blocky calcite cement (visual estimation). Grain types include bryozoans (62.5µ – 4mm), crinoids (62.5µ – 1mm), and ostracods (250µ – 500µ).

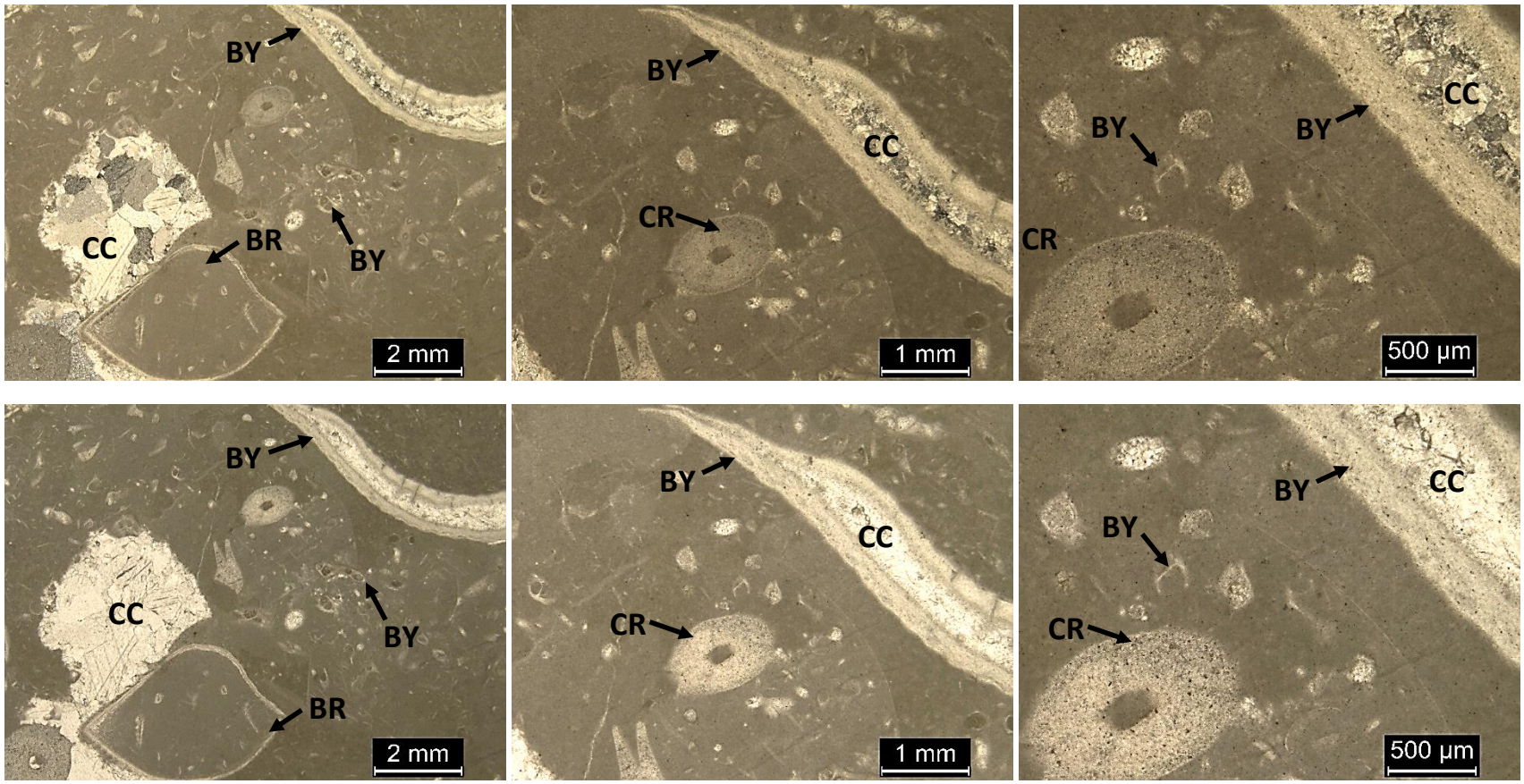

JC7 (Block 1): Bryozoan-crinoidal wackestone, poorly sorted, grain size ranges from fine sand to fine pebbles. Contains 15% skeletal grains, 82% micrite matrix, and 3% blocky calcite cement (visual estimation). Grain types include bryozoans (125µ – 5mm), crinoids (125µ – 1mm), and brachiopods (500µ – 4mm).

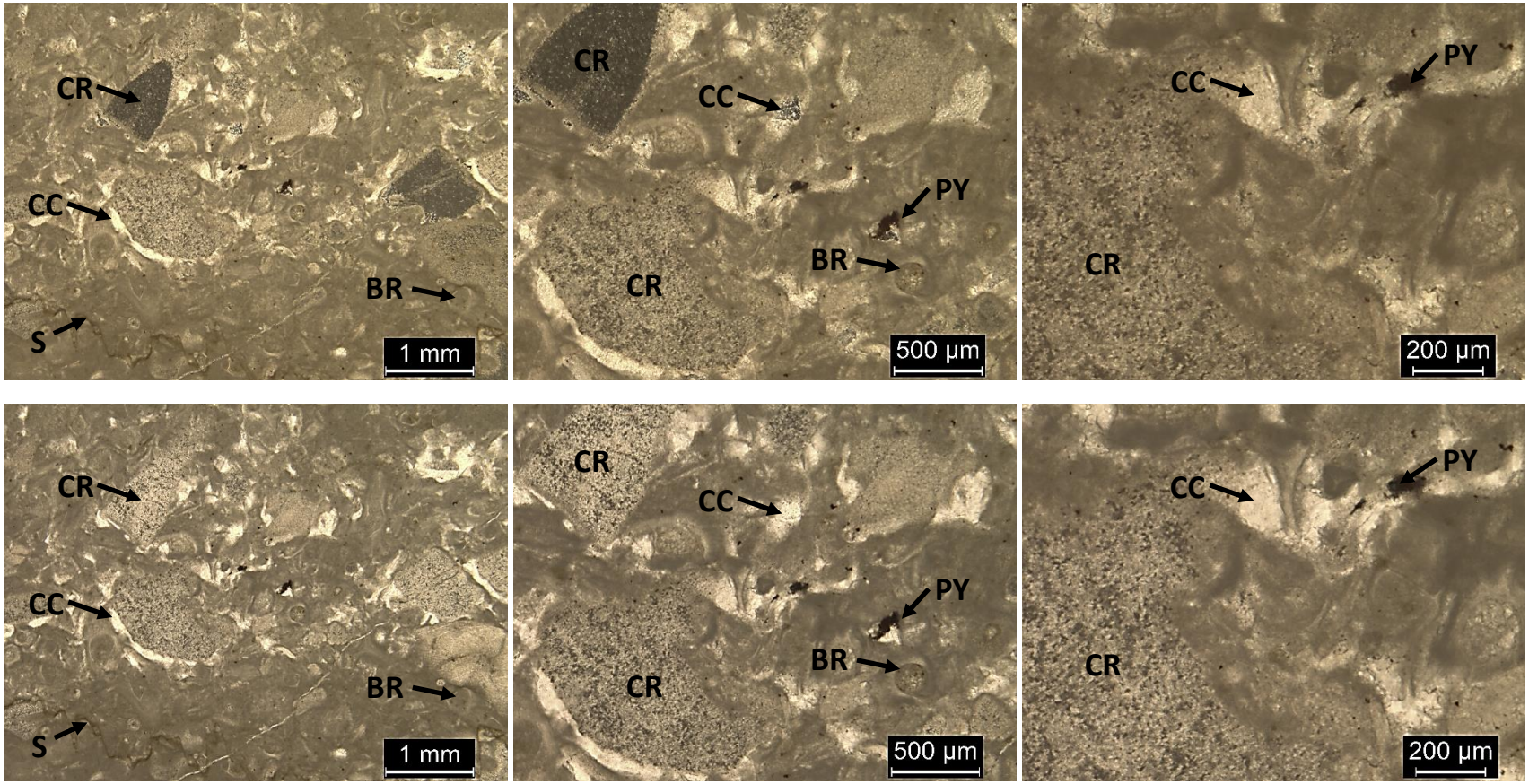

JC8 (Block 1): Crinoidal-bryozoan wackestone-packstone, fine to very coarse grained, poorly sorted. Contains 45% skeletal grains, 54% micrite matrix, and 1% blocky calcite cement and pyrite (visual estimation). Skeletal grains include crinoids (200µ – 2mm) and bryozoans (125µ – 400µ)

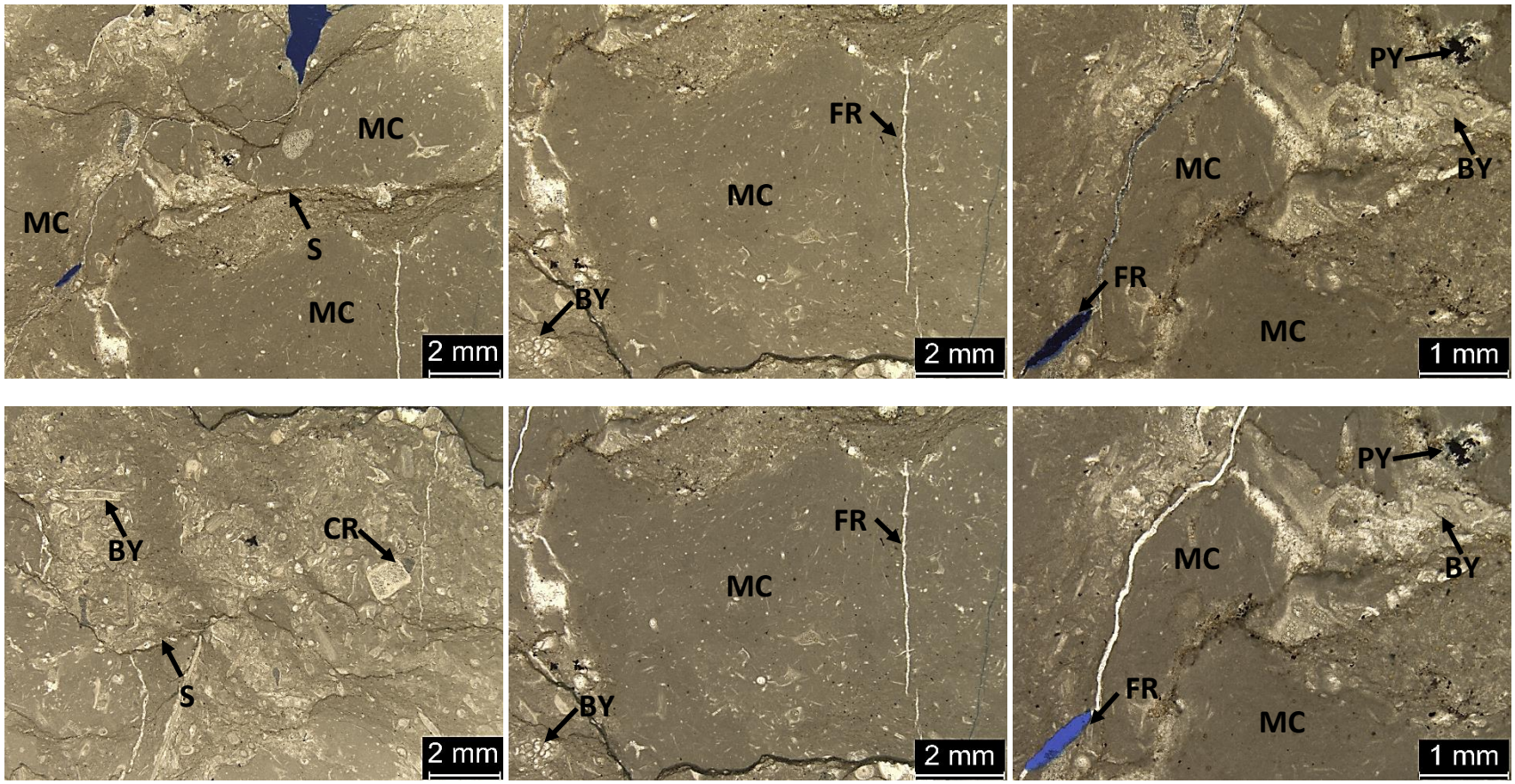

Block 2: Top left photomicrograph is the upper half of the thin section in CPL. The bottom left photograph is the lower portion of the thin section in CPL. Skeletal wackestone containing mud clasts broken up within. The mud clasts range in size from very coarse sand to fine pebbles. Skeletal grains include crinoids (250µ – 2mm) and bryozoans (125µ – 2mm). Pyrite and calcite cement have filled in fractures and void spaces within the micrite matrix. Stylolites have been filled with dolomite.

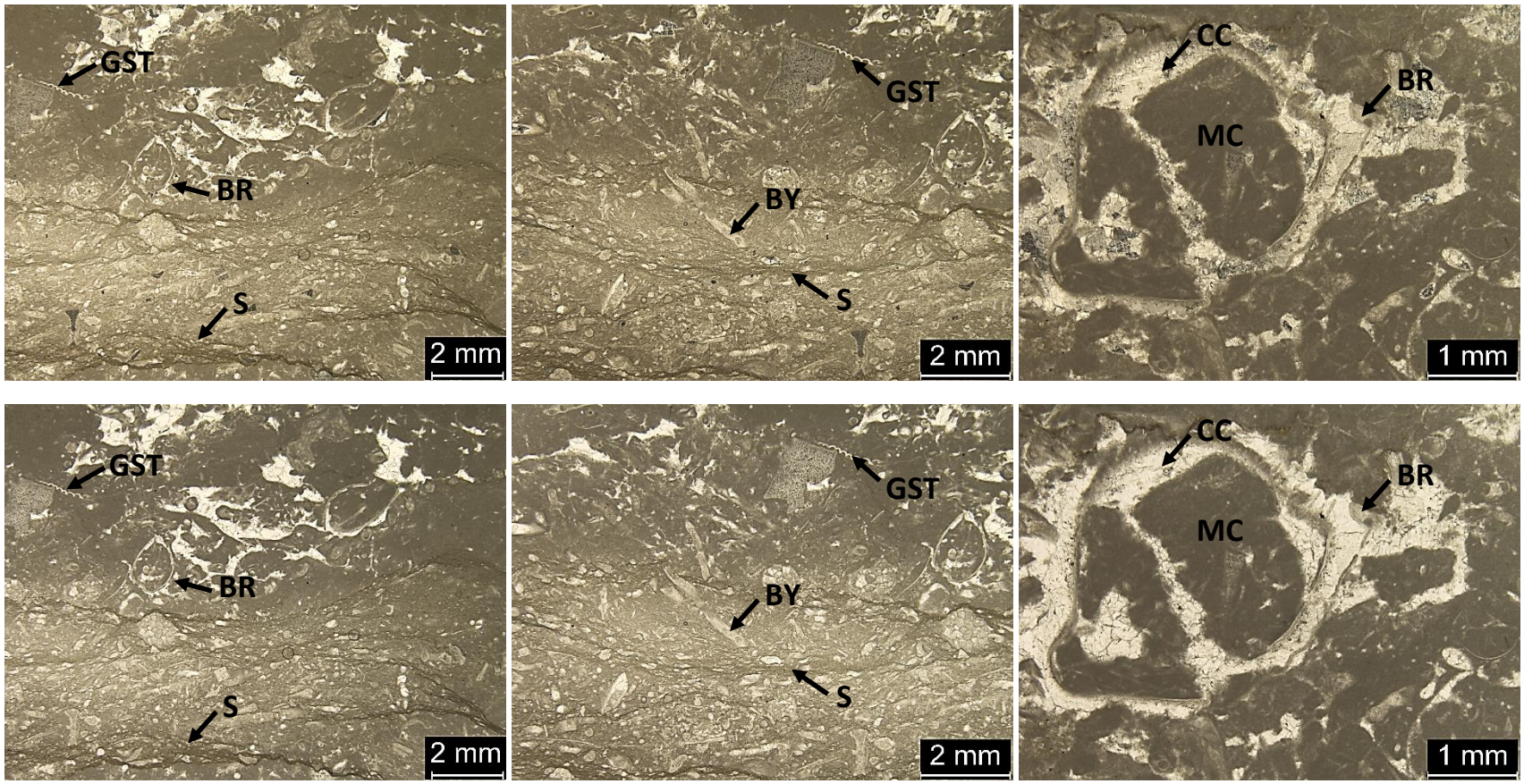

Block 3: Skeletal wackestone, grain size ranges from fine sand to very fine pebbles, poorly sorted. Contains crinoids (500µ – 2mm), bryozoans (125µ – 1mm), brachiopods (500µ – 2mm), ostracods (125µ – 450µ), and gastropods (750µ – 2mm). Calcite cement has filled in stromatactis-like structures throughout the upper half of the thin section. Wispy stylolites filled with dolomite occur throughout the lower half of the thin section. The photos at the far right show a brachiopod that was initially filled in with micrite. Upon block movement and deformation of the brachiopod, calcite cement filled in void space within the skeletal grain.

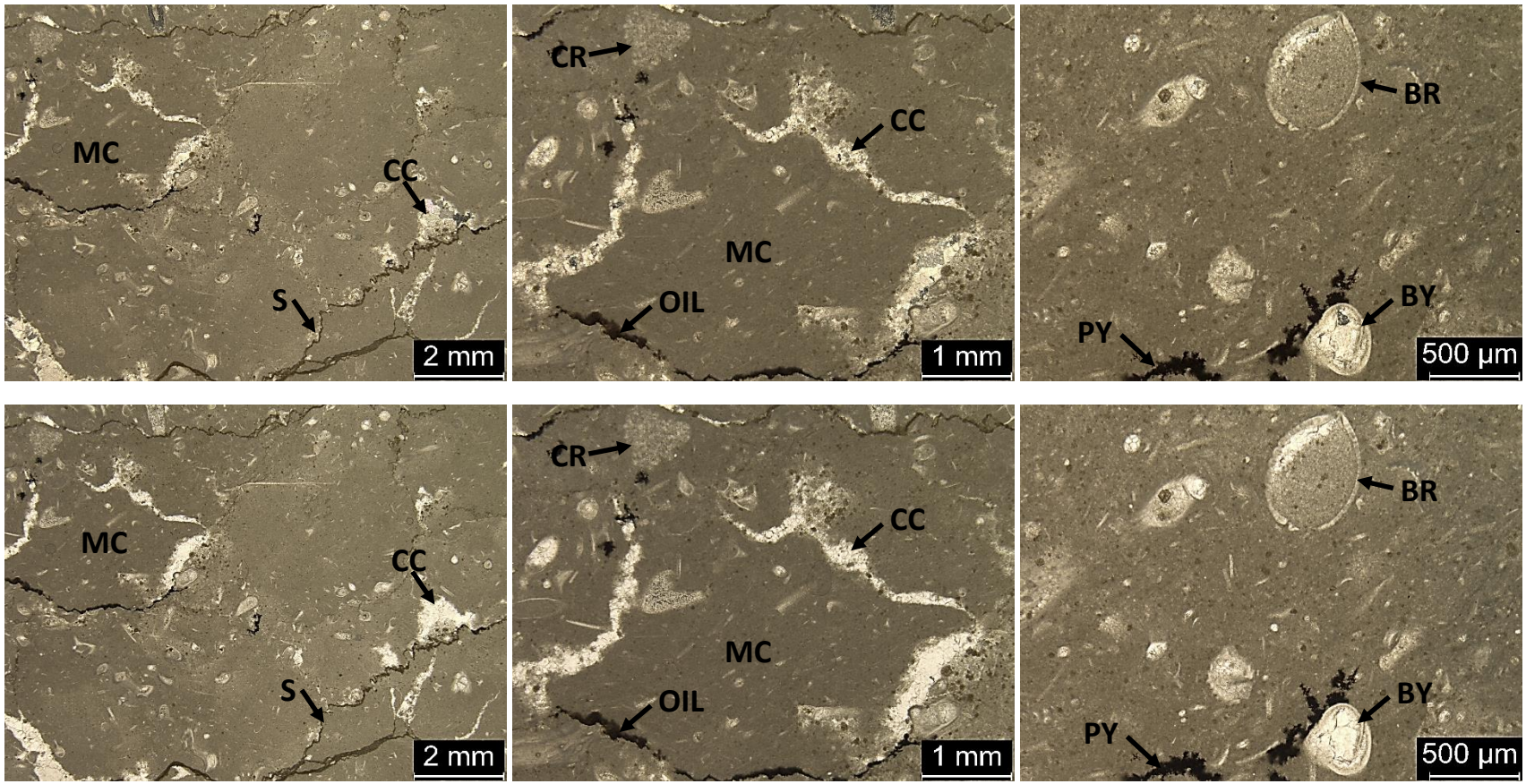

Block 4: Wackestone, very fine to coarse grained, moderately sorted. Contains crinoids (250µ – 1mm), bryozoans (62.5µ – 400µ), and brachiopods (400µ – 750µ). Pyrite and dead oil occur throughout. Calcite cement has filled in some skeletal grains and surrounded mud clasts.

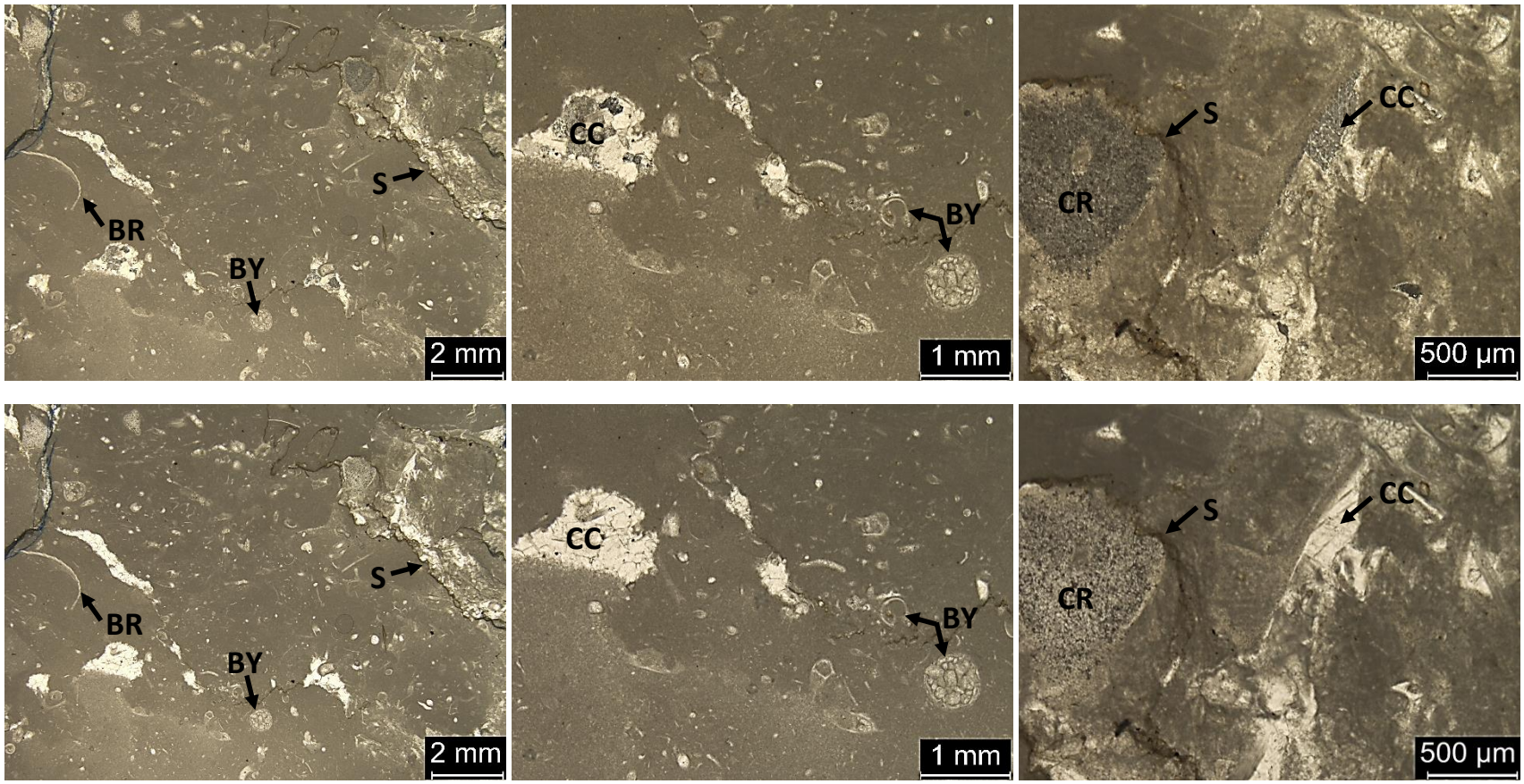

Block 5: Wackestone, fine to very coarse grained, poorly sorted. Contains 20% skeletal grains, 75% micrite matrix, and 5% calcite cement (visual estimation). Skeletal grains include crinoids (250µ – 1mm), brachiopods (750µ – 2mm), and bryozoans (125µ – 750µ). Dead oil occurs along the stylolites.

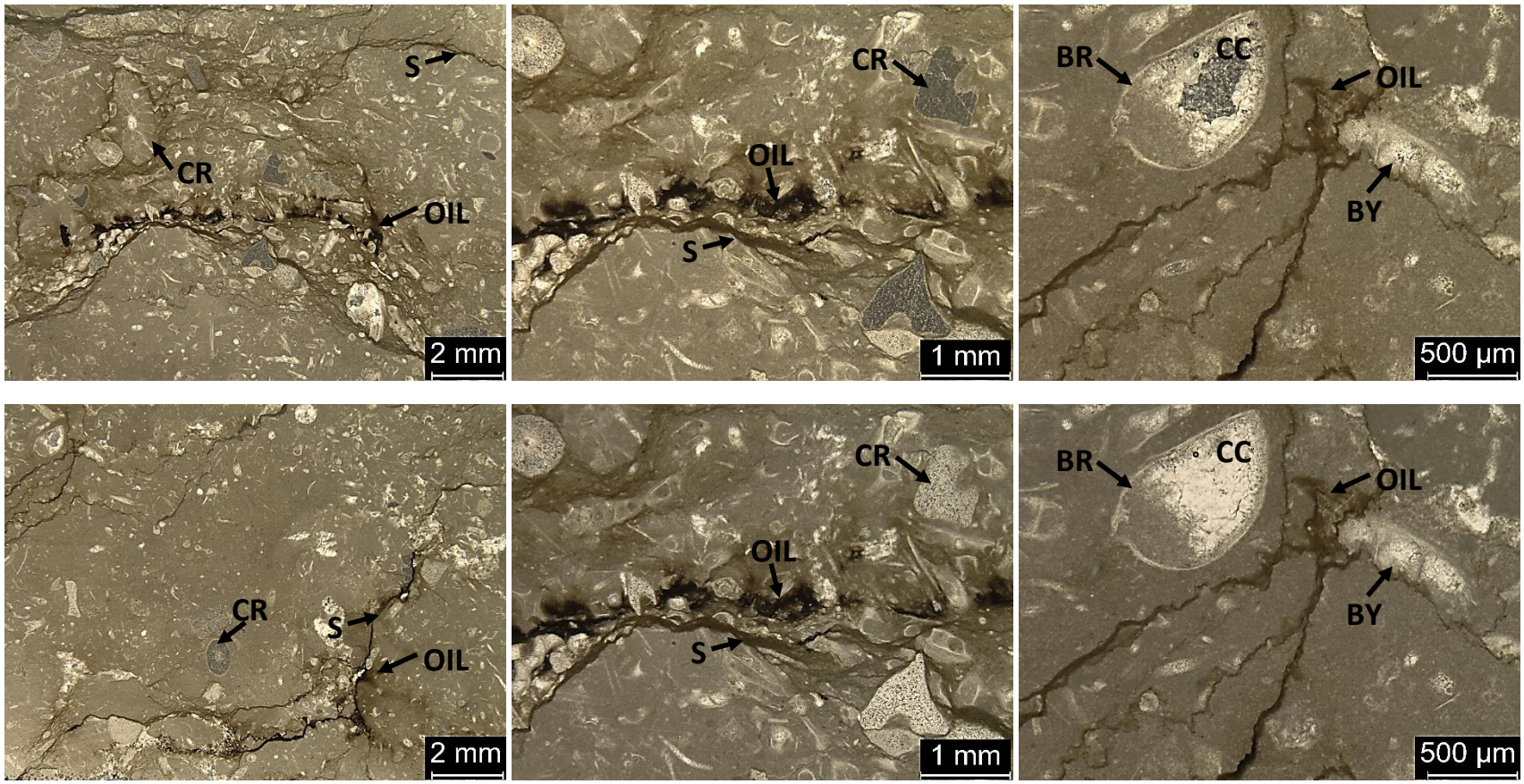

Block 6: Top left photomicrograph is the upper half of the thin section in CPL. The bottom left photograph is the lower portion of the thin section in CPL. Skeletal wackestone, very fine to very coarse grained, poorly sorted. Contains 25% skeletal grains, 65% micrite matrix, 4% dead oil, and 6% blocky calcite cement (visual estimation). Skeletal grains include brachiopods (400µ – 750µ), crinoids (62.5µ – 1mm), bryozoans (62.5µ – 2mm). Dead oil can be seen along the stylolites. A geopetal structure in the form of a brachiopod can be seen at the far right.

Debris Flow

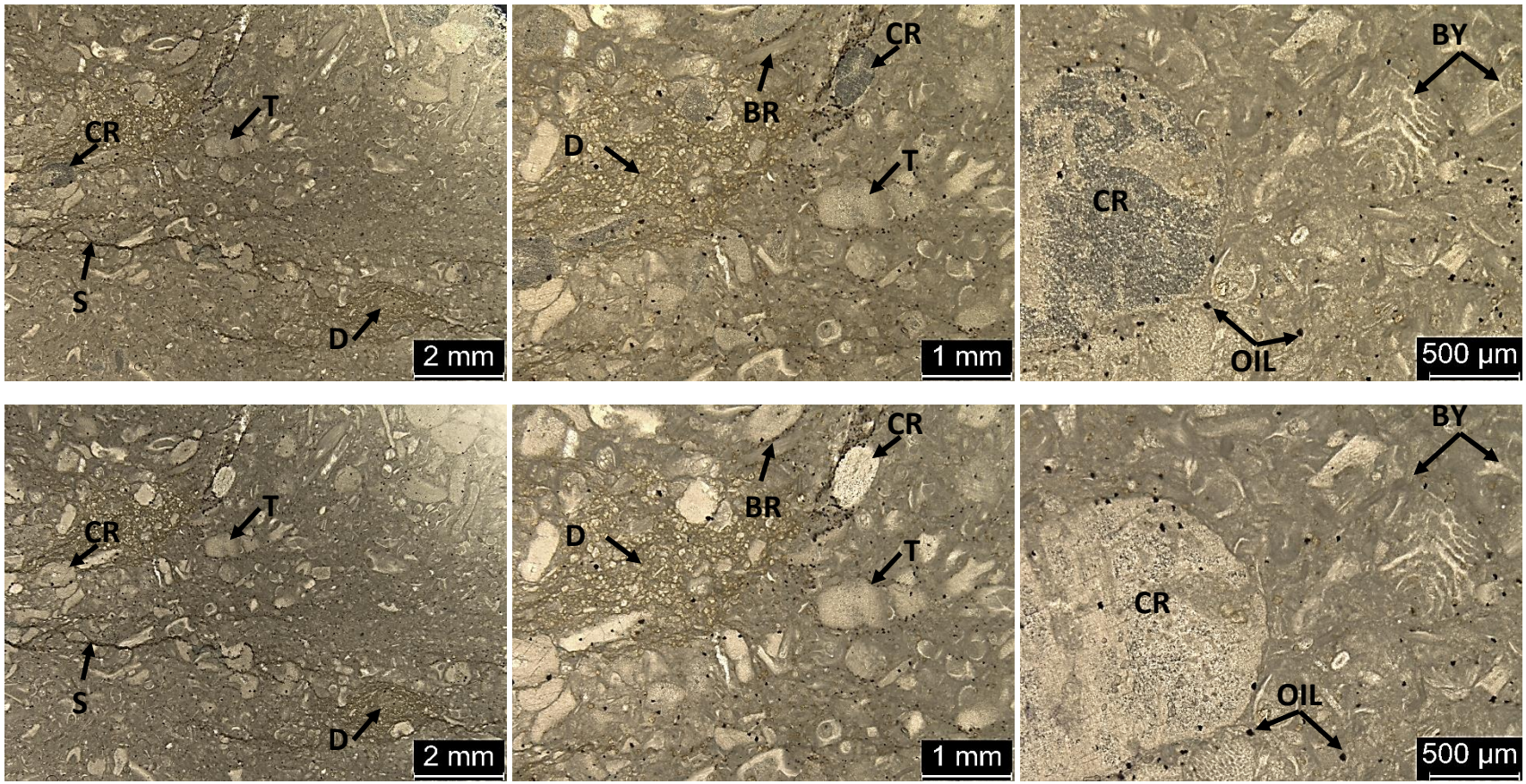

DF 1: Skeletal packstone, very fine to very coarse grained, poorly to moderately sorted. Contains 35% skeletal grains, 60% micrite matrix, 3% dead oil and pyrite, and 2% calcite cement (visual estimation). Skeletal grains include crinoids (62.5µ – 1mm), bryozoans (62.5µ – 500µ), brachiopods (500µ – 750µ)and trilobites (700µ – 2mm). Dolomite occurs throughout the thin section.

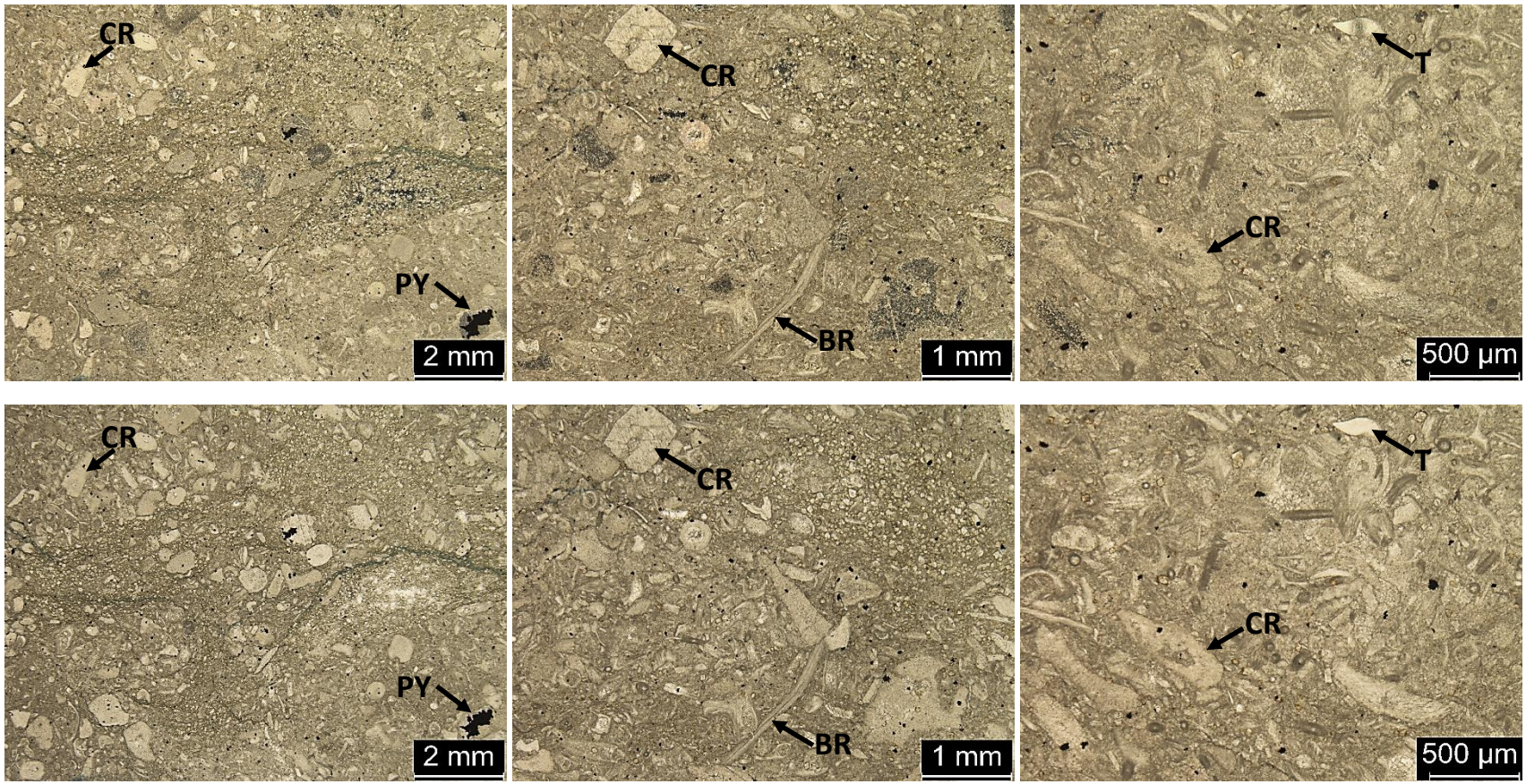

DF 2: Skeletal packstone, very fine to coarse grained, moderately to poorly sorted. Contains 40% skeletal grains, 55% micrite matrix, and 5% dolomite and dead oil (visual estimation). Skeletal grains include crinoids (62.5µ – 1mm), bryozoans (62.5µ – 650µ), brachipods (500µ – 1mm), and trilobites (250µ – 500µ).

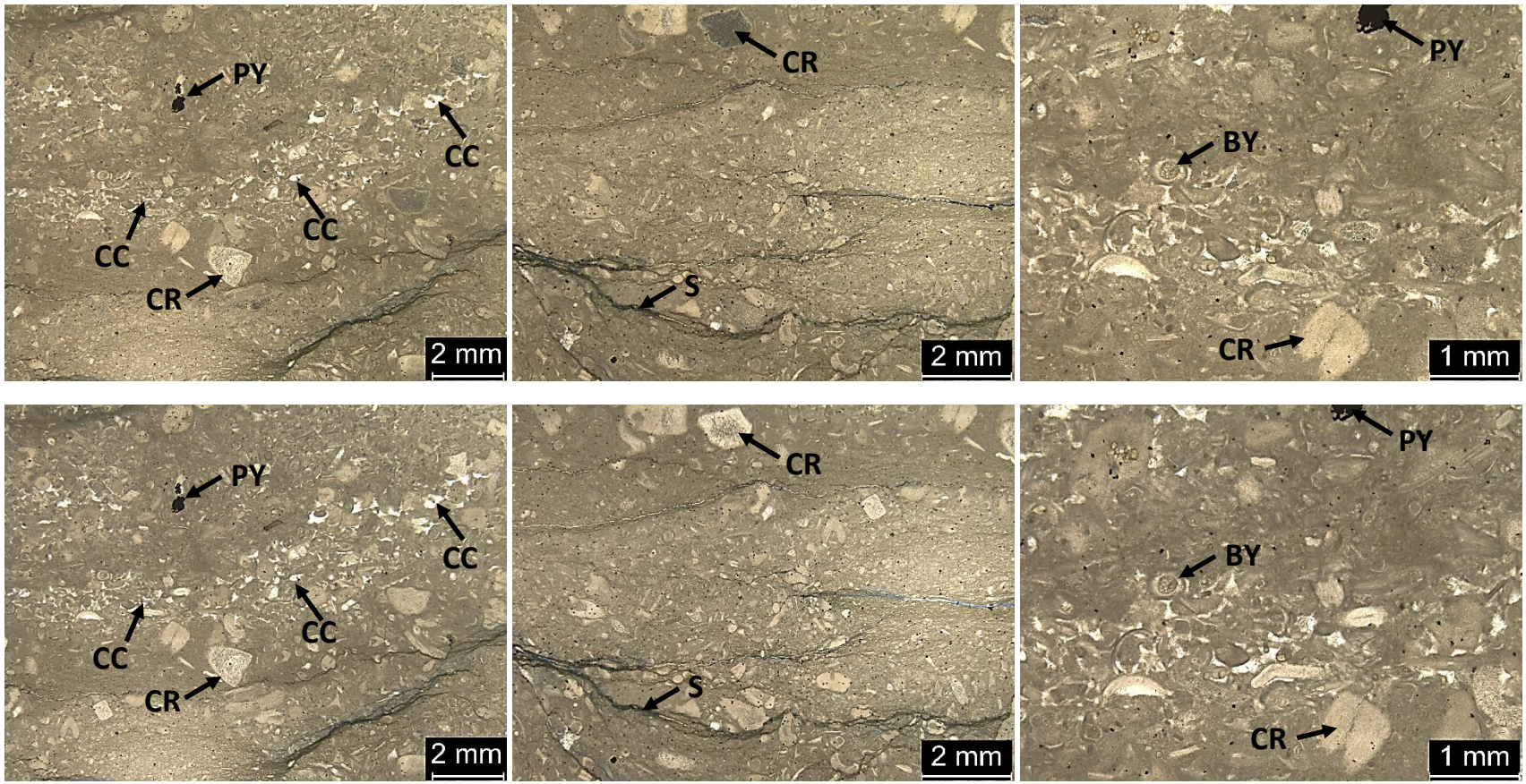

DF 3: Wackestone, fine to coarse grained, moderately to poorly sorted. Contains 30% skeletal grains, 65% micrite matrix, and 5% calcite cement, pyrite and dead oil (visual estimation). Skeletal grains include crinoids (125µ – 2mm), bryozoans (125µ – 500µ), and brachiopods (400µ – 700µ). As seen at the far left, calcite cement has preferentially filled in between grains in a streak shape, possibly void space left after movement of the block down the ramp.

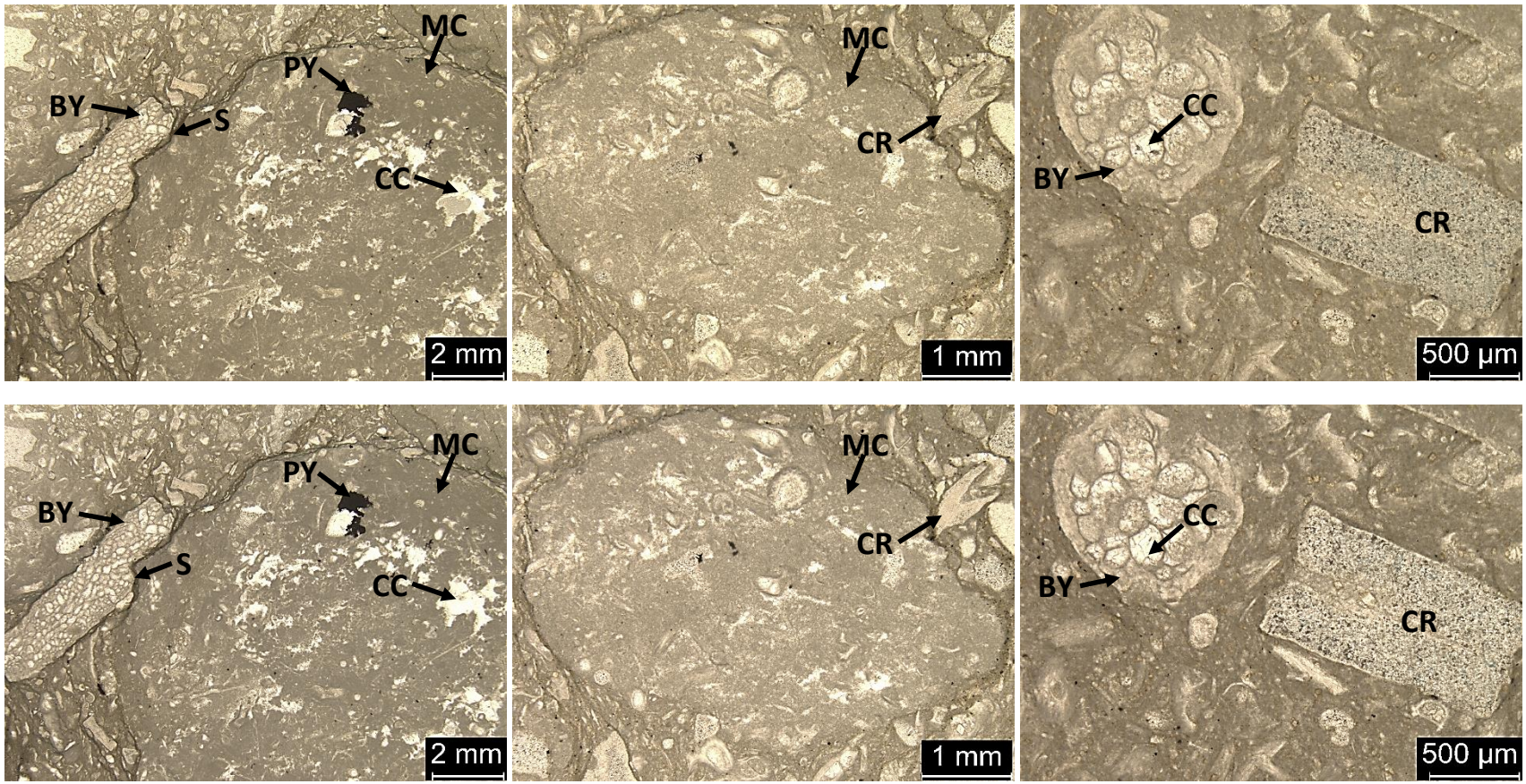

3c-6.5: Wackestone-packstone from the debris flow unit within the Compton Formation. Contains mudstone clasts ranging in size from very coarse sand to very coarse pebbles. The mudstone clasts are surrounded by a matrix of fine to coarse grained bryozoans (125 µ – 1mm), brachiopods (400 µ – 700 µ), and crinoids (125 µ – 2mm). These skeletal components are also contained within the mud clasts. Muddy stylolites, calcite cement, and pyrite can also be seen throughout.

APPENDIX B

SCANNING ELECTRON MICROSCOPE IMAGES

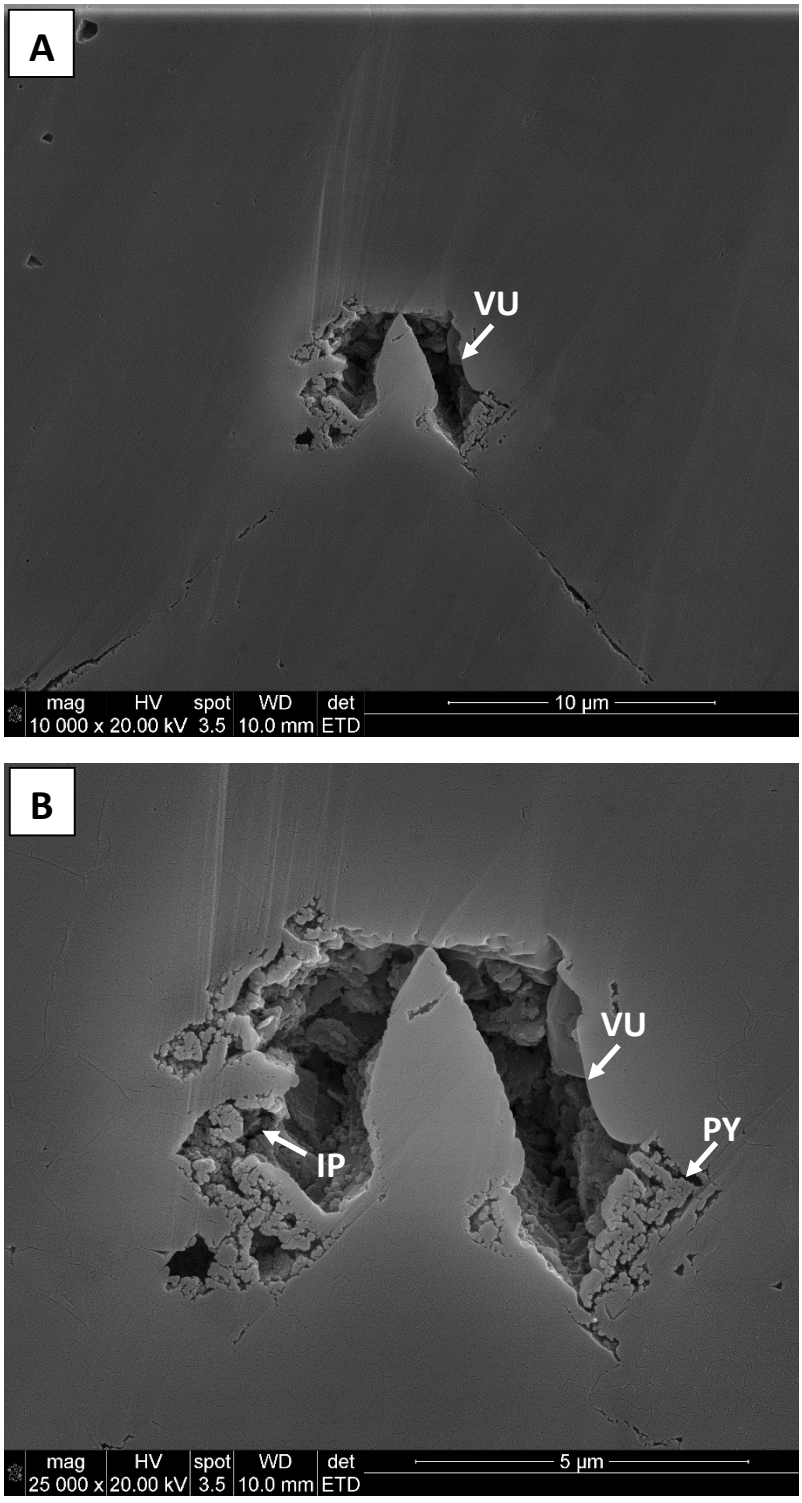

3c-0.0: SEM image of Facies 1 (bryozoan-crinoidal wackestone). **A.** 25,000X, vug containing interparticle porosity can be seen. **B.** closer view of the interparticle porosity seen within A. Pore-filling and pore-lining pyrite occurs throughout the vug. Pores fall into the micro- to nanopore classes, while pore throats are primarily in the nanopore class.

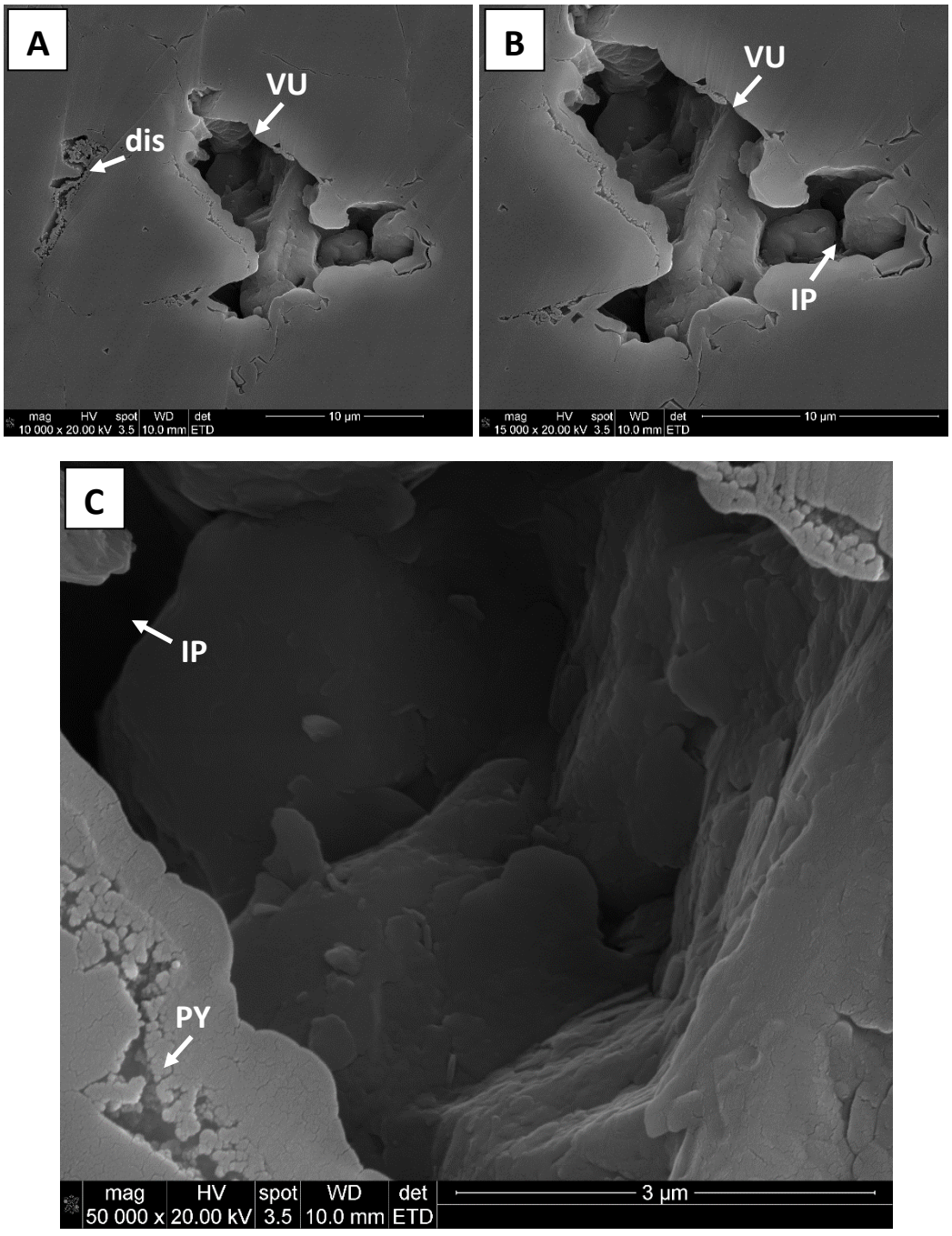

3c-0.0**:** Facies 1 (bryozoan- crinoidal wackestone facies (continued). **A.** Vug containing interparticle porosity is shown at 10,000x. The curved features surrounding the main vug maybe dissolution-related features (dis). **B.** Vug is shown at 15,000x. Pyrite lines the walls of the vug. **C.** Magnification of the upper left corner of the vug at 50,000x. Pores and pore throats fall into the micro- to nanopore classes.

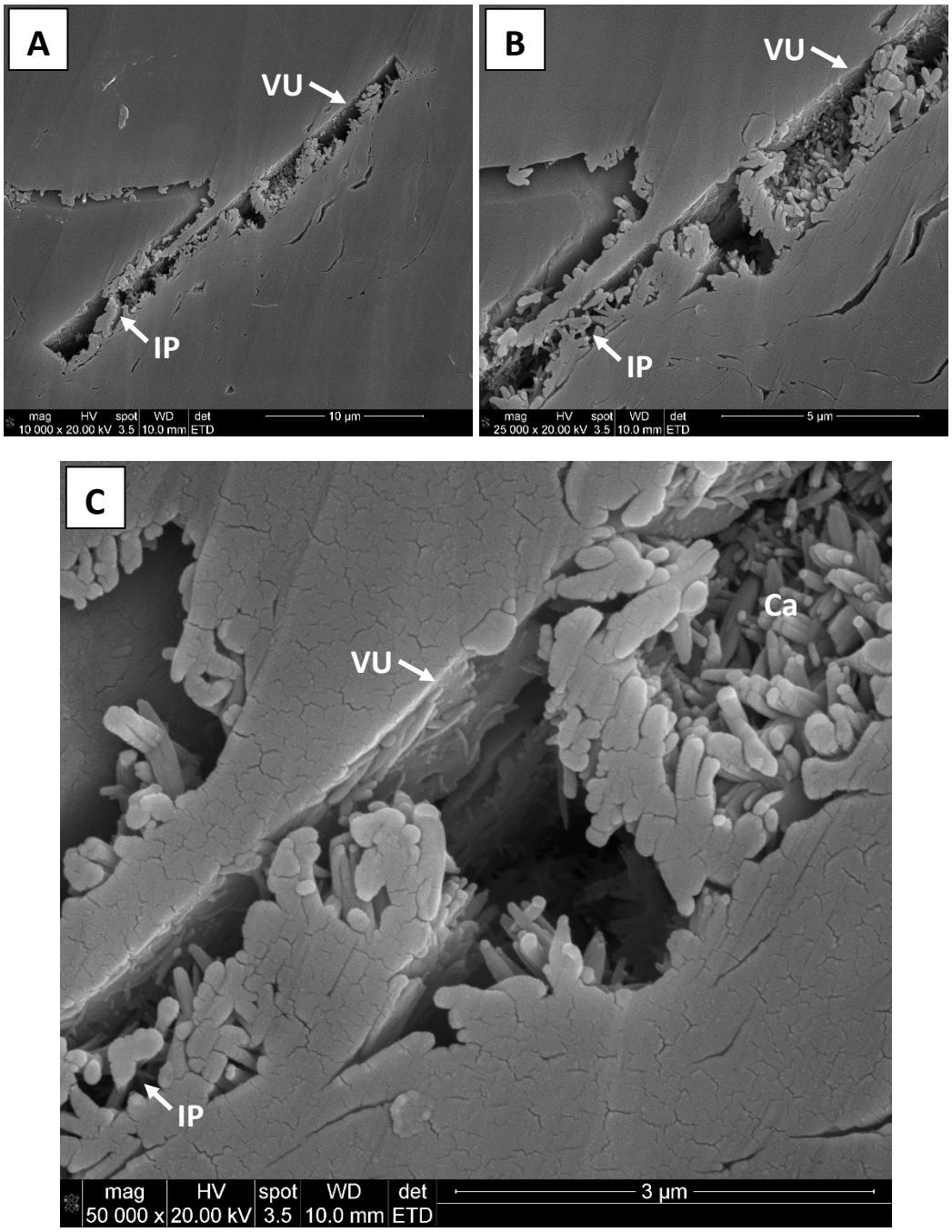

3nv-2.5: Facies 2 (crinoidal wackestone to packstone). **A.** Rectangular-shaped pore along a cleavage plane containing interparticle porosity. **B.** View of the rectangular-shaped pore at 25,000x. porosity occurs around the calcite crystals (Ca) within the vugs. **C.** View of the vug magnified to 50,000x. Pores fall into the micro- to nanopore classes, while pore throats are primarily in the nanopore class.

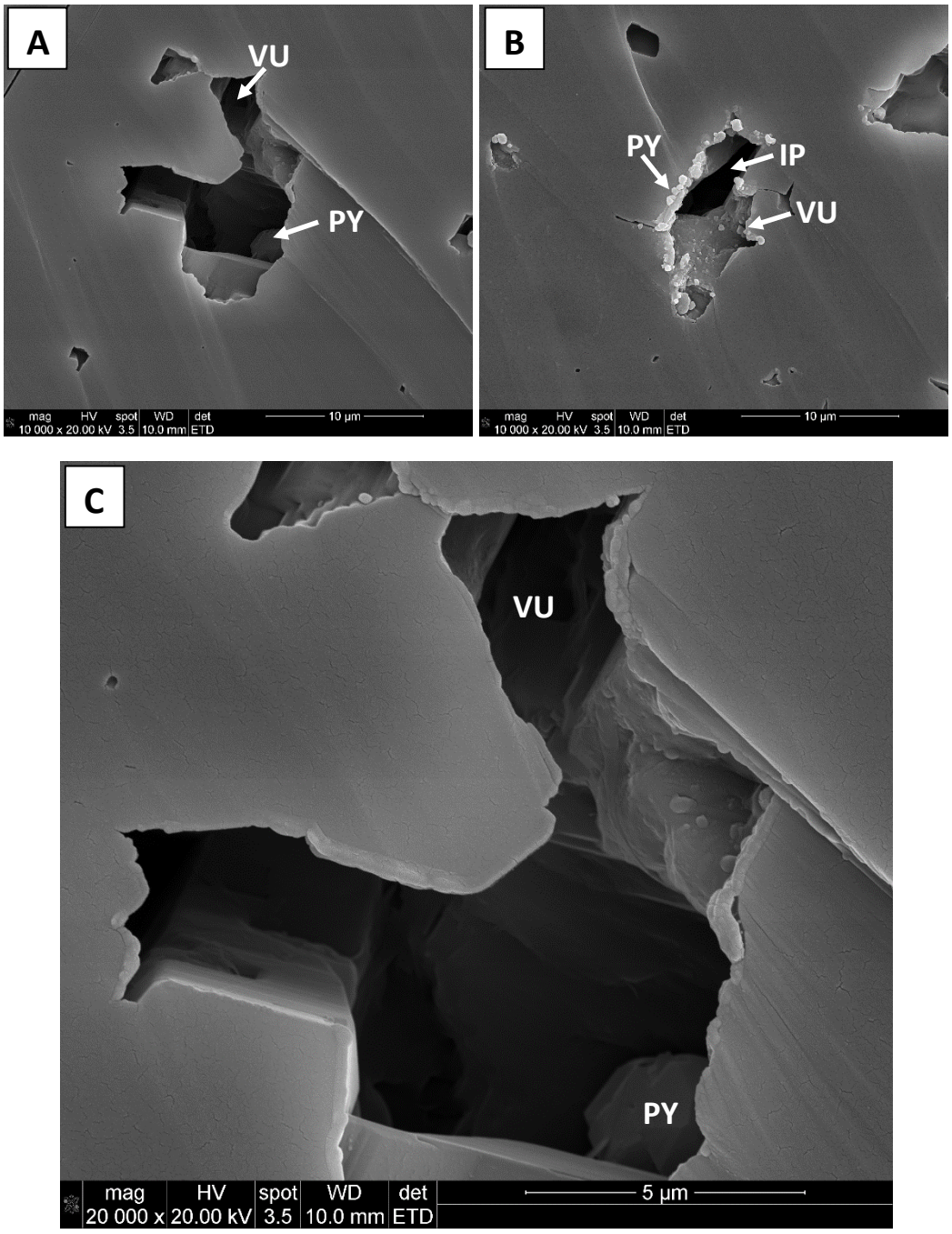

2nv-1.25: Facies 3 (bryozoan-crinoidal mud-lean packstone to grainstone). There are significantly more pores present within this sample relative to the others. **A.** Vug with pore-lining and pore-filling pyrite at 10,000x. **B.** Additional vug at 10,000x lined with pyrite. **C.** Magnification of vug in A. at 20,000x. Pore size falls into the micropore class. This facies contains the largest pore throats of each facies defined in this study, which falls into the nano- and micropore classes.

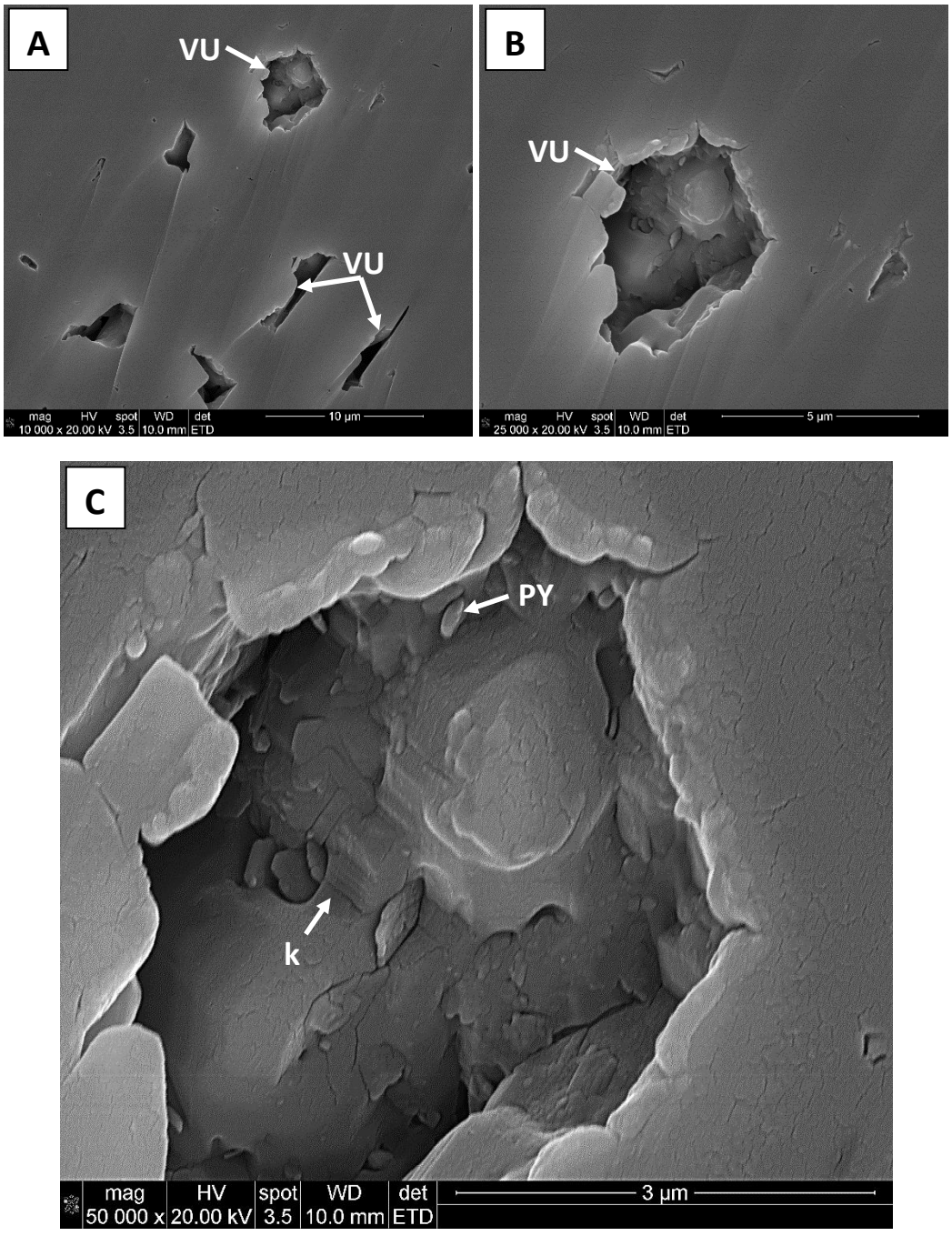

2p2-9.0: Facies 4 (skeletal grainstone). **A.** 10,000x view of vuggy porosity.**B.** Magnified view of vug at 25,000x containing pyrite and clay lining the walls of the pore. **C.** View at 50,000X shows vug partially filled with kaolinite and pyrite. Pores fall into the micro- to nanopore classes, while pore throats are primarily in the nanopore class.

APPENDIX C

OUTCROP FIELD PHOTOGRAPHS

Vertical Section 2

Base of the Compton of Vertical Section 2-3C at the southeast end of the outcrop. Massive bedding at the base of the photograph transitions into thinly bedded wackestone-packstone units. The top-most unit is part of the debris flow bed associated with mobilized blocks. Note each red mark on the Jacob's staff is 1 foot (0.3 m).

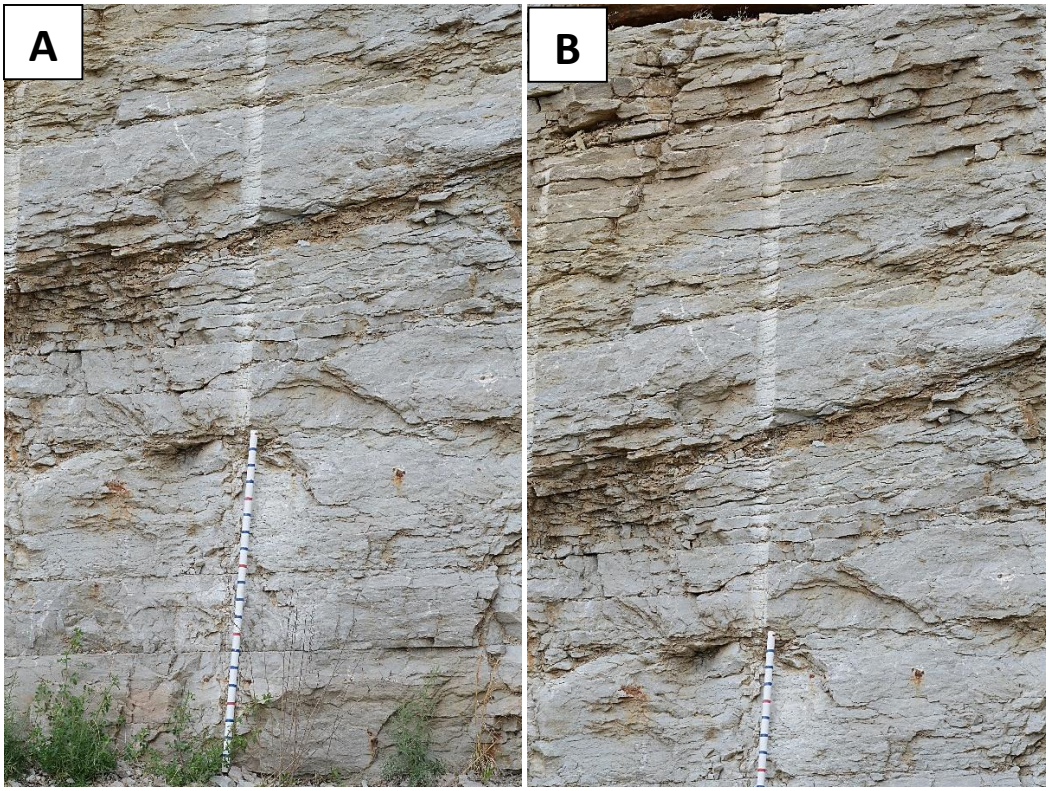

Base of the Compton Formation at Vertical Section 2, just to the right of Block 1 (not pictured). Truncated bedding can be seen, likely the result of block movement down-dip. Bedding thickness changes considerably in the vertical direction, suggesting blocks moved in multiple events throughout depositional time. Note each red mark on the Jacob's staff is 1 foot (0.3 m).

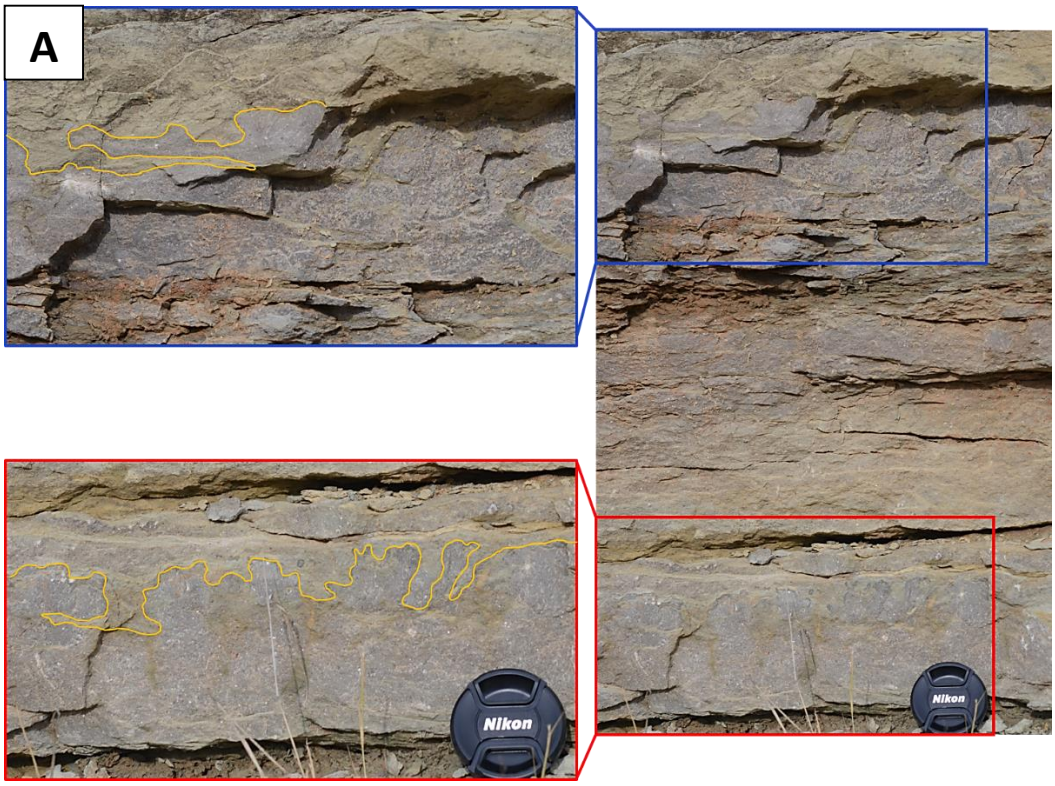

Photographs of the Northview Formation at Vertical Section 2. A. Multiple subaerial exposure surfaces (traced in yellow) serve as evidence for periods of regression in 4th order high frequency sequences. B. Lenticular bedding, a common feature of tidal flats. Note lens cap and finger for scale.

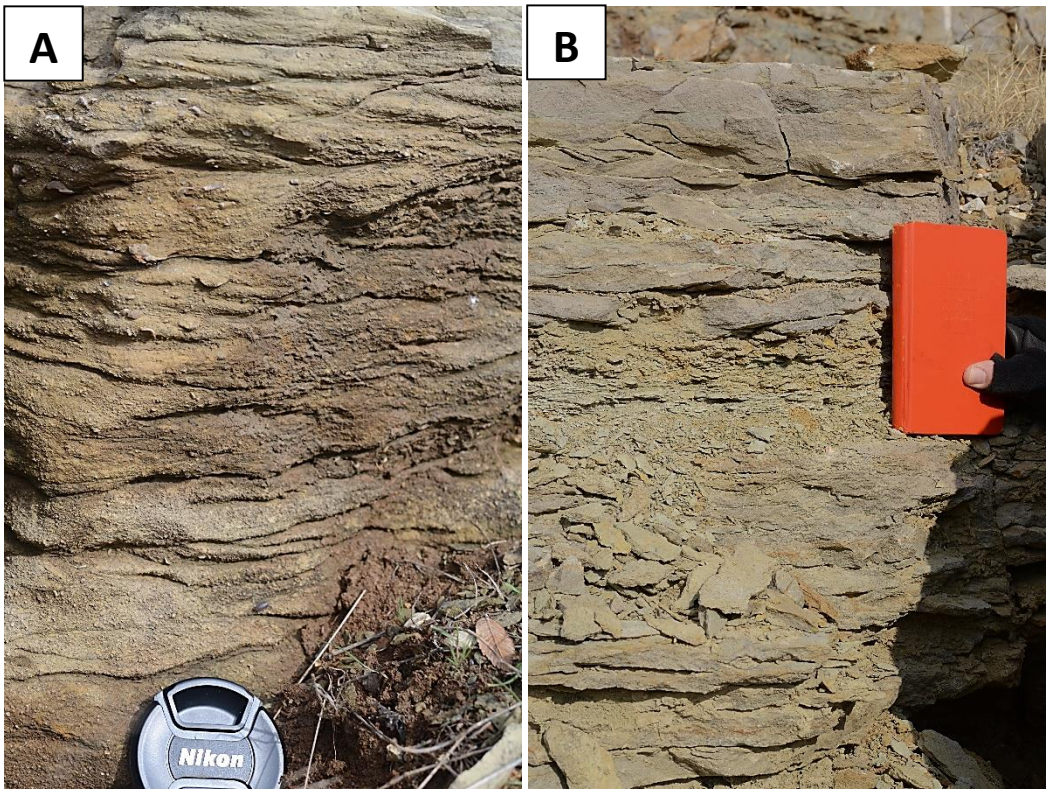

Photographs of the Northview Formation near Vertical Section 2. A. Bi-directional ripples serve as further evidence the Northview Formation was deposited in a tidal flat depositional environment. B. Thinly bedded mud-lean packstone to grainstone facies of the Northview Formation. This facies contains the most porosity according to thin section and SEM analyses. Note lens cap and field book for scale.

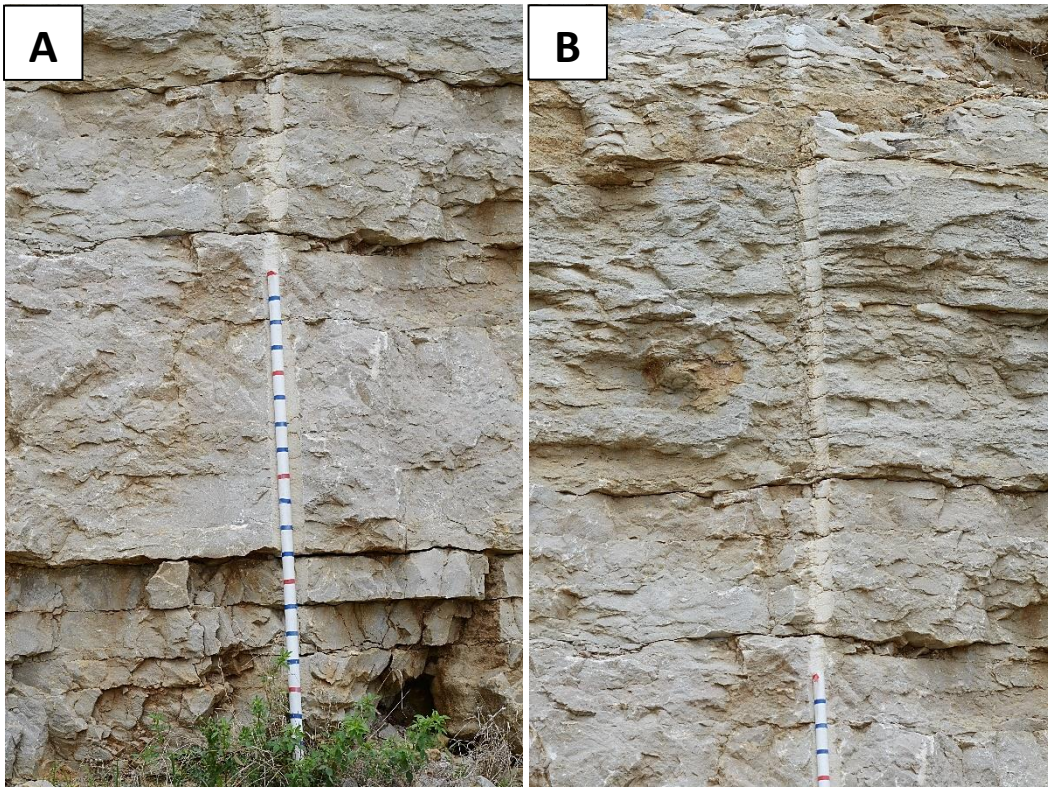

Field photographs of the first ledge of the Pierson Formation. A. Base of ledge 1, showing the bed transition from thin to massive. B. Top of ledge 1, which is dominated by thinly bedded packstones-grainstones. Note Jacob's staff for scale, red marks are 1 ft (0.3 m).

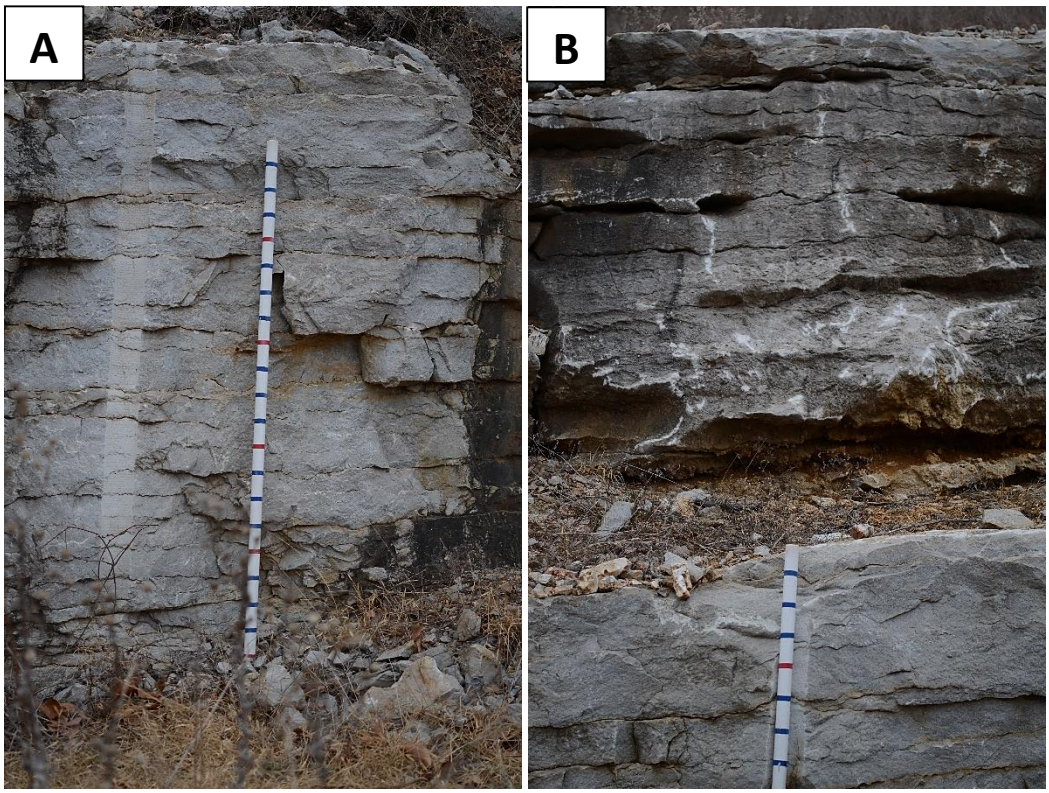

Field photographs of ledge 2 and 3 of the Pierson Formation at Vertical Section 2. A. Base and top of ledge 2, dominated by thinly bedded grainstones. B. Top of ledge 2 and entire ledge 3. Ledge 3 is highly weathered and dominated by thinly bedded grainstones. Note Jacob's staff for scale, red marks are 1 ft (0.3 m).

Vertical Section 3

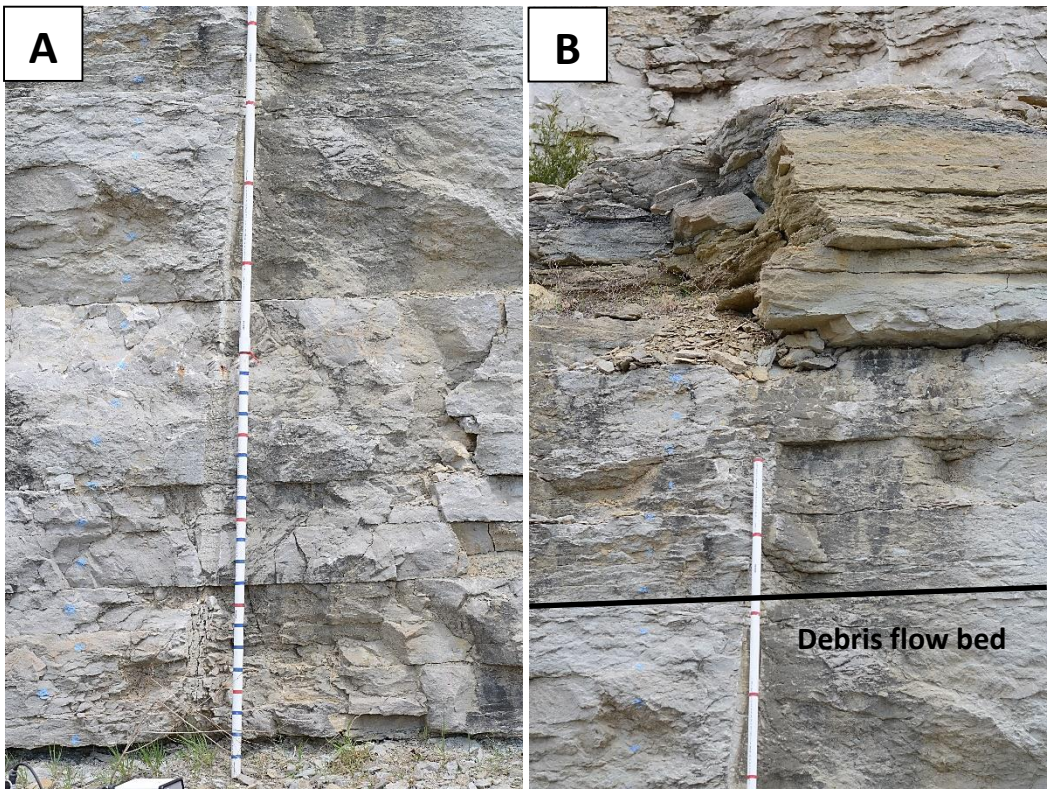

Field photographs of the first ledge of the Compton Formation and the overlying Northview Formation at Vertical Section 3. A. Bottom half of the bottom ledge of the Compton Formation. Thinly bedded wackestones change into massively bedded wackestones to packstones from bottom to top. B. Upper portion of the Compton Formation and overlying Northview Formation. The debris flow bed of the Compton Formation can be seen. The changing colors of the Northview Formation each represent a lithology change from light brown to gray silty shale at the base to thinly bedded mud-lean packstone to grainstone at the top (see next page). Note Jacob's staff for scale, red marks are 1 ft (0.3 m).

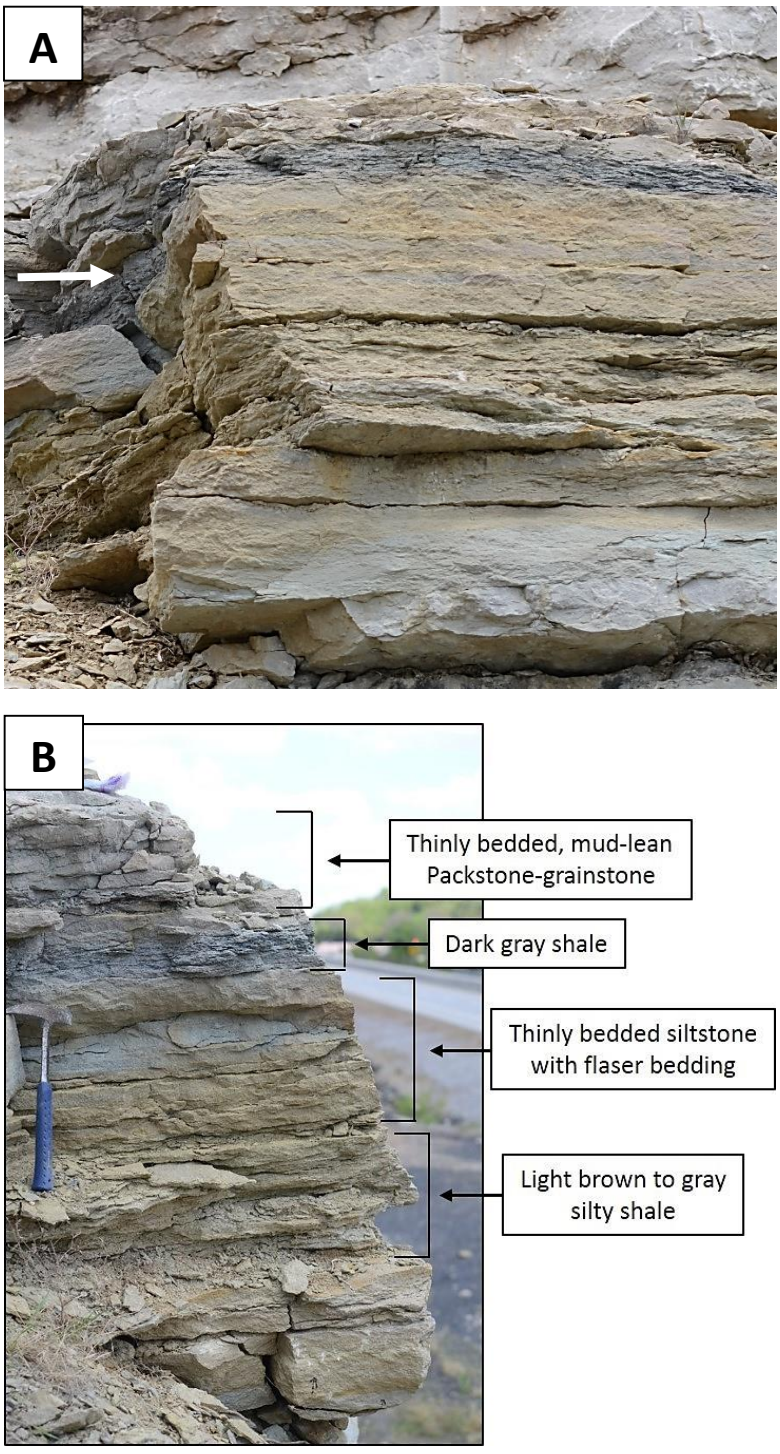

Outcrop photographs of the Northview Formation. A. shows the front face of the Northview Formation, which facies the road. B. shows the side of the Northview Formation (white arrow in photo A) labeled from base to top. Note rock hammer for scale.

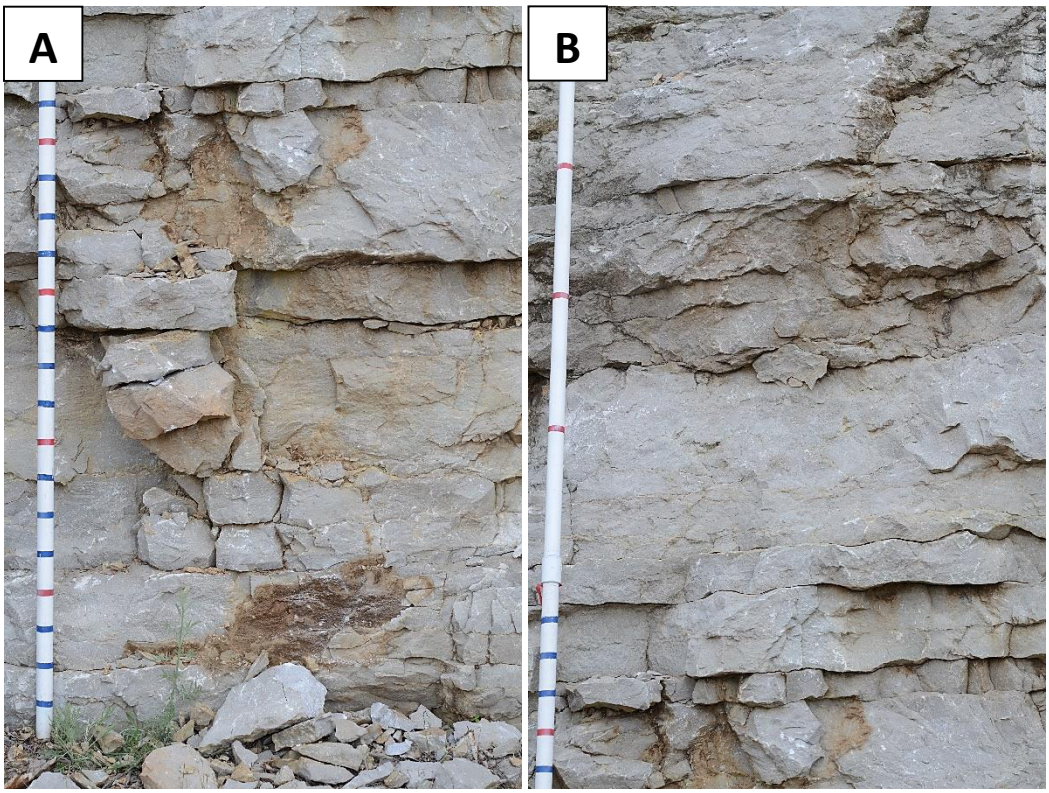

Field photographs of the first ledge of the Pierson Formation at Vertical Section 3. A. Bottom portion of the first ledge. B. Middle portion of the first ledge. Moving from bottom to top, massively bedded packstones give way to thinly bedded mud-lean packstones. Note Jacob's staff for scale, red marks are 1 ft (0.3 m).

Field photograph of the top portion of the first ledge of the Pierson Formation at Vertical Section 3. This ledge is dominated by thin and wavy bedded packstones to mud-lean packstones and grainstones. Note Jacob's staff for scale.

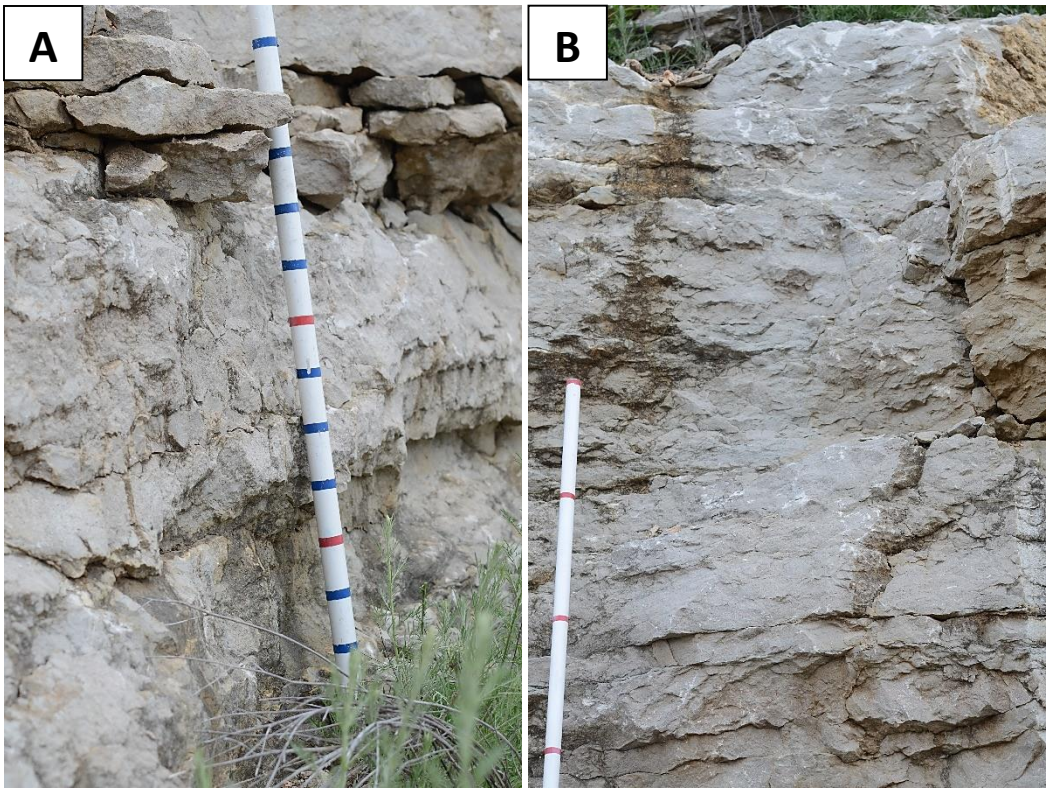

Field photographs of the second ledge of the Pierson Formation at Vertical Section 3. This ledge is dominated by packstones to grainstones. A. shows the base of the second ledge. B. shows the top of the second ledge. Note Jacob's staff for scale.

VITA

Miranda Nichole Childress

Candidate for the Degree of

Master of Science

Thesis: HIGH RESOLUTION SEQUENCE STRATIGRAPHIC ARCHITECTURE OF A MID-CONTINENT MISSISSIPPIAN OUTCROP IN SOUTHWEST MISSOURI

Major Field: Geology

Biographical:

Education:

Completed the requirements for the Master of Science in Geology at Oklahoma State University, Stillwater, Oklahoma in May, 2015.

Completed the requirements for the Bachelor of Science in Geology at Oklahoma State University, Stillwater, OK/USA in 2012.

Experience: Interned at Devon Energy in Oklahoma City, OK in 2014

Began full-time job as a geologist at Devon Energy in Oklahoma City, OK in 2015

Professional Memberships:

American Association of Petroleum Geologists